Hydrogel Encapsulated Droplet Interface Bilayer Networks as a Chassis for Artificial Cells and a Platform for Membrane Studies

A thesis submitted *in accordance with the conditions governing candidates* for the degree of Philosophiae Doctor in Cardiff University

by

Divesh K. Baxani

September 2017
Cardiff School of Pharmacy and Pharmaceutical Science
Cardiff University

Abstract

There has been increasing interest in droplet interface bilayers (DIBs) as novel devices for the study of lipid membranes and the development of artificial cell systems. Although DIBs have demonstrated to be useful in a number of laboratory applications, their wider use is hampered by a limited ability to exist untethered and remain mechanically stable beyond controlled laboratory environments.

In this thesis, a microfluidic system is developed which enables the facile generation of hydrogel-encapsulated DIB networks which are freestanding and can exist in air, water and oil environments, without compromise to their ability to interface with the surrounding environment. Electrophysiology is employed in order to demonstrate the formation of bilayers between the encapsulated DIBs (eDIBs) and their external environment, achieved via the incorporation of the transmembrane pore α-Hemolysin. The eDIBs produced here are able to form higher-order structures akin to tissues via their assembly and adherence to one another, further demonstrating their potential to act as a chassis for artificial cells. Furthermore, the potential of eDIBs to be used as a platform for membrane studies is demonstrated via their use as a high-throughput array for membrane disruption fluorescence measurements using a plate reader, which makes use of the ability of eDIBs to be generated in large numbers as well as to be mechanically handled and placed in the wells of a 96-well plate. Fluorescence measurements were taken on up to 47 eDIBs simultaneously, and were able to detect bilayer leakage through pores as well as bilayer failure.

The above experiments comprise the design, manufacture and use of a novel kind of DIB construct as a chassis for artificial cells and a platform for high-throughput membrane studies. It is proposed that eDIBs may help in realising the unfulfilled potential of DIB networks in applications in healthcare and beyond.

Table of Contents

Table of Contents

Table of Contents

List of Abbreviations

µTAS	Micro total analysis system
2.5D	2.5 dimenisons
2D	2 dimensions
2PP	2-photon polymerisation
3D	3 dimensions
A	Amperes
Ag	Silver
AgCl	Silver chloride
ALM	Artificial lipid membrane
APTES	(3-aminopropyl) Triethoxysilane
APTMS	(3-aminopropyl) Trimethoxysilane
BLM	Black lipid membrane
Ca	Calcium
$CaCO_3$	Calcium carbonate
CH_3	Methyl group
CMC	Critical micelle concentration
CNC	Computer numerical control
CO_2	Carbon dioxide
COC	Cyclin olefin copolymer
CoM	Center of mass
CVD	Chemical vapour deposition
DIB	Droplet interface bilayer
DNA	Deoxyribonucleic acid
DOPC	1,2-dioleoyl-sn-glycero-3-phosphocholine
DPhPC	1,2-diphytanoyl-sn-glycero-3-phosphocholine
eDIB	Encapsulated droplet interface bilayer
EDTA	Ethylenediaminetetraacetic acid
ETFE	Ethylene tetrafluoroethylene
F	Frequency
FEP	Fluorinated ethylene propylene
FFF	Fused filament fabrication
G/M	Guluronate/mannurate
GUV	Giant unilamellar vesicle
H	Hydrogen
H_2O	Dihydrogen monoxide
HEPES	4-(2-hydroxyethyl)-1-piperazineethanesulfonic acid
HPLC	High-performance liquid chromatography
hr	Hour
Hz	Hertz
i3DP	Initiator integrated 3D-printing

List of Abbreviations

ID	Internal diameter
ID	Identity
KCl	Potassium chloride
L	Litre
LBL	Layer-by-layer
LoC	Lab-on-chip
m	Metre
MEMS	Micro electromechanical system
Mg	Magnesium
MLV	Multilamellar vesicle
MPEOTMS	3-Methoxy(polyethyleneoxy)propyl]trimethoxysilane
MPTS	3-Mercaptopropyltrimethoxysilane
NaCl	Sodium chloride
O	Oxygen
O/W	Oil in water
O/W/O	Oil in water in oil
OD	Outer diameter
OH	Hydroxyl group
OTMS	Octadecyl trimethoxysilane
OTS	Octadecyl trichlorosilane
P	Pressure
Pa	Pascal
PCR	Polymerase chain reaction
PDMS	Polydimethoxysilane
PEEK	Polyether ether ketone
PEG	Polyethylene glycol
PEO	Polyethylene oxide
PFS	Polytetrafluoroethylene silane
pH	Potential of hydrogen
PLA	Poly lactic acid
PS	Phosphatidylserine
PS	Polystyrene
PTFE	Polytetrafluoroethylene
PVA	Polyvinyl alcohol
Q	Flow rate
Re	Reynold Number
RNA	Ribonucleic acid
rpm	Sevolutions per minute
s	Seconds
S	Siemens
SAM	Self-assembled monolayer
SDS	Sodium dodecyl sulphate
Si	Silicon
SLA	Stereolithography
SLB	Supported lipid bilayer

List of Abbreviations

SMH	Shai-Matsuzaki-Huang model
SUV	Small unilamellar vesicle
SWR	Standard well read
TEOSPEO	N-(Triethoxysilylpropyl)-O-poly(ethylene oxide)urethane
Tg	Glass transition temperature
TIRF	Total internal reflection microscopy
UK	United Kingdom
USA	United States of America
USB	Universal serial bus
UV	Ultraviolet
V	Voltage
v/v	volume/volume
v/w	volume/weight
W/O	Water in oil
W/O/W	Water in oil in water
W/O/W/O	Water in oil in water in oil
WS	Well scanning
XPS	X-ray photoelectron Spectroscopy

Chapter 1: Introduction and Literature Review

1.1 Synthetic Biology

1.1.1 Introduction

Synthetic biology is an emerging field of study that can be defined as "the design and construction of new biological, biological-based or biological inspired parts, devices and systems and the modification of existing biological systems"[1]. The field has been made increasingly possible thanks to the global ability to share and interpret data and knowledge across different fields of study, in order to gain multi-disciplinary insight into biological systems[2]. The broad aim is to give rise to new technologies inspired by biological systems to counter persistent grand challenges that face humanity within healthcare, energy production and the environment. It is expected to have as great a global impact as the advent of information and computing technology throughout the last century[3].

Appreciation of the "circuit-like connectivity" of biological parts and the ability of biological systems to collectively process sequential, feedback and logical operations has enabled a distinct engineering approach to synthetic biology[4], applying concepts such as the standardization of components, decoupling of whole systems into parts and abstraction via mathematical modelling, for example[5]. One aspect of synthetic biology that has advanced significantly in the recent years is the development of synthetic genetic pathways and their inclusion in microorganisms for biochemical engineering applications, such as the production of biofuels[6] and pharmaceuticals[7, 8].

The engineering aspect is evident in the development of "biobricks"[9], which is a standardized, modular format of building blocks used to assemble genetic circuits.

1.1.2 Artificial cells

Central to the field of synthetic biology is the development of artificial cells. Since the proposition of cell theory in 1839 by Matthias Schleiden and Theodor Schwann[10], the cell has been considered the basic structural and functional component of all known living systems. With the sheer amount of functionality packed into cells and the applications that have developed from their study (biochemical engineering, cell therapies, studies into the origin of life etc.), it has become desirable to produce artificial mimics of cells which can overcome their inherent complexity and *ex vivo* frangibility[11], as well as to develop novel devices and technologies which make use of some of the fundamental concepts that make cells so incredibly functional.

a)

Compartmentalization
Identity & containment

Metabolism
maintenance, growth and replication

Information
selection & inheritance

b)

Compartmentalization
Identity & containment

Metabolism
maintenance, growth and replication
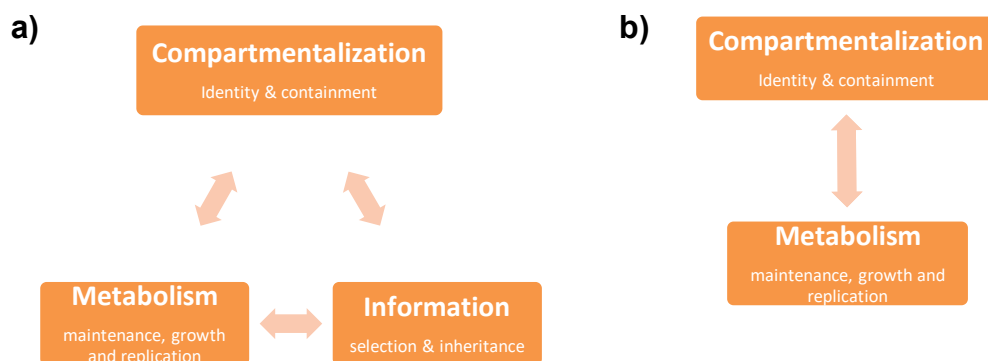
Figure 1.1 The minimum component requirements for a cell to be considered "living" (a). It is likely that simpler systems capable of self-replication existed prior to the evolution of DNA and RNA information systems (b)[12].

In order to produce artificial cells one must first understand the key features of living cells that would need to be replicated. From a reductionist point of view, it can be said that biological cells are "living" due to the collective operations of compartmentalization, metabolism and information (Figure 1.1), allowing for self-preservation, replication and evolution[13]. In modern cells, these processes are based on three main components[12]:

1. A semi-permeable membrane container that protects the internal contents of the cell and defines its boundaries, allowing for selective material and energy exchanges with an environment.

2. Molecular complexes that carry inheritable information and control cell function, such as DNA and RNA.

3. Metabolic pathways that allow cells to maintain and repair themselves, as well as perform functions of growth and replication.

The debate concerning which of these three processes preceded which has been on-going since Alexander Oparin first popularised the idea of the emergence of life from non-living materials in 1924[14-16]. However, it is likely that that in early scenarios of the evolution of cells, compartmentalisation and metabolism were sufficient in achieving replication (Figure 1.1), as growth achieved via metabolism might have been able to force-split a compartment into "daughters"[12]. Here, it is proposed that compartmentalisation is the primordial aspect required to generate life, as life is fundamentally defined as being separated from an environment at large (i.e. cellular life).

It can be said that "typical" artificial cells aim to possess all of the above features of living cells in order to give rise to a system containing the minimum requirements to be considered "alive" (however difficult such a definition may be), such as self-replication, metabolism and evolution. "Non-typical" artificial cells on the other hand aim to produce constructs that do not necessarily confine to the all of the criteria defined above, but nevertheless display functionalities that mimic those of biological cells, in order to provide biological insight or novel, bio-inspired devices[17].

1.1.2.1 Bottom-up vs. Top-down approaches

Synthetic biology aims to produce and modify cells in order to understand how cells developed from non-living matter, and how they function and evolve, as well as to engineer new, useful life forms. Such efforts can be divided into two main approaches: the top-down approach and the bottom-up approach[18] (Figure 1.2).
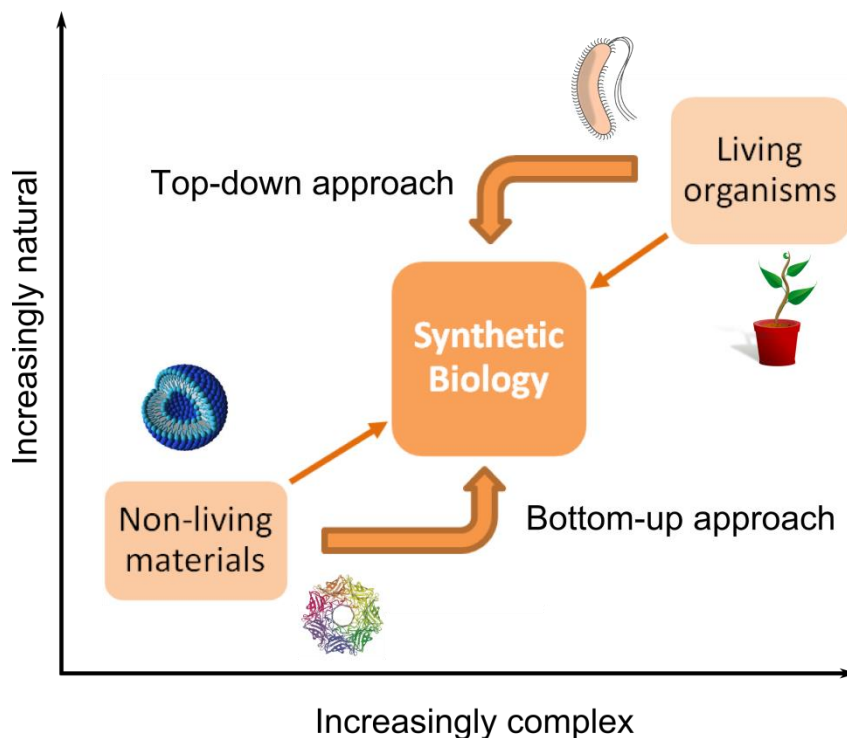
Figure 1.2 Bottom-up and top-down synthetic biology approaches in producing artificial cells[19].

The top-down approach has insofar been the dominant approach, in which existing organisms are modified with the intention of reducing complexity and re-purposing cells[20]. Top-down approaches primarily focus on genetic modifications including the introduction of synthetic gene pathways and the elimination of non-essential genes, as the other "living" aspects such as metabolism, compartmentalisation and containment are provided by the host organism. A significant milestone in the top-down approach was achieved in 2010 by Craig Venter´s research team, who managed to produce a

viable cell by introducing a synthetic genome into a cell containing no genome[21]. Experiments with a variety of synthetic organisms[22] created in Venter´s lab provide promising proof of concept as well as a good platform for the development and commercial re-purposing of cells. Criticism has been sustained against claims that a truly synthetic life form had been created as only the genome is synthetic, but not the biochemical machinery and environment critical to its function[23]. However, this approach remains a pragmatic method of producing artificial cells that is both functional and tailored to specific applications, such as their use in biochemical engineering as bio-factories.

Whilst the top-down approach is an exercise in reducing the complexity of existing organisms, bottom-up approaches attempt to increase complexity via the assembly of biological or non-biological materials into a synthetic, life-like system "from scratch", often leaning on self-organizing processes[24]. This approach comes hand in hand with the philosophy of the late Richard Feynman, crystallised in his quote: "What I cannot create, I do not understand"[25]. This hints at the limitations of our understanding and ability to integrate information regarding highly complex systems, such as cells. Indeed, top-down synthetic biologists often have to worry about genetic and metabolic crosstalk, cell death, noise, mutations etc. when working with natural cells[26], which exemplifies such complexities. The phrase makes reference to the virtues of understanding systems via the bottom-up, where one often has to engage in reiterative design and consider the pragmatisms and trade-offs required in order to generate functional and self-sustaining systems[27].

Bottom-up synthetic biology offers the potential to provide a conceptual bridge between non-living and living matter, and thus aid in our understanding of how life originated in the first place[28]. Additionally, artificial cells created in this approach would likely offer

higher degrees of tailorability and control than top-down artificial cells, and therefore their potential in technological applications remains enticing.

For many bottom-up synthetic biologists, the first point of call in producing artificial cells has been in producing a suitable structural chassis which delineates the cell boundary, and allows for the maintenance of a cellular environment and the selective exchange of solutes across a semi-permeable membrane[29]. A number of different structures have been explored, including polymersomes[30-32] and coacervates[33], but phospholipid membranes have thus far been the most studied due to their biological relevance and ability to produce sub-compartmentalised structures. Phospholipids, phospholipid membranes and artificial cells constructed using such structures will be overviewed in section 1.2.

1.2 Lipid membranes

Lipid membranes are ubiquitous structures within the realm of biology that mediate compartmentalisation[34]. They form semi-permeable barriers that delineate cell boundaries as well as certain organelles, such as the nucleus, lysosomes and mitochondria, whilst being the main structural component of other organelles such as the Golgi apparatus and endoplasmic reticulum. The compartmentalisation offered by lipid membranes is essential for the function of biological systems for their ability to selective include or exclude different molecular species, and maintain concentration gradients between different cellular compartments as well as with their extracellular environment. Aside from this, lipid membranes also perform a variety of other functions such as cell signalling and small molecule transport, often aided by a variety of macromolecules such as transmembrane proteins, which are embedded within the membrane. Lipid membranes are formed via the self-assembly of lipid molecules into bimolecular leaflets.

1.2.1 Lipids

Lipids are a broad class of non-polar, biological molecules. This includes fatty acids, sterols, triglycerides, waxes, phospholipids and others. Although cell membranes are composed from a large variety of lipids, this section will focus on the main class of bilayer-forming lipids in biological membranes, which are phospholipids. The phospholipid structure is based on a hydrophilic "head" group, which is attached to a hydrophobic "tail", usually composed of two fatty acid chains with even number carbon atoms (usually 16-18 per fatty acid) and come in varying degrees of saturation, usually containing 1-4 unsaturated carbons. As such, they are amphiphillic and display interesting self-assembling properties. Phospholipids are usually classified according to their head group, which are formed from a phosphoric acid group with either a glycerol, choline, ethanolamine or serine moiety. Phosphocholine and ethanolamine phospholipids are neutral as their head is zwitterionic, whilst glycerol and serine phospholipids are charged.

1.2.2 Lipid polymorphism

Phospholipids self-assemble into higher order structures to form thermodynamically favourable states when present in a polar solvent such as water, as a result of their amphiphillic nature and the hydrophobic effect. The presence of non-polar molecular regions in phospholipids disrupts hydrogen bond networks between water molecules, a process that is energetically unfavourable. Thus, phospholipids aggregate into structures that shield their hydrophobic tails from the water whilst maintaining their heads hydrated, giving rise to a variety of lamellar and non-lamellar lipid phase structures[35] as shown in Table 1. Factors that affect the formation of lamellar phases will be overviewed in the following section, due to their relevance to the formation of lipid bilayer structures within biology.

16
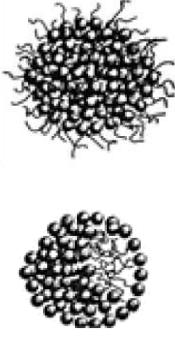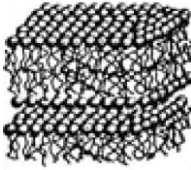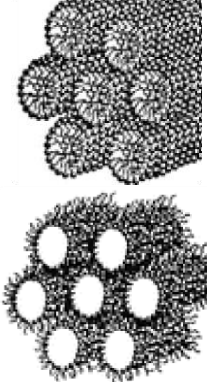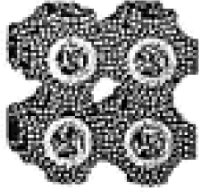
Diagram	Name	Notes
	Micelles and inverse micelles	In polar solvents, lipids aggregate into spheres where the lipid head groups shield the tail groups. The inverse occurs in non-polar solvents. Micelles form in solvents when lipids are sufficiently concentrated in a solvent, defined by the critical micelle concentration (CMC).
	Lamellar phase	Lamellar phases are composed of a bimolecular layer of lipids where lipid tail groups face each other and head groups are in contact with the polar solvent. This is the most important phase from a biological perspective.
	Hexagonal and inverse hexagonal	Lipids in low quantities of water may form tubular structures with hydrocarbon chains on the inside in contact with each other, and the polar heads facing the water. Tubes form bundles of six, hence hexagonal phase. This disposition is thought to be a result of the hydrophobic effect[36]. Inverse hexagonal phases form in non-polar solvents, in a similar fashion to inverse micelles[37].
	Cubic phases	Various cubic phases (such as Fd3m, Im3m, Ia3m, Pn3m, and Pm3m) form in water under certain conditions, such as high temperatures and high lipid concentrations[38]. Cubic phases are liquid crystalline bicontinuous structures that are not strongly favoured and involve high energy of activation barriers[39].

Table 1 Table depicting the main, different kinds of structures that lipids can give rise to. Images adapted from referenced publication[40].

1.2.2.1. Factors that affect lipid polymorphism

The kinds of structures that are formed depend on a variety of physical and chemical factors. One obvious factor is the solvent, as lipids will dissolve in non-polar solvents such as alkane oils, but form emulsions in non-polar solvents. The presence of salts and the pH of the solvent affects lipid polymorphism as the pH alters the protonation of hydrophilic head groups and cationic salts can affect its polarity by interacting with carbonyl regions. These factors, among others, define the relative size and hydrophillicity of lipid head groups[41]. Along with the type of lipid head and the length and unsaturation of lipid tail groups, this affects the overall shape of the lipid molecule and hence its packing into supramolecular structures. Agitation and the application of external forces such as electric fields define the degree of ionisation and interaction between lipid molecules which can modify the type and size of structures that they give rise to[42]. Other important factors include lipid concentration, the presence of other kinds of lipids, such as cholesterol, hydration levels, temperature and pressure[43].

1.2.2.2 Lamellar phase properties

Lamellar phases, or lipid bilayers, can exist in a number of conformations depending on the type of lipids used and physical conditions such as temperature.

1.2.2.2.1 Fluidity

Lipid bilayers exist in various phases where individual lipid molecules have different levels of fluidity to move laterally within the bilayer leaflets. This depends on the temperature and hydration of the system[44]. At low temperatures, lipid bilayers exist in an orderly crystalline lattice with tightly packed lipids. Increasing temperature causes the bilayer to transition into a gel phase where lipids exhibit limited freedom of lateral movement. Higher temperatures cause the lipid bilayer to "melt", and exist in a liquid-

crystalline state where lipids exhibit a higher cross-sectional area and are more able to diffuse laterally[45]. In this state, lipid bilayers can be considered 2D-fluids, able to reseal holes and with varying degrees of mechanical rigidity[34]. The transition temperature between the gel and liquid states (T_g) depends on the nature of the lipid employed. For example, longer fatty acid chains give rise to higher T_g whilst chain unsaturation lowers it.

The movement of lipids across the bilayer from leaflet to another is also possible although occurs at a slow rate in the absence of specialised enzymes[46], due to the energetically unfavourable process of lipid heads having to traverse the hydrophobic region within the bilayer[47].

1.2.2.2.2 Curvature

Depending on the overall geometry and the lateral stress profile of lipids, lipids can have a natural tendency to induce curvature in their supramolecular assembly, giving rise to different lipid structures. The relative widths of the head and tail groups of a particular lipid will give rise to different packing conformations, some of which are conducive to giving rise to curved structures, driven by the hydrophobic effect described earlier[48]. This varies depending on the relative polarity of the head group, the number and length of the fatty acid chains that form the lipid tail, and the degree of fatty acid chain unsaturation, which gives rise to kinks in the chain. Broadly, there are three main types of lipid geometric profiles which are shown in Figure 1.3[48]. Cylindrical lipids are more likely to give rise to lamellar phases, whilst conical lipids with wider heads than tails will have a tendency to form micelles. Inversely conical lipids will tend to curve in the opposite direction, giving rise to inverse lipid phases as described in Table 1.
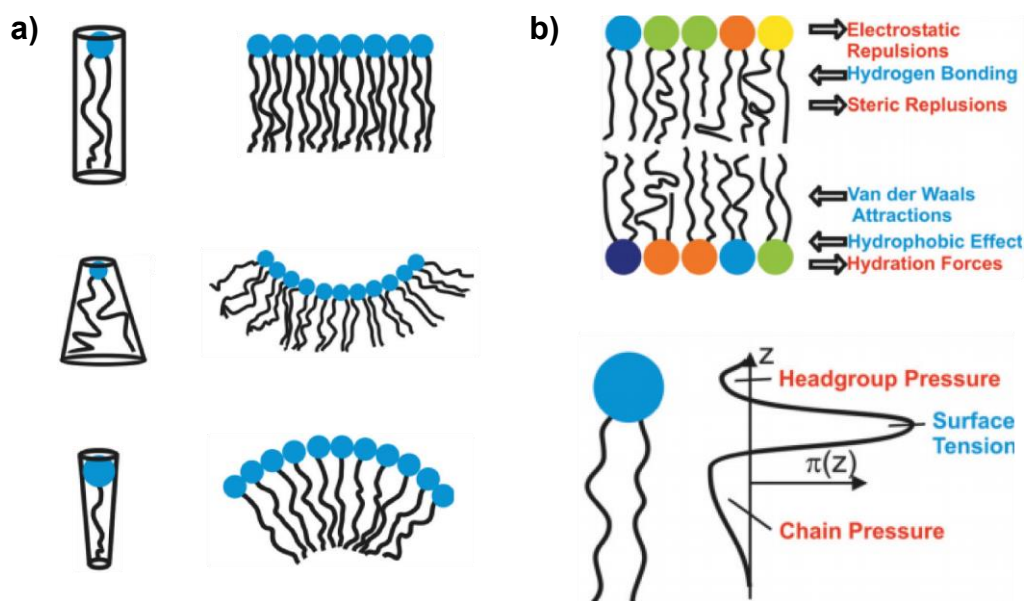
Figure 1.3 Diagrams depicting geometrical aspects of lipids that affect their packing into supramolecular structures. a) Different lipids have different head to tail size ratios, which gives rise to a natural preference in packing. Type O lipids can naturally pack without any curvature, whilst type I and II lipids will tend to form concave and convex packing structures, respectively. b) Images depicting the lateral stress profile of lipids in the context of their packing, and the main forces that are implicated in lipid packing. Images adapted from referenced publication[48].

The lateral stress profile describes the relative effect of the different forces that act on individual lipids within a lamellar conformation, affected by the polarity of its head and the length of the fatty acid chains as well as their saturation. Lateral stress profile also applies to transmembrane proteins. A relative difference in the magnitude of forces acting along the length of the lipid molecule can aid in understanding the inclination of lipids to form curved structures beyond the structural geometry of the lipid[48].

1.2.2.2.3 Permeability

Overton´s rule, pioneered in 1899, describes that the permeability of lipid bilayers to a given molecule is given by its solubility in lipid solutions[49]. Thus, the partition coefficient (LogP) of a given molecule between water and octanol can indicate its permeability through a lipid bilayer. LogP is given by:

20

$$LogP = Log \frac{[solute]in\ octanol}{[solute]in\ water}$$

However, it has since been found that the permeability of lipid bilayers depend on a number of factors other than solubility[50]. For example, lipids are amphiphillic molecules, so molecules need to pass through both hydrophilic and hydrophobic portions of the molecule. Indeed, evidence exists showing a decrease in permeability for highly hydrophobic substances[51], which is likely due to this reason. Secondly, many substances exist in an ionised state which affects its ability to cross through a lipid bilayer[52]. Thus, LogP can be modified in the following manner (referred to as LogD):

$$LogD = Log \frac{[solute]in\ octanol}{[solute]in\ ionised\ water + [solute]in\ neutral\ water}$$

The rate at which small, nonpolar molecules diffuse through a lipid bilayer can be given by a modification of Fick´s Law[53], which takes into account membrane properties such as its thickness and surface area:

$$\frac{dn}{dt} = \frac{AKD}{x}(C_1 - C_2)$$

Where A is bilayer area, K is the partition coefficient of the transported substance, D is the diffusion coefficient of the substance within the bilayer, x is bilayer thickness, and C_1 and C_2 are the concentrations of the substance at either side of the lipid bilayer.

1.2.2.2.4 Electrical properties

It is common to find situations where two aqueous compartments are separated by a lipid bilayer. In such cases, the lipid bilayer can act as an electrical capacitor, as it separates two conductive regions and impedes the flow of charged species, but is able

to store charge at either side of the membrane[54]. Bilayer capacitance is proportional to bilayer area and inversely proportional to bilayer thickness, and can be measured via electrophysiology, where electrodes are placed at either side of the membrane and the current can be measured under an applied voltage.

1.2.3 Biological membranes

Lipid bilayers can be considered the main structural component of biological membranes, although they significantly differ from pure lipid membranes in their structure and function. This section will look at the main features of cell membranes, how they differ from pure lipid bilayers, and their significance within research.

1.2.3.1 Gross structure and function

The fluid mosaic model is the main conceptual representation via which cell membranes are understood (Figure 1.4), although the model has been updated significantly since its conception in 1972[55]. The fluid mosaic model touches upon two basic features of cell membranes: they are fluid as described in section 1.2.2.2.1, where molecules are able to laterally diffuse with various degrees of freedom within the 2-dimensional space of the bilayer; and they are composed of a large variety of different kinds of molecules.
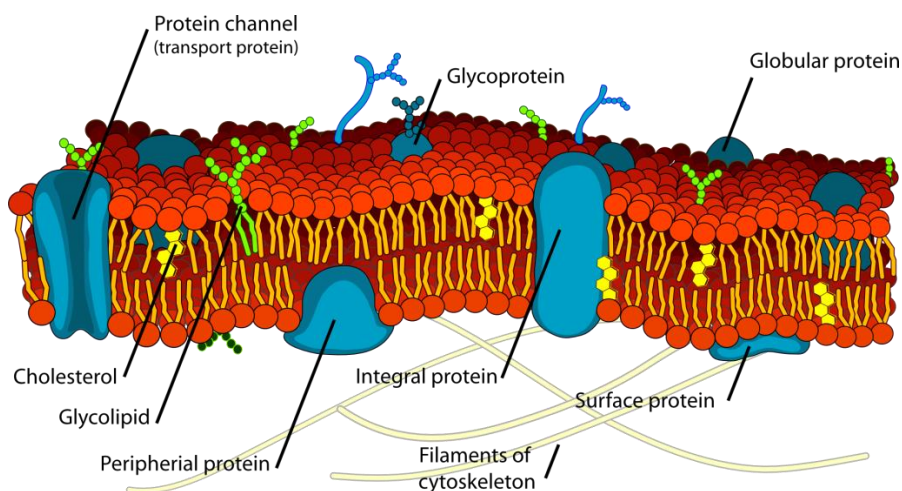
Figure 1.4 Diagram depicting the main features of a cell membrane, including lipids and membrane proteins. The region containing cytoskeleton filaments represent the intracellular region. Image adapted from Wikimedia Commons.

Typically, lipids compose around 50% of the mass of a cell membrane, with the remainder being mostly protein[56]. Glycolipids and glycoproteins are common which display carbohydrate moieties to the inside or the outside of the cell. The glycocalyx refers to the layer of carbohydrate moieties that forms on the exterior of cell membranes, with some being particularly dense such as with animal epithelial cells and certain bacteria. The interior face of the cell membrane is attached to the cell cytoskeleton, in particular with the actin cytoskeleton, which mediates cell structure as well as performing a variety of other signalling and transport functions.

Being the main interface between a cell and its environment, the cell membrane performs a large variety of important cellular functions. Structurally, it provides a self-repairing boundary to the cell and maintains it shape and integrity[34]. It provides an interface where molecular assemblies can come together and perform various functions, such as the signal transduction processes arising from G protein-coupled receptors. Other membrane proteins aid in the transport of molecules across the membrane and aid in setting up membrane action potentials. The glycocalyx is used for cell recognition, adhesion and signalling. The cell membrane is also involved in cell division and other whole-cell processes such as certain kinds of cellular motility.

1.2.3.2 Components

1.2.3.2.1 Membrane lipids

Cell membranes usually contain thousands of different lipids, which vary immensely between different animal kingdoms[57]. They are also characterised by being asymmetrical, where one leaflet significantly differs from the other in terms of lipid composition[58]. This asymmetry is actively regulated by the cell via use of specialised enzymes which aid in the directional movement of lipids from one leaflet to another[46]. Membrane asymmetry mediates a number of membrane functions, which can be exemplified by the localisation of phosphatidylserine (PS) phospholipids in mammalian cells. PS lipids are located primarily on the interior leaflet of a cell membrane and serve as a co-factor for various membrane-bound enzymes such as the Na^+/K^+ ATPase[58]. However, cells can actively display PS on their outer leaflet which is known to promote apoptotic and blood coagulation pathways. Additionally, cholesterols are present in the mix, which sit in the non-polar regions of the cell membrane lipid bilayer. This modifies the biophysical properties of the membrane, such as bilayer fluidity, by intercalating between lipids[59]. The heterogeneity of lipids and the presence of cholesterol profoundly affect the packing, permeability, curvature, fluidity and electrical properties of the cell membrane in comparison to pure lipid bilayers. For example, a bilayer containing saturated and unsaturated lipids will leave "gaps" in their packing which increases the membrane´s permeability to small molecules.

A particular feature of cell membranes is the formation of lipid rafts, which are localised patches that are rich in cholesterol and sphingolipids, and therefore exhibit less fluidity and a higher packing density than their surrounding membrane[60, 61]. Due to their more ordered structure, transient nature, and their affinity for certain proteins, lipid rafts are thought to be involved in a variety of cell signalling processes, such as those regarding

receptor tyrosine kinases and G protein-coupled receptors[60]. Lipid rafts are also thought to be involved in the mediation of caveolae, which are specialised invaginations in cell membranes. Lipid rafts are an intense subject of investigation within the field, with on-going debates regarding their significance, existence, and mechanisms of function[62].

1.2.3.2.2 Membrane proteins

It is estimated that around 30% of the proteome of a typical cell are membrane proteins[63]. Membrane proteins can be classified by localisation within the membrane: integral membrane proteins span across the membrane while peripheral membrane proteins attach to a particular side of the membrane. Their localisation is aided by their structure, with integral proteins containing hydrophobic regions that sit with the hydrophobic regions of the lipid bilayer, for example. Many proteins are able to rotate and diffuse laterally within the lipid membrane[59]. Membrane proteins mediate a large number of functions[56]:

Transport: many integral membrane proteins function as pores and transporters, with some actively transporting molecules or ions at the expense of energy, and others passively transporting molecular species by providing a channel in the membrane. Certain protein pores act as toxins produced by pathogenic microorganisms, by inserting in their host´s membranes and causing lysis. For example, *Staphylococcus aureus* produce water-soluble hemolysins which lyse red blood cells via the production of pores in their membranes[64]. Electrophysiology techniques can measure the presence and activity of certain transport proteins due to their ability to modulate the flow of charge across a membrane[65].

Receptor: certain proteins can recognise specific signalling molecules in their extracellular face and give rise to intracellular signal transduction mechanisms. Two

major classes of receptor membrane proteins are G protein-coupled receptors and receptor tyrosine kinases.

Enzymes: certain enzymes are anchored to cell membranes and mediate cell transduction mechanisms and other cellular functions. For example, receptor tyrosine kinases use their intracellular enzymatic activity to transmit signals upon extracellular ligand recognition.

Adhesion: certain cells adhere to each other or to extracellular matrices and other surfaces. Transmembrane glycoproteins such as selectins and cadherins mediate cell adhesion processes.

1.2.3.3 Importance of studying lipid membranes

Biological membranes are the interface via which cells interact with the World and a biological surface that facilitates a large number of cellular processes. As such, many diseases and pathogenic pathways involve the cell membrane in one way or another, and over 60% of pharmaceutical drugs for a variety of applications target the cell membrane[66]. The design of many other drugs need to take membranes into consideration as the bioavailability of intracellular drugs will depend on their ability to cross membranes, and many other drugs need to be screened for toxicity against membrane components that perform vital functions, such as cardiac membrane proteins. Additionally, their biological significance and material properties make membranes a valuable topic of study for biophysicists and synthetic biologists. For all of these reasons, the understanding of the structure and function of membrane components is of tremendous value for both fundamental and applied sciences.

1.2.4 Artificial lipid membranes

Biological sciences have largely benefitted from a reductionist method where biological systems are studied via their dissection into parts[67]. Due to the complexity and heterogeneity of biological membranes, the isolation of membrane part and processes *in situ* is challenging. Thus, the fabrication of artificial lipid membranes (ALMs) is a valuable technique that promises to give rise to a platform via which lipid bilayers can be studied in the absence of the influence of other biological components. Such biological components can also be individually incorporated into the ALMs in order to study their activity in isolation. The ability to form ALMs is aided by lipid self-assembly, as is the study of certain membrane proteins that are also able to self-assemble into lipid bilayers.

ALMs are not only useful as a method to study the fundamental properties of biological membranes, but can be used in the pharmaceutical industry to screen substances against lipid bilayers or proteins reconstituted into them[68]. Certain ALM types can be used as encapsulation devices for drug delivery and cell transfections[69], or as chassis for artificial cells[70, 71].

Different methods exist in the production of ALMs, including black lipid membranes (BLM)[72], supported lipid membranes[73], vesicles[74] and droplet interface bilayers (DIBs)[75]. The following sections will focus mostly on DIBs as they are extensively used throughout this thesis, and vesicles, which have given rise to interesting biomimetic and artificial cell developments.

1.2.4.1 Vesicles

Vesicles are spherical constructs that are composed of a volume of water encapsulated by a lipid bilayer (Figure 1.5). The addition of water to a dried lipid film will give rise to multi-lamellar vesicles (MLVs) composed of a number of concentric lipid bilayer

spheres, as lipid bilayers assemble into spheres to minimise their surface area[74]. These can be further processed via membrane extrusion or sonication to give rise to smaller, unilamellar vesicles (SUVs) up to 100 nm in diameter[74], and filtered to produce solutions containing vesicles of a particular size range. Numerous methods also exist that give rise to giant unilamellar vesicles (GUVs) up to 50 μm in diameter[76], some of which assemble GUVs individually in comparison to the "bulk" methods of producing most other kinds of vesicles[76].
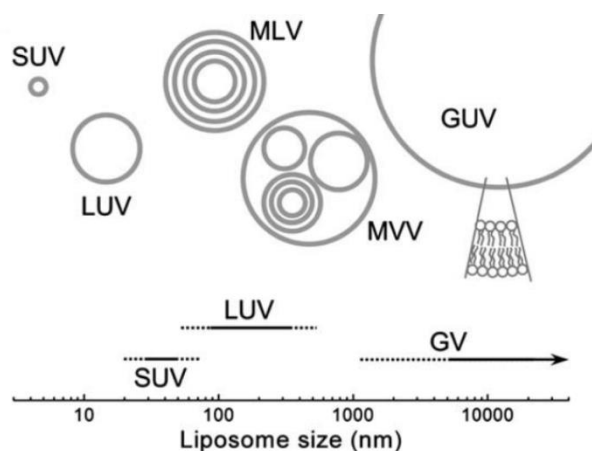
Figure 1.5 Diagram representing the basic structure and size of different kinds of lipid vesicles. Image adapted from referenced publication[77].

The structure of vesicles is fundamentally biomimetic, as they are found naturally in cells as certain organelles such as lysosomes and peroxisomes. They are also involved in cell secretions (exocytosis), cell uptake (phagocytosis and endocytosis), and the maintenance of the cell membrane via the fusion of vesicles containing newly synthesized membrane proteins, for example. Furthermore, they represent the basic architecture of a cell, as they are a volume of liquid encapsulated in a lipid bilayer that can encapsulate biological macromolecules and incorporate biological membrane constituents such as transmembrane proteins. This has given rise to a number of studies where minimal cell systems are incorporated into vesicles as artificial cells, and vesicles have been theorised to have been a necessary precursor of cellular life on Earth[16, 78, 79].

The ability of vesicles to maintain concentration gradients has enabled their use in a variety of applications. Biological studies commonly employ them to measure the leakage or rupture of lipid bilayers in response to pore-forming substances[80], via the encapsulation of reporter substances such as fluorescent dyes. They are also used as vehicles of delivery, may it be into cell culture transfections, or as therapeutic devices in drug delivery[81].

1.2.4.1.1 Vesicles as artificial cells

It has been theorised that the spontaneous formation of fatty acid vesicles may have been the precursor to life as we know it, during the early stages of abiogenesis[82, 83]. Along with their ease of production, they make an attractive chassis to produce artificial cells. Fatty acid vesicles have been known to spontaneously self-reproduce in the presence of fatty acid anhydrides (such as oleic anhydride for oleic acid vesicles) for as far back as 1994[84]. A notable advocate for vesicle-based artificial cells is Nobel laureate Jack Szostak, who´s research group has demonstrated that fatty acids containing RNA replicase as a model genome can spontaneously grow and self-divide, providing a route towards self-sustaining "protocells"[79, 85]. Subsequent experiments performed by other research groups have shown that DNA can be contained and replicated via polymerase chain reaction (PCR) cycles within phospholipid vesicles, and the amplification of such DNA can be linked to the division of the vesicles in the presence of a vesicle membrane precursor[86]. Furthermore, full protein expression systems have been incorporated into vesicles[87], and have been maintained for up to four days by incorporating the transmembrane protein pore α-Hemolysin, which allowed the vesicle to uptake synthesis precursors from its environment[70]. Other interesting, biomimetic functions performed with vesicles have involved their interaction with microorganisms. Also, vesicles have been made to synthesise complex carbohydrates in the presence of precursors and exert an influence over the quorum

sensing mechanisms of a bacterial culture[88]. With all of these demonstrations involving a single vesicle compartment, the works of Elani et al. have focused on producing multi-compartment vesicles[89], which have demonstrated to be able to functionally compartmentalise a multi-step chemical reaction via the transfer of substances across lipid bilayers through transmembrane pores[90, 91].

1.2.4.2 Droplet Interface Bilayers
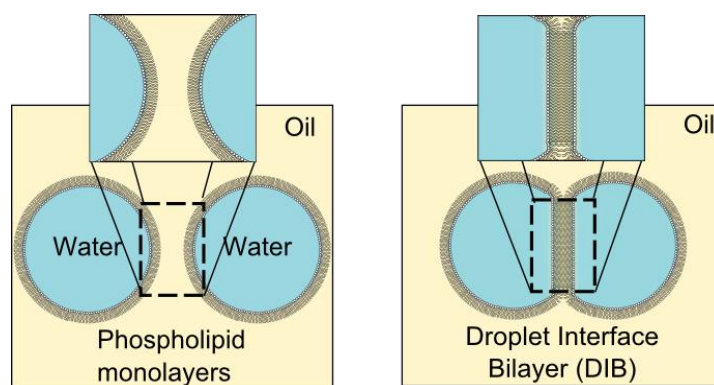
Figure 1.6 Diagrams representing the basic method of forming droplet interface bilayers (DIBs) from the contact of two droplets of water in oil in the presence of a bilayer-forming lipid.

Droplet interface bilayers (DIBs) are typically formed from the contact of two aqueous droplets in oil in the presence of lipid, supplied either dissolved in the oil phase or as vesicles in the aqueous solutions (Figure 1.6). Lipid monolayers self-assemble at the oil/water interfaces and bilayers are formed where two monolayers are brought into close proximity[92]. This method of bilayer formation was first reported many decades ago, but interestingly only started gaining traction as an ALM study for various applications in the past two decades, notably by Hagan Bayley's research group at Oxford[75] and Takeuchi´s in Tokyo[93]. Since then, a large variety of applications and different DIB incarnations have arisen (Figure 1.7). DIBs have been formed between an aqueous droplet and hydrogel surfaces[92], between hydrogel shapes[94] and between aqueous droplets in air[95]. Physical encapsulation of DIBs has also been explored in order to develop shippable or storable ALM platforms[96, 97].

30
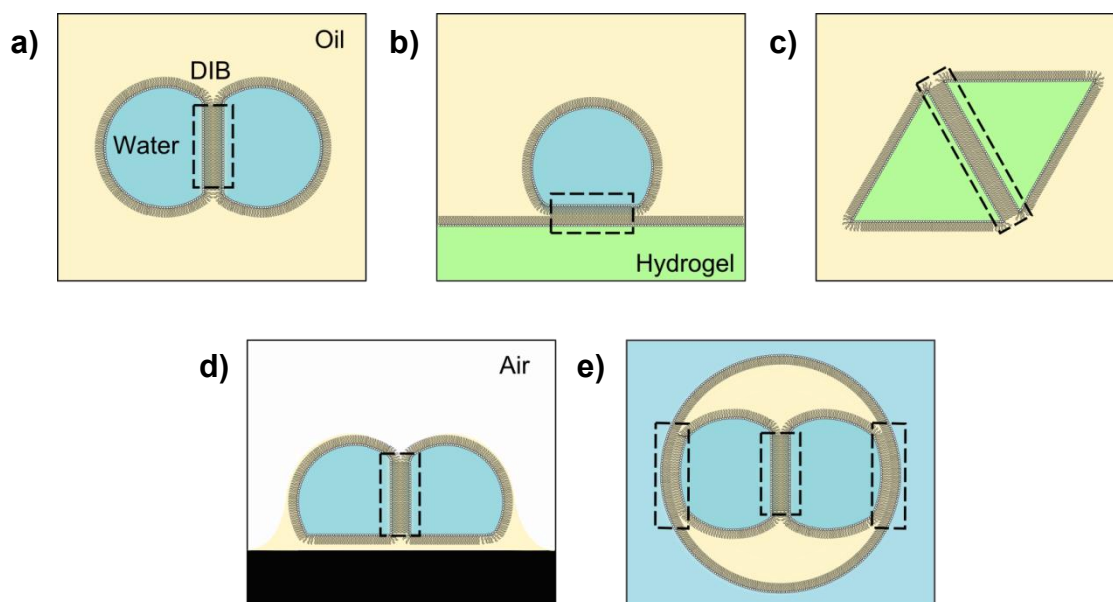
Figure 1.7 Different methods of forming DIBs (DIBs outlined with dotted line box). In all of the incarnations, phospholipid is present in the oil phase. a) DIB formed between two aqueous droplets in oil. b) DIB formed between an aqueous droplet contacting a hydrogel surface, submerged in oil. c) DIB formed between two hydrogel shapes in oil. d) Air-stable DIB formed between two aqueous droplets on a surface coated in oil. e) DIBs formed between two aqueous droplets contained within a droplet of oil in water. DIBs also form between the internal droplets and the external aqueous environment.

Notable benefits of DIBs include their stability, reported to be able to survive indefinitely under conditions that prevent evaporation[92]. They also exhibit a relative ease in incorporating membrane proteins, with a large variety of prokaryotic and eukaryotic proteins reported to have been introduced and studied in DIBs[98-100]. The ability to provide the lipid as vesicles suspended in the aqueous phases allows for the facile production of asymmetric bilayers[101], important for the characterisation of biological membranes that exhibit this property. The use of droplets allows for novel methods to be developed due to their ease of manipulation. For example, the area of DIBs formed from droplets that are anchored on electrodes can be dynamically controlled by moving the electrode[102], and reconstituted membrane proteins can be corralled[103]. DIBs can be formed and reformed indefinitely between many droplets, allowing for automation techniques[104] and multiplexed bilayer formation, which can be employed to give rise to

high-throughput assay platforms[105]. DIBs also lend themselves well to the microfluidic realm for which numerous droplet manipulation techniques exist[104, 106-108] (see section 1.3). For many of these reasons, DIBs have increasingly been used to study membrane proteins[99, 100, 109], model cell membranes[110, 111] and nanopore sensing[112], with some of these applications involving unprecedented, high-throughput bilayer arrays[100, 112].

1.2.4.2.1 DIB Networks

A particular, paradigm-shifting aspect of DIBs is their ability to give rise to networks[75, 113], where DIBs are formed between any number of contacting droplets. This provides a foundation for the use of DIBs as novel devices, and for collective properties to arise and be studied. For example, "biobatteries"[75] and wave rectifiers[114] have been produced from DIBs, which offer the potential to give rise to soft matter electronic components. The use of DIBs as logical gate operators has briefly been explored as well[115].

The network forming properties of DIBs are of particular interest within the field of bottom-up synthetic biology; in its ability to give rise to biologically inspired multi-compartmentalised structures[91]. Pioneering work employing this concept was performed by Gabriel Villar in Bayley´s group, who devised freestanding droplet networks by containing aqueous droplets within a larger oil droplet (Figure 1.8), allowing the formation of DIBs between the aqueous droplets and also between the aqueous droplets and an external, aqueous environment[116]. These structures, termed multisomes, have been manufactured via manual methods using micropipettes and by tethering the oil droplet to a silver wire "frame" in water, to avoid the structure from rising and rupturing at the water/air interface. Thus, work is still required in order to generate robust and freestanding multisomes. Work performed by Elani et al. has

32

taken this concept further by producing multisomes using microfluidic methods, and using them as "cell-like reactors", where ethanolamine in one droplet within the multisome crosses a bilayer into a second, reaction compartment where pyrylium is converted into pyridinium.

Villar et al. also developed droplet printing method which allowed for the creation of DIB network-based "tissue-like materials" (Figure 1.8), formed from thousands of picolitre droplets[117]. This novel material exhibited mechanical properties comparable to soft tissues, such as brain tissue, and was able to give rise to selective conductive paths with use of α-Hemolysin pores and self-assembled morphological changes.
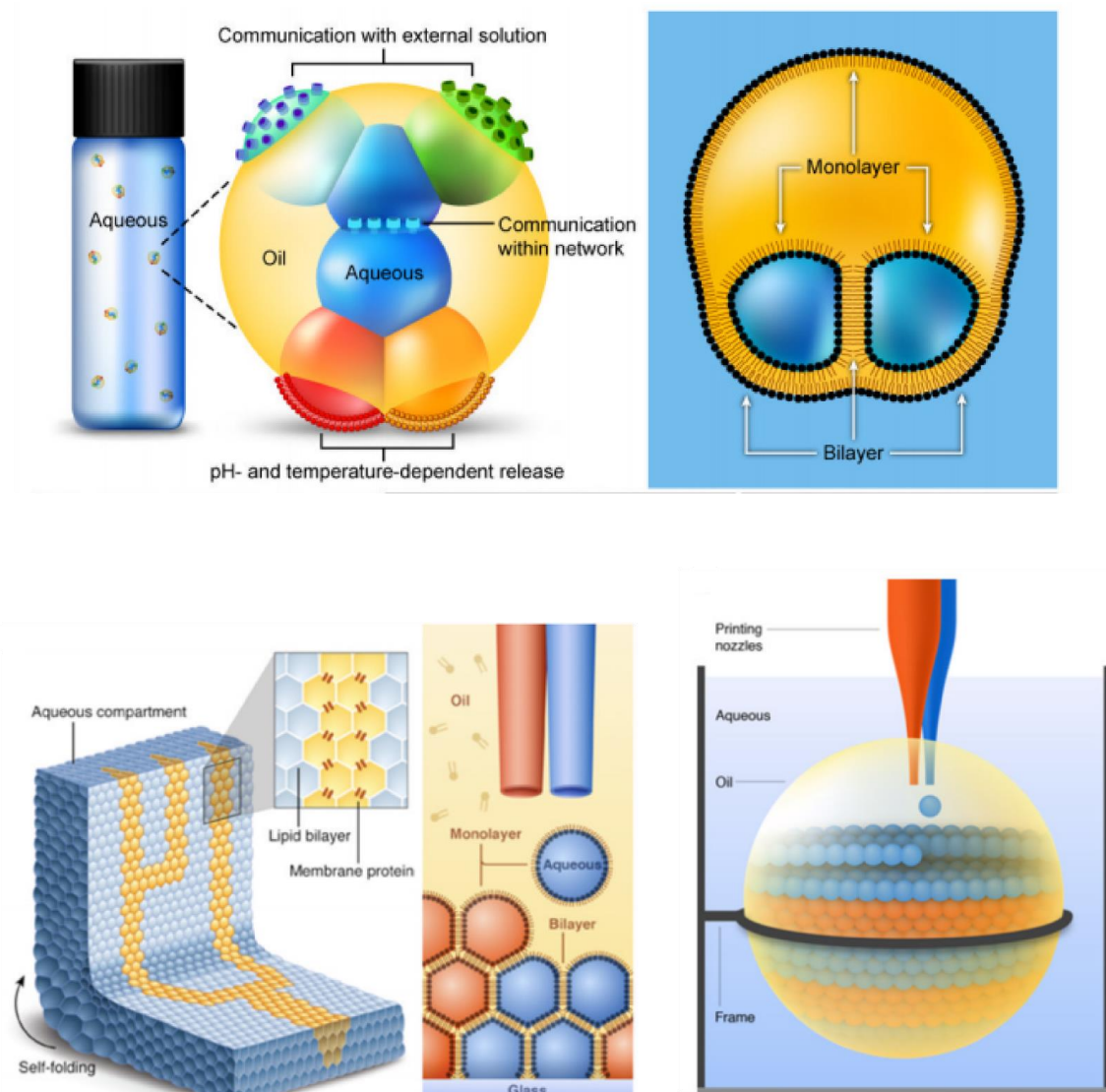
Figure 1.8 Diagrams depicting different two different DIB technologies developed by Dr. Villar in Hagan Bayley´s research group. a) the conception of multisome structures, formed from a number of aqueous droplets contained within a larger droplet of oil in the presence of lipid. Bilayers form between the internal aqueous compartments of the multisome and also between the compartments and the external aqueous environment. b) The development of a droplet printing technology allowing for the formation of tissue-like materials consisting of thousands of picolitre droplets forming a large bilayer network. Images are adapted from referenced publications[116, 117].

1.3 Microfluidics

Microfluidics has been mentioned in previous sections as a technology that is used to produce droplet-based constructs for the generation on lipid bilayer structures, as well as artificial cell systems. This is because microfluidics offers the ability to produce microscale droplets and capsules in large numbers and with excellent control, by exploiting the characteristic behaviour of fluid flow in the microscale[118]. This section will provide a brief overview of the field with emphasis on the mechanisms of droplet generation.

1.3.1 Introduction

Microfluidics concerns the manipulation of fluids in channels and structures in the microscale, which can range in size from from 1 -1000 µm in diameter. Unique fluid flow characteristics emerge as channels decrease in diameter, giving rise to novel liquid handling techniques[119] which are employed in many scientific and consumer technologies.   Along with miniaturisation in itself, microfluidics has found diverse applications within chemical[120], biological[121] and biomedical fields[122] of study. Microfluidic technology has given rise to the concept of Lab-on-a-Chip (LoC)[123] and micro Total Analysis Systems (µTAS)[124], which aim to provide novel laboratory and diagnostic methods that are portable, disposable, or that simplify, automate or increase the throughput of large-scale processes[125]. Aside from the wealth of technological applications that microfluidics offers, it also provides insight into the fundamental physical laws that govern the behaviour of microscopic systems in their environment[126].

1.3.1.1 Advantages

The radically different fluid behaviours that are evident in microscale flows enables the emergence of potential new functionalities, experimental paradigms and. Low reagent volumes and increased surface area to volume ratios are inherent benefits of miniaturisation. Miniaturisation allows for enhanced process parallelization for high-throughput processes and the integration of sequential reactions that would usually involve large or laborious laboratory set-ups[127, 128]. It also allows for portability, which has given rise to novel point-of-care diagnostic devices[129]. High control over physical and chemical properties allow for uniform reaction conditions to obtain high purity products[130]. Efficient heat transfer and a low footprint make microfluidics environmentally friendly[120]. Predictable fluidic environments and integration with microelectromechanical systems (MEMS) enable large-scale multi-process automation[131-133]. The creation of miniature, controlled environments allow for the study of biological cells in unprecedented manners[134]. Furthermore, droplet microfluidics allows for a new liquid handling paradigm and enables further advancements with regards to volume reductions, high-throughput[135] and large surface to volume ratios for interfacial processes[106], via the ability to generate large numbers of highly monodisperse droplets that can act as individual experimental units. One commercially successful example of a droplet microfluidic technology is the development of digital PCR[136]. Droplets can be selectively transported, sorted, fused, split etc.[137], and can embody Boolean logic within fluidic systems[138]. Novel microencapsulation techniques have also emerged from droplet microfluidics, such as the ability to encapsulate individual biological cells[139], or generate hierarchically encapsulated droplets (droplets inside droplets)[140].

1.3.1 Fluid Flow in the Microscale

All organisms, including ourselves, live in some form of liquid or gaseous fluid. The intuitions that we have developed over the course of our lifetimes regarding our interactions with our fluidic environments are subject to a size scale dependency that becomes apparent when examining a radically different scale, such as the microscale. For example, in swimming, we produce a forward force by some form of stroke, in which we cause a turbulent, overall directional movement of fluid around us, propelling us forward even for some time after the stroke has been performed. Due to our relatively large mass, the force we generate with a stroke is large enough to greatly overcome the resistance offered by the fluid around us to being deformed (i.e. viscous forces), giving rise to turbulence and inertia. The way in which we swim would be fundamentally different if we were the size of a microorganism, as we would no longer be able to generate forces that out-compete other inherent forces in the system, such as viscosity and surface tension. This scenario exemplifies how fluid flow changes from the macro to the microscale, due to a relativistic difference in the magnitude of the different forces that govern a given fluidic system.

The Reynolds number describes the ratio of inertial to viscous forces, and can thus be used to predict the scale dependencies of fluid flow depicted in the analogy. As the scale decreases, or as channels become microfluidic channels, viscous forces start to dominate inertial forces[118]. This viscosity is given by the velocity of flow caused by a given shear stress, such as a pressure gradient, and is a measure of the internal friction within the particles that constitute a fluid. Newtonian fluids display a linear relationship profile between shear stress and velocity, whilst the viscosity of Non-Newtonian fluids varies depending on the rate of shear stress applied[141].

The Reynolds number (Re) is given by the following equation:

$$Re = \frac{inertia\ forces}{viscous\ forces} = \frac{\rho v L}{\mu}$$

Where ρ is density (kg m^{-3}), v is velocity (m s^{-1}), L is characteristic length (commonly channel diameter), and μ is dynamic viscosity (N s m^{-2}).

Low Re flows are governed by viscous forces and are described as being laminar, due to a tendency of fluid to flow in layers parallel to the overall direction of flow. Higher Re numbers give rise to turbulent flow, governed by inertial forces (Figure 1.9).

Re < 2000   **Re > 2000**
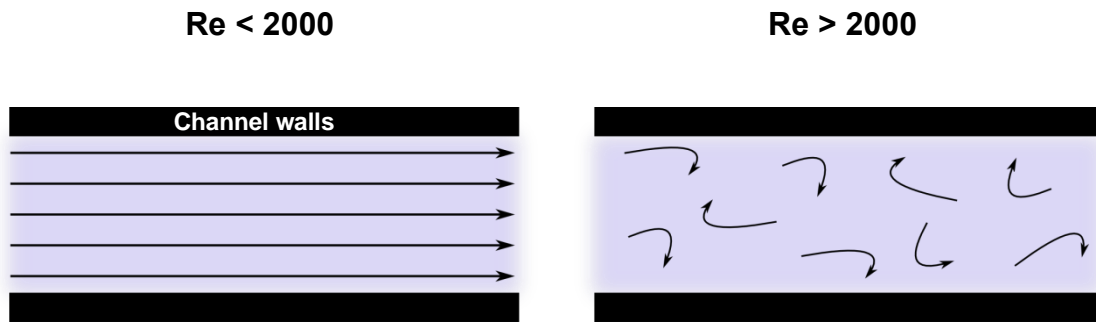
Figure 1.9 Representation of laminar (left) vs. turbulent (right) flow in a situation where a fluid (blue) is flowing in a channel. Flow is represented by arrows. At low Re numbers, fluid flows in parallel layers. As Re increases, flow becomes turbulent and is characterised by a chaotic regime with swirls and eddies.

For a straight channel, a transition from laminar to turbulent typically occurs around Re = 2000 – 2500. From the equation described above, different parameters can be modified in order to attain low Re fluidic flows, including fluid density, viscosity, velocity, and small channel diameters, with the latter being the obvious primary method within microfluidics. Laminar flows have the virtue of being of a more orderly and predictable nature[141], and can be exploited to create concentration gradients[142], efficient reagent technologies[143], and to generate microdroplets[144].

1.3.2.1 Multiphase Microfluidics

Multiphase flow refers to the flow of two (or more) immiscible phases in contact with each other. When two immiscible phases, such as water and oil, flow in the same channel, different fluidic regimes can occur (Figure 1.10).
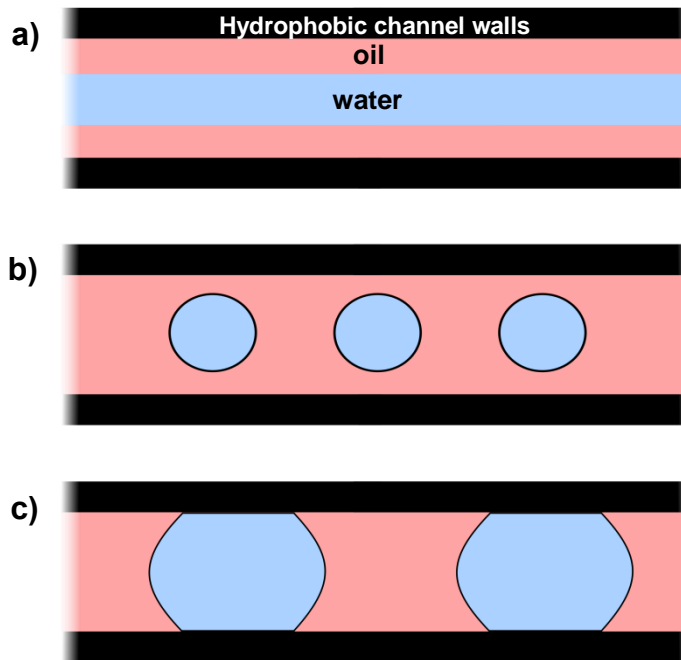
Figure 1.10 Representation of common fluidic conformations in multiphase microfluidics. a) Sub-streaming b) droplets and c) slugs. Red and blue represent different immiscible phases, where the red fluid preferentially wets the channel surfaces (black).

Due to the laminar nature of microfluidics, the fluids may flow in streams parallel to each other. However, this creates a large contact surface area between one fluid and the other, which can be energetically unfavourable. Also, the surface of the channel may preferentially wet one fluid over the other, causing a drive of the non-wetting fluid to minimise its contact with channel walls[145]. Furthermore, viscous instabilities may arise from the flow of one immiscible fluid in another, and pressures may build up when one fluid occludes the channel from another[146]. For all of the above reasons, it is common in the microfluidic scenario described above for one fluid to segment in the other, forming droplets or channel-occluding slugs. The process of droplet formation

can be controlled in order to give rise to the rapid production of monodisperse droplets encouraged by droplet-generating flow geometries[147].

1.3.2.1.1 Physics of droplet formation

In a liquid-liquid multiphase system, droplet formation is governed by the shear force generated from one fluid onto another and the interplay of surface tensions between the fluids and also the channel walls[145]. Surface tension is defined as energy per unit area and is an important driver in the formation of droplets, as it drives a segment of fluid to adopt a spherical shape in order to minimise its surface area to volume ratio. In droplet formation, the wettability of the different fluids with the channel walls will define which of the fluids will form droplets in the other, where the fluid with the highest surface tension with the channel walls forming droplets, and the other fluid constituting a "carrier" phase. For example, hydrophobic channels will produce water in oil (W/O) droplets and not vice versa, to give rise to the most energetically favourable scenario. The interplay of surface tensions can be understood via the measurement of contact angles (figure 1.11), which quantifies the degree at which a liquid wets a solid surface[148]. The angle of a droplet on a surface represents the relative strength of forces between the liquid, solid and the surrounding air. Strategies exist to modify the surface tension between the different fluids, such as the use of surfactants[149], and also to modify the surface energy of the channel walls via surface modification techniques[150, 151] (Section 2.2.1.4).
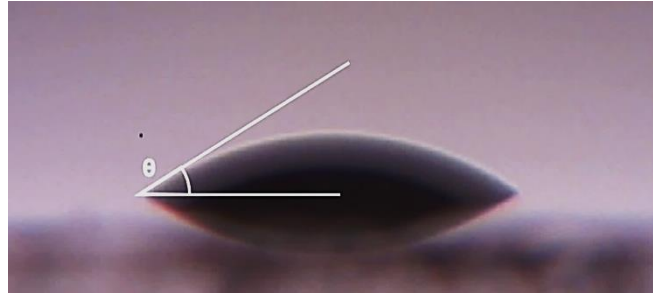
Figure 1.11 Droplet of water on a surface depicting the contact angle between the droplet and the surface. The relatively low angle here indicated a relatively high wettability of the droplet against the surface.

Whilst surface forces encourage the formation of droplets in certain scenarios, viscous forces provide a resistance to fluid deformation required to break a fluid stream into segments. Thus the relative strength between these forces determines the manner in which droplets are formed in a particular droplet-generating scenario. This interplay is described by the Capillary number (Ca), which is given by the following equation:

$$Ca = \frac{viscous\ forces}{surface\ forces} = \frac{\mu v}{\sigma}$$

Where μ is dynamic viscosity (N s m^{-2}), v is velocity (m s^{-1}) and σ is surface tension (N m^{-1}).

The weber number can also be of importance when analysing the formation of droplet formation, and relates to the interplay between fluidic inertia and surface tension along an interface[152]. Although inertia is usually negligible for microfluidic purposes, this can differ for high flow rate values and/or large diameters[153]. It is given by the following equation:

$$We = \frac{inertial\ forces}{surface\ forces} = \frac{\rho v^2 l}{\sigma}$$

Where ρ is density (kg m^{-3}), v is velocity (m s^{-1}), l is characteristic length (typically droplet diameter), and σ is surface tension (N m^{-1}).

1.3.2.1.2 Droplet Coalescence

A dispersion of droplets in an immiscible carrier phase is a thermodynamically unfavourable system due to the total interfacial area between the droplets and the carrier fluid, in comparison to a system where the fluids are separated by a continuous interface. This drives smaller, miscible droplets present in a system to coalesce with each other when in close proximity in order to minimize the total surface area between both fluids, in a mechanism called Ostwald ripening[154]. In a system without any surface-active molecules, the only resistance to coalescence is the thinning and evacuation of the immiscible fluid between one droplet and another, which is affected by the proximity of the droplets and the viscosity of the carrier phase[155]. Therefore, in order to avoid the coalescence of droplets into larger droplets, surfactant molecule solutions are used, which adsorb at immiscible interfaces (i.e. water and oil) due to their amphiphillic structure. Surfactants decrease the surface tension between the fluids which decreases the drive for coalescence, as well as providing electrostatic or steric repulsion between droplet interfaces[149]. This has an overall effect of droplet stabilization, and droplet microfluidics makes extensive use of surfactants for this particular purpose.

1.3.3 Droplet-generating Geometries

In order to generate droplets in multiphase microfluidics, two (or more) immiscible fluids need to be delivered into a common channel. It is at the point where the two fluids meet that droplet formation occurs, often aided by specific channel geometries that encourage monodisperse droplet formation of a desired size or configuration. Here, the T-junction, flow-focusing and coaxial geometries will be described.

1.3.3.1 T-junction

T-junctions comprise two perpendicular channels with one phase flowing in each and delivering fluid into a common channel. Depending on the physical characteristics and flow rates of the fluids, different mechanisms of droplet formation occur, based on the interplay between three forces that act at the droplet/carrier phase junction. These are the surface tension force at the interface, the shear stress caused by the flow of the carrier phase on the droplet phase, and the hydrodynamic resistance the carrier phase flow experiences as the droplet phase interface occludes the channel[147]. The formation of droplets at high Ca numbers is caused by the exertion of shear stress from the carrier phase onto the growing droplet interface at the junction (Figure 1.12a). For lower Ca numbers (≈Ca < 0.1), shear stress alone is unable to deform the growing interface sufficiently to cause droplet formation, due to the relative effect of surface tension. Here, forming droplets obstruct the flow of the carrier phase and cause a build-up of hydrodynamic pressure upstream to the forming droplet, which causes the channel-occluding droplet to break off alleviating the pressure build up (Figure 1.12b). It is likely that the ratio of channel diameters affects this form of droplet formation, especially for low Ca number scenarios, as channel occlusion by the forming droplet will depend on this.

a)   Ca > 0.1

                                                    Ca < 0.1

b)
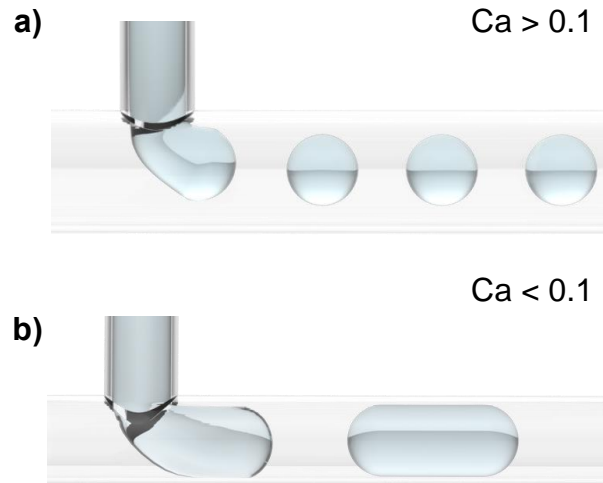
Figure 1.12 Different methods of droplet formation in T-junctions. a) For higher Ca numbers, droplet break-up is governed by the shear stress provided by the continuous phase onto the droplet phase. b) For low Ca numbers, pressure builds up as the forming droplet obstructs the flow of the continuous phase, which causes droplet break-up. Images adapted from Elveflow[156].

1.3.3.3 Flow Focusing Junctions

As the name suggests, flow-focusing geometries involve the focusing of the flow of both the carrier and droplet fluids through a nozzle into a common channel (Figure 1.13). Such geometries are usually symmetric in the radial plane, where the droplet fluid channel flows parallel to the output channel, and is flanked at either side by channels delivering the carrier fluid[157].
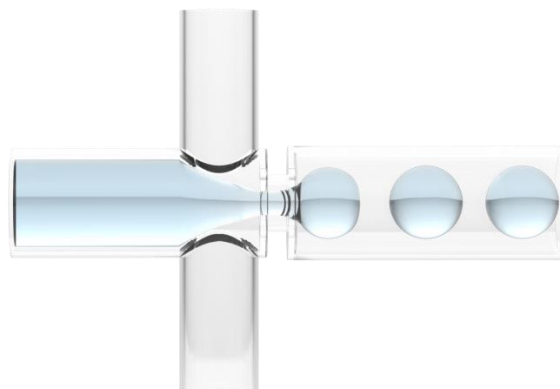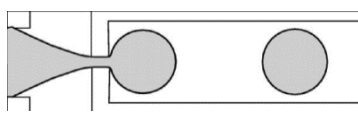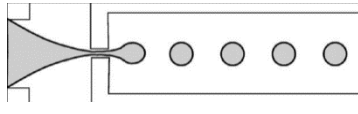
Figure 1.13 Depiction of a flow-focusing junction producing droplets under a dripping regime. Image adapted from Elveflow[156].

The focusing of at least two channels of carrier fluid into a common channel provides shear stress to the growing interface of the droplet fluid as well as a build-up of hydrodynamic pressure as seen in T-junctions, causing droplet break off[158]. The coaxial co-flow of the droplet and carrier phase fluids can also give rise to Plateau-Rayleigh instabilities[159], which arise in elongated cylindrical fluidic interfaces under shear stress and unconstrained flow, and cause droplet break-up[153]. A large diversity exists within flow-focusing geometries, where the carrier fluids can be delivered parallel, perpendicular or diagonal to the droplet phase channel, different ratios of channel diameter can be used, the output channel can be widened after the droplet-forming junction, etc. Flow-focusing geometries give rise to different mechanisms of droplet formation which relate to the interplay of the dominance of viscous or surface forces, and thus can be characterised with the use of the Ca number[153]. These mechanisms are summarised in Table 2.

Name	Depiction	Description
Geometrically-controlled		This regime occurs at low Ca numbers (≈0.1) and is driven by the upstream build-up of hydrodynamic pressure caused by the occluding formation of the droplet. The "finger" of the droplet phase retracts back to the orifice one droplet pinch-off occurs. This method gives rise to droplets that are highly monodisperse and of a diameter roughly equal to the channel.
Dripping		Higher Ca numbers (≈0.2) give rise to this regime where the droplet phase fluid finger of the droplet fluid remains at a fixed location. Here, droplet break-up occurs once the finger is elongated enough to sustain a Plateau-Rayleigh instability. Droplet diameter is less than that of geometrically-controlled droplet break-

		up although remains highly monodisperse.
Jetting		Even higher Ca numbers (≈1) display a jetting mode of droplet formation, where the droplet phase finger elongates beyond the orifice forming an elongated cylinder of fluid, which breaks due to Plateau-Rayleigh instabilities along the jet. The droplets formed tend to be smaller than in dripping regimes and are not considered to be monodisperse.
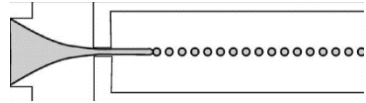
Table 2 Modes of droplet generation seen for microfluidic flow focusing junctions. Diagrams adapted from referenced publication[158].

It is difficult to ascertain the exact Ca numbers at which droplet generation regime changes occur, due to its dependency on a number of factors. For example, the use of surfactants shifts the Ca numbers at which transition occurs upwards, as well as high droplet to carrier phase flow rate ratios[153].

1.3.3.3 Coaxial droplet generation

The droplet-generating configurations described in the previous two sections comprise planar channels, in what is commonly referred to as 2.5D. However, another method of droplet-generation exists which involves the coaxial alignment of tubes and channels in 3D[160]. In this configuration, a tube flowing the droplet phase terminates within a larger tube flowing the dispersed phase, which gives rise to a coaxial geometry where the carrier fluid flow envelopes the flow of the droplet fluid (Figure 1.14). The study of droplet formation at a capillary nozzle predates the emergence of droplet microfluidics as it has been employed in many engineering applications including ink-jet printing, liquid/liquid dispersing and separation applications[160].

Similar to flow-focusing junctions, coaxial droplet generation can give rise to dripping and jetting regimes (Figure 1.14b), where a droplet is formed directly at the tip of the inner tube dominated by surface and hydrodynamic pressure forces, or where they

break up from an extended finger of fluid downstream due to Plateau-Rayleigh instabilities, respectively[161].
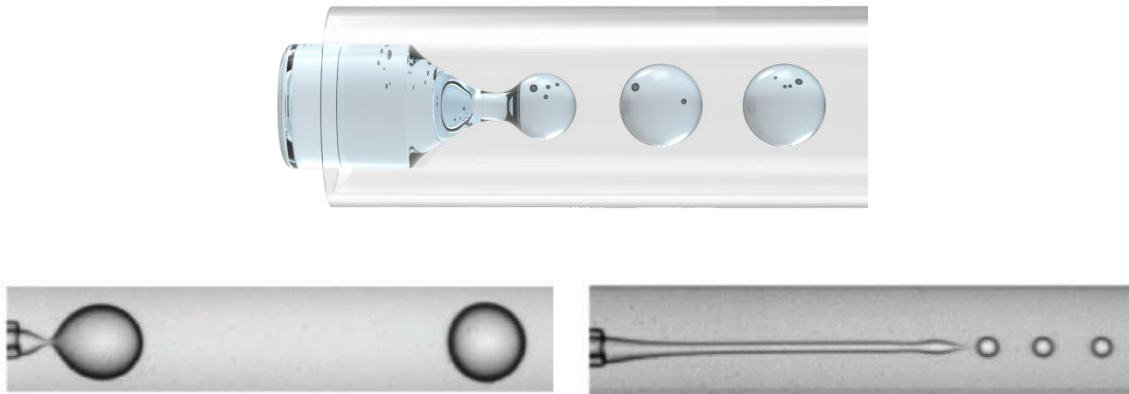
Figure 1.14 Coaxial droplet-generating regimes. a) Depiction of a coaxial droplet generator where a channel flowing the droplet phase is inserted inside a larger channel flowing the carrier phase. Image taken from Elveflow[156]. b) Dripping (left) and jetting (right) regimes of droplet generation in coaxial geometries. Photographs adapted from referenced publication[162].

The transition from dripping to jetting has been found to depend on a number of factors and to occur once the carrier phase velocity surpasses a critical value. Dripping regimes have been found to occur below We numbers of ≈1 and Ca numbers of ≈0.2[162]. The We number is taken into account for coaxial devices and not for flow-focusing devices as the former usually comprises larger channels due to manufacturing constraints, whilst characterisation of the latter tends to ignore the Weber number due to the effect of inertia being negligible at smaller dimensions[147, 153]. Parameters that affect droplet formation include the ratio of channel sizes, the surface energy of channel walls, fluid velocity, flow rate ratio, the use of surfactants and the viscosity, density, and surface energy of the fluids. It is expected that geometrically-controlled droplet generation can occur in coaxial systems when the diameter ratio between the inner and outer tubes is sufficiently low so that the size of the growing droplet is equal or larger than the outer tube diameter.

1.3.4 Complex Emulsions

Complex emulsions refer to fluidic constructs comprised of droplets containing droplets of an immiscible phase. Commonly produced complex emulsions are water-in-oil-in-water (W/O/W) or oil-in-water-in-oil (O/W/O) emulsions. These can be described as double emulsions. Complex emulsions are considered to be metastable constructs[163], as droplets contained within another droplet of an immiscible phase are likely to get ejected in order to minimise contacting surface areas. However, they can maintain their structure for extended periods of time when surfactants are used to stabilise the interfaces.

Although first described in 1924[164], interest in complex emulsions had not garnered much interest until the recent decades. Due to their compartmentalised nature, double emulsions have gained interest for applications in pharmaceuticals[165], foods[166] and cosmetics[167]. Particularly, a number of studies have focused on the potential pharmaceutical use of W/O/W emulsions as targeted delivery systems for water-soluble drugs[168]. Double emulsions have also been regarded as a thin liquid film chemical extraction method, for example for the removal of mercury from waste water[169]. Alternatively, double emulsions can be used as intermediate structures to produce solid capsules via solidification methods[170, 171].

Prior to the development of microfluidic techniques, complex emulsions have been generated in a bulk and heterogeneous manner via the use of valve homogenisers and membranes[172]. One notable example of this was performed by Higashi et al., who used a porous glass membrane to produce W/O/W emulsions composed of epirubicin-containing water droplets within an iodinated poppy seed oil droplet, which preferentially accumulates in hepatocellular carcinoma tumours[173]. Although double emulsions could be generated with a low coefficient of variation in terms of the total emulsion size (below 10%), there was no control over the number or size of

encapsulated droplets using these bulk methods and hence their applicability was limited. Regardless, the prospect of using double emulsions for drug delivery due to their ability to transport and deliver water-soluble substances in a controlled or sustained manner remained enticing[168].

1.3.4.1 Microfluidic production of complex emulsions

Microfluidic methods for complex emulsion generation often involve sequential droplet-generating geometries, but other methods exist which produce complex emulsions in an integrated manner (single-step methods). Surface modification techniques are often employed for the production of complex emulsions due to the common requirement of having to generate droplets of two immiscible phases, which requires the preferential wetting of the channel walls with one phase or another.

1.3.4.1.1 Sequential emulsification

In 2005, Okushima et al. provided the first instance of double emulsion production using microfluidic techniques[174], which harnessed the high degree of control that microfluidics offers in terms of monodisperse droplet generation and droplet manipulation to produce W/O/W emulsions containing a prescribed number of inner droplets as well as containing droplets of different identities (i.e. one containing a red dye and another containing a blue dye). First, droplets of water in oil are created using a T-junction design constructed out of PTFE tubes, comprising the hydrophobic portion of the device. The PTFE tubing is then connected to a glass capillary flowing water in a perpendicular manner, forming a second T-junction (Figure 1.15a). Similar devices fabricated from PDMS have also been produced[175], with some available commercially[176].

Furthermore, Abate et al. found that a similar method could be implemented which not only allows for the production of double emulsions, but for higher order emulsions including triple, quadruple and quintuple emulsions[177], by sequentially aligning flow-focusing droplet-generating geometries in series with alternating channel surface wettabilities (Figure 1.15b). Although these higher order emulsions have not yet found practical applications, their production is a feat in itself, demonstrates the capabilities of microfluidic emulsion generation.

Other implementations of this sequential method have involved the use of coaxial droplet-generating geometries formed from glass capillaries (Figure 1.15c)[178]. Control of droplet size and the number of encapsulated droplets is achieved via the adjustment of the capillary orifice dimensions and flow rates. These devices have also demonstrated to be able to produce further, higher order emulsions, via the sequential alignment of an additional droplet-generating geometry following the generation of double emulsions (W/O/W), producing triple emulsions (W/O/W/O) [179].
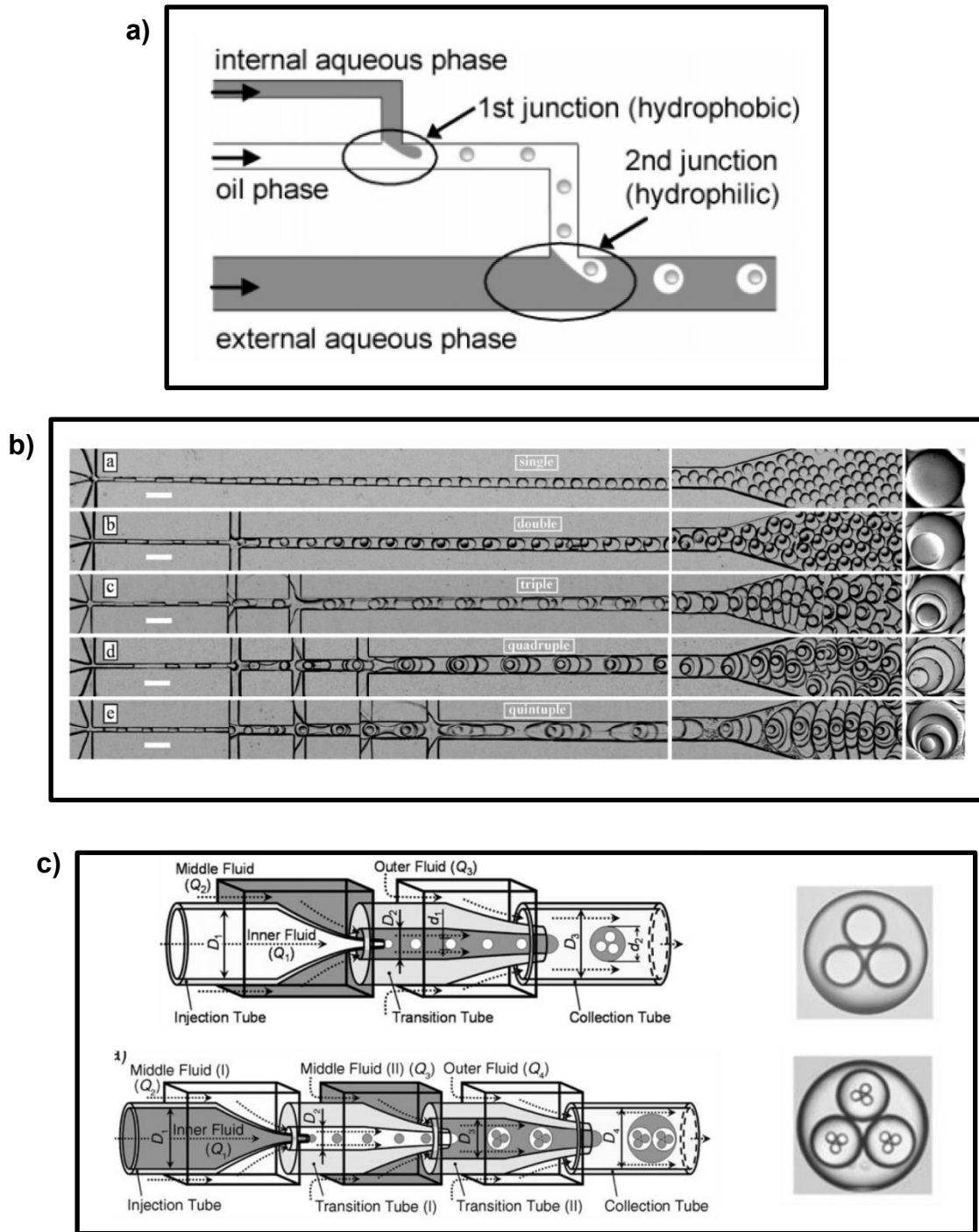
Figure 1.15 Sequential emulsification microfluidic methods for the generation of complex emulsions. a) Droplets of water in oil are generated in a PTFE T-junction, which is connected to a hydrophilic glass capillary flowing water, producing W/O/W emulsions[174]. b) Sequential flow-focussing geometries in PDMS with alternating hydrophobic/hydrophilic wettabilities are employed to generate double, triple, quadruple and quintuple complex emulsions[177]. c) Glass capillaries of alternative hydrophobic/hydrophilic wettabilities are aligned to create coaxial droplet-generating geometries, able to generate W/O/W and W/O/W/O emulsions[179].

1.3.4.1.2 Single-step emulsification

Double emulsions can also be produced in a single step via the specific arrangement of glass capillaries and the tailoring of glass surface wettabilities. One such example is illustrated in Figure 1.16a. This method has demonstrated to produce monodisperse double emulsions with good control over the size and number of droplets produced as well as being able to encapsulate droplets of different solutions via the use of double-bore capillaries[140]. It is noted that the device fabrication is tricky due to the fragile nature of the glass capillaries and the requirement to precisely align the channels with each other and also with the oil/water interface inside the larger glass capillary. Attempts have been made to aid in the device fabrication and alignment of the capillaries via the use of 3D-printed parts[180].
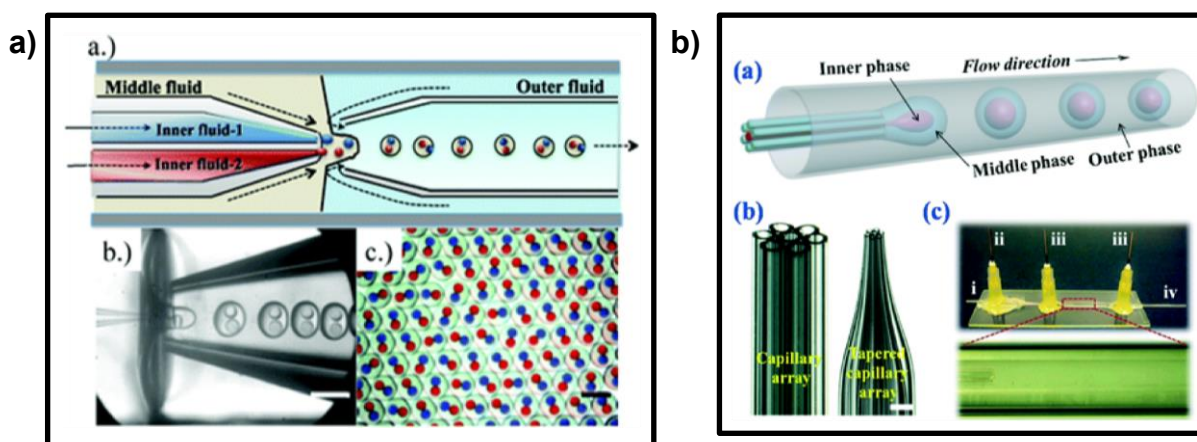
Figure 1.16 Single-step formation of double emulsions. a) A capillary flowing the water droplet phase flows through an oil interface into another capillary, where water flowing around this capillary produces a 3D, flow focusing junction which breaks off W/O/W emulsions[140]. b) Multi-bore glass capillaries generate double emulsions in a coaxial droplet-generating geometry where the outer ring of capillaries flow oil and the inner capillaries flow the water droplet phase[181].

Another single-step method reported uses multi-bore glass capillaries and a coaxial droplet-generating geometry to produce W/O/W emulsions (Figure 1.16b)[181]. The multi-bore capillary is composed of a ring of capillaries flowing the oil phase, surrounding 1-3

capillaries flowing the internal aqueous phase(s). The outer capillary flows the external aqueous phase. Thus, the oil flowing from the multi-bore capillary fuse together, enveloping a number of droplets contained inside, defined by the number of inner capillaries and the flow rates used. Although elegant, this method does not appear to give rise to the same degree of control over droplet size and the number of encapsulated droplets as other methods described here. However, its straightforward device fabrication and operation make it an attractive method to generate double emulsions.

1.3.4.2 Applications

The development of microfluidic methods for the production of complex emulsions revived the interest in them for applications mostly in controlled release systems for pharmaceutical applications[168]. Adams et al. developed double emulsion systems with the ability to encapsulate up to three different aqueous solution droplets within a single oil droplet with control over their number and size, as well as wax-based double emulsion systems which allowed for the temperature-controlled release or coalescence of internal, aqueous cargoes[140]. These developments could be envisaged as a method to deliver a cocktail of drugs, or drug precursors for short-lived drugs into specific areas or tissues within the human body for triggered or sustained release.

W/O/W double emulsions have been employed for the encapsulation of cells[182] and the generation of multicellular spheroids[183]. The use of these double emulsions allows for cells to be encapsulated and a microenvironment to be maintained, which allows for individual cell secretome analysis[184] as well as the maintenance of cell viability[182]. The encapsulation of cells in double emulsions has been proposed as a method for next-generation single-cell screening[184] as well as a vehicle for cell therapies and tissue engineering[182].

Furthermore, double emulsions have been employed in order to generate artificial cells and artificial lipid bilayer systems. For example, Ho et al. developed W/O/W emulsions which were able to sense mechanical disturbances[185] akin to many biological cells, as the compression of the emulsions resulted in the thinning of the oil phase which allowed for the transfer of calcium ions from the aqueous environment around the emulsion to the aqueous droplet within the emulsion. The increased influx of calcium could be envisaged as an artificial cell signalling trigger. Furthermore, Elani et al.[186] generated W/O/W emulsions to create multisomes[116] comprised of aqueous droplets separated by droplet interface bilayers (DIBs), capable of communicating with the external aqueous environment through lipid bilayers. This provided with an important step forward in generating encapsulated DIB structures in a reproducible manner and in large numbers, for their development as artificial cells or compartmentalised chemistry vehicles, for example.

1.4 Thesis aims

The broad aim of this thesis is the production of robust and freestanding droplet interface bilayer networks that are compatible with a range of different environments, and that can be used as a chassis for artificial cells and for high-throughput membrane studies. Droplet microfluidic techniques will be used in order to produce such constructs, as it offers the ability to produce highly monodisperse droplets as well as droplets-within-droplets. Proof-of-concept demonstrations will be performed to assess the performance of such constructs as a high-throughput assay platform to characterise pore-forming molecular species. Additionally, we aim to demonstrate that the constructs can act as artificial cells via their ability to form higher order structures (i.e. artificial tissues) and also via communication with an external environment. All of this aims to widen the scope of applications for droplet interface bilayer networks as well as increase the practicality of their use via a facile, automated manufacture

method and the enhanced stability of the constructs. The project can be divided into the following aims:

1. Development of a microfluidic device that is capable of producing droplets-within-droplets in order to produce droplet interface bilayer networks within an oil droplet, forming bilayers with an external aqueous environment.

2. Encapsulation of droplet interface bilayer networks within a hydrogel shell using microfluidic methods. This ensures that the constructs are robust whilst at the same time able to communicate with their external environment.

3. Demonstration of the formation of lipid bilayers within such constructs via the use of electrophysiological methods and the incorporation of pore-forming membrane proteins.

4. Development of a high-throughput, fluorescence assay capable of assessing the interaction of pore-forming species, such as peptides, on lipid bilayers.

5. Demonstration of the ability of such constructs to form higher-order structures such as artificial tissues, via the tethering of constructs to one another.

1.5 References

1.   A Synthetic Biology Roadmap for the UK - Research Councils UK.
2.   Zhang, J. Y., The art of trans-boundary governance: the case of synthetic biology. *Systems and Synthetic Biology* **2013,** *7* (3), 107-114.
3.   Oecd, *Symposium on Opportunities and Challenges in the Emerging Field of Synthetic Biology Synthesis Report: Synthesis Report.* Royal Society: 2010; p 51.
4.   Khalil, A. S.; Collins, J. J., Synthetic biology: applications come of age. *Nature Reviews Genetics* **2010,** *11* (5), 367-379.
5.   Andrianantoandro, E.; Basu, S.; Karig, D. K.; Weiss, R., Synthetic biology: new engineering rules for an emerging discipline. *Molecular Systems Biology* **2006,** *2* (1), 2006.0028.
6.   d'Espaux, L.; Mendez-Perez, D.; Li, R.; Keasling, J. D., Synthetic biology for microbial production of lipid-based biofuels. *Current Opinion in Chemical Biology* **2015,** *29*, 58-65.
7.   Vogl, T.; Hartner, F. S.; Glieder, A., New opportunities by synthetic biology for biopharmaceutical production in Pichia pastoris. *Current Opinion in Biotechnology* **2013,** *24* (6), 1094-1101.
8.   Paddon, C. J.; Keasling, J. D., Semi-synthetic artemisinin: a model for the use of synthetic biology in pharmaceutical development. *Nature Reviews Microbiology* **2014,** *12* (5), 355-367.
9.   Shetty, R. P.; Endy, D.; Knight, T. F., Engineering BioBrick vectors from BioBrick parts. *Journal of Biological Engineering* **2008,** *2*, 5.
10.   Schwann, T., *Microscopical researches into the accordance in the structure and growth of animals and plants.* Sydenham Society: 1847; p 320.
11.   Pohorille, A.; Deamer, D., Artificial cells: prospects for biotechnology. *Trends in Biotechnology* **2002,** *20* (3), 123-128.
12.   Solé, R. V., Evolution and self-assembly of protocells. *The International Journal of Biochemistry & Cell Biology* **2009,** *41* (2), 274-284.
13.   Mann, S., Life as a nanoscale phenomenon. *Angewandte Chemie (International Ed. in English)* **2008,** *47* (29), 5306-5320.
14.   Boozer, C.; Yu, Q.; Chen, S.; Lee, C.-Y.; Homola, J.; Yee, S. S.; Jiang, S., Surface functionalization for self-referencing surface plasmon resonance (SPR) biosensors by multi-step self-assembly. *Sensors and Actuators B: Chemical* **2003,** *90* (1–3), 22-30.
15.   Miller, S. L.; Schopf, J. W.; Lazcano, A., Oparin's ``Origin of Life'': Sixty Years Later. *Journal of Molecular Evolution* **1997,** *44* (4), 351-353.
16.   Lazcano, A.; Miller, S. L., The Origin and Early Evolution of Life: Prebiotic Chemistry, the Pre-RNA World, and Time. *Cell* **1996,** *85* (6), 793-798.
17.   Xu, C.; Hu, S.; Chen, X., Artificial cells: from basic science to applications. *Materials Today* **2016,** *19* (9), 516-532.
18.   Bedau, M. A.; McCaskill, J. S.; Packard, N. H.; Parke, E. C.; Rasmussen, S. R., Introduction to Recent Developments in Living Technology. *Artificial Life* **2013,** *19* (3_4), 291-298.
19.   Max Planck, G., Synthetic Biology: Life, Remixed.
20.   Stano, P., Advances in Minimal Cell Models: a New Approach to Synthetic Biology and Origin of Life. **2011**.
21.   Gibson, D. G.; Glass, J. I.; Lartigue, C.; Noskov, V. N.; Chuang, R.-Y.; Algire, M. A.; Benders, G. A.; Montague, M. G.; Ma, L.; Moodie, M. M.; Merryman, C.; Vashee, S.; Krishnakumar, R.; Assad-Garcia, N.; Andrews-Pfannkoch, C.; Denisova, E. A.; Young, L.; Qi, Z.-Q.; Segall-Shapiro, T. H.; Calvey, C. H.; Parmar, P. P.; Hutchison, C. A.; Smith, H. O.; Venter, J. C., Creation of a bacterial cell controlled by a chemically synthesized genome. *Science (New York, N.Y.)* **2010,** *329* (5987), 52-56.
22.   Gibson, D. G.; Benders, G. A.; Andrews-Pfannkoch, C.; Denisova, E. A.; Baden-Tillson, H.; Zaveri, J.; Stockwell, T. B.; Brownley, A.; Thomas, D. W.; Algire, M. A.; Merryman, C.; Young, L.; Noskov, V. N.; Glass, J. I.; Venter, J. C.; Hutchison, C. A.; Smith, H. O., Complete chemical synthesis, assembly, and cloning of a Mycoplasma genitalium genome. *Science (New York, N.Y.)* **2008,** *319* (5867), 1215-1220.
23.   Life after the synthetic cell. *Nature* **2010,** *465* (7297), 422-424.

24.   Benner, S. A.; Sismour, A. M., Synthetic biology. *Nature Reviews. Genetics* **2005,** *6* (7), 533-543.

25.   Richard Feynman's blackboard at time of his death | Caltech.

26.   Purnick, P. E. M.; Weiss, R., The second wave of synthetic biology: from modules to systems. *Nature Reviews Molecular Cell Biology* **2009,** *10* (6), 410-422.

27.   Simpson, M. L., Cell-free synthetic biology: a bottom-up approach to discovery by design. *Molecular Systems Biology* **2006,** *2* (1), 69.

28.   Schwille, P., Bottom-Up Synthetic Biology: Engineering in a Tinkerer's World. *Science* **2011,** *333* (6047), 1252-1254.

29.   Elani, Y., Construction of membrane-bound artificial cells using microfluidics: a new frontier in bottom-up synthetic biology. *Biochemical Society Transactions* **2016,** *44* (3), 723-730.

30.   Meng, F.; Engbers, G. H. M.; Feijen, J., Biodegradable polymersomes as a basis for artificial cells: encapsulation, release and targeting. *Journal of Controlled Release* **2005,** *101* (1–3), 187-198.

31.   Chandrawati, R.; Caruso, F., Biomimetic liposome- and polymersome-based multicompartmentalized assemblies. *Langmuir: the ACS journal of surfaces and colloids* **2012,** *28* (39), 13798-13807.

32.   Peters, R. J. R. W.; Marguet, M.; Marais, S.; Fraaije, M. W.; van Hest, J. C. M.; Lecommandoux, S., Cascade Reactions in Multicompartmentalized Polymersomes. *Angewandte Chemie International Edition* **2014,** *53* (1), 146-150.

33.   Tang, T. Y. D.; Hak, C. R. C.; Thompson, A. J.; Kuimova, M. K.; Williams, D. S.; Perriman, A. W.; Mann, S., Fatty acid membrane assembly on coacervate microdroplets as a step towards a hybrid protocell model. *Nature Chemistry* **2014,** *6* (6), 527-533.

34.   Alberts, B.; Johnson, A.; Lewis, J.; Raff, M.; Roberts, K.; Walter, P., The Lipid Bilayer. **2002**.

35.   Chandler, D., Interfaces and the driving force of hydrophobic assembly. *Nature* **2005,** *437* (7059), 640-647.

36.   Funari, S. S.; Mädler, B.; Rapp, G., Cubic topology in surfactant and lipid mixtures. *European Biophysics Journal* **1996,** *24* (5), 293-299.

37.   Seddon, J. M., An inverse face-centered cubic phase formed by diacylglycerol-phosphatidylcholine mixtures. *Biochemistry* **1990,** *29* (34), 7997-8002.

38.   Landau, E. M.; Rosenbusch, J. P., Lipidic cubic phases: A novel concept for the crystallization of membrane proteins. *Proceedings of the National Academy of Sciences* **1996,** *93* (25), 14532-14535.

39.   Shyamsunder, E.; Gruner, S. M.; Tate, M. W.; Turner, D. C.; So, P. T. C.; Tilcock, C. P. S., Observation of inverted cubic phase in hydrated dioleoylphosphatidylethanolamine membranes. *Biochemistry* **1988,** *27* (7), 2332-2336.

40.   G. Mouritsen, O., Lipidology and lipidomics— quo vadis ? A new era for the physical chemistry of lipids. *Physical Chemistry Chemical Physics* **2011,** *13* (43), 19195-19205.

41.   Cullis, P. R.; De Kruijff, B., Lipid polymorphism and the functional roles of lipids in biological membranes. *Biochimica et Biophysica Acta (BBA) - Reviews on Biomembranes* **1979,** *559* (4), 399-420.

42.   Li, X.; Schick, M., Theory of lipid polymorphism: application to phosphatidylethanolamine and phosphatidylserine. *Biophysical Journal* **2000,** *78* (1), 34-46.

43.   Katsaras, J.; Gutberlet, T., *Lipid Bilayers: Structure and Interactions*. Springer Science & Business Media: 2013; p 304.

44.   Sperelakis, N., *Cell Physiology Source Book: Essentials of Membrane Biophysics*. Elsevier: 2012; p 1262.

45.   Lewis, R. A. H.; McElhaney, R., The Mesomorphic Phase Behavior of Lipid Bilayers. In *The Structure of Biological Membranes, Third Edition*, CRC Press: 2011; pp 19-89.

46.   Clark, M. R., Flippin' lipids. *Nature Immunology* **2011,** *12* (5), 373-375.

47.   Nakano, M.; Fukuda, M.; Kudo, T.; Matsuzaki, N.; Azuma, T.; Sekine, K.; Endo, H.; Handa, T., Flip-flop of phospholipids in vesicles: kinetic analysis with time-resolved small-angle neutron scattering. *The Journal of Physical Chemistry. B* **2009,** *113* (19), 6745-6748.

48.   Ces, O.; Mulet, X., Physical coupling between lipids and proteins: a paradigm for cellular control. *Signal Transduction* **2006,** *6* (2), 112-132.

49.   Overton, E., Vierteljahreszeitschrift Naturforsch. *Gesellschaft Zürich* **1899,** *44*, 88-135.

50.   Al-Awqati, Q., One hundred years of membrane permeability: does Overton still rule? *Nature Cell Biology* **1999,** *1* (8), E201-E202.

51.   Grime, J. M. A.; Edwards, M. A.; Unwin, P. R., Reply to Missner et al.: Timescale for passive diffusion across bilayer lipid membranes. *Proceedings of the National Academy of Sciences of the United States of America* **2008,** *105* (52), E124.

52.   Paula, S.; Deamer, D. W., Chapter 4 Membrane Permeability Barriers to Ionic and Polar Solutes. *Current Topics in Membranes* **1999,** *48*, 77-95.

53.   Lodish, H.; Berk, A.; Zipursky, S. L.; Matsudaira, P.; Baltimore, D.; Darnell, J., Diffusion of Small Molecules across Phospholipid Bilayers. **2000**.

54.   Alvarez, O.; Latorre, R., Voltage-dependent capacitance in lipid bilayers made from monolayers. *Biophysical Journal* **1978,** *21* (1), 1-17.

55.   Singer, S. J.; Nicolson, G. L., The fluid mosaic model of the structure of cell membranes. *Science (New York, N.Y.)* **1972,** *175* (4023), 720-731.

56.   Lodish, H.; Berk, A.; Zipursky, S. L.; Matsudaira, P.; Baltimore, D.; Darnell, J., Membrane Proteins. **2000**.

57.   van Meer, G.; Voelker, D. R.; Feigenson, G. W., Membrane lipids: where they are and how they behave. *Nature Reviews. Molecular Cell Biology* **2008,** *9* (2), 112-124.

58.   Fadeel, B.; Xue, D., The ins and outs of phospholipid asymmetry in the plasma membrane: roles in health and disease. *Critical reviews in biochemistry and molecular biology* **2009,** *44* (5), 264-277.

59.   Haynie, D. T., *Biological Thermodynamics*. Cambridge University Press: 2008; p 369.

60.   Simons, K.; Toomre, D., Lipid rafts and signal transduction. *Nature Reviews. Molecular Cell Biology* **2000,** *1* (1), 31-39.

61.   Pike, L. J., Lipid rafts bringing order to chaos. *Journal of Lipid Research* **2003,** *44* (4), 655-667.

62.   Munro, S., Lipid rafts: elusive or illusive? *Cell* **2003,** *115* (4), 377-388.

63.   Tan, S.; Tan, H. T.; Chung, M. C. M., Membrane proteins and membrane proteomics. *Proteomics* **2008,** *8* (19), 3924-3932.

64.   Wiseman, G. M., The hemolysins of Staphylococcus aureus. *Bacteriological Reviews* **1975,** *39* (4), 317-344.

65.   Krasilnikov, O. V.; Merzlyak, P. G.; Yuldasheva, L. N.; Rodrigues, C. G.; Bhakdi, S.; Valeva, A., Electrophysiological evidence for heptameric stoichiometry of ion channels formed by Staphylococcus aureus alpha-toxin in planar lipid bilayers. *Molecular Microbiology* **2000,** *37* (6), 1372-1378.

66.   Terstappen, G. C.; Reggiani, A., In silico research in drug discovery. *Trends in Pharmacological Sciences* **2001,** *22* (1), 23-26.

67.   Regenmortel, M. H. V. V., Reductionism and complexity in molecular biology. *EMBO Reports* **2004,** *5* (11), 1016-1020.

68.   Haverkamp, W.; Breithardt, G.; Camm, A. J.; Janse, M. J.; Rosen, M. R.; Antzelevitch, C.; Escande, D.; Franz, M.; Malik, M.; Moss, A.; Shah, R., The potential for QT prolongation and pro-arrhythmia by non-anti-arrhythmic drugs: clinical and regulatory implications. Report on a Policy Conference of the European Society of Cardiology. *Cardiovascular Research* **2000,** *47* (2), 219-233.

69.   Jesorka, A.; Orwar, O., Liposomes: technologies and analytical applications. *Annual Review of Analytical Chemistry (Palo Alto, Calif.)* **2008,** *1*, 801-832.

70.   Noireaux, V.; Libchaber, A., A vesicle bioreactor as a step toward an artificial cell assembly. *Proceedings of the National Academy of Sciences of the United States of America* **2004,** *101* (51), 17669-17674.

71.   Baxani, D. K.; Morgan, A. J. L.; Jamieson, W. D.; Allender, C. J.; Barrow, D. A.; Castell, O. K., Bilayer Networks within a Hydrogel Shell: A Robust Chassis for Artificial Cells and a Platform for Membrane Studies. *Angewandte Chemie International Edition* **2016,** *55* (46), 14240-14245.

72.   Montal, M.; Mueller, P., Formation of Bimolecular Membranes from Lipid Monolayers and a Study of Their Electrical Properties. *Proceedings of the National Academy of Sciences of the United States of America* **1972,** *69* (12), 3561-3566.

73.   Kalb, E.; Frey, S.; Tamm, L. K., Formation of supported planar bilayers by fusion of vesicles to supported phospholipid monolayers. *Biochimica Et Biophysica Acta* **1992,** *1103* (2), 307-316.

74.   F Szoka, Jr.; Papahadjopoulos, a. D., Comparative Properties and Methods of Preparation of Lipid Vesicles (Liposomes). *Annual Review of Biophysics and Bioengineering* **1980,** *9* (1), 467-508.

75.   Bayley, H.; Cronin, B.; Heron, A.; Holden, M. A.; Hwang, W.; Syeda, R.; Thompson, J.; Wallace, M., Droplet interface bilayers. *Molecular bioSystems* **2008,** *4* (12), 1191-1208.

76.   Matosevic, S.; Paegel, B. M., Stepwise Synthesis of Giant Unilamellar Vesicles on a Microfluidic Assembly Line. *Journal of the American Chemical Society* **2011,** *133* (9), 2798-2800.

77.   Stano, P.; Carrara, P.; Kuruma, Y.; Souza, T. P. d.; Luisi, P. L., Compartmentalized reactions as a case of soft-matter biotechnology: synthesis of proteins and nucleic acids inside lipid vesicles. *Journal of Materials Chemistry* **2011,** *21* (47), 18887-18902.

78.   Boiteau, L., *Prebiotic Chemistry: From Simple Amphiphiles to Protocell Models*. Springer Science & Business Media: 2005; p 248.

79.   Zhu, T. F.; Szostak, J. W., Coupled growth and division of model protocell membranes. *Journal of the American Chemical Society* **2009,** *131* (15), 5705-5713.

80.   Benachir, T.; Lafleur, M., Study of vesicle leakage induced by melittin. *Biochimica et Biophysica Acta (BBA) - Biomembranes* **1995,** *1235* (2), 452-460.

81.   van der Meel, R.; Fens, M. H. A. M.; Vader, P.; van Solinge, W. W.; Eniola-Adefeso, O.; Schiffelers, R. M., Extracellular vesicles as drug delivery systems: Lessons from the liposome field. *Journal of Controlled Release* **2014,** *195*, 72-85.

82.   Chen, I. A.; Walde, P., From Self-Assembled Vesicles to Protocells. *Cold Spring Harbor Perspectives in Biology* **2010,** *2* (7).

83.   Blain, J. C.; Szostak, J. W., Progress Toward Synthetic Cells. *Annual review of biochemistry* **2014,** *83*, 615-640.

84.   Walde, P.; Wick, R.; Fresta, M.; Mangone, A.; Luisi, P. L., Autopoietic Self-Reproduction of Fatty Acid Vesicles. *Journal of the American Chemical Society* **1994,** *116* (26), 11649-11654.

85.   Chen, I. A.; Szostak, J. W., A kinetic study of the growth of fatty acid vesicles. *Biophysical Journal* **2004,** *87* (2), 988-998.

86.   Kurihara, K.; Tamura, M.; Shohda, K.-I.; Toyota, T.; Suzuki, K.; Sugawara, T., Self-reproduction of supramolecular giant vesicles combined with the amplification of encapsulated DNA. *Nature Chemistry* **2011,** *3* (10), 775-781.

87.   Tan, C.; Saurabh, S.; Bruchez, M.; Schwartz, R.; LeDuc, P., Molecular crowding shapes gene expression in synthetic cellular nanosystems. *Nature nanotechnology* **2013,** *8* (8), 602-608.

88.   Gardner, P. M.; Winzer, K.; Davis, B. G., Sugar synthesis in a protocellular model leads to a cell signalling response in bacteria. *Nature Chemistry* **2009,** *1* (5), 377-383.

89.   Elani, Y.; Gee, A.; Law, R. V.; Ces, O., Engineering multi-compartment vesicle networks. *Chemical Science* **2013,** *4* (8), 3332-3338.

90.   Elani, Y.; Law, R. V.; Ces, O., Vesicle-based artificial cells as chemical microreactors with spatially segregated reaction pathways. *Nature Communications* **2014,** *5*, 5305.

91.   Elani, Y.; V. Law, R.; Ces, O., Protein synthesis in artificial cells: using compartmentalisation for spatial organisation in vesicle bioreactors. *Physical Chemistry Chemical Physics* **2015,** *17* (24), 15534-15537.

92.   Leptihn, S.; Castell, O. K.; Cronin, B.; Lee, E.-H.; Gross, L. C. M.; Marshall, D. P.; Thompson, J. R.; Holden, M.; Wallace, M. I., Constructing droplet interface bilayers from the contact of aqueous droplets in oil. *Nature Protocols* **2013,** *8* (6), 1048-1057.

93.   Funakoshi, K.; Suzuki, H.; Takeuchi, S., Lipid Bilayer Formation by Contacting Monolayers in a Microfluidic Device for Membrane Protein Analysis. *Analytical Chemistry* **2006,** *78* (24), 8169-8174.

94.   Sapra, K. T.; Bayley, H., Lipid-coated hydrogel shapes as components of electrical circuits and mechanical devices. *Scientific Reports* **2012,** *2*, 848.

95.   Boreyko, J. B.; Polizos, G.; Datskos, P. G.; Sarles, S. A.; Collier, C. P., Air-stable droplet interface bilayers on oil-infused surfaces. *Proceedings of the National Academy of Sciences* **2014**, 201400381.

96.   Sarles, S. A.; Stiltner, L. J.; Williams, C. B.; Leo, D. J., Bilayer formation between lipid-encased hydrogels contained in solid substrates. *ACS applied materials & interfaces* **2010,** *2* (12), 3654-3663.

97.   Sarles, S. A.; Leo, D. J., Physical encapsulation of droplet interface bilayers for durable, portable biomolecular networks. *Lab on a Chip* **2010,** *10* (6), 710-717.

98.   Leptihn, S.; Thompson, J. R.; Ellory, J. C.; Tucker, S. J.; Wallace, M. I., In vitro reconstitution of eukaryotic ion channels using droplet interface bilayers. *Journal of the American Chemical Society* **2011,** *133* (24), 9370-9375.

99.	Barriga, H. M. G.; Booth, P.; Haylock, S.; Bazin, R.; Templer, R. H.; Ces, O., Droplet interface bilayer reconstitution and activity measurement of the mechanosensitive channel of large conductance from Escherichia coli. *Journal of the Royal Society, Interface / the Royal Society* **2014,** *11* (98), 20140404.

100.	Castell, O. K.; Berridge, J.; Wallace, M. I., Quantification of Membrane Protein Inhibition by Optical Ion Flux in a Droplet Interface Bilayer Array. *Angewandte Chemie International Edition* **2012,** *51* (13), 3134-3138.

101.	Hwang, W. L.; Chen, M.; Cronin, B.; Holden, M. A.; Bayley, H., Asymmetric Droplet Interface Bilayers. *Journal of the American Chemical Society* **2008,** *130* (18), 5878-5879.

102.	Gross, L. C. M.; Heron, A. J.; Baca, S. C.; Wallace, M. I., Determining Membrane Capacitance by Dynamic Control of Droplet Interface Bilayer Area. *Langmuir* **2011,** *27* (23), 14335-14342.

103.	Gross, L. C. M.; Castell, O. K.; Wallace, M. I., Dynamic and Reversible Control of 2D Membrane Protein Concentration in a Droplet Interface Bilayer. *Nano Letters* **2011,** *11* (8), 3324-3328.

104.	Barlow, N. E.; Bolognesi, G.; Flemming, A. J.; Brooks, N. J.; Barter, L. M. C.; Ces, O., Multiplexed droplet Interface bilayer formation. *Lab on a Chip* **2016,** *16* (24), 4653-4657.

105.	Syeda, R.; Holden, M. A.; Hwang, W. L.; Bayley, H., Screening Blockers Against a Potassium Channel with a Droplet Interface Bilayer Array. *Journal of the American Chemical Society* **2008,** *130* (46), 15543-15548.

106.	Stanley, C. E.; Elvira, K. S.; Niu, X. Z.; Gee, A. D.; Ces, O.; Edel, J. B.; Demello, A. J., A microfluidic approach for high-throughput droplet interface bilayer (DIB) formation. *Chemical Communications (Cambridge, England)* **2010,** *46* (10), 1620-1622.

107.	A microfluidic platform for size-dependent generation of droplet interface bilayer networks on rails. *Biomicrofluidics* **2015,** *9* (6), 064121.

108.	Schlicht, B.; Zagnoni, M., Droplet-interface-bilayer assays in microfluidic passive networks. *Scientific Reports* **2015,** *5*.

109.	Taylor, G. J.; Sarles, S. A. In *Model Neural Membrane Droplet Interface Bilayers from Brain Total Lipid Extract for Studying Membrane-Peptide Interactions with Amyloid-β*, 2015; 2015.

110.	Tamaddoni, N.; Sarles, S. A., Toward cell-inspired materials that feel: measurements and modeling of mechanotransduction in droplet-based, multi-membrane arrays. *Bioinspiration & Biomimetics* **2016,** *11* (3), 036008.

111.	Barlow, N. E.; Smpokou, E.; Friddin, M. S.; Macey, R.; Gould, I. R.; Turnbull, C.; Flemming, A. J.; Brooks, N. J.; Ces, O.; Barter, L. M. C., Engineering plant membranes using droplet interface bilayers. *Biomicrofluidics* **2017,** *11* (2), 024107.

112.	Huang, S.; Romero-Ruiz, M.; Castell, O. K.; Bayley, H.; Wallace, M. I., High-throughput optical sensing of nucleic acids in a nanopore array. *Nature Nanotechnology* **2015,** *10* (11), 986-991.

113.	Holden, M. A.; Needham, D.; Bayley, H., Functional Bionetworks from Nanoliter Water Droplets. *Journal of the American Chemical Society* **2007,** *129* (27), 8650-8655.

114.	Maglia, G.; Heron, A. J.; Hwang, W. L.; Holden, M. A.; Mikhailova, E.; Li, Q.; Cheley, S.; Bayley, H., Droplet networks with incorporated protein diodes show collective properties. *Nature Nanotechnology* **2009,** *4* (7), 437-440.

115.	Yasuga, H.; Kawano, R.; Takinoue, M.; Tsuji, Y.; Osaki, T.; Kamiya, K.; Miki, N.; Takeuchi, S. In *Droplet-box*, 17th International Conference on Miniaturized Systems for Chemistry and Life Sciences, MicroTAS 2013, 2013; 2013.

116.	Villar, G.; Heron, A. J.; Bayley, H., Formation of droplet networks that function in aqueous environments. *Nature Nanotechnology* **2011,** *6* (12), 803-808.

117.	Villar, G.; Graham, A. D.; Bayley, H., A Tissue-Like Printed Material. *Science (New York, N.Y.)* **2013,** *340* (6128), 48-52.

118.	Reynolds, O., An Experimental Investigation of the Circumstances Which Determine Whether the Motion of Water Shall Be Direct or Sinuous, and of the Law of Resistance in Parallel Channels. *Philosophical Transactions of the Royal Society of London* **1883,** *174*, 935-982.

119.	Solvas, X. C. i.; deMello, A., Droplet microfluidics: recent developments and future applications. *Chemical Communications* **2011,** *47* (7), 1936-1942.

120.   Elvira, K. S.; i Solvas, X. C.; Wootton, R. C. R.; deMello, A. J., The past, present and potential for microfluidic reactor technology in chemical synthesis. *Nature Chemistry* **2013,** *5* (11), 905-915.

121.   David, J. B.; Glennys, A. M.; Walker, a. G. M., Physics and Applications of Microfluidics in Biology. *Annual Review of Biomedical Engineering* **2002,** *4* (1), 261-286.

122.   Fujii, T., PDMS-based microfluidic devices for biomedical applications. *Microelectronic Engineering* **2002,** *61–62*, 907-914.

123.   Herold, K. E.; Rasooly, A., *Lab on a Chip Technology: Fabrication and microfluidics*. Horizon Scientific Press: 2009; p 425.

124.   Manz, A.; Graber, N.; Widmer, H. M., Miniaturized total chemical analysis systems: A novel concept for chemical sensing. *Sensors and Actuators B: Chemical* **1990,** *1* (1), 244-248.

125.   Yeo, L. Y.; Chang, H.-C.; Chan, P. P. Y.; Friend, J. R., Microfluidic devices for bioapplications. *Small (Weinheim an Der Bergstrasse, Germany)* **2011,** *7* (1), 12-48.

126.   Binz, M.; Lee, A. P.; Edwards, C.; Nicolau, D. V., Motility of bacteria in microfluidic structures. *Microelectronic Engineering* **2010,** *87* (5–8), 810-813.

127.   Gómez-Sjöberg, R.; Leyrat, A. A.; Pirone, D. M.; Chen, C. S.; Quake, S. R., Versatile, Fully Automated, Microfluidic Cell Culture System. *Analytical Chemistry* **2007,** *79* (22), 8557-8563.

128.   Melin, J.; Quake, S. R., Microfluidic Large-Scale Integration: The Evolution of Design Rules for Biological Automation. *http://dx.doi.org/10.1146/annurev.biophys.36.040306.132646* **2007**.

129.   Chin, C. D.; Laksanasopin, T.; Cheung, Y. K.; Steinmiller, D.; Linder, V.; Parsa, H.; Wang, J.; Moore, H.; Rouse, R.; Umviligihozo, G.; Karita, E.; Mwambarangwe, L.; Braunstein, S. L.; van de Wijgert, J.; Sahabo, R.; Justman, J. E.; El-Sadr, W.; Sia, S. K., Microfluidics-based diagnostics of infectious diseases in the developing world. *Nature Medicine* **2011,** *17* (8), 1015-1019.

130.   Chip in a lab: Microfluidics for next generation life science research. *Biomicrofluidics* **2013,** *7* (1), 011302.

131.   Hughes, A. J.; Lin, R. K. C.; Peehl, D. M.; Herr, A. E., Microfluidic integration for automated targeted proteomic assays. *Proceedings of the National Academy of Sciences* **2012,** *109* (16), 5972-5977.

132.   Kim, S.; De Jonghe, J.; Kulesa, A. B.; Feldman, D.; Vatanen, T.; Bhattacharyya, R. P.; Berdy, B.; Gomez, J.; Nolan, J.; Epstein, S.; Blainey, P. C., High-throughput automated microfluidic sample preparation for accurate microbial genomics. *Nature Communications* **2017,** *8.*

133.   Njoroge, S. K.; Chen, H.-W.; Witek, M. A.; Soper, S. A., Integrated microfluidic systems for DNA analysis. *Topics in Current Chemistry* **2011,** *304*, 203-260.

134.   Lee, P.; Chen, C. S. Y.; Gaige, T.; Hung, P. J., Automated live cell imaging of cell migration across a microfluidic-controlled chemoattractant gradient. *Nature Methods* **2015,** *12* (11).

135.   Wootton, R. C. R.; deMello, A. J., Microfluidics: Analog-to-digital drug screening. *Nature* **2012,** *483* (7387), 43-44.

136.   Baker, M., Digital PCR hits its stride. *Nature Methods* **2012,** *9* (6), 541-544.

137.   Niu, X.; deMello, A. J., Building droplet-based microfluidic systems for biological analysis. *Biochemical Society Transactions* **2012,** *40* (4), 615-623.

138.   Katsikis, G.; Cybulski, J. S.; Prakash, M., Synchronous universal droplet logic and control. *Nature Physics* **2015,** *11* (7), 588-596.

139.   Lagus, T. P.; Edd, J. F., High Throughput Single-cell and Multiple-cell Micro-encapsulation. *Journal of Visualized Experiments : JoVE* **2012,** (64).

140.   Adams, L. L. A.; Kodger, T. E.; Kim, S.-H.; Shum, H. C.; Franke, T.; Weitz, D. A., Single step emulsification for the generation of multi-component double emulsions. *Soft Matter* **2012,** *8* (41), 10719-10724.

141.   Ong, S.-E.; Zhang, S.; Du, H.; Fu, Y., Fundamental principles and applications of microfluidic systems. *Frontiers in Bioscience: A Journal and Virtual Library* **2008,** *13*, 2757-2773.

142.   Kim, S.; Joon Kim, H.; Li Jeon, N., Biological applications of microfluidic gradient devices. *Integrative Biology* **2010,** *2* (11-12), 584-603.

143.   Weigl, B. H.; Yager, P., Microfluidic Diffusion-Based Separation and Detection. *Science* **1999,** *283* (5400), 346-347.

144.   Teh, S.-Y.; Lin, R.; Hung, L.-H.; Lee, A. P., Droplet microfluidics. *Lab on a Chip* **2008,** *8* (2), 198-220.

145.   Günther, A.; Jensen, K. F., Multiphase microfluidics: from flow characteristics to chemical and materials synthesis. *Lab on a Chip* **2006,** *6* (12), 1487-1503.

146.   Garstecki, P.; Stone, H. A.; Whitesides, G. M., Mechanism for Flow-Rate Controlled Breakup in Confined Geometries: A Route to Monodisperse Emulsions. *Physical Review Letters* **2005,** *94* (16), 164501.

147.   Garstecki, P.; Fuerstman, M. J.; Stone, H. A.; Whitesides, G. M., Formation of droplets and bubbles in a microfluidic T-junction—scaling and mechanism of break-up. *Lab on a Chip* **2006,** *6* (3), 437-446.

148.   Cassie, A. B. D., Contact angles. *Discussions of the Faraday Society* **1948,** *3* (0), 11-16.

149.   Rosen, M. J.; Kunjappu, J. T., *Surfactants and Interfacial Phenomena*. John Wiley & Sons: 2012; p 618.

150.   Soper, S. A.; Henry, A. C.; Vaidya, B.; Galloway, M.; Wabuyele, M.; McCarley, R. L., Surface modification of polymer-based microfluidic devices. *Analytica Chimica Acta* **2002,** *470* (1), 87-99.

151.   Zhou, J.; Khodakov, D. A.; Ellis, A. V.; Voelcker, N. H., Surface modification for PDMS-based microfluidic devices. *Electrophoresis* **2012,** *33* (1), 89-104.

152.   Christopher, G. F.; Anna, S. L., Microfluidic methods for generating continuous droplet streams. *Journal of Physics D: Applied Physics* **2007,** *40* (19), R319.

153.   Microscale tipstreaming in a microfluidic flow focusing device. *Physics of Fluids* **2006,** *18* (12), 121512.

154.   Schramm, L. L., *Emulsions, Foams, and Suspensions: Fundamentals and Applications*. John Wiley & Sons: 2006; p 466.

155.   Riechers, B.; Maes, F.; Akoury, E.; Semin, B.; Gruner, P.; Baret, J.-C., Surfactant adsorption kinetics in microfluidics. *Proceedings of the National Academy of Sciences* **2016,** *113* (41), 11465-11470.

156.   Elveflow, Elveflow Plug and Play microfluidics. *Elveflow*.

157.   Anna, S.; Bontoux, N.; Stone, H., Formation of dispersions using ``flow focusing'' in microchannels. *Applied Physics Letters* **2003,** *82* (3), 364-366.

158.   Sullivan, M. T.; Stone, H. A., The role of feedback in microfluidic flow-focusing devices. *Philosophical Transactions of the Royal Society of London A: Mathematical, Physical and Engineering Sciences* **2008,** *366* (1873), 2131-2143.

159.   Rayleigh, L., On The Instability Of Jets. *Proceedings of the London Mathematical Society* **1878,** *s1-10* (1), 4-13.

160.   Cramer, C.; Fischer, P.; Windhab, E. J., Drop formation in a co-flowing ambient fluid. *Chemical Engineering Science* **2004,** *59* (15), 3045-3058.

161.   The generation of highly monodisperse droplets through the breakup of hydrodynamically focused microthread in a microfluidic device. *Applied Physics Letters* **2004,** *85* (17), 3726-3728.

162.   Utada, A. S.; Fernandez-Nieves, A.; Stone, H. A.; Weitz, D. A., Dripping to Jetting Transitions in Coflowing Liquid Streams. *Physical Review Letters* **2007,** *99* (9), 094502.

163.   Ficheux, M. F.; Bonakdar, L.; Leal-Calderon, F.; Bibette, J., Some Stability Criteria for Double Emulsions. *Langmuir* **1998,** *14* (10), 2702-2706.

164.   Seifriz, W., Studies in Emulsions. III-V. *The Journal of Physical Chemistry* **1924,** *29* (6), 738-749.

165.   Davis, S. S.; Walker, I. M., Multiple emulsions as targetable delivery systems. *Methods in Enzymology* **1987,** *149*, 51-64.

166.   Matsumoto, S., W/O/W-Type Multiple Emulsions with a View to Possible Food Applications1. *Journal of Texture Studies* **1986,** *17* (2), 141-159.

167.   Yoshida, K.; Sekine, T.; Matsuzaki, F.; Yanaki, T.; Yamaguchi, M., Stability of vitamin A in oil-in-water-in-oil-type multiple emulsions. *Journal of the American Oil Chemists' Society* **1999,** *76* (2), 1-6.

168.   Garti, N.; Bisperink, C., Double emulsions: Progress and applications. *Current Opinion in Colloid & Interface Science* **1998,** *3* (6), 657-667.

169.   Boyadzhiev, L.; Bezenshek, E., Carrier mediated extraction: application of double emulsion technique for mercury removal from waste water. *Journal of Membrane Science* **1983,** *14* (1), 13-18.

170.   Ren, P.-W.; Ju, X.-J.; Xie, R.; Chu, L.-Y., Monodisperse alginate microcapsules with oil core generated from a microfluidic device. *Journal of Colloid and Interface Science* **2010,** *343* (1), 392-395.
171.   Lee, T. Y.; Choi, T. M.; Shim, T. S.; Frijns, R. A. M.; Kim, S.-H., Microfluidic production of multiple emulsions and functional microcapsules. *Lab on a Chip* **2016,** *16* (18), 3415-3440.
172.   Garti, N., Double emulsions — scope, limitations and new achievements. *Colloids and Surfaces A: Physicochemical and Engineering Aspects* **1997,** *123–124*, 233-246.
173.   Higashi, S.; Setoguchi, T., Hepatic arterial injection chemotherapy for hepatocellular carcinoma with epirubicin aqueous solution as numerous vesicles in iodinated poppy-seed oil microdroplets: clinical application of water-in-oil-in-water emulsion prepared using a membrane emulsification technique. *Advanced Drug Delivery Reviews* **2000,** *45* (1), 57-64.
174.   Okushima, S.; Nisisako, T.; Torii, T.; Higuchi, T., Controlled production of monodisperse double emulsions by two-step droplet breakup in microfluidic devices. *Langmuir: the ACS journal of surfaces and colloids* **2004,** *20* (23), 9905-9908.
175.   Chang, F.-C.; Su, Y.-C., Controlled double emulsification utilizing 3D PDMS microchannels. *Journal of Micromechanics and Microengineering* **2008,** *18* (6), 065018.
176.   Dolomite, Double Emulsion System.
177.   Abate, A. R.; Weitz, D. A., High-Order Multiple Emulsions Formed in Poly(dimethylsiloxane) Microfluidics. *Small* **2009,** *5* (18), 2030-2032.
178.   Utada, A. S.; Lorenceau, E.; Link, D. R.; Kaplan, P. D.; Stone, H. A.; Weitz, D. A., Monodisperse Double Emulsions Generated from a Microcapillary Device. *Science* **2005,** *308* (5721), 537-541.
179.   Chu, L.-Y.; Utada, A. S.; Shah, R. K.; Kim, J.-W.; Weitz, D. A., Controllable Monodisperse Multiple Emulsions. *Angewandte Chemie* **2007,** *119* (47), 9128-9132.
180.   Martino, C.; Berger, S.; Wootton, R. C. R.; deMello, A. J., A 3D-printed microcapillary assembly for facile double emulsion generation. *Lab on a Chip* **2014,** *14* (21), 4178-4182.
181.   Shang, L.; Cheng, Y.; Wang, J.; Ding, H.; Rong, F.; Zhao, Y.; Gu, Z., Double emulsions from a capillary array injection microfluidic device. *Lab on a Chip* **2014,** *14* (18), 3489-3493.
182.   Choi, C.-H.; Wang, H.; Lee, H.; Kim, J. H.; Zhang, L.; Mao, A.; Mooney, D. J.; Weitz, D. A., One-step Generation of Cell-laden Microgels Using Double Emulsion Drops with a Sacrificial Ultra-thin Oil Shell. *Lab on a chip* **2016,** *16* (9), 1549-1555.
183.   Chan, H. F.; Zhang, Y.; Ho, Y.-P.; Chiu, Y.-L.; Jung, Y.; Leong, K. W., Rapid formation of multicellular spheroids in double-emulsion droplets with controllable microenvironment. *Scientific Reports* **2013,** *3*.
184.   Terekhov, S. S.; Smirnov, I. V.; Stepanova, A. V.; Bobik, T. V.; Mokrushina, Y. A.; Ponomarenko, N. A.; Belogurov, A. A.; Rubtsova, M. P.; Kartseva, O. V.; Gomzikova, M. O.; Moskovtsev, A. A.; Bukatin, A. S.; Dubina, M. V.; Kostryukova, E. S.; Babenko, V. V.; Vakhitova, M. T.; Manolov, A. I.; Malakhova, M. V.; Kornienko, M. A.; Tyakht, A. V.; Vanyushkina, A. A.; Ilina, E. N.; Masson, P.; Gabibov, A. G.; Altman, S., Microfluidic droplet platform for ultrahigh-throughput single-cell screening of biodiversity. *Proceedings of the National Academy of Sciences* **2017,** *114* (10), 2550-2555.
185.   Ho, K. K. Y.; Lee, L. M.; Liu, A. P., Mechanically activated artificial cell by using microfluidics. *Scientific Reports* **2016,** *6*.
186.   Elani, Y.; Solvas, X. C. I.; Edel, J. B.; Law, R. V.; Ces, O., Microfluidic generation of encapsulated droplet interface bilayer networks (multisomes) and their use as cell-like reactors. *Chemical Communications* **2016,** *52* (35), 5961-5964.

Chapter 2 – Development of a Microfluidic Device for the Generation of Hierarchical Emulsions.

2.0 Chapter Summary

Microfluidics offers the ability to produce droplets of water in oil in a reproducible and monodisperse manner, which should allow for the generation of encapsulated artificial lipid bilayer constructs. This chapter will explore different manufacture methods for droplet microfluidic devices that are capable of generating hierarchical droplet emulsions for this purpose. Such methods include CNC machining and 3D-printing, as well as ancillary methods such as silanisation of microfluidic channels for tuneable surface wettabilities (i.e. hydrophilic/hydrophobic). The main outcome of this chapter is the development and assessment of a novel, hybrid 3D-printed microfluidic system capable of producing double and triple emulsions from sequentially aligned coaxial droplet-generating geometries, which will be employed to produce encapsulated droplet interface bilayer (DIB) soft matter constructs in the following chapters.

2.1 Introduction

Numerous fabrication methods exist for the generation of microfluidic devices and channels, each of which are compatible with a range of different materials, and can give rise to different channel properties and planar (2.5D) or 3D microfluidic features. Methods that allow for rapid prototyping are generally preferable due to the iterative design approach commonly employed in device engineering. For the particular purpose

of generating hierarchical emulsions, such as water-in-oil-in-water (W/O/W) or W/O/W/O emulsions, which provide a basic architecture to develop freestanding, encapsulated droplet interface bilayer networks, the choice of channel substrate is of particular importance due to the requirements to produce channels that allow for both water and oil droplet generation within the same device. Thus, materials and methods that allow for different surface properties within the same device are required in order to assemble devices that can produce both water-in-oil (W/O) droplets and oil-in-water (O/W) droplets at different locations within a microfluidic chip, for the ultimate assembly of W/O/W and W/O/W/O emulsions. This can be achieved by using different materials within the same microfluidic device that display different surface wettabilities, or by employing materials that are compatible with surface modification techniques. The overarching objective of this chapter is to produce a microfluidic device that is able to sequentially generate droplets of alternating phases using surface modification techniques.

2.1.1 Microfluidic Device Fabrication

Microfluidic device fabrication methods can be divided into categories relating to the substrates that they are compatible with. The use of PDMS with photolithographic techniques is widely employed in the microfluidic community[1, 2] due to a cheap and relatively straightforward manufacture process that allows for rapid, iterative prototyping. PDMS can be cast against a mold with a <100 nm fidelity and presents with favourable physicochemical properties for a number of microfluidic applications[3]. These include transparency, low reactivity and surface energy, impermeability to water, permeability to gases, good thermal and electrical insulation, elastomeric properties, and general biocompatibility[1]. However, PDMS-based devices may sometimes be unsuitable due to its permeability to organic solvents[4], such as for the production of hierarchical droplet emulsions which employ organic solvents as intended here.

Alternative methods involve the use of thermoplastics such as polymethyl methacrylate (PMMA), polycarbonate (PC), polystyrene (PS) and cyclic olefin copolymer (COC), which can be machined or hot-embossed to produce planar microfluidic channels and structures[5, 6]. These materials have been used for cell biology applications where PDMS can be problematic due to its ability to leach uncured oligomers into microfluidic channels and absorb small hydrophobic molecules[7]. Their excellent optical properties, biocompatibility, low inherent fluorescence and high manufacturability have contributed to their emergence as popular materials within commercial biomedical applications[4]. Fabrication of glass capillary microfluidic devices has gained recent traction due to the ability to easily generate channels within channels forming coaxial droplet-generating geometries, allowing for hierarchical droplet generation[8-15], as well as the amenability of glass surfaces to be surface modified[16]. 3D-printing has also garnered attention as a method to produce microfluidic devices offering fast and easy fabrication compatible with rapid prototyping and device disposability[17]. Other fabrication methods exist which give rise to high-resolution micro and nano- fluidics, such as laser lithography[18] and dry[19] and wet etching[20]. The following sections will focus on glass capillary and 3D-printing microfluidics as well as surface modification techniques, which are employed here due to their amenability in producing microfluidic devices for hierarchical emulsion generation in a straight-forward and low cost manner.

2.1.1.1 Glass Capillary Devices

Microfluidic devices comprised of glass capillaries are commonly used to prepare particles and hierarchically-assembled droplet emulsions[9-12, 14, 21], as outlined in section 1.4. These are often constructed via the assembly of glass capillaries within each other, giving rise to coaxial droplet-generating geometries. In the majority of instances, these devices are constructed using manual methods, adhesives such as epoxy resin, and re-purposed materials (i.e. modified syringe tips as inlets), although there have

been attempts to standardise the process of device assembly using 3D-printed scaffolds that aid in the alignment of channels[13]. Nevertheless, glass microfluidics offers an attractive way of producing double and triple emulsions due to its fabrication simplicity and material compatibility with surface modification techniques.

2.1.1.2 3D-printing in Microfluidic Manufacture

3D-printing has emerged as a versatile tool and method of manufacture of microfluidic devices in the recent years, sparked by the increased availability, quality and reduced cost of 3D-printing resources. A variety of different 3D-printing techniques exist, each offering different capabilities and limitations. Inkjet (i3DP) is a technique borrowed from inkjet printing which relies on pulses generated thermally or via piezoelectric effects to push either powder or a photopolymer out of a nozzle on demand[22]. It offers good printing resolution (down to 50 µm in the x or y directions[23]), however the difficulties in removing scaffolds limits its use in generating microfluidic structures. 2-photon polymerisation uses a laser alongside a photocurable, transparent epoxy resin which allows for the direct production of 3-dimensional structures[24]. It allows for the generation of microfluidic channels that are 25 µm in diameter down to the nano-range[25], but the technique is very infrastructure-heavy which limits its availability and practicality for many microfluidic applications. Stereolithography (SLA) involves printing layer upon layer of a photocurable resin and offers good resolution[26], but is limited to the use of certain photocurable resins and also offers difficulties in printing closed microfluidic channels[27]. Fused filament fabrication (FFF) 3D-printers work by extruding layers of a thermoplastic through a high-temperature nozzle. It is a low resolution method of 3D-printing (typically can´t produce channels below 100 µm in diameter[27]), but is tremendously practical due to its low cost, high accessibility and compatibility with a range of thermoplastics. Off-the-shelf 3D-printers have been demonstrated to be able to produce self-contained microfluidic devices able to generate droplets and

66

encapsulated stem cells using a modular system[28]. Although these channels are 800 μm in diameter, it is expected that the fidelity and resolution of consumer-ready 3D-printers will increase as the technology advances. Therefore, with the ability of 3D printing to greatly increase the availability and accessibility of microfabrication for microfluidics, its potential to democratise microfluidic manufacture, or at least become a significant tool in rapid prototyping, remains large[17].

2.1.2 Surface Modification of Microfluidic Devices

Due to the dependency of microfluidics on channel surface chemistry, it is not surprising that surface modification techniques are extensively used within the microfluidic realm and fulfil a variety of different roles. Broadly, surface modification techniques serve to either encourage or inhibit the adhesion or absorption of different molecules on channel surfaces. This is of particular importance within the biological applications of microfluidics, as protein and biomolecule surface immobilization[29-32] are useful for biosensing and lab-on-a-chip applications[33], as well as preventing unwanted protein adsorption[34]. Similarly, droplet microfluidics rely on surface modification to change the wetting properties of the surface, as this technique inherently involves the non-interaction of the dispersed phase with channel walls[35] and hence surface wettability must be tailored in order to produce a desired droplet regime (i.e. hydrophilic channels for oil droplets hydrophobic channels for aqueous droplets).

Naturally, surface modifications strategies will depend on the material used to fabricate the microfluidic channels. With polydimethoxysilane (PDMS) being by far the most popular material used for microfluidic fabrication[2, 3], most instances of techniques found in the literature focus on the surface modification of this particular polymer[36, 37], although many of these techniques may be used with other materials depending on surface chemistry and reactivity. On the other hand, surface modification techniques also exist within and beyond microfluidics, and for other common materials such as

67

PMMA[30, 38-40], glass[15, 41-43], and others due to the extensive and broad use of surface modification for applications unrelated or preceding microfluidics.

A 2011 review on the surface modification of PDMS[37] listed the following surface modification techniques: plasma treatment, silanisation, chemical vapour deposition (CVD), layer-by-layer (LBL) deposition, surfactant treatment, protein adsorption and graft-polymer based. Some of these techniques, including silanisation, CVD, surfactant treatment, protein adsorption and LBL can be grouped into self-assembled monolayer (SAM) techniques that rely on molecules that expose a desired surface chemistry to self-assemble and bond to the native surface (i.e. PDMS), and often to cross-link to form a stable layer[43]. Beyond these techniques, topographic techniques exist which involve the nanopatterning[44] or the use of nanocomposite materials[45, 46] such as carbon nanotubes[47, 48] to surface modify microfluidic channels, which is envisaged to give rise to a next generation of higher performance microfluidic devices[37].

With most microfluidic fabrication materials being sufficiently hydrophobic in nature (PDMS, PMMA, glass, polycarbonate, fluoropolymers etc.) to naturally generate droplets of water in oil, this section will focus on the use of surface modification techniques to generate droplets of oil in water. Many of the techniques described above are regarded as cumbersome (i.e. LBL and graft-polymer)[37], whilst some are more suited towards biological applications (i.e. protein adsorption), and others involve the use of surfactant layers which are non-permanent and incompatible with certain studies, such as those involving the study of artificial lipid bilayers. As such, this section will focus mainly on plasma modification, silanisation, and other instances where channel surfaces are hydrophillised using relatively uncomplicated techniques.

2.1.2.1 Plasma activation

Plasma activation relies on the exposure of a surface to gas plasma. Plasma is one of the four fundamental states of matter and is a gaseous mixture composed of positive ions and negative electrons that occur when gaseous substances are subjected to high temperatures or strong electromagnetic fields.

In the context of plasma activation, the commonly used oxygen plasma acts as a source of high energy, short-lived reactive oxygen species which can break bonds within a polymer backbone[49]. For both PDMS and glass surfaces, silanol groups develop (Si-OH) upon exposure to oxygen plasma at the expense of methyl groups (-CH_3)[50]. In PDMS, some of these combine with each other to form Si-O-Si bonds[51]. This is further evidenced by tapping mode atomic force microscopy (AFM) which demonstrates increased stiffness after plasma exposure[52], indicating increased cross-linking and bond formation at the PDMS surface. However, the surface is nevertheless thought to contain a richness in polar –OH groups. PMMA surfaces develop carboxyl, carbonate and carbonyl groups at its surface according to XPS studies[53]. There is evidence that the use of water vapour plasma instead of the commonly used oxygen may increase the density of hydroxyl groups for this material[54]. These chemical groups increase the surface energy and hydrophillicity albeit in a short-lived manner, due to the process of hydrophobic recovery[55-58] wherein the highly reactive surface groups exchange with polymer oligomers in the bulk material phase in order to minimize surface energy. This appears to be true for PDMS, glass and PMMA surfaces. Although methods exist to circumvent this issue to varying degrees[55, 59], this renders plasma treatment in itself ineffective at producing lasting hydrophilic surfaces for the production of droplets of oil in water. However, it enables the permanent or semi-permanent bonding of other hydrophilic species to the activated, reactive layer it produces to produce long-lasting hydrophilic surface modifications. Thus it can be said

that due to the highly effective but short-lived nature of plasma surface treatment, the direct use of plasma within microfluidic surface modification is limited, but critical to other surface modification techniques that require surface activation, such as silanisation.

2.1.2.2 Silanisation

Silanisation is a surface modification technique that relies on the covalent bonding of organosilanes onto a surface and their formation of an interfacial self-assembled monolayer (SAM). SAMs are usually formed from linearly structured molecules that contain a surface reactive group on one end and a functional group on the other[60]. The first observed example of a SAM was the spontaneous assembly of organic thiols on a gold surface[61]. The self-assembly of fatty acids on alumina surfaces is another example[60]. Organosilanes are commonly used due to their ability to form monolayers on a large variety of surfaces and the availability of organosilanes with different functional groups to decorate the surfaces of a channel[43]. Methoxy- or chloro- groups are present on the surface reactive end of organosilane molecules, which react with trace amounts of water to form silanol groups (Figure 2.1). These can then covalently bond to other free hydroxyl groups present on a surface, and lateral hydroxyl groups cross-link with adjacent silane molecules to form a SAM. These reactions are very sensitive to the amount of water present in the system, and although the formation of a high-quality monolayer is often challenging, consistent and uniform surface chemistry and wetting profiles are anyhow achievable[60]. Thus, organosilanes are able to surface modify practically any surface that contains a richness in hydroxyl groups, which, as explained previously, can be actively encouraged using plasma activation for common microfluidic manufacture materials such as PDMS, glass and PMMA.
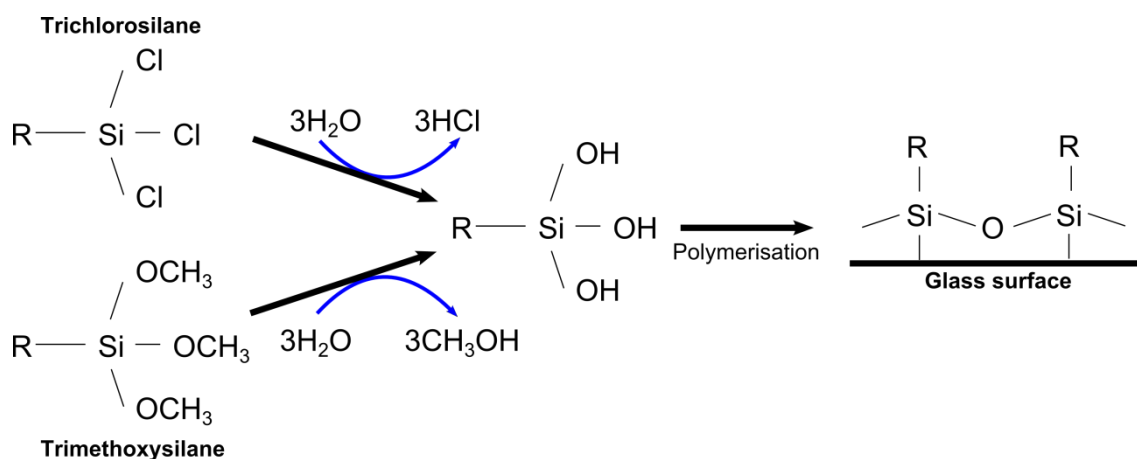
Figure 2.1 The steps that give rise to the polymerisation of a trichlorosilane and a trimethoxysilane onto a glass surface containing surface hydroxyl groups. "R" denotes the apical portion of the molecule that forms the new surface once the glass is surface modified. The chloro groups on the trichlorosilane and the Methoxy groups on the trimethoxysilane react with trace amounts of water to form hydroxyl groups, producing hydrochloric acid and methanol as side products, respectively. The hydroxyl groups can then covalently bond with a surface containing other hydroxyl groups, and cross-link with adjacent organosilanes.

The selection of organosilanes that contain surface-reactive methoxy- or chloro- groups will depend on the surface that is modified, as the reaction products of the covalent bonding are either methanol or chloride ions, respectively, which can damage the material that is being surface modified. For example, the latter risks the localised production of hydrochloric acid[62] which may corrode certain substrates.

Silanisation methods invariably involve the selection of an appropriate organosilane depending on the surface-exposed functional groups desired and the suitable surface-reactive groups. The surface needs to be cleaned and modified, via plasma treatment for example, to contain surface hydroxyl groups. Then, the surface is exposed to the selected organosilanes and excess organosilane removed after a period of time. Optional baking of the surface can be performed to improve SAM quality as this enhances the cross-linking of the organosilanes side-chains[43]. Common silanes for surface modification are listed in Table 1.

Silane	Hydrophobic/hydrophilic	Common use(s)
3-Aminopropyltriethoxysilane/3-aminopropyltrimethoxysilane (APTES/APTMS)	Hydrophilic	Generation of amine-rich surfaces which can be used to immobilise biomolecules[63].
3-Mercaptopropyltrimethoxysilane (MPTS)	Hydrophilic	Generation of thiol-rich surfaces which can be used to immobilise thiol-containing molecules[64].
Octadecyl organosilanes	Hydrophobic	Generation of hydrophobic surfaces and protein adsorption[65].
Polytetrafluoroethylene organosilanes (PFS)	Hydrophobic	Generation of hydrophobic surfaces or used as a resist for electron beam lithiography[66].
PEG and PEO organosilanes	Hydrophilic	Generation of hydrophilic surfaces [13].

Table 1 Different organosilanes and their common uses within microfluidics**.**

Oxygen plasma, piranha solutions or UV/ozone exposure can be used for the introduction of surface hydroxyl groups, the selection of which will depend on material compatibility[43]. Exposure to organosilanes can be achieved via liquid phase deposition via submerging the desired surfaces in an organosilanes solution or chemical vapour deposition (CVD), with the latter reported to give rise to SAMs of a higher order and quality[67].

2.1.2.3 Other strategies

Other surface modification strategies exist, especially for PDMS and glass. One example involves the coating of PMMA walls with poly vinyl alcohol (PVA) or hydroxypropylmethyl cellulose following substrate oxidation with UV/ozone or nitric

acid, which is reported to reduce water contact angle down to 18.9º (for PVA-coated polymer oxidised with UV/ozone)[38]. In these methods, oxidisation serves to increase hydrogen bonds between the substrate and the modifier, but it is considered that only a physical coating is achieved as there is no covalent bonding to the surface. Another method involves submerging PMMA in a solution of potassium iodide and iodine[68]. This method induces an increase in surface roughness and water contact angle is not reduced below 50º, and is therefore less preferable than other methods described here.

2.2 PMMA Devices

Initially, the production of flow-focusing, droplet-generating devices made from PMMA was explored, owing to the ease of manufacture by CNC machining and existing experience within the research group. Since the wetting profile of PMMA favours preferential wetting of oil over water, resulting in water in oil droplet formation, surface modification strategies were evaluated in order to attempt to produce oil in water emulsions. The ability to selectively modify PMMA to tailor its wetting profile would enable the production of sequential water and oil droplets to make hierarchical emulsions for later application as encapsulated DIB systems.

2.2.1 Methods

2.2.1.1 Microfluidic Fabrication

Fabrication of PMMA microfluidic devices for the generation of W/O/W emulsions consisted of device design, PMMA milling and surface modification via silanisation. PMMA was purchased from Arkema (France).

2.2.1.1.1 CAD Design

Computer Assisted Design was employed to design 2.5D and 3D microfluidic chips and assemblies. This was done using the software Solidworks (Dassault Systemes, France).

2.2.1.1.2 CNC Machining

Computer Numerical Control (CNC) micromilling (C30, LPKF, Germany) was used to manufacture PMMA chips. 2D designs were exported from SOLIDWORKS as .dxf files into the software CircuitCAM 5.0 (LPKF, Germany), which performed the contour routing for the milling of channels and holes. The file is then exported to the software Boardmaster (LPKF), which operates the C30 milling machine. The software automatically controls the milling tool movement in the X and Y dimensions, whilst the Z dimension (depth) had to be controlled manually. This required the milling of channels to occur in multiple steps, with each step milling a depth equivalent to a quarter of the width of the tip of the milling tool employed. This minimises the formation of material debris, protects the tool from damage and ensures a smooth surface finish. Typically, 0.15 mm and 0.8 mm end mill tools (LPKF) were employed, depending on the width of the channels. A rotational speed of 24,000 rpm and a travel speed of 20 mm s^{-1} were used. The relatively slow rotational speed and relatively fast travel speed ensure that the PMMA substrate does not melt. Debris was collected using a vacuum line attached to the milling head. After the channels had been milled, a hand drill (Dremel, Germany) was used to drill holes for the microfluidic chip inlets and outlets using a 0.8 mm drill tool.

74

2.2.1.2 Surface modification

Surface modification involved the plasma activation of glass and PMMA surfaces and their subsequent exposure to organosilanes to form a SAM.

2.2.1.2.1 Plasma activation

Plasma activation of glass or PMMA surfaces and capillaries was carried out using a Femto Plasma Cleaner (Diener, Germany). Prior to plasma activation, glass surfaces and capillaries were sonicated for 10 minutes in neat acetone, then methanol and then isopropanol. PMMA surfaces were sonicated in isopropanol only as acetone is able to dissolve the polymer, and methanol and ethanol can induce crazing and swelling of PMMA solids. The surfaces were then vacuum-dried for at least 10 minutes in the plasma cleaner. Oxygen plasma is generated using an oxygen stream at a flow rate of 10 sccm and a pressure of 0.35 mbar. Oxygen plasma is qualitatively confirmed visually, as it generates white/blue light, as opposed to the purple light emitted by air plasma (Figure 2.2). During the method development process, surfaces were exposed to plasma for between 0 and 12 minutes.
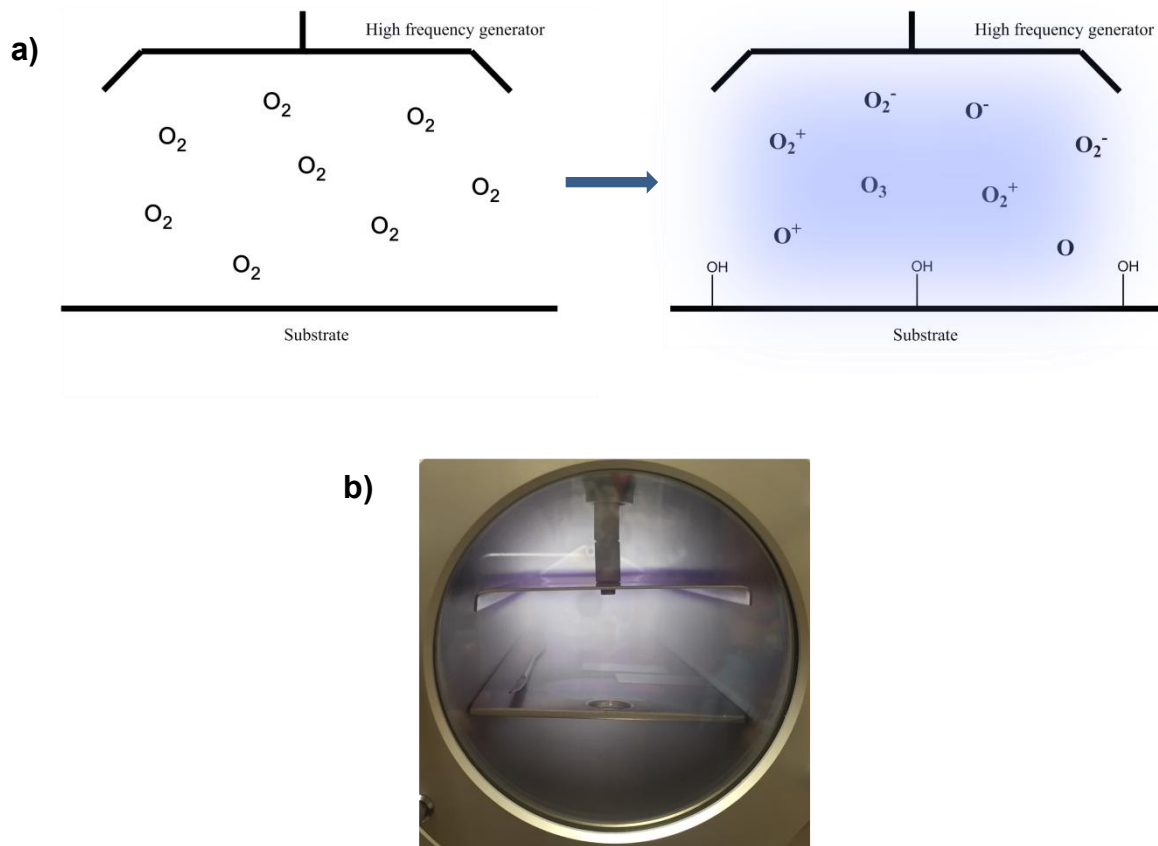
Figure 2.2 Activation of glass or PMMA surfaces using oxygen plasma. a) Schematic of the formation of oxygen plasma using a high frequency generator (Diener, Germany) from oxygen gas (0.35 mbar). b) Photograph of plasma chamber displaying the generation of white/blue plasma, indicating oxygen plasma. This colour varies depending on the gas composition.

2.2.1.2.2 Silanisation

Glass or PMMA is silanised using 3-[Methoxy(polyethyleneoxy)propyl]trimethoxysilane (MPEOTMS) **or** N-(Triethoxysilylpropyl)-O-poly(ethylene oxide)urethane (TEOSPEO) to achieve hydrophilic surfaces (Figure 2.3). Following oxygen plasma activation (0.35 mbar O_2, 10 sccm, 10 minutes), substrates are submerged overnight in a 2% v//v solution of the desired silane in isopropanol. Care is taken in order to minimise the time between the end of plasma exposure and incubation with silane. Following silane incubation, the now silanised materials are washed with deionised water and cured at

76

120ºC overnight for glass and 70ºC for 24 hours for PMMA. The lower temperature of

PMMA ensures that the polymer does not melt and hence disrupt its surface chemistry.

3-[Methoxy(polyethyleneoxy)propyl]trimethoxysilane   N-(Triethoxysilylpropyl)-O-poly(ethylene   oxide)

a)

b)

Incubation with silane

$+CH_3OH$

Curing at high temperature

$+CH_3OH$
$-H_2O$

Figure 2.3 Silanisation of glass or PMMA surfaces. a) Two hydrophilic silanes (ABCR, Germany) used to produce hydrophilic glass or PMMA surfaces. b) Diagram depicting the functionalization of plasma activated surfaces using trimethoxysilanes.
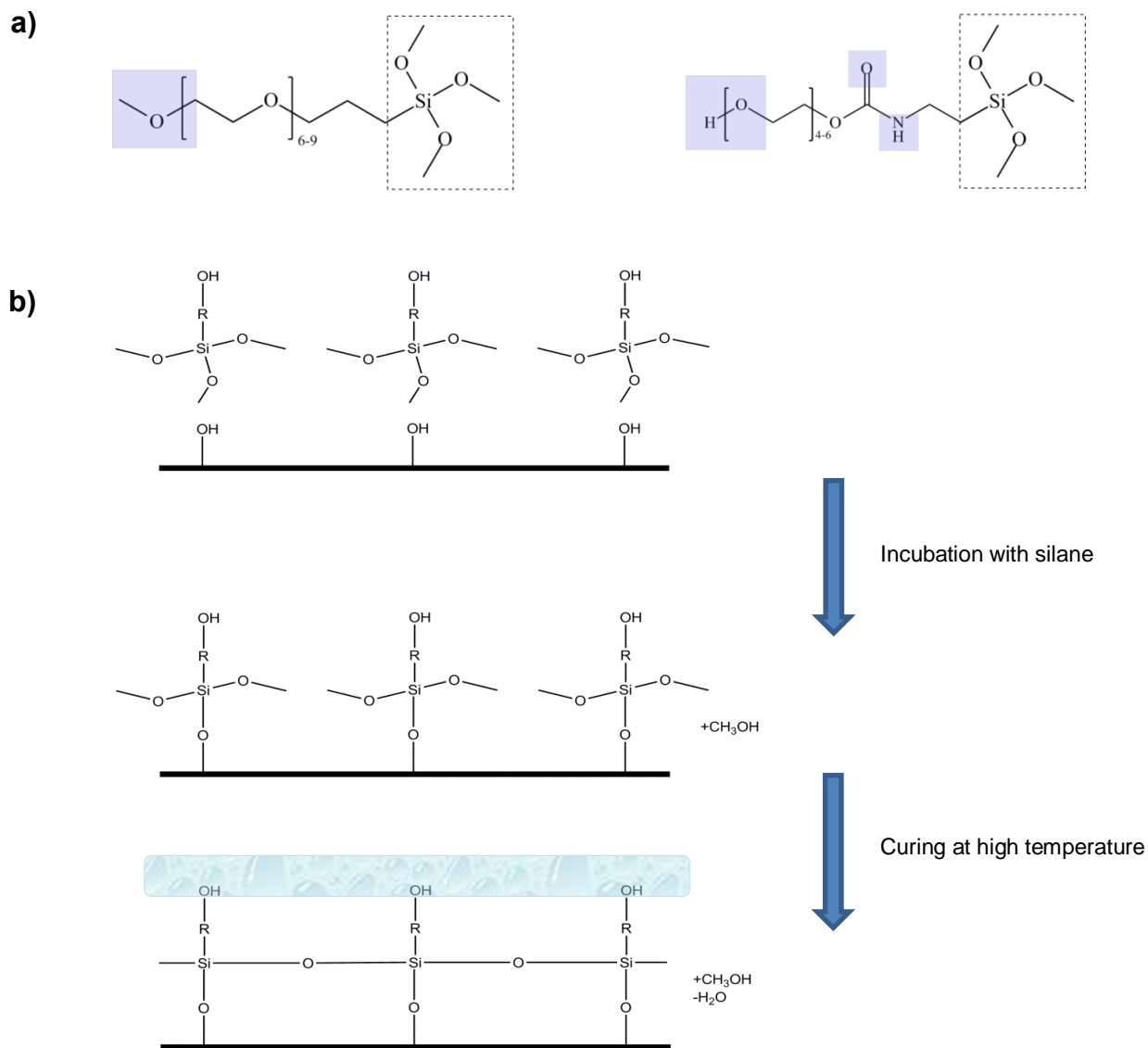
2.2.1.2.3 Contact angle measurements

Contact angle measurements were taken using custom-made equipment. Sample surfaces were placed upon a movable z-stage and imaged using a digital USB microscope (Celestron, USA). A transmitted light base was used to produce high contrast images (Figure 2.4a). 1 µL droplets of either deionised water or squalene were placed on the desired surface using a pipette. Care was taken in order to dispense the droplet without touching the surface as well as to dispense the same volume of liquid for every experiment. Droplets were then given 10 seconds to rest before any images were taken. Droplet images were processed using ImageJ software using the "sharpen" and then the "find edges" functions in order to more accurately ascertain the edges of the droplet. The contact angle was then taken using the "angle" tool (Figure 2.4b). For every contact angle measurement, an average was calculated from both sides of the droplet.

a)
b)
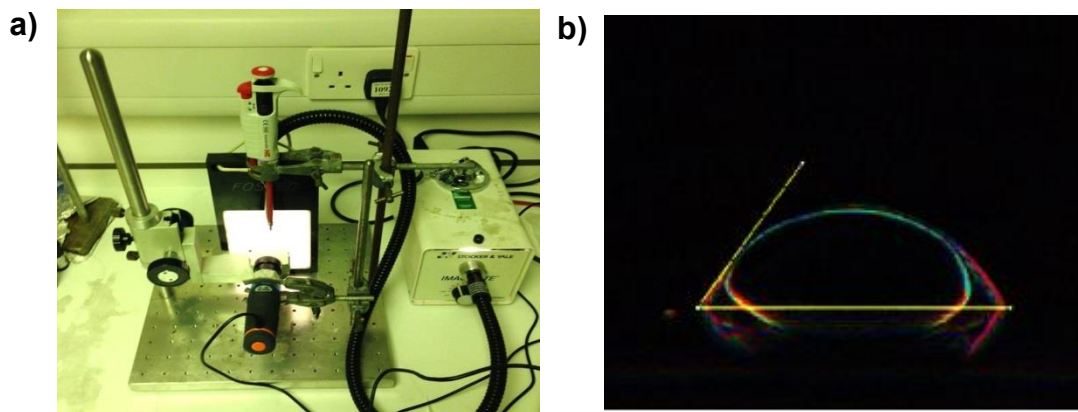
Figure 2.4 Contact angle measurements. a) Photograph of the custom equipment assembled to image sessile droplet contact angles. Droplets are placed on a stage which is imaged using a USB microscope (Celestrion, USA) and illuminated with a transmitted light base. A clamped pipette is used to dispense droplets onto the desired surface which can move in the z dimension. b) Photograph of a droplet of water on a surface imaged as shown in a), after processing using the "sharpen" and "find edges" tools of the ImageJ software. Contact angle data was extracted from these images.

2.2.1.3 Microfluidic set-up

PMMA microfluidic devices consisted of a machined steel sandwich manifold, as described by Castell et al.[69], containing the PMMA micromilled chip as well as a PMMA "lid" to enable the sealing and visualisation of the channels (Figure 2.5). Inlet and outlet FEP tubing (Kinesis, UK) with an inner diameter of 0.5 mm and an outer diameter of 0.76 mm were inserted into the appropriate holes that are drilled into the microfluidic chip and aligned with the manifold, facilitated by PEEK fingertight fluidic connectors (Kinesis, UK) that are screwed into the manifold. Nitrile rubber O-rings were used to seal these inlets and outlets via compression. The steel manifold is compression sealed via eight steel screws that go through the whole device, which avoids any leakage that may occur from the channels.
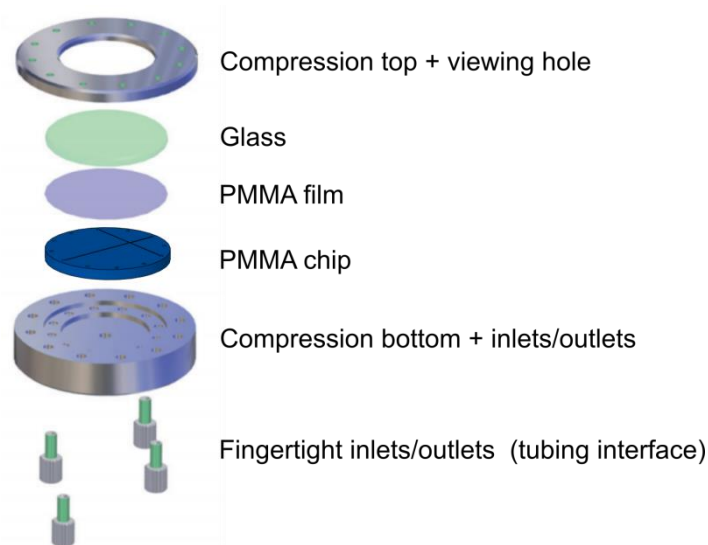
Figure 2.5 Steel sandwich manifold components used for the microfluidic operation of micromilled PMMA chips[69]. Steel screws are used to compress the PMMA chip with a PMMA film, in order to seal the channels. A glass cylinder is placed on the PMMA film in order to aid in the compression whilst allowing for observation of the channels. Tubing inlets and outlets are inserted through the bottom and interfaced with the bottom compression manifold using PEEK fingertight fittings and rubber O-rings.

2.2.1.4 Microfluidic operation

Fluids were delivered into the device using 3 mL luer lock plastic syringes mounted on syringe pumps (KD Scientific, USA), connected to the microfluidic device inlets using FEP tubing. The flow rates employed here ranged between 1 and 10 ml hr^{-1}.

2.2.1.5 Materials

De-ionised water was used, Squalene was purchased from Sigma-Aldrich (USA), and the silanes 3-[Methoxy(polyethyleneoxy)propyl]trimethoxysilane (MPEOTMS) and N-(Triethoxysilylpropyl)-O-poly(ethylene oxide)urethane (TEOSPEO) were purchased from ABCR (Germany).

2.2.2 Results and Discussion

2.2.2.1 Silanisation of PMMA

Unmodified PMMA surfaces were found to give rise to the production of water droplets in oil (W/O). Thus, silanisation of PMMA was attempted in order to produce hydrophilic channels which would allow for the formation of oil in water (O/W) emulsions and subsequently double emulsions (W/O/W). In order to do this, the surfaces were first plasma activated using oxygen plasma and then exposed to hydrophilic organosilanes.

The effect of plasma activation times was explored (0 – 12 minutes), which produced increasingly hydrophilic surfaces indicating an increase in surface activation as described in Section 2.3.1.2.2 (Figure 2.5a). Subsequent silanisation resulted in hydrophilic surfaces (Figure 2.5b), with the highest achieved hydrophillicity involving a plasma activation time of 5 minutes and the use of MPEOTMS silane. Silanisation following 11 minutes of plasma activation resulted in less hydrophilic surfaces than when exposed to 5 minutes, contrary to what one would expect, as increasing plasma times appear to cause a more complete surface activation (Figure 2.5a). It is possible

80

that the increased heat that the PMMA surfaces are exposed to when subject to 11 minutes of plasma activation affects the surface chemistry or topology in a manner that is detrimental to subsequent silanisation.

Microfluidic flow was then attempted by flowing water (2 ml hr^{-1}) and squalene oil (0.5 ml hr^{-1}) through a micromilled PMMA microfluidic chip that had been surface modified using the conditions that led to the highest hydrophillicity as shown in Figure 2.5b (blue bar). After initial successful oil droplet formation, the surface modification appeared to wear off with time and continued flow, as the oil phase was observed to adhere to the channel walls as the experiment progressed. This can be seen in Figure 2.5c, as an elongated sub-stream of oil advances further down the channel after the T-junction, adhering to the channel wall. This occurred within a minute of oil and water flow, and it was therefore found that the surface modification was only temporary and inadequate as a technique for the sustained production of hierarchical emulsions.

a)

b)

c)

Flow-focusing geometry for the generation of oil droplets in water

5 s intervals
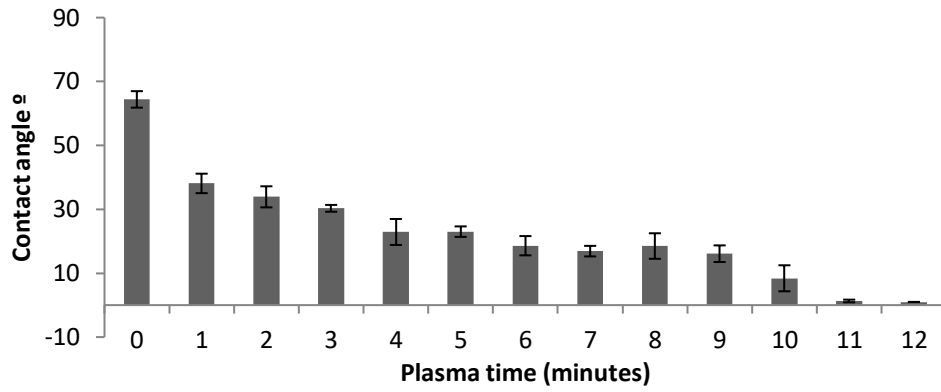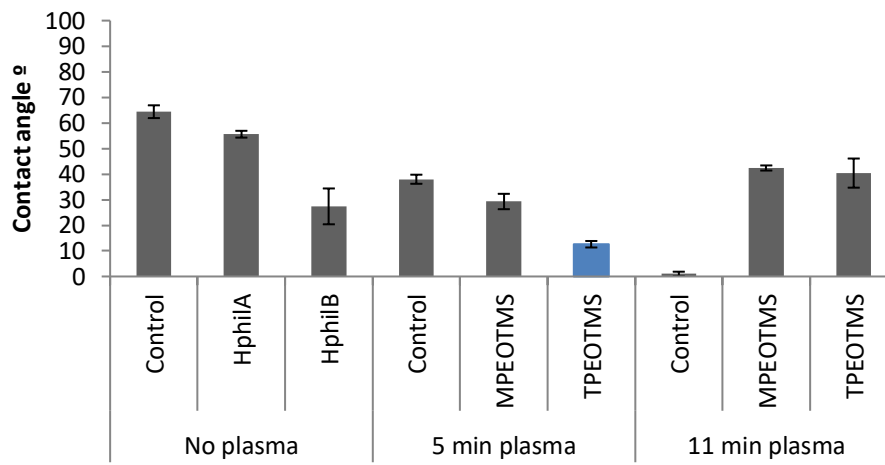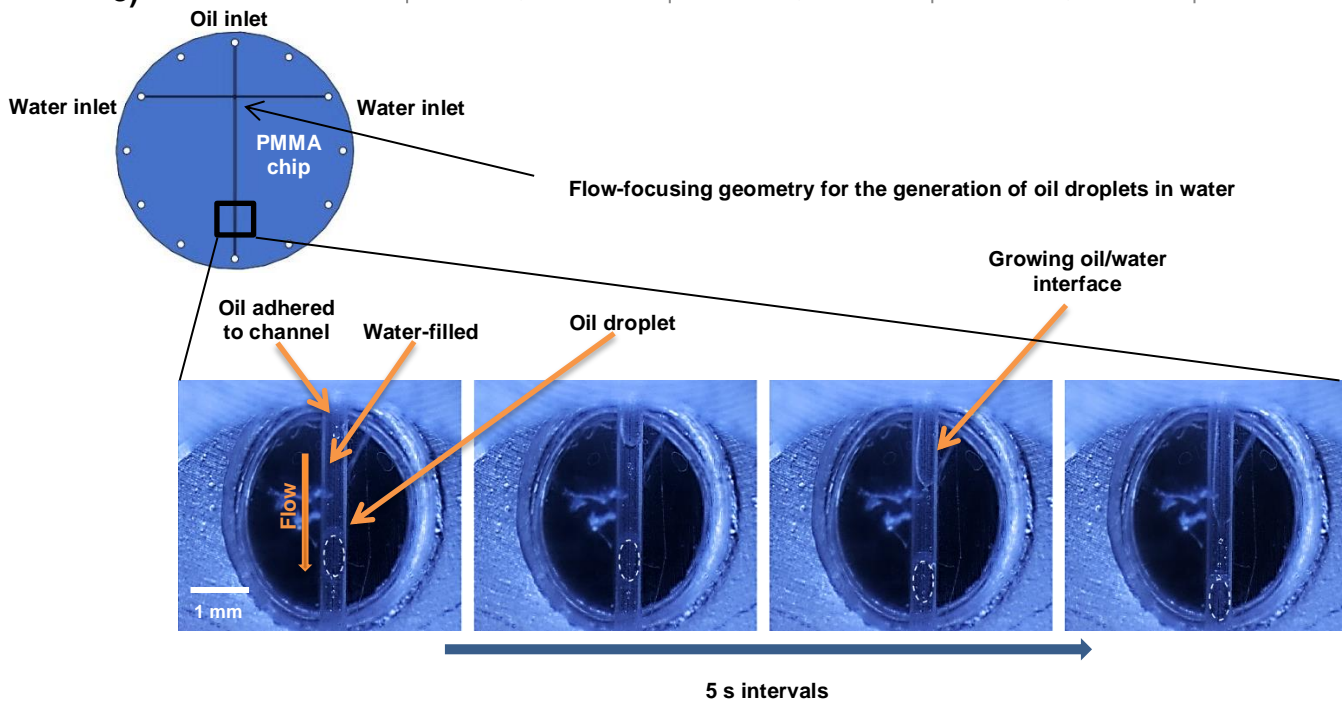
Figure 2.6 Surface modification of poly (methyl methacrylate) (PMMA) by silanisation. a) The effect of plasma activation time on PMMA water contact angle (n = 3). b) Water contact angles for PMMA exposed to different silanisation conditions, using the silanes 3-[Methoxy(polyethyleneoxy)propyl] trimethoxysilane (MPEOTMS) and N-(Triethoxysilylpropyl)-O-poly(ethylene oxide) urethane (TPEOTMS) (n = 3). The bar in blue represents the condition which appears to give the best hydrophilic surface modification and is thus used in the microfluidic experiments shown in c). c) Images of a surface modified microfluidic channel (diameter = 500 μm) flowing droplets of oil in water generated upstream in a milled T-junction. As flow occurs, the oil interface grows in the direction of flow as the silane treatment wears off and the oil adheres to the channel surface, leading to droplets breaking off further down in the channel. The flow rates employed here are 0.5 ml hr^{-1} for the oil phase and 1 ml hr^{-1} for each of the water inlets.

This is contrary to evidence in the literature that suggests that PMMA can be silanised[54], although this evidence characterises surface modification via water contact angle which might not address the issue that such modification is not permanent. Silanisation with both of the hydrophilic silanes (as shown in section 2.2.1.2) was attempted as well as an experimental method to produce water vapour plasma as suggested in the literature[54]. The use of water vapour plasma was expected to give rise to a higher density of hydroxyl terminals on the PMMA surface, enhancing the silanisation process. This method consisted in subliming a 50 μL frozen droplet of deionised water within the plasma cleaner chamber up to the same chamber pressure as used for oxygen plasma (0.35 mbar), without any other gas flow. However, similar results were obtained for both oxygen and water vapour plasma silanisation. The non-permanent nature of the silanisation was demonstrated by simulating water flow across the surface by washing freshly modified PMMA surfaces which had been surface activated with either oxygen or water vapour plasma prior to silanisation. Each washing event was found to increase the water contact angle (Figure 2.7), demonstrating that the silane layer was only weakly bound to the PMMA surface if bound at all.
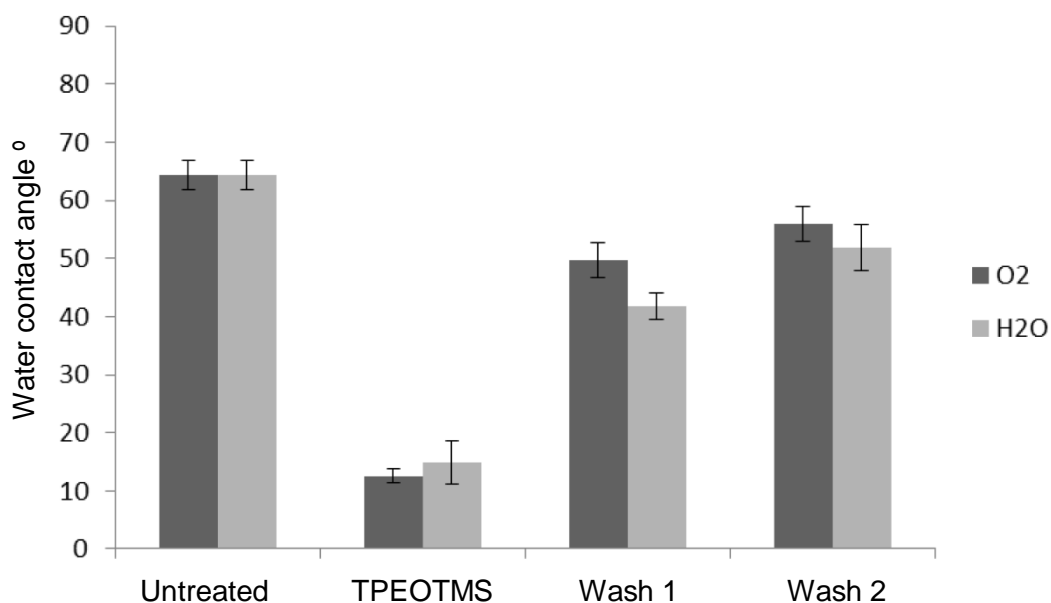
Figure 2.7 Water contact angles of PMMA before (control) and after silanisation with N-(Triethoxysilylpropyl)-O-poly(ethylene oxide) urethane (TPEOTMS), using either oxygen or water vapour plasma to activate the surface prior to silanisation. The substrates were then washed twice for 30 seconds with a stream of deionised water and the contact angles measured, demonstrating the washing off of the surface modification technique employed. The error bars represent standard deviation (n = 5).

It is noted that silanisation can be a sensitive process, and it is therefore possible that the methodology employed led to ineffective silanisation. For example, the process is not carried out in a clean room as commonly suggested[43], and curing is performed at a temperature below the boiling point of water, as it was necessary to choose a temperature below the melting point of PMMA. Also, the use of trichlorosilanes instead of trimethoxysilanes could have been attempted. Another explanation for the ineffective silanisation could be the diversity of functional groups present on the PMMA surface following oxygen plasma activation, as noted in section 2.1.2, of which only one type contains –OH terminals to which silanes can bond. This might give rise to a heterogeneous, low-density silanisation where silane molecules are not able to sufficiently cross-link. It was therefore concluded that, due to the difficulties in controlling the surface wettability of PMMA substrates, a different method relying on

surface modified glass capillaries would be explored due to its more prevalent use in the literature regarding the formation of W/O/W emulsions.

2.3 Hybrid, 3D-printed glass capillary devices for the generation of W/O/W and W/O/W/O emulsions

The inability to produce PMMA channels that are hydrophilic led to the exploration of an alternative method of producing W/O and O/W using microfluidics. Thus, the idea of a hybrid, 3D-printed microfluidic device based on the coaxial alignment of channels of alternating wettability was explored, as glass capillaries can be used which are known to be more amenable to silanisation techniques.

2.3.1 Methods

CAD design and surface modification techniques were performed as described in Section 2.2.1.

2.3.1.1 3D-Printing

3D-printing was performed using an Ultimaker 2 (Ultimaker, Netherlands) fused filament fabrication (FFF) 3D-printer, primarily extruding 3 ± 0.005 mm transparent poly (lactic acid) (PLA) filament (Faberdashery, UK). Devices designed in Solidworks were converted to .stl files and then imported into the Cura software (Ultimaker, Netherlands), which was used to virtually slice and parameterise designs into printer-ready files (.gcode). The main printer parameters employed are adapted from Morgan et al.[28] and summarised in Table 2. Such parameters allowed for high printing fidelity as well as a transparent and leak-free device.

Parameter	Value
Nozzle diameter	0.4 mm
Layer height	0.06 mm
Wall thickness	1.2 mm
Top/bottom Thickness	1.2 mm
Infill density	70%
Print speed	30 mm s^{-1}
Travel speed	120 mm s^{-1}
Print cooling	yes
Nozzle temperature	215 ºC
Build plate temperature	70 ºC
Build plate adhesion	skirt
Enable support	No

Table 2 3D-printing parameters selected in the slicing software Cura (Ultimaker, Netherlands) for the manufacture of 3D-printed microfluidic devices.

2.3.1.2 Microfluidic device assembly

A microfluidic device for the production of hierarchical emulsions was assembled using a custom-designed, 3D-printed assembly along with glass capillaries (internal diameter = 2 mm, external diameter = 2.4 mm) (CM Scientific, UK), an ethylene tetrafluoroethylene (ETFE) T-junction (ID = 0.5 mm) (Kinesis, UK) and FEP tubing (ID = 0.8 mm, OD = 1.6 mm) (Kinesis, UK). The device schematic and dimensions are shown in Figure 2.8.
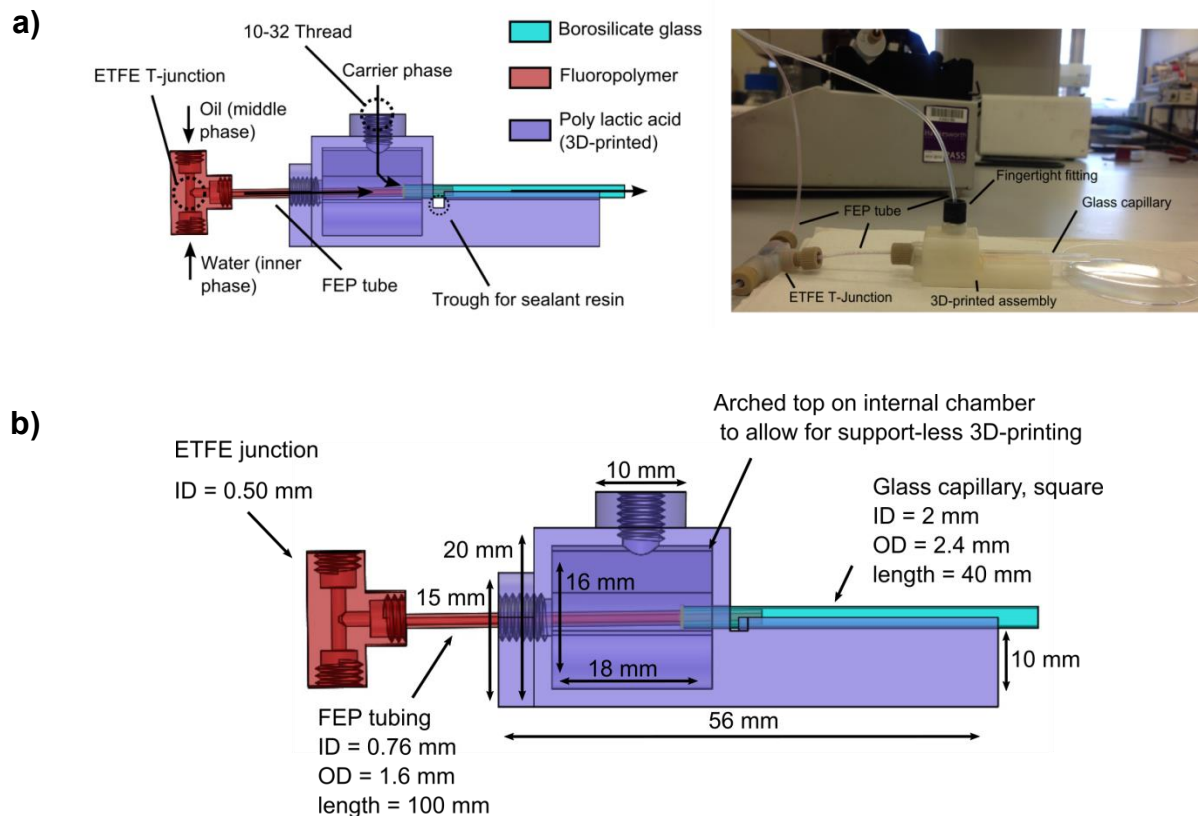
Figure 2.8 a) CAD design showing the main device features and photograph of hybrid, 3D-printed device used to generate W/O/W emulsions. b) Dimensions of the device.

As shown in Figure 2.8, the ETFE junction is employed in order to produce water droplets in oil, and is then delivered coaxially into a hydrophilic, silanised glass capillary using FEP tubing. A second aqueous phase flows between the FEP tubing and the glass capillary, which allows for the coaxial formation of W/O/W hierarchical emulsions.

The glass capillary is glued to a hole designed into the 3D-printed assembly using a two-part epoxy resin (Loctite, Germany). The output FEP tube of the ETFE junction is then inserted into the glass capillary through a chamber within the 3D-printed assembly so that it terminates ≈ 0.5 mm into the glass capillary, and screwed into the horizontal input of the 3D-printed assembly using a fingertight fitting (Kinesis, UK). The second aqueous phase is delivered into the 3D-printed assembly chamber using the vertical input on top of the device, which delivers fluid into the 3D-printed chamber and the glass capillary to form the coaxial, droplet-generating junction. The 3D-printed assembly aids in the alignment of the FEP tube with the glass capillary, and also allows

the fluidic inputs to be appropriately sealed with use of fingertight fittings. PTFE tape is wrapped around the thread of the fingertight fittings in order to secure a water-tight seal within the 3D-printed assembly.

2.3.1.3 Microfluidic operation

Fluids were delivered to the device as described for PMMA devices (Section 2.2.1.4).

2.3.2 Results & Discussion

2.3.2.1 Production of W/O and O/W emulsions using a hybrid, 3D-printed microfluidic device.

The production of W/O/W emulsions in a sequential manner requires the independent generation of W/O emulsions and O/W emulsions. The microfluidic device shown in Figure 2.8 is employed for this, where water droplets are generated in the ETFE T-junction and oil droplets are generated in the coaxial droplet-generating geometry.

2.3.2.1.1 W/O emulsions

It was found that a commercially available ETFE junction was able to produce aqueous droplets in oil at a variety of different flow rates (between 2 – 10 ml hr^{-1} for both oil and water phases), as well as being able to output these droplets into FEP tubing. Fingertight fittings between the ETFE and FEP materials were found to sufficiently seal the channels avoiding any leakage. An example of the generation of water droplets using an ETFE T-junction is shown in Figure 2.9.
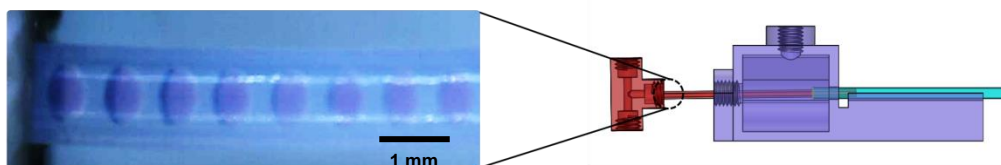
Figure 2.9 The production of a stream of droplets of water in oil produced in the ETFE T-junction and output into an FEP tube. The water is dyed pink with 25 µM sulphorhodamine B, and the oil phase is composed of squalene with 1% (v/v) Span-80. The flow rates employed are 4 ml hr^{-1} for the water phase and 10 ml hr^{-1} for the oil phase.

The frequency of droplet generation and the volume of the resultant droplets were analysed (Figure 2.10a and b). Frequency was calculated by measuring the time between the pinching-off of droplets, whilst droplet volumes were calculated from droplet dimensions in photographs, which were assumed to be ellipsoid in geometry (Appendix 1). Flow rate regimes where the water flow rate is higher than the oil flow rate are excluded as they failed to give rise to periodic droplet generation (Appendix 2).
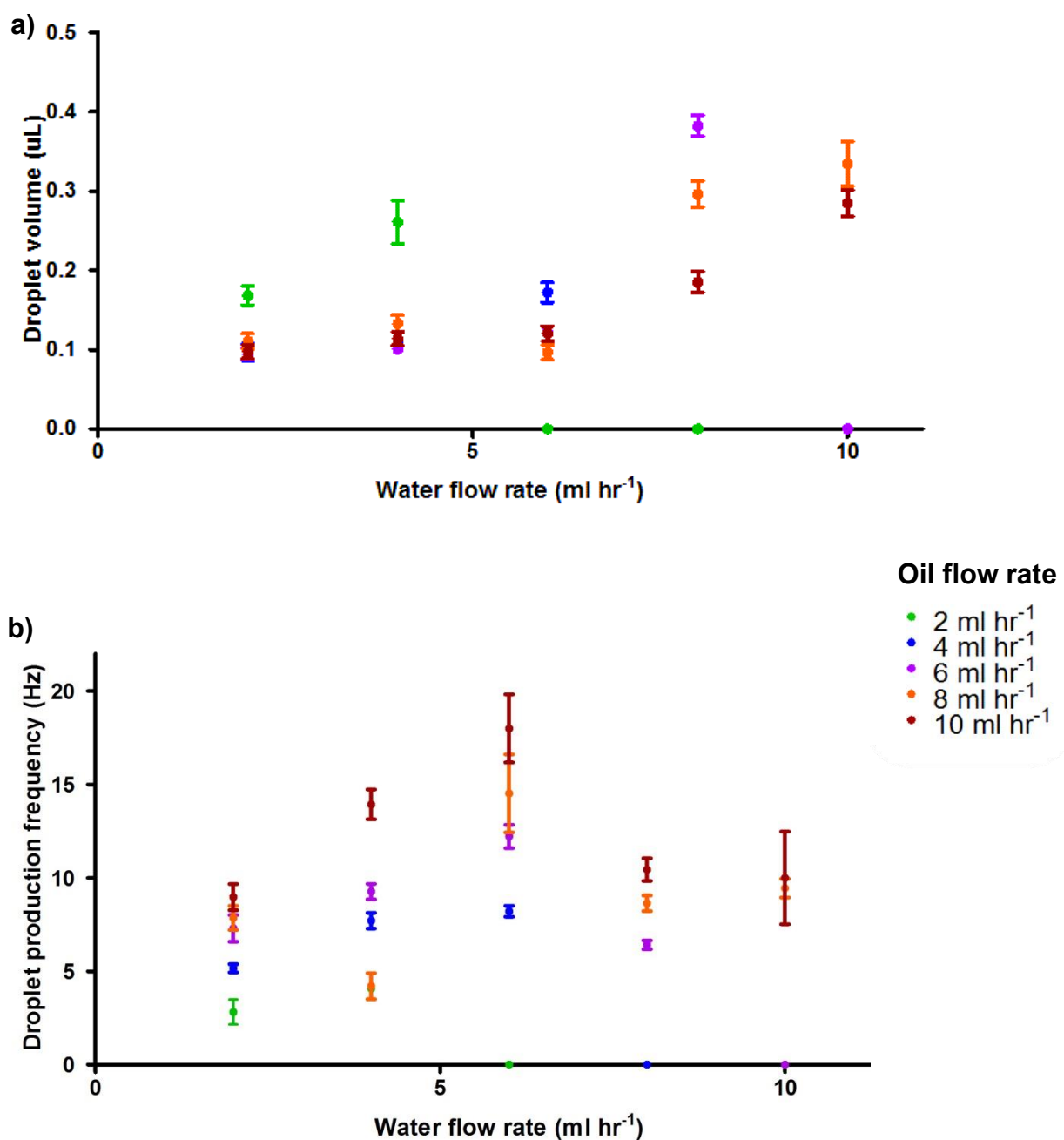
Figure 2.10 The effect of water and oil flow rates in the production of W/O droplets in an ETFE T-junction. a) Droplet volume vs. flow rate. b) Droplet generation frequency vs. flow rate.

The relationship between the frequency of W/O formation and water flow rate appears to be erratic across the range of water flow rates explored (Figure 2.10b), as a somewhat linear increase in frequency is visible for aqueous flow rates between 2 and 6 ml hr^{-1}, followed by a drop in frequency for the higher flow rates. Increasing oil flow

rates appear to give rise to a higher frequency of droplet generation for a given water flow rate. The relationship between flow rates and droplet volume seems to be erratic as well (Figure 2.10a), which is very likely related to the variability in frequency. Additionally, droplet generation frequencies appear to inversely relate to droplet volume. This is expected as for any given aqueous flow rate, the same volume of water per given amount of time is divided by a larger number of droplets for higher droplet generation frequencies. It does appear that increasing water flow rates, particularly above 6 ml hr^{-1}, gives rise to larger droplets, especially for low oil flow rates. This is expected as for higher water flow rates, a higher shear force is required from the oil phase in order to break the stream of water into droplets.

The erratic nature of droplet formation within the ETFE junction could be because of droplets forming in close proximity with each other and coalescing, giving rise to a lower frequency of droplet generation as well as larger droplets. This is somewhat supported by the increase in droplet volume for aqueous flow rates of 8 and 10 ml hr^{-1} (Figure 2.10a), and the fact that formed droplets transition from a 0.5 mm channel within the ETFE junction to a 0.8 mm channel in the FEP tube, which is a likely point for coalescence due to the expected drop in flow velocity. Another explanation of this could be the presence of void volumes between the tubing and the ETFE junction, as it is often challenging to cut the tubing perfectly flat. Such void volumes may cause a transient drop in velocity aiding in droplets coalescing at this junction. An alternative explanation for the difference could be a transitioning of one type of droplet-generating regime to another, as the Ca number varies for different flow velocities (as described in section 1.3). However, all estimated Ca numbers for these experiments except for the lowest flow rates employed appear to be >0.1 (Appendix 3), which is defined as being the transition point from "squeezing" to "dripping" regimes (see section 1.3.1). Thus, reproducibility, control and predictability of the number of droplets encapsulated per W/O/W should be achievable by maintaining a constant velocity following droplet

formation. It is likely that the system would benefit from the selection of a different method of aqueous droplet generation, such as using a PMMA chip or a coaxial droplet-generating geometry downstream.

The formation of droplets in the ETFE T-junction appears to be governed by shear stress forces for all except one (2 ml hr^{-1} for both water and oil phases) of the flow rates employed, according to the Ca numbers obtained (see section 1.3.1). Ca numbers were calculated to be between 0.99 and 0.5, with transitions from one type of droplet generation to another thought to occur around Ca = 0.1 according to reports in the literature[70]. Increasing the flow rate of either of the fluids increases the resultant capillary number resulting in increased dominance of viscous over surface tension forces.

2.3.2.1.2 O/W emulsions

Further downstream in the microfluidic device, a coaxial junction is produced via the alignment of an FEP tube (ID = 0.8 mm) inside a larger glass capillary (ID = 2 mm). The FEP tube flows the squalene oil phase, whilst the glass capillary flows the water phase through the 3D-printed assembly. As with the T-junction upstream, fingertight fittings are used to seal the fluid inlets of the 3D-printed parts. Although glass is somewhat hydrophilic, in itself it was not able to produce oil droplets as oil would adhere to the surface. Silanisation with MPEOTMS was employed to increase the hydrophillicity of the channels, which contact angle measurements on glass coverslips confirmed (Figure 2.11).
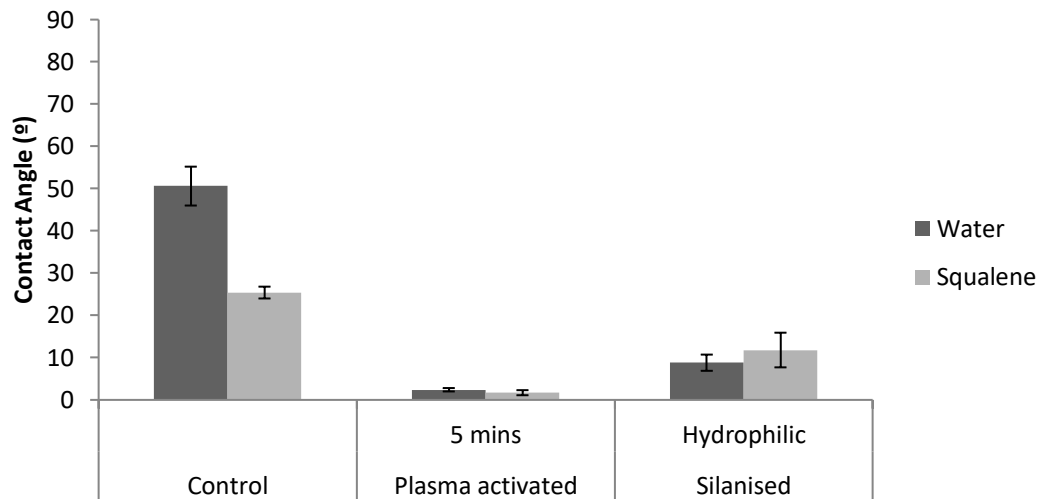
Figure 2.11 Contact angles of both water and squalene oil on glass coverslips. Glass is silanised with 3-[Methoxy(polyethyleneoxy)propyl] trimethoxysilane.

An example of the production of droplets of oil in water in the coaxial, droplet-generating geometry using a silanised glass capillary is shown in Figure 2.12. Importantly, in contrast to PMMA, the channel remained hydrophilic under oil and water flow and was found to remain so for up to 3 months of non-continuous use.
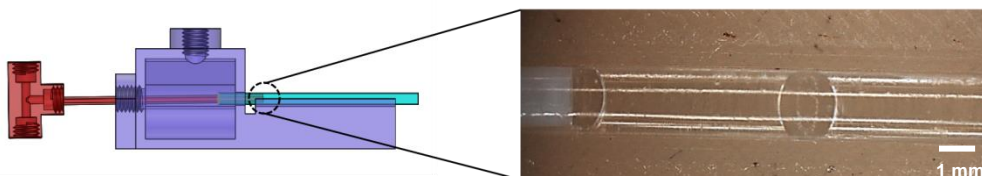
Figure 2.12 The production of droplets of oil in water in the coaxial, droplet-generating geometry within the 3D-printed microfluidic device. The oil phase is composed of squalene and the aqueous phase is deionised water. The oil flow rate is 10 ml hr^{-1} ad the water flow rate is 100 ml hr^{-1}.

Oil droplets appear to break off after the diameter of the glass channel is occluded by the forming droplet, demonstrating a dominance of surface over viscous forces. For the whole range of flow rates employed (2 – 10 ml hr^{-1} for the oil, 100 – 500 m hr^{-1} for the carrier aqueous phase), the highest Ca number obtained is 0.00016, which indicates a

geometrically-driven regime of oil droplet formation as described in section 1.3.2. Because of this regime of droplet formation, it is likely that droplet size is highly influenced via the diameter of the glass channel and the FEP channel delivering the oil into the glass channel. Increasing carrier flow rates as well as lower oil flow rates give rise to smaller droplets, although droplet diameters remain between 1.6 mm and 2 mm for the majority of flow rates tested, further demonstrating the geometrically-driven regime of droplet formation and the dependency of droplet diameters to channel diameters (Figure 2.13).
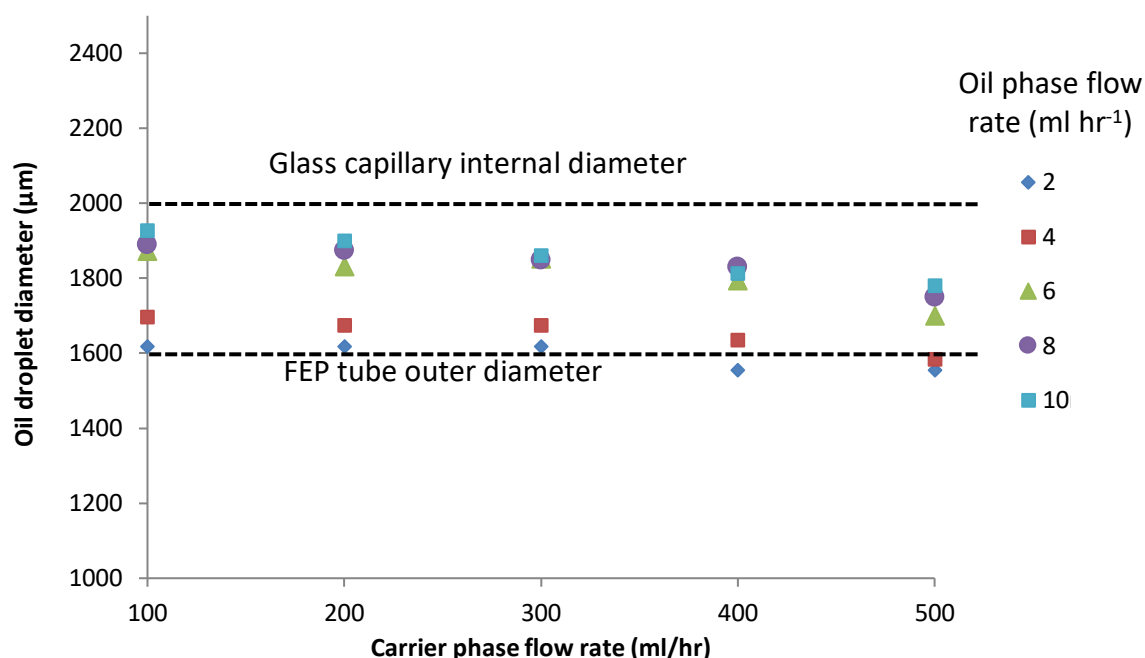
Figure 2.13 The effect of oil and carrier aqueous flow rates on oil droplet diameter, for droplets generating using a coaxial, droplet-generating geometry in the hybrid, 3D-printed device.

The size of the resulting oil droplets is also likely dependent on the ratio of diameters between the FEP and glass channels[15]. Furthermore, it would be necessary to attempt oil droplet formation using different sized channels in order to better establish the relationship between channel diameter and resulting droplet diameter. This would be focus of future experiments as it would be beneficial to scale-down the device in order

to produce smaller oil droplets and hence smaller W/O/W emulsions, as discussed in section 2.4.4.

In order to further characterise oil droplet formation, the frequency and volume of oil droplets generated in this way was characterised for the range of flow rates employed (Figure 2.14a and b).
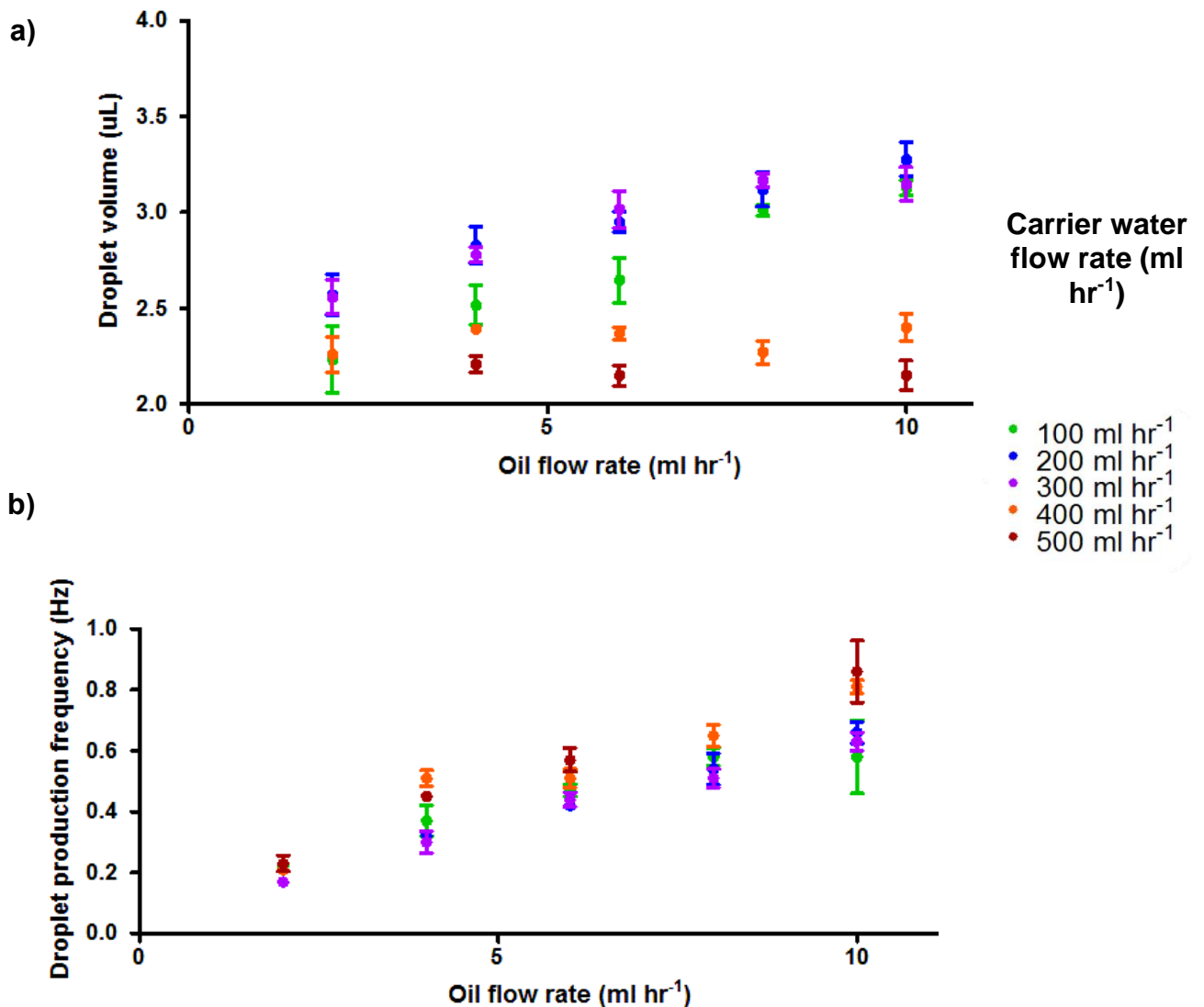
Figure 2.14 The effect of oil and water flow rates in the production of O/W droplets in a coaxial droplet generating geometry. a) Droplet volume vs. flow rate. b) Droplet generation frequency vs. flow rate.

Increasing oil flow rates gave rise to increasing frequency of droplet generation where the effect of the carrier flow rates appears to be minimal (Figure 2.14b). There also appears to be higher variability in droplet generation frequency at higher oil flow rates.

95

Increasing oil flow rates gives rise to larger droplets for carrier flow rates below 300 ml hr^{-1}; although oil droplet volumes remain between 2 and 2.5 µL for the higher flow rates explored (Figure 2.14a). This difference does not appear to be due to a difference in droplet-generating regime as Capillary numbers for all flow rate conditions remain well below 0.1, which is the Ca number at which transitions into other kinds of droplet-generating regimes are thought to occur for flow-focusing junctions according to reports in the literature[70], as seen in section 1.3.2. This data shows a higher predictability of O/W formation in the coaxial junction than for W/O formation in the ETFE junction for the range of flow rates explored. This is likely because of the geometrically-driven droplet formation regime, which has been reported to be highly stable, as well as the maintenance of constant channel diameters in comparison to droplet formation in the ETFE junction, which allows for the oil droplets to be sufficiently spaced from each other and thus avoid coalescence between multiple droplets.

2.3.2.2 Production of W/O/W emulsions using a hybrid, 3D-printed microfluidic device.

Using the device depicted in Figure 2.8, and the surface modification techniques and flow rate regimes described in the previous section, it was possible to generate W/O/W emulsions. First, water droplets are generated as shown in an ETFE junction as shown in Figure 2.9. The flow of droplets of water in oil is then passed into the 3D-printed microfluidic device, which is then broken up into droplets of oil containing a number of aqueous droplets within, in the coaxial, droplet-generating geometry downstream (Figure 2.12). The formation of W/O/W double emulsions using the flow regimes presented in section 2.3.2.1 is shown in Figure 2.15a.

A second mode of droplet generation was also possible that gave rise to a jetting regime of droplet, and did not require the use of surface modification techniques

(Figure 2.15b). In this method, the carrier phase contained 10 mM oleic acid dissolved in a pH 12 aqueous solution, and acted as a surfactant dissolved in the aqueous phase as oleate. This reduces the surface tension between the carrier aqueous phase and the forming oil droplets, and appeared to significantly alter the method of coaxial droplet formation as W/O/W emulsions broke off into droplets much before the forming oil droplet occluded the majority of the glass channel, due to fluid flow instabilities. This is characteristic of a domination of viscous over surface forces, and a high Ca number is expected due to the decrease in surface tension between the oil and water phases.

For both modes of fluidic operation, squalene is used as the oil phase with Span-80 surfactant (1% v/v) in order to avoid the coalescence of the aqueous droplets contained within the W/O/W emulsions. For the subsequent application of these emulsions as artificial lipid bilayer constructs, the use of a surfactant in the oil phase is somewhat comparable to the presence of a dissolved phospholipid required in order to produce droplet interface bilayers within the fluidic constructs.
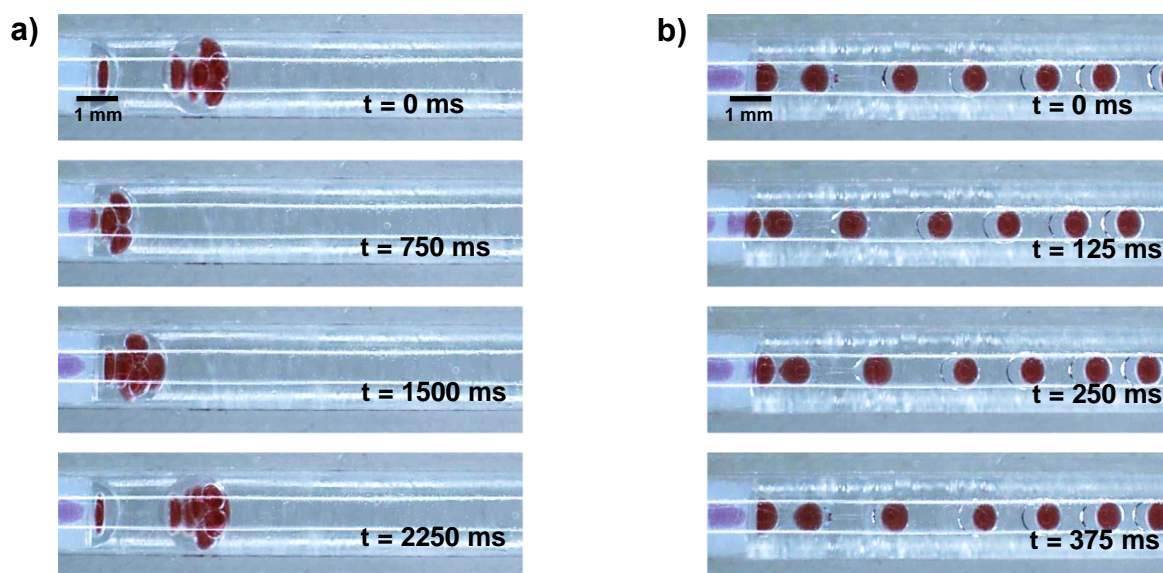
Figure 2.15 Time lapse photographs depicting the formation of W/O/W emulsions using the hybrid, 3D-printed device depicted in Figure 2.8. Aqueous droplets are dyed red and contain a pH 7.4 phosphate buffer. Flow rates are 4 ml hr^{-1} for the internal aqueous phase, 8 ml hr^{-1} for the oil phase and 300 ml hr^{-1} for the aqueous carrier phase. Although the flow rates are the same for a) and b), different flow regimes are observed as a) uses a hydrophilic, surface modified glass channel, no surfactant in the aqueous, and a pH 7.4 phosphate buffer as the

aqueous carrier phase, and b) uses no surface modification and a 10 mM solution of oleic acid in pH 12 water as the carrier phase.

For both of the flow regimes described in Figure 2.15, emulsions could be produced for a wide range of flow rates (2 – 10 ml hr^{-1} for internal aqueous and oil phases, 100 – 500 ml hr^{-1} for the external aqueous phase), giving rise to emulsions containing a different number of internal aqueous cores. Jetting regimes gave rise to little variability in the number of aqueous droplet encapsulated per emulsion for the range of flow rates, encapsulating between one and three aqueous cores. On the other hand, geometrically-controlled regimes allowed for the encapsulation of between 6 and 22 aqueous droplets, as shown in Figure 2.16. This difference is likely because the geometrically-controlled regime involves a low frequency of oil droplet generation and a relatively high frequency of water droplet generation downstream. So, as the oil droplet is in its forming stages, a number of aqueous droplets can flow into it before it is pinched off into a W/O/W emulsion. This is expected to give rise to a more predictable regime of droplet encapsulation.

Legend (nº droplets per W/O/W emulsion)
0-7
8-10
11-14
15-19
>20

Carrier aqueous flow rate = 100 ml hr^{-1}

		Oil flow rate (ml hr^{-1})				
		2	4	6	8	10
Water flow rate (ml hr^{-1})	2	14±0.82	14.75±1.26	14.25±0.96	14±0.21	14±0.82
	4	x	18.75±0.96	18.5±0.58	19±0.82	17±0.82
	6	x	x	21	21±0.82	21
	8	x	x	x	20.25±0.5	21.25±0.96
	10	x	x	x	x	21.5±1.73

Carrier aqueous flow rate = 300 ml hr^{-1}

		Oil flow rate (ml hr^{-1})				
		2	4	6	8	10
Water flow rate (ml hr^{-1})	2	7.5±0.58	6.75±1.26	7.25±0.96	8.25±0.5	9
	4	x	8.25±1.5	7.5±0.58	6.5±0.58	7.75±0.96
	6	x	x	12.75±0.96	12.25±2.36	13.75±0.5
	8	x	x	x	12.5±1.73	12.5±0.58
	10	x	x	x	x	12.25±0.5

Carrier aqueous flow rate = 500 ml hr^{-1}

		Oil flow rate (ml hr^{-1})				
		2	4	6	8	10
Water flow rate (ml hr^{-1})	2	7±0.82	8.25±0.5	8	6.75±0.5	7.5±1
	4	x	9.25±0.96	9.75±0.5	11±0.82	11±0.82
	6	x	x	9.75±0.96	12.5±0.58	12.5±1
	8	x	x	x	8.5±1.91	17±1.63
	10	x	x	x	x	12.25±1.71

Figure 2.16 The number of aqueous droplets encapsulated per oil droplet at a variety of different flow rates in the generation of water-in-oil-in-water (W/O/W) emulsions using a hybrid, 3D-printed coaxial device. Flow rates marked "x" were excluded as they gave rise to non-periodic water droplet formation (see Appendix 1).

As shown in Figure 2.16, the flow rates of all three phases have an effect on the number of aqueous droplets encapsulated per oil droplet. Generally, increasing water and oil flow rates give rise to emulsions with a greater number of encapsulated droplets, as higher water flow rates generate water droplets at a higher frequency and higher oil flow rates give rise to smaller water droplets and larger oil droplets (See Figure 2.10 and Figure 2.14). The water flow rate appears to have a larger impact on the number of encapsulated droplet than the oil flow rate. Increased carrier water phase flow rates decrease the number of droplets encapsulates per emulsion, which is expected as this increases the frequency at which oil droplets are generated (see Figure 2.14), thus providing less time for the growing oil droplet to encapsulate aqueous droplets before being pinched-off.

2.3.2.2.1 Predicting the number of aqueous cores encapsulated per W/O/W emulsions produced using a geometrically-controlled regime of droplet generation

As previously established, the geometrically-driven method of W/O/W emulsion formation allows for a wide range of aqueous droplets encapsulated per emulsion depending on the flow rates employed. In this section, a prediction model for the number of encapsulated droplets per W/O/W emulsion will be attempted based on the frequency of W/O and O/W generation for different flow rates, as seen in section 2.3.2.1, by dividing the former with the latter. For example, if water droplets are being generated at 10 Hz, and oil droplets are being generated upstream at 1 Hz, then it stands to reason that 10 droplets are encapsulated per oil droplet. However, this simple calculation does not take into account that the presence of the flow of water droplets within the oil stream, as the frequency of oil droplet formation was determined experimentally in the absence of an aqueous phase forming droplets in the oil phase. To account for the flow of aqueous droplets in oil, the frequency of oil droplet formation is taken for the flow rate of the water and oil phases combined, which can be extrapolated from the linear trends seen for oil droplet frequency of generation (Figure 2.17). The oil phase flow rate is kept constant at 10 ml hr^{-1} as it allows for the use of a wide range of internal aqueous flow rates (2 – 10 ml hr^{-1}).
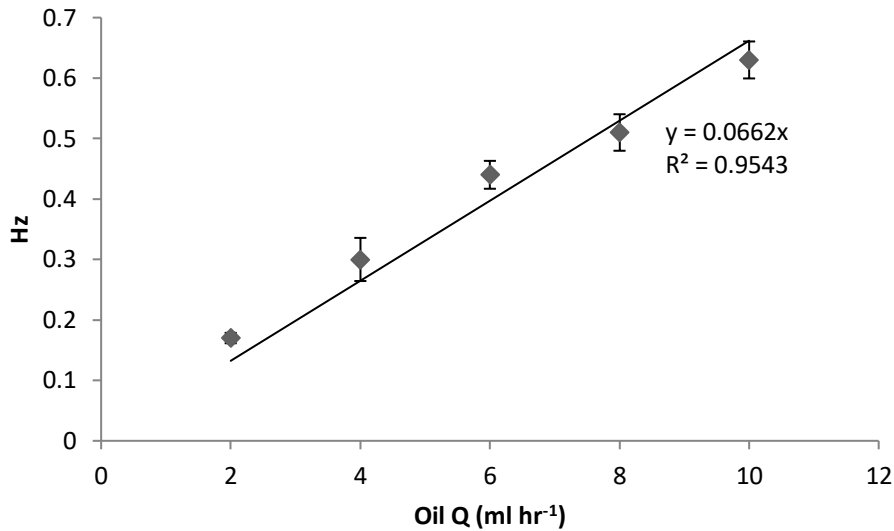
Figure 2.17 Variation of oil droplet generation frequency using the coaxial droplet generator in response to varying oil flow rate (0 - 10 ml hr^{-1}). A linear regression is fitted displaying an R^2 value of 0.9543. This allows for the frequency of oil droplet generation to be predicted for a given oil flow rate when the external water phase is kept constant. Error bars represent standard deviation (n = 5).

The linear trend in Figure 2.17 gives the following relationship for oil droplet frequency of generation:

$$F_o = 0.0662 Q_o$$

Where F_o is the frequency of oil droplet generation (Hz) and Q_o is the oil flow rate (ml hr^{-1}). The *y* intercept is forced to 0 as no droplets are generated when $Q_o = 0$.

This gives the following equation to predict the number of internal aqueous droplets encapsulated for a given frequency of aqueous droplet generation, at an oil flow rate of 10 ml hr^{-1} and a carrier aqueous phase flow rate of 300 ml hr^{-1}:

$$n = \frac{F_w}{0.0662(Q_o + Q_w)}$$

Where n is the predicted number of aqueous droplets encapsulated per W/O/W emulsion, F_w is the frequency of generation of water droplets, and Q_w is the flow rate of the droplet-forming water phase.

101

This could be performed for a variety of carrier aqueous phase flow rates, and compared against empirical data as shown in Figure 2.16 regarding the number of aqueous droplets per W/O/W for the selected flow rates (Figure 2.18).

100 ml hr^{-1}

300 ml hr^{-1}

500 ml hr^{-1}
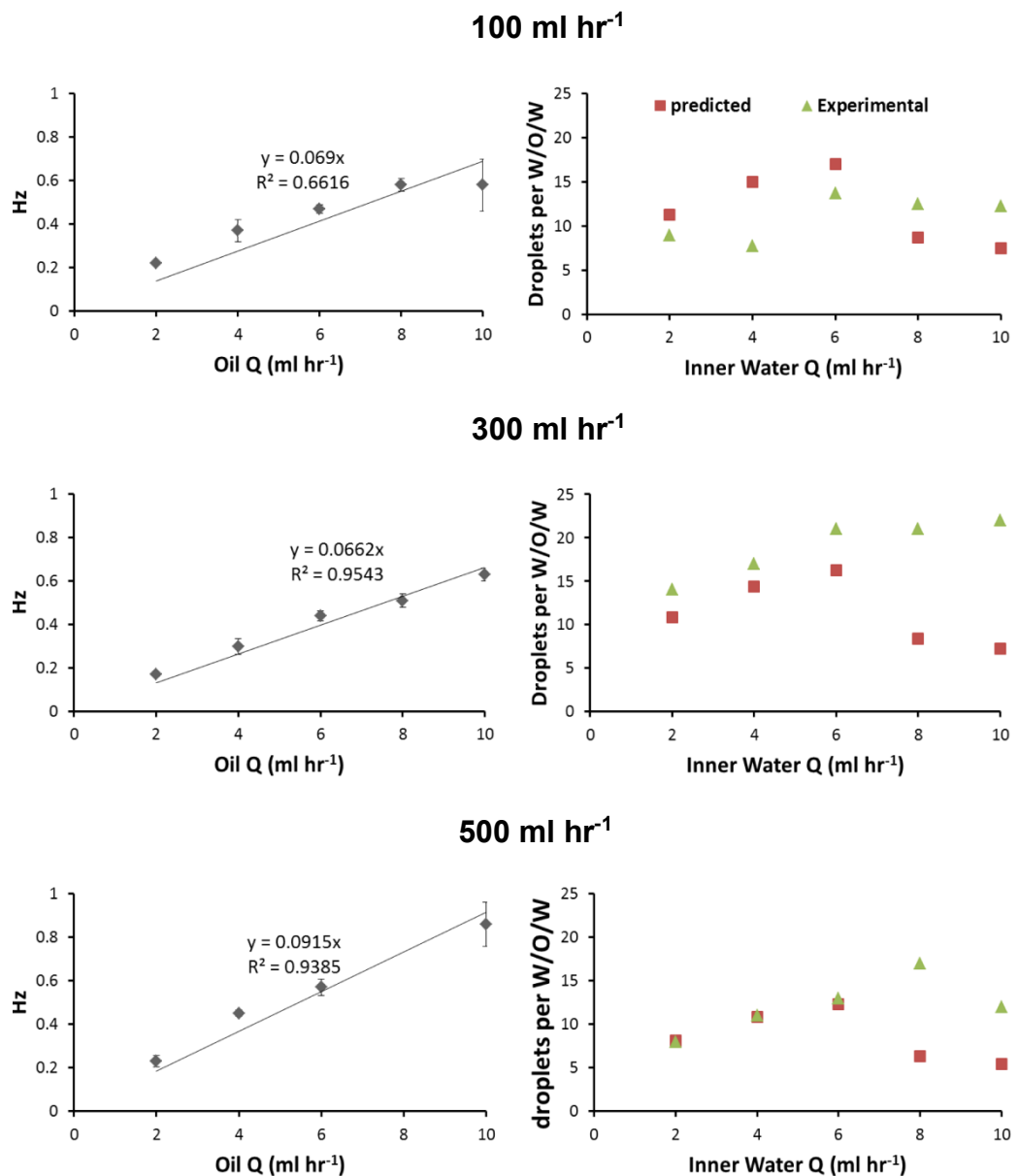
Figure 2.18 The linear trend seen for the generation of O/W droplets for different oil and aqueous carrier flow rates (left). This linear trend can be used to predict the number of aqueous droplets encapsulated per W/O/W emulsions for a given frequency of W/O generation (right – "predicted" in graph). This prediction can then be compared to empirical data (right – "experimental" in graph) obtained. Error bars represent standard deviation (n = 5).

The prediction model described is not able to accurately predict the number of droplets encapsulated per W/O/W emulsion for the majority of flow rates tested, although for an aqueous carrier flow rate of 500 ml hr^{-1} and aqueous flow rates below 6 ml hr^{-1}, the

prediction is accurate ±1 droplet. This is likely because the volume of oil droplets for the aqueous carrier flow rate of 500 ml hr^{-1} is affected less by the oil (and presumably inner aqueous) flow rate than when lower aqueous carrier flow rates are used, as seen in Figure 14a. Also, for the aqueous flow rate of 100 ml hr^{-1}, the data fits a linear regression with low fidelity (R^2 = 0.6639). Overall, the irregularity of aqueous droplet volume and generation frequency in relation to flow rate is likely the reason why these predictions are inaccurate, especially for inner aqueous flow rates above 6 ml hr^{-1}. Thus, the production of W/O/W emulsions would likely benefit from an alternative method of water droplet generation, such as the use of a PMMA chip or a coaxial droplet generator as the one used for oil droplet generation, employing a hydrophobic silane to modify the glass channel in which such droplets are formed. This would likely give rise to a more predictable regime of water droplet formation and hence a higher degree of control and predictability over the number and volume of aqueous droplets encapsulated per oil droplet.

2.3.2.3 Production of W/O/W/O emulsions using a hybrid 3D-printed microfluidic device

The production of W/O/W emulsions as established in the previous section can be used as a chassis to produce DIB networks within an oil droplet, as demonstrated by Elani et al.[71], for example. However, these constructs are inherently fragile because of their fluidic nature, and thus an extra, aqueous layer around the oil droplet would provide the foundation to encapsulate such DIB networks within a solid shell, with appropriate use of polymerisable aqueous fluids such as those that form hydrogels. This would allow for encapsulated DIB networks to be more rugged whilst at the same time able to communicate with an aqueous environment. One route to achieving this is the development of a device capable of producing W/O/W/O emulsions.

The hybrid, 3D-printed microfluidic device shown in Figure 2.8 allows for the alignment of further coaxial, droplet-generating geometries in series. In theory, this set-up would allow for the formation of double, triple and further hierarchical emulsions by aligning a number of coaxial, droplet-generating geometries and channels of alternating hydrophilic/hydrophobic wettabilities and increasing channel diameters. Thus, a device containing two sequentially aligned coaxial, droplet-generating geometries was designed and assembled for the production of W/O/W/O emulsions, using the same design principles as for the production of W/O/W emulsions (Figure 2.8). This device is shown in Figure 2.19.
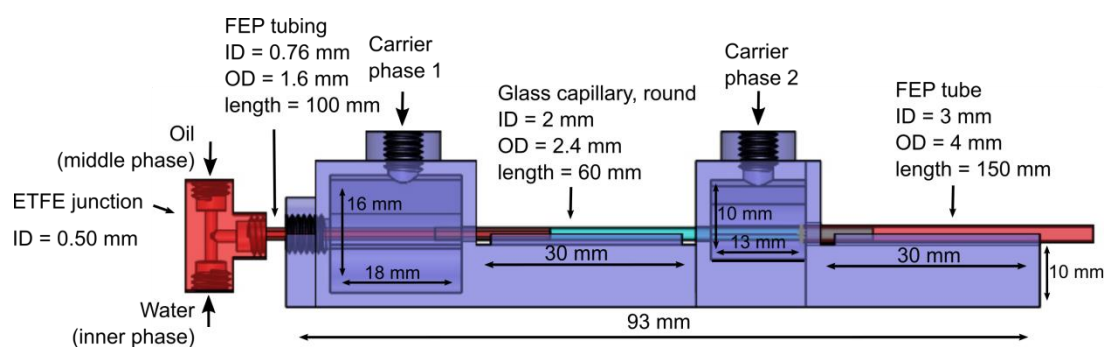
Figure 2.19 CAD image of a hybrid, 3D-printed device to generate W/O/W/O emulsions, where carrier phase 1 is an aqueous fluid and carrier phase 2 is hydrophobic and immiscible with carrier phase 1. The device is composed of a ETFE fluidic connector to generate W/O droplets, and two coaxial droplet-generating geometries as depicted in Figure 2.8, aligned in series. The first geometry is composed hydrophobic channel terminating within a larger hydrophilic channel, enabling the formation of W/O/W emulsions, whilst the second comprises this same hydrophilic channel terminating within a larger hydrophobic channel. This would allow for W/O/W emulsions to be segmented in a second oil flow, forming W/O/W/O emulsions.

With double emulsions considered to be metastable fluidic constructs[72], the production of triple emulsions was challenging as double emulsions formed at the first coaxial geometry would need to pass through a second coaxial geometry, which exerts shear force onto the double emulsion, and can result in coalescence of the different miscible phases. For example, the internal aqueous droplets could coalesce with the external aqueous droplets they are contained in, or the oil droplet containing aqueous droplets could coalesce with the external oil phase. In order to avoid this, surfactants were selected and used to avoid the coalescence of miscible phases (Table 3).

Phase	Surfactant (% v/v)	Comments
Inner water	No surfactant	No surfactant required
Inner oil (squalene)	Span-80 1%	Avoids the coalescence of inner water droplets
Outer water	Tween 0.5%	Avoids the coalescence of inner and outer water phases during the second coaxial geometry in the device.
Outer oil (mineral oil)	Span-80 0.5%	Avoids the coalescence of the inner oil phase and the outer oil phase in the second coaxial geometry and also after W/O/W/O droplets have been formed.

Table 3 Table showing the use of surfactants in the different phases used to form W/O/W/O emulsions. Comments address the rationale for using the surfactants.

Hydrophilic surface modification was employed for the glass capillary (as described in section 2.4.3) and an FEP tube was used as the outer channel of the second coaxial junction, due to its inherent hydrophobicity. The production of W/O/W/O emulsions is shown in Figure 2.20.
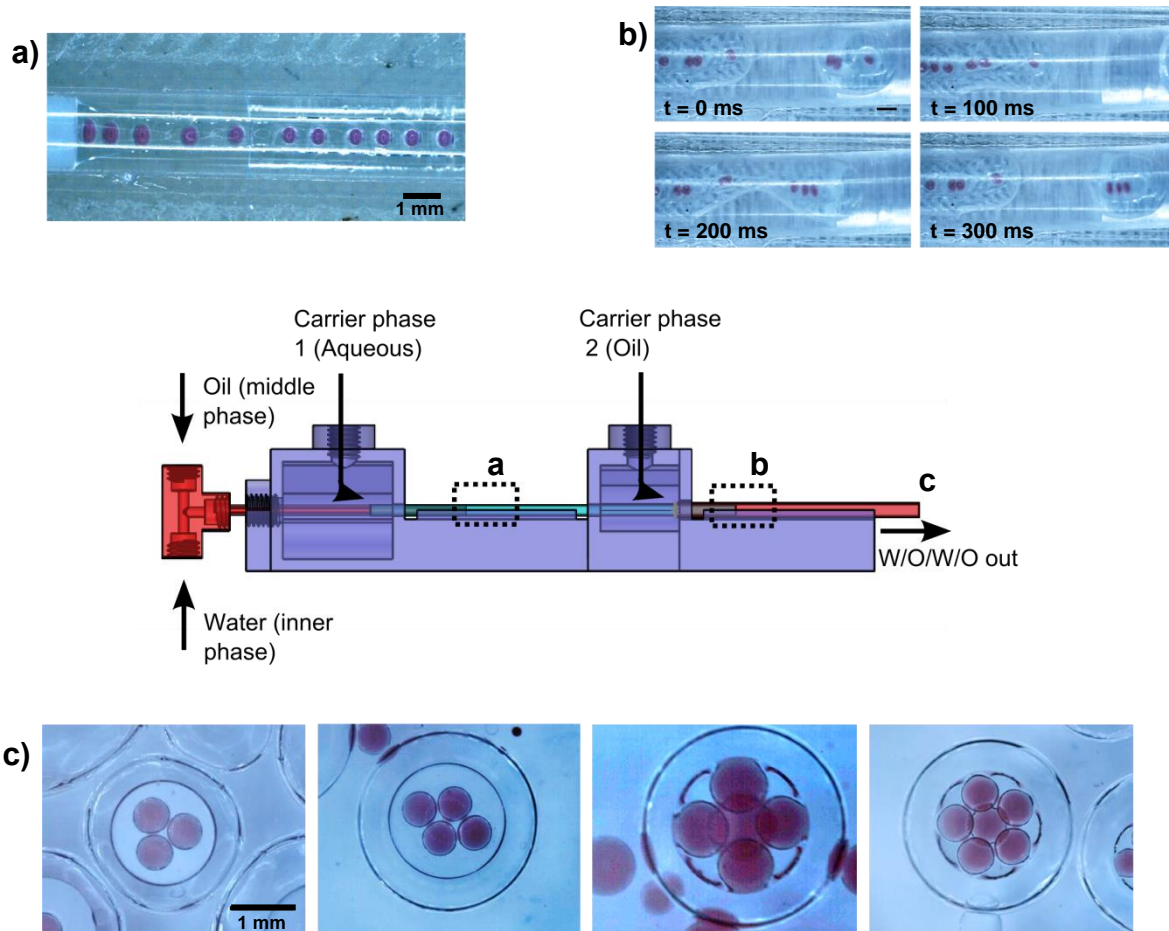
Figure 2.20 Photographs showing the generation of W/O/W/O emulsions and a CAD diagram depicting the hybrid, 3D-printed microfluidic device used, displaying the regions where photographs a), b) and c) are taken. a) Formation of a sub-stream of water droplets in oil flowing parallel to an outer aqueous phase at the first coaxial geometry. b) formation of W/O/W/O emulsions at the second coaxial geometry stage. Here, both the internal oil and external water phase break up into droplets in the external oil phase. c) W/O/W/O emulsions collected from the device containing 3-6 inner aqueous cores. The flow rates employed are 6 ml hr^{-1} for the inner aqueous phase, 8 ml hr^{-1} for the inner oil phase, 200 ml hr^{-1} for the outer water phase and 250 ml hr^{-1} for the outer oil phase.

The use of surfactants in the inner oil and outer water phases changed the manner in which W/O/W emulsions formed in the first coaxial geometry. In comparison to section 2.3.2.2 where W/O/W emulsion formation exhibited a geometrically-controlled regime, here the stream of water droplets in oil did not break up into W/O/W emulsions within the glass capillary, but flowed as a sheath surrounded by the aqueous carrier phase within the same channel (Figure 2.20a). This is likely due to a decrease in surface tension caused by the assembly of surfactants at the oil/water interface, which reduces the drive of the oil to minimise its surface area and assume spherical geometries. This

106

results in fluid flows that are characteristic of high Capillary numbers[15]. The break-up of this sheath flow into droplets occurred in the second coaxial geometry (Figure 2.20b) alongside the breakup of the outer aqueous phase. This gave rise to variability in the number of aqueous droplets encapsulated per W/O/W/O emulsion, as emulsions containing 3-6 inner aqueous were formed using the same set of flow rates (Figure 2.20c). These constructs were output from the device into a petri dish where they were submerged in Mineral oil with 0.5% (v/v) Span-80. They did not remain intact for more than 5 minutes, as the inner oil phase would coalesce with the external oil phase (Figure 2.21). It is likely that this is due to the relatively large size of the droplets and the density difference between the different fluids that compose the emulsion. This behaviour could be exploited for applications requiring controlled release of an aqueous substance, such as for drug delivery.
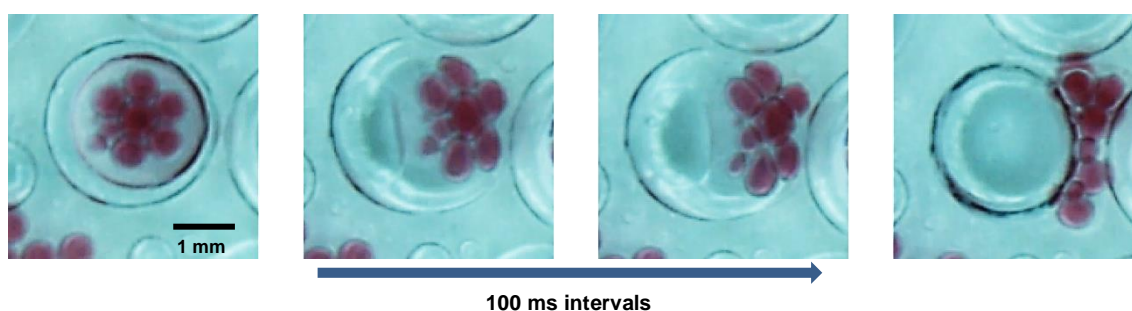
Figure 2.21 W/O/W/O emulsion ejecting the internal oil droplet (containing aqueous droplets) after ≈1 minute of remaining intact in a petri dish filled with the oil carrier phase. Coalescence between the internal oil droplet and the external oil environment ensues, leading to the un-encapsulation of the internal aqueous droplets (dyed red). Scale bar = 1 mm.

2.4 General discussion

2.4.1 Fabrication of a novel, hybrid 3D-printed glass capillary device for the generation of hierarchically assembled higher order emulsions

Using devices fabricated with surface modified glass capillaries, a 3D-printed assembly, and fluidic tubing and connectors, it was possible to produce W/O/W and W/O/W/O emulsions in a facile and cost-effective manner. Glass capillaries displayed

an effective hydrophilic surface modification allowing for the prolonged generation of oil droplets in water; the 3D-printed scaffold aided in the coaxial assembly of the different hydrophilic and hydrophobic channels; and fluidic connectors such as fingertight fittings demonstrated good compatibility with the 3D-printed scaffold in the ability to interface without any leaks.

Devices were constructed for the formation of W/O/W emulsions via the generation of droplets of W/O and its subsequent coaxial flow with an external aqueous fluid, which pinched-off W/O emulsions into W/O/W emulsions. A second, similar device constituting two coaxial droplet-generating geometries allowed for the subsequent pinching off of W/O/W emulsions in oil, forming W/O/W/O emulsions. This method of hierarchical droplet encapsulation offers the potential to add even more emulsification stages, aided via a basic 3D-printed scaffold which can be added and aligned with each other in series.

A particular benefit of the microfluidic devices designed here are their accessibility, ease of use and cost. The devices are assembled from common laboratory materials. For example, glass capillaries are cheap and are used for electrophysiology applications; and fingertight fittings, ETFE junctions and FEP tubing are commonly found as part of high performance liquid chromatography (HPLC) rigs. 3D-printers are likely to be accessible to many research institutions and can be remarkably low cost. 3D-printing also offers the ability for designs to be digitally shared which aids in the accessibility of the devices to other researchers. Specialised equipment or clean room environments are not required except for the surface modification techniques, which require the use of a plasma cleaner. However, as described in section 2.2.1.1, alternatives surface modification techniques exist. All of this serves to increase the ease via which researchers can produce double or triple emulsions for diverse applications, overcoming the microfluidic fabrication barrier[28].

2.4.2 Stability

The stability of W/O/W and W/O/W/O was not thoroughly assessed as the experiments focused on the ability to generate such emulsions. However, W/O/W emulsions were observed to remain intact for at least 1 hour when contained in a glass channel, likely due to the presence of surfactants. This was not true for the case of W/O/W/O emulsions, where the internal oil phase would coalesce with the external oil phase. This is likely due to the compound effect of the emulsions being relatively large and the density difference between the inner oil and outer water phase, causing the inner oil phase to rise in relation to the outer water phase. It is likely that this can be circumvented via the solidification of the outer shell of the emulsion. It remains unknown whether emulsions stabilised with lipid instead of surfactants will be sufficiently stable for droplets to survive the mechanical stress provided by droplet-generating junctions. This is explored in the following chapter. However, there is evidence that that lipid bilayers can form in the presence of Span-80 surfactant, which has been reported to become excluded from a DIB once it has formed[73]. This can provide an alternative route to producing stable encapsulated DIBs if lipid alone fails to stabilise the emulsion interfaces, although further assessment of the mechanism and effectiveness of surfactant exclusion from lipid bilayers would be required.

2.4.3 Monodispersity

The monodispersity of the aqueous droplets, W/O/W and W/O/W/O emulsions remains untested for these experiments. It was observed that droplets were relatively monodisperse, and for droplet volume and frequency of generation as explored in section 2.3.2.1, low standard deviations were obtained (n = 5 for all experiments and conditions). Due to the geometrically-controlled regime of droplet formation and reports in the literature it is likely that high monodispersity is achievable.

2.4.4 Emulsions Size

The emulsions produced here are in the millimetre range and therefore larger than desirable for many most applications including the generation of encapsulated droplet interface bilayers. For this particular application, smaller hierarchical emulsions would allow for higher surface area to volume ratios as well as bilayers of a smaller surface are which would likely increase the stability of the constructs, cheaper experiments due to less usage of reagents, increased efficiency of chemical reactions that require the maintenance of chemical concentrations, as well as the potential to use these constructs as parenteral medical devices for drug delivery, for example. Similar fluidic set-ups for the generation of hierarchical emulsions are seen in the literature, which operate in the micrometre range, giving rise to double emulsions that are 100 - 500 μm in diameter[12, 74].

The geometrically-driven nature of droplet formation, alongside the ability to purchase glass capillaries in the micrometre range and easily scale-down the size of the 3D-printed assembly, mean that it is very likely that the devices presented in this chapter could be scaled down in order to produce smaller emulsions in the ≈100 μm range. This would be the focus of future experiments.

2.5 Conclusion

The work performed in this chapter provides a suitable foundation in order to produce encapsulated droplet interface bilayers templated from hierarchically assembled emulsions. The use of PMMA devices has proved to be challenging due to difficulties in preparing suitably hydrophilic channels. However, a novel microfluidic system has been developed instead which provides the means to generate W/O/W and W/O/W/O using sequentially aligned coaxial droplet-generating geometries, and offers advantages in terms of versatility, accessibility, ease and cost of fabrication. W/O/W emulsion

generation was demonstrated to be possible via dripping and jetting coaxial droplet-generating, with the former involving the use of glass silanisation in order to render channels hydrophilic, and the latter involving the use of surfactants. This adds to the accessibility of the methods described here as a method can be selected depending on the equipment available to the user. The reliability of production in terms of droplet volume, frequency of generation and the number of aqueous droplets encapsulated per W/O/W has been explored here for dripping regimes, which demonstrates some control over these parameters although improvements can be made in order to increase the reliability of double emulsion production. Additional experiments exploring a wider range of flow rates, different sized channels and also the monodispersity of the emulsions produced would support the characterization of the devices explored here. The addition of lipid to the oil phase should allow for the generation of multisome-like structures, and the use of W/O/W/O emulsion can allow for further encapsulation of multisomes allowing for their increased stability by using polymerisable outer shell fluids. Their ability to release internal cargoes (Figure 2.21) may prove useful for applications in controlled release, such as in drug delivery or in food technology and cosmetics[75].

2.6 References

1.   Fujii, T., PDMS-based microfluidic devices for biomedical applications. *Microelectronic Engineering* **2002,** *61–62*, 907-914.

2.   McDonald, J. C.; Duffy, D. C.; Anderson, J. R.; Chiu, D. T.; Wu, H.; Schueller, O. J.; Whitesides, G. M., Fabrication of microfluidic systems in poly(dimethylsiloxane). *Electrophoresis* **2000,** *21* (1), 27-40.

3.   McDonald, J. C.; Whitesides, G. M., Poly(dimethylsiloxane) as a Material for Fabricating Microfluidic Devices. *Accounts of Chemical Research* **2002,** *35* (7), 491-499.

4.   Berthier, E.; Young, E. W. K.; Beebe, D., Engineers are from PDMS-land, Biologists are from Polystyrenia. *Lab on a Chip* **2012,** *12* (7), 1224-1237.

5.   Liu, K.; Fan, Z. H., Thermoplastic microfluidic devices and their applications in protein and DNA analysis. *The Analyst* **2011,** *136* (7), 1288-1297.

6.   Tsao, C.-W., Polymer Microfluidics: Simple, Low-Cost Fabrication Process Bridging Academic Lab Research to Commercialized Production. *Micromachines* **2016,** *7* (12), 225.

7.   Regehr, K. J.; Domenech, M.; Koepsel, J. T.; Carver, K. C.; Ellison-Zelski, S. J.; Murphy, W. L.; Schuler, L. A.; Alarid, E. T.; Beebe, D. J., Biological implications of polydimethylsiloxane-based microfluidic cell culture. *Lab on a Chip* **2009,** *9* (15), 2132-2139.

8.   Okushima, S.; Nisisako, T.; Torii, T.; Higuchi, T., Controlled production of monodisperse double emulsions by two-step droplet breakup in microfluidic devices. *Langmuir: the ACS journal of surfaces and colloids* **2004,** *20* (23), 9905-9908.

9.   Utada, A. S.; Lorenceau, E.; Link, D. R.; Kaplan, P. D.; Stone, H. A.; Weitz, D. A., Monodisperse Double Emulsions Generated from a Microcapillary Device. *Science* **2005,** *308* (5721), 537-541.

10.   Shah, R. K.; Shum, H. C.; Rowat, A. C.; Lee, D.; Agresti, J. J.; Utada, A. S.; Chu, L.-Y.; Kim, J.-W.; Fernandez-Nieves, A.; Martinez, C. J.; Weitz, D. A., Designer emulsions using microfluidics. *Materials Today* **2008,** *11* (4), 18-27.

11.   Ren, P.-W.; Ju, X.-J.; Xie, R.; Chu, L.-Y., Monodisperse alginate microcapsules with oil core generated from a microfluidic device. *Journal of Colloid and Interface Science* **2010,** *343* (1), 392-395.

12.   Adams, L. L. A.; Kodger, T. E.; Kim, S.-H.; Shum, H. C.; Franke, T.; Weitz, D. A., Single step emulsification for the generation of multi-component double emulsions. *Soft Matter* **2012,** *8* (41), 10719-10724.

13.   Martino, C.; Berger, S.; Wootton, R. C. R.; deMello, A. J., A 3D-printed microcapillary assembly for facile double emulsion generation. *Lab on a Chip* **2014,** *14* (21), 4178-4182.

14.   Shang, L.; Cheng, Y.; Wang, J.; Ding, H.; Rong, F.; Zhao, Y.; Gu, Z., Double emulsions from a capillary array injection microfluidic device. *Lab on a Chip* **2014,** *14* (18), 3489-3493.

15.   Nabavi, S. A.; Vladisavljević, G. T.; Gu, S.; Ekanem, E. E., Double emulsion production in glass capillary microfluidic device: Parametric investigation of droplet generation behaviour. *Chemical Engineering Science* **2015,** *130*, 183-196.

16.   Mike Wei, R. S. B., Wetting properties and stability of silane-treated glass exposed to water, air, and oil. *Journal of Colloid and Interface Science - J COLLOID INTERFACE SCI* **1993,** *157* (1), 154-159.

17.   Bhattacharjee, N.; Urrios, A.; Kang, S.; Folch, A., The upcoming 3D-printing revolution in microfluidics. *Lab Chip* **2016,** *16* (10), 1720-1742.

18.   Malek, C. G. K., Laser processing for bio-microfluidics applications (part II). *Analytical and Bioanalytical Chemistry* **2006,** *385* (8), 1362-1369.

19.   Garra, J.; Long, T.; Currie, J.; Schneider, T.; White, R.; Paranjape, M., Dry etching of polydimethylsiloxane for microfluidic systems. *Journal of Vacuum Science & Technology A: Vacuum, Surfaces, and Films* **2002,** *20* (3), 975-982.

20.   Grosse, A.; Grewe, M.; Fouckhardt, H., Deep wet etching of fused silica glass for hollow capillary optical leaky waveguides in microfluidic devices. *Journal of Micromechanics and Microengineering* **2001,** *11* (3), 257.

21.   Choi, C.-H.; Kim, J.; Nam, J.-O.; Kang, S.-M.; Jeong, S.-G.; Lee, C.-S., Microfluidic Design of Complex Emulsions. *ChemPhysChem* **2014,** *15* (1), 21-29.

22.   Walczak, R.; Adamski, K., Inkjet 3D printing of microfluidic structures—on the selection of the printer towards printing your own microfluidic chips. *Journal of Micromechanics and Microengineering* **2015,** *25* (8), 085013.

23.   Sachs, E.; Cima, M.; Williams, P.; Brancazio, D.; Cornie, J., Three Dimensional Printing: Rapid Tooling and Prototypes Directly from a CAD Model. *Journal of Engineering for Industry* **1992,** *114* (4), 481-488.

24.   Xing, J.-F.; Zheng, M.-L.; Duan, X.-M., Two-photon polymerization microfabrication of hydrogels: an advanced 3D printing technology for tissue engineering and drug delivery. *Chemical Society Reviews* **2015,** *44* (15), 5031-5039.

25.   Jariwala, S.; Venkatakrishnan, K.; Tan, B., Single step self-enclosed fluidic channels via two photon absorption (TPA) polymerization. *Optics Express* **2010,** *18* (2), 1630-1636.

26.   Au, A. K.; Lee, W.; Folch, A., Mail-order microfluidics: evaluation of stereolithography for the production of microfluidic devices. *Lab on a Chip* **2014,** *14* (7), 1294-1301.

27.   Waheed, S.; Cabot, J. M.; Macdonald, N. P.; Lewis, T.; Guijt, R. M.; Paull, B.; Breadmore, M. C., 3D printed microfluidic devices: enablers and barriers. *Lab Chip* **2016,** *16* (11), 1993-2013.

28.   Morgan, A. J. L.; Jose, L. H. S.; Jamieson, W. D.; Wymant, J. M.; Song, B.; Stephens, P.; Barrow, D. A.; Castell, O. K., Simple and Versatile 3D Printed Microfluidics Using Fused Filament Fabrication. *PLOS ONE* **2016,** *11* (4), e0152023.

29.   Breguet, V.; Gugerli, R.; Pernetti, M.; von Stockar, U.; Marison, I. W., Formation of microcapsules from polyelectrolyte and covalent interactions. *Langmuir: the ACS journal of surfaces and colloids* **2005,** *21* (21), 9764-9772.

30.   Fixe, F.; Dufva, M.; Telleman, P.; Christensen, C. B. V., Functionalization of poly(methyl methacrylate) (PMMA) as a substrate for DNA microarrays. *Nucleic Acids Research* **2004,** *32* (1), e9.

31.   Hughes, A. J.; Lin, R. K. C.; Peehl, D. M.; Herr, A. E., Microfluidic integration for automated targeted proteomic assays. *Proceedings of the National Academy of Sciences* **2012,** *109* (16), 5972-5977.

32.   Soper, S. A.; Henry, A. C.; Vaidya, B.; Galloway, M.; Wabuyele, M.; McCarley, R. L., Surface modification of polymer-based microfluidic devices. *Analytica Chimica Acta* **2002,** *470* (1), 87-99.

33.   Wink, T.; Zuilen, S. J. v.; Bult, A.; Bennekom, W. P. v., Self-assembled Monolayers for Biosensors. *Analyst* **1997,** *122* (4), 43R-50R.

34.   Huang, T. T.; Sturgis, J.; Gomez, R.; Geng, T.; Bashir, R.; Bhunia, A. K.; Robinson, J. P.; Ladisch, M. R., Composite surface for blocking bacterial adsorption on protein biochips. *Biotechnology and Bioengineering* **2003,** *81* (5), 618-624.

35.   Mashaghi, S.; Abbaspourrad, A.; Weitz, D.; Oijen, A., Droplet microfluidics: A tool for biology, chemistry and nanotechnology. *TrAC Trends in Analytical Chemistry* **2016**.

36.   Makamba, H.; Kim, J. H.; Lim, K.; Park, N.; Hahn, J. H., Surface modification of poly(dimethylsiloxane) microchannels. *Electrophoresis* **2003,** *24* (21), 3607-3619.

37.   Zhou, J.; Khodakov, D. A.; Ellis, A. V.; Voelcker, N. H., Surface modification for PDMS-based microfluidic devices. *Electrophoresis* **2012,** *33* (1), 89-104.

38.   Shah, J. J.; Geist, J.; Locascio, L. E.; Gaitan, M.; Rao, M. V.; Vreeland, W. N., Surface modification of poly(methyl methacrylate) for improved adsorption of wall coating polymers for microchip electrophoresis. *Electrophoresis* **2006,** *27* (19), 3788-3796.

39.   Subramanian, B.; Kim, N.; Lee, W.; Spivak, D. A.; Nikitopoulos, D. E.; McCarley, R. L.; Soper, S. A., Surface Modification of Droplet Polymeric Microfluidic Devices for the Stable and Continuous Generation of Aqueous Droplets. *Langmuir : the ACS journal of surfaces and colloids* **2011,** *27* (12), 7949-7957.

40.   Zhang, Y.; Ping, G.; Kaji, N.; Tokeshi, M.; Baba, Y., Dynamic modification of poly(methyl methacrylate) chips using poly(vinyl alcohol) for glycosaminoglycan disaccharide isomer separation. *ELECTROPHORESIS* **2007,** *28* (18), 3308-3314.

41.   Cras, J. J.; Rowe-Taitt, C. A.; Nivens, D. A.; Ligler, F. S., Comparison of chemical cleaning methods of glass in preparation for silanization. *Biosensors and Bioelectronics* **1999,** *14* (8–9), 683-688.

42.   Erb, R. M.; Obrist, D.; Chen, P. W.; Studer, J.; Studart, A. R., Predicting sizes of droplets made by microfluidic flow-induced dripping. *Soft Matter* **2011,** *7* (19), 8757-8761.

43.   Glass, N. R.; Tjeung, R.; Chan, P.; Yeo, L. Y.; Friend, J. R., Organosilane deposition for microfluidic applications. *Biomicrofluidics* **2011,** *5* (3), 036501-036501-7.

44.   Mukhopadhyay, S.; Roy, S. S.; D'Sa, R. A.; Mathur, A.; Holmes, R. J.; McLaughlin, J. A., Nanoscale surface modifications to control capillary flow characteristics in PMMA microfluidic devices. *Nanoscale Research Letters* **2011,** *6* (1), 411.

45.   Sershen, S. R.; Mensing, G. A.; Ng, M.; Halas, N. J.; Beebe, D. J.; West, J. L., Independent Optical Control of Microfluidic Valves Formed from Optomechanically Responsive Nanocomposite Hydrogels. *Advanced Materials* **2005,** *17* (11), 1366-1368.

46.   Fu, X.; Mavrogiannis, N.; Ibo, M.; Crivellari, F.; Gagnon, Z. R., Microfluidic free-flow zone electrophoresis and isotachophoresis using carbon black nano-composite PDMS sidewall membranes. *ELECTROPHORESIS* **2017,** *38* (2), 327-334.

47.   Rubner, M.; Wardle, B. L.; Cohen, R. E.; Toner, M.; Fachin, F. High definition nanomaterials. US9506846 B2, 2016/11/29/, 2016.

48.   Wang, C. F.; Wang, W. N.; Yang, S. Y.; Chen, L. T.; Tsai, H. Y. In *Preparation and characterization of biomimetic superhydrophobic expanded graphite/carbon nanotube/polymer composites*, 2016 International Conference on Electronics Packaging (ICEP), 2016/04//; 2016; pp 673-676.

49.   Lai, J. Y.; Lin, Y. Y.; Denq, Y. L.; Shyu, S. S.; Chen, J. K., Surface modification of silicone rubber by gas plasma treatment. *Journal of Adhesion Science and Technology* **1996,** *10* (3), 231-242.

50.   Bhattacharya, S.; Datta, A.; Berg, J. M.; Gangopadhyay, S., Studies on surface wettability of poly(dimethyl) siloxane (PDMS) and glass under oxygen-plasma treatment and correlation with bond strength. *Journal of Microelectromechanical Systems* **2005,** *14* (3), 590-597.

51.   Hillborg, H.; Ankner, J. F.; Gedde, U. W.; Smith, G. D.; Yasuda, H. K.; Wikström, K., Crosslinked polydimethylsiloxane exposed to oxygen plasma studied by neutron reflectometry and other surface specific techniques. *Polymer* **2000,** *41* (18), 6851-6863.

52.   Bar, G.; Delineau, L.; Häfele, A.; Whangbo, M. H., Investigation of the stiffness change in, the indentation force and the hydrophobic recovery of plasma-oxidized polydimethylsiloxane surfaces by tapping mode atomic force microscopy. *Polymer* **2001,** *42* (8), 3627-3632.

53.   I. Uba, F.; R. Pullagurla, S.; Sirasunthorn, N.; Wu, J.; Park, S.; Chantiwas, R.; Cho, Y.-K.; Shin, H.; A. Soper, S., Surface charge, electroosmotic flow and DNA extension in chemically modified thermoplastic nanoslits and nanochannels. *Analyst* **2015,** *140* (1), 113-126.

54.   Long, T. M.; Prakash, S.; Shannon, M. A.; Moore, J. S., Water-vapor plasma-based surface activation for trichlorosilane modification of PMMA. *Langmuir: the ACS journal of surfaces and colloids* **2006,** *22* (9), 4104-4109.

55.   David T Eddington, J. P. P., Thermal aging and reduced hydrophobic recovery of polydimethylsiloxane. *Sensors and Actuators B* **2006,** *114*, 170-172.

56.   Fritz, J. L.; Owen, M. J., Hydrophobic Recovery of Plasma-Treated Polydimethylsiloxane. *The Journal of Adhesion* **1995,** *54* (1-4), 33-45.

57.   Hillborg, H.; Tomczak, N.; Olàh, A.; Schönherr, H.; Vancso, G. J., Nanoscale hydrophobic recovery: A chemical force microscopy study of UV/ozone-treated cross-linked poly(dimethylsiloxane). *Langmuir: the ACS journal of surfaces and colloids* **2004,** *20* (3), 785-794.

58.   Jokinen, V.; Suvanto, P.; Franssila, S., Oxygen and nitrogen plasma hydrophilization and hydrophobic recovery of polymers. *Biomicrofluidics* **2012,** *6* (1), 016501.

59.   Vickers, J. A.; Caulum, M. M.; Henry, C. S., Generation of hydrophilic poly(dimethylsiloxane) for high-performance microchip electrophoresis. *Analytical Chemistry* **2006,** *78* (21), 7446-7452.

60.   Ulman, A., Formation and Structure of Self-Assembled Monolayers. *Chemical Reviews* **1996,** *96* (4), 1533-1554.

61.   Bain, C. D.; Troughton, E. B.; Tao, Y. T.; Evall, J.; Whitesides, G. M.; Nuzzo, R. G., Formation of monolayer films by the spontaneous assembly of organic thiols from solution onto gold. *Journal of the American Chemical Society* **1989,** *111* (1), 321-335.

62.   Nihonyanagi, S.; Eftekhari-Bafrooei, A.; Hines, J.; Borguet, E., Self-Assembled Monolayer Compatible with Metal Surface Acoustic Wave Devices on Lithium Niobate. *Langmuir* **2008,** *24* (9), 5161-5165.

63.   Koyano, T.; Saito, M.; Miyamoto, Y.; Kaifu, K.; Kato, M., Development of a Technique for Microimmobilization of Proteins on Silicon Wafers by a Streptavidin−Biotin Reaction. *Biotechnology Progress* **1996,** *12* (1), 141-144.

64.   Rao, S. V.; Anderson, K. W.; Bachas, L. G., Oriented immobilization of proteins. *Microchimica Acta* **1998,** *128* (3-4), 127-143.

65.   Schmitt, Y.; Hähl, H.; Gilow, C.; Mantz, H.; Jacobs, K.; Leidinger, O.; Bellion, M.; Santen, L., Structural evolution of protein-biofilms: Simulations and experiments. *Biomicrofluidics* **2010,** *4* (3).

66.   Zhang, G.-J.; Tanii, T.; Zako, T.; Hosaka, T.; Miyake, T.; Kanari, Y.; Funatsu, T.; Ohdomari, I., Nanoscale Patterning of Protein Using Electron Beam Lithography of Organosilane Self-Assembled Monolayers. *Small* **2005,** *1* (8-9), 833-837.

67.   Singh, J.; Whitten, J. E., Adsorption of 3-Mercaptopropyltrimethoxysilane on Silicon Oxide Surfaces and Adsorbate Interaction with Thermally Deposited Gold. *The Journal of Physical Chemistry C* **2008,** *112* (48), 19088-19096.

68.   Fabrication, sealing and hydrophilic modification of microchannels by hot embossing on PMMA substrate. *ResearchGate*.

69.   K. Castell, O.; J. Allender, C.; A. Barrow, D., Liquid–liquid phase separation: characterisation of a novel device capable of separating particle carrying multiphase flows. *Lab on a Chip* **2009,** *9* (3), 388-396.

70.   Garstecki, P.; Fuerstman, M. J.; Stone, H. A.; Whitesides, G. M., Formation of droplets and bubbles in a microfluidic T-junction—scaling and mechanism of break-up. *Lab on a Chip* **2006,** *6* (3), 437-446.

71.   Elani, Y.; Solvas, X. C. I.; Edel, J. B.; Law, R. V.; Ces, O., Microfluidic generation of encapsulated droplet interface bilayer networks (multisomes) and their use as cell-like reactors. *Chemical Communications* **2016,** *52* (35), 5961-5964.

72.   Ficheux, M. F.; Bonakdar, L.; Leal-Calderon, F.; Bibette, J., Some Stability Criteria for Double Emulsions. *Langmuir* **1998,** *14* (10), 2702-2706.

73.   Jeong, D.-W.; Jang, H.; Choi, S. Q.; Choi, M. C., Enhanced stability of freestanding lipid bilayer and its stability criteria. *Scientific Reports* **2016,** *6*, 38158.

74.   Chu, L.-Y.; Utada, A. S.; Shah, R. K.; Kim, J.-W.; Weitz, D. A., Controllable Monodisperse Multiple Emulsions. *Angewandte Chemie* **2007,** *119* (47), 9128-9132.

75.   Garti, N., Double emulsions — scope, limitations and new achievements. *Colloids and Surfaces A: Physicochemical and Engineering Aspects* **1997,** *123–124*, 233-246.

Chapter 3 – Hydrogel Encapsulated Droplet Interface Bilayers (eDIBs)

3.0 Chapter Summary

In the previous chapter, a microfluidic method was developed in order to produce hierarchical droplet assemblies comprising droplet within droplets, including water-in-oil-in-water (W/O/W) and W/O/W/O. In this chapter, this technology is adapted to produce novel soft matter constructs comprising droplet interface bilayers encapsulated in a hydrogel shell (eDIBs). The construct also allows for the formation of lipid bilayers between the internal compartments and its external environment, enabling the ability of the internal compartments to selectively communicate with an aqueous environment. The presence of artificial lipid bilayers within these constructs is demonstrated via electrophysiology, in addition to the functional insertion of the membrane protein α-Hemolysin. The alginate shell enables the construct to remain stable in different aqueous, air and oil environments, and they are able to withstand mechanical handing which enhances their practicality and applicability as constructs for membrane studies. These properties are demonstrated in this chapter, and along with the high-throughput methods employed to generate eDIBs, they represent a promising platform to carry out high-throughput membrane studies as well as to create artificial cell-like constructs for applications in bottom up synthetic biology.

3.1 Introduction

Artificial mimics of lipid bilayers may not only aid in our understanding of biology via the reduction of complexity necessary to isolate and scrutinise individual processes, but may also find a place within the field of bottom-up synthetic biology[1], as they are a prime candidate to carry out biomimetic compartmentalisation[1].
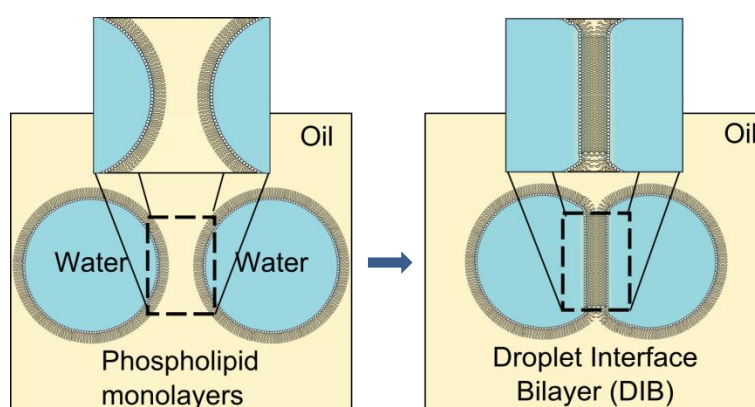

Figure 3.1 Diagram depicting the formation of a droplet interface bilayer (DIB) by contacting two droplets of water in oil with lipid.

Droplet interface bilayers offer a simple and robust method to form artificial lipid membranes (ALMs) via the contact of droplets of water in oil in the presence of lipid [2, 3] (Figure 3.1). In comparison to other methods of forming ALMs (as reviewed in section 1.2.4), DIBs offer practical advantages such as the ability to insert electrodes and spatially control and monitor individual droplets bound by lipid bilayers [2, 4]. As such, DIBs have widened the scope of biophysical membrane study and aided in the advance of single-channel membrane protein studies [5-9]. DIBs can survive for periods of weeks when conditions are such so that evaporation is prevented, such as when the droplets are submerged in oil, further widening their potential applications as device components. The collection of favourable aspects of DIBs as described above grant DIBs great potential in a variety of applications within membrane studies and synthetic

biology. For example, DIB networks have been used as biomimetic electrical components [10, 11] and to complete compartmentalised enzymatic pathways [12, 13]. For a more comprehensive review of DIBs, see section 1.2.4.2.

DIBs have traditionally been prepared manually and individually[2], and, whilst numerous developments have been made in this way, DIB formation methods could benefit from methods that reduce manual preparation and increase experimental throughput. Microfluidics offers an alternative method of producing and experimenting with DIBs, due to its ability to produce highly monodisperse droplets in a rapid and automatic manner (see section 1.3.2) [14-18]. A number of microfluidic methods have been employed to generate DIBs by exploiting the rapid assembly of lipid monolayers caused by the flow of droplets of water in oil[19], and device geometries that allow these droplets to be kept in close contact with each other[14, 16-18, 20].

Whilst conventional DIB formation occurs in a bulk oil phase (Figure 3.1), the ability to form DIB networks that are freestanding in an aqueous environment would allow them to act as individual synthetic cells and would open up a wealth of possibilities if able to form bilayers with an external aqueous environment. By being untethered, the constructs could be used outside of laboratory environments or in high-throughput endeavours, and allow for novel handling capabilities. Sub-compartmentalisation within a network of bilayer-connected droplets would allow for the potential of spatially segregated chemical pathways and cascades which may be useful in biosensing or biochemical engineering applications for the production of valuable chemicals and pharmaceuticals[21]. Thus, value exists in producing a DIB system with such characteristics.
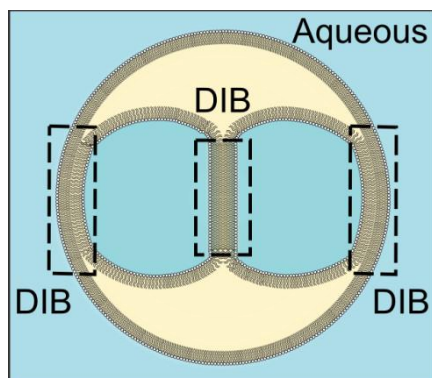
3.1.1 Multisomes

Figure 3.2 A multisome, comprised of a number of aqueous droplets contained within an oil droplet (containing lipid) in water. Monolayers assemble at the oil/water interface, and form bilayers when in close proximity with each other. Thus, DIBs form between the internal droplets and also between the internal droplets and the external aqueous environment.

In 2011, Villar et al. conceived a system which comprised of DIB networks that can exist and interface with an external environment with lipid bilayers [22, 23]. Multisome structures constitute aqueous droplets that are encapsulated within a droplet of oil, facilitating the formation of interface bilayers between the internal droplets and the external environment via the close contact of the different water/oil interfaces (Figure 3.2). This allows for the function of DIB networks in aqueous environments where communication with its surroundings can be achieved through the incorporation of membrane proteins, not unlike biological cells [22, 23]. Similar bilayer networks have since been developed by Elani et al. that dispense with the oil phase, by passing a network of DIBs in oil through an oil/water interface, yielding multi-compartment vesicles (MCVs), as the monolayer formed between the oil/water interface wraps around the monolayer that surrounds the DIB network in oil[12]. These constructs might be useful for applications where the oil phase in multisomes can be a burden, such as in potential drug delivery systems, however the multisome oil phase may be useful in providing with buoyancy, structural stability or as a reservoir for oil-soluble substances such as lipids.

Multisomes and MCVs have demonstrated to be able to spatially segregate enzymatic pathways[12, 13] and communicate with their surrounding environment via membrane proteins[13, 23], and multisomes have been produced using microfluidic methods[13]. These systems therefore embody potential candidate structures for development into future medical and industrial applications for their ability to incorporate selectively-communicating compartments that can interface with physiological (i.e. aqueous) environments.

However, multisomes are hampered by the inherent fragility of fluidic constructs which is necessary to survive in environments that do not enjoy precise laboratory control. Current demonstrations thus far have remained limited to structurally supported droplets[23] or contained within a microfluidic channel[13], which limits their potential as they are not truly freestanding. Multisomes often rupture when in contact with water-air interfaces or with container walls, requiring careful control of buoyancy in order for them to remain intact. This is demonstrated in section 3.3.2.1 (Figure 3.10). As such, a step-change is hereby proposed by embedding DIB networks within a permeable, yet mechanically rigid shell composed of a suitable hydrogel (Figure 3.3). This would provide the necessary foundation in order for DIB networks to be used as truly freestanding devices that may be able to function outside of a controlled laboratory environment and survive mechanical handling. Alginate is selected as a hydrogel-forming agent as its transition from liquid to hydrogel can be controlled within a microfluidic device (see section 3.1.2.2), and also presents with a number of suitable properties as listed in Appendix 4.
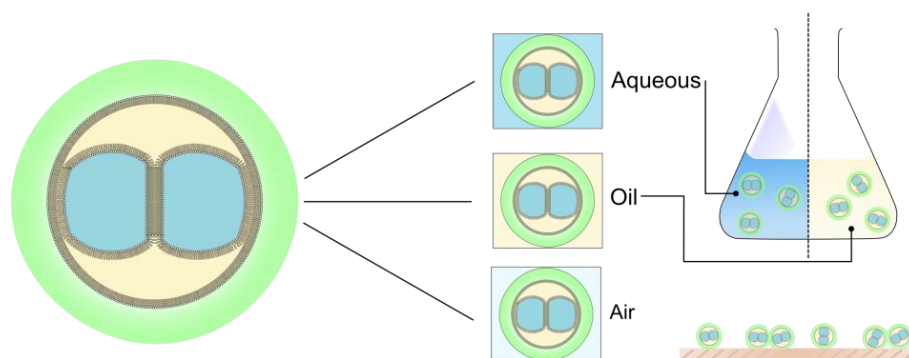
Figure 3.3 An encapsulated droplet interface bilayer (eDIB) construct, comprised of a number of aqueous droplets (blue) in an oil droplet (orange) which is encapsulated in a hydrogel shell (green). This would allow DIBs to contained within a solid structure and therefore gain in ruggedness and stability, whilst at the same time still able to form DIBs between the internal droplet and external environment, conceded by the aqueous nature of the hydrogel. In this manner, eDIBs should be able to exist in both aqueous, oil and air environments.

3.1.2 Alginate

Alginates are polysaccharide polymers that are found abundantly in the cell walls of brown seaweed (Phaephyceae). Alginic acid is a linear polymer with homopolymeric blocks of (1-4)-linked β-D-mannuronate and its C-5 epimer α-L-guluronate (Figure 3.4), separated by blocks of random or alternating mannuronic and guluronic acids[24].
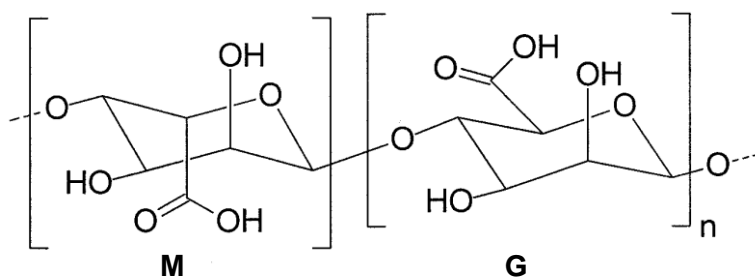
Figure 3.4 Chemical Structure of a typical alginate monomer. M and G denote the mannuronate and guluronate blocks, respectively.

The proportion of such blocks as well as the molecular weight of the alginate differs per alginate source and preparation, resulting in different physical properties[25]. Importantly, alginic acid can be hydrated forming viscous hydrogels that are heat-stable at room temperature[25], where the water molecules are entrapped within the alginate matrix due to capillary forces, but are still able to move within the polymer[26].

Figure 3.5 The ionotropic cross-linking of alginate using calcium ions. The calcium ions specifically bind the guluronic acid blocks, and co-ordinated alginate chains overlay adjacent chains forming an "egg box" structure. Diagram adapted from referenced publication[27].
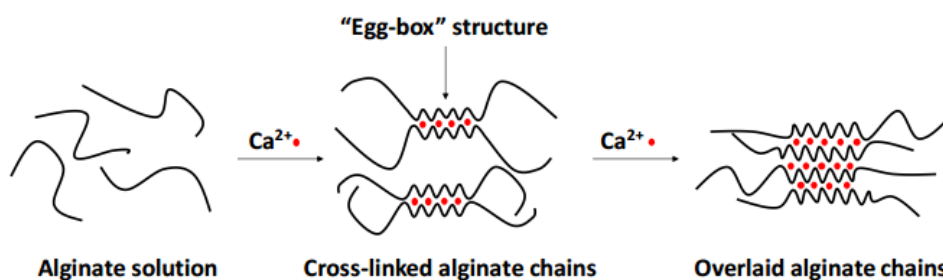
Alginate can exist in a soluble salt form, such as when bound to sodium ($NaC_6H_7O_6$). Monovalent metal ions form soluble alginate salts, whilst multivalent cations (such as Ca^{2+} but excluding Mg^{2+}) cross-link guluronic acid blocks within the alginate to form ionotropic alginate hydrogels via what is commonly known as the "egg-box" model [28] (Figure 3.5). Covalently bonded alginate hydrogels can also occur when alginate chains are cross-linked using poly(ethylene glycol)-diamines [25]. Alginate polymers can be degraded using enzymatic processes[29] or microwaves exposure[30]. Ionotropic alginate hydrogels can be easily dissolved using a calcium ion chelation agent such as EDTA [31].

3.2.2.1 Alginate properties and applications

The physical properties of alginate hydrogels are dependent on the ratio of guluronic to mannuronate blocks (G/M ratio), with alginates rich in guluronic presenting higher gel strength, swelling and viscoelasticity due to the higher affinity of guluronic acid residues to divalent ions. Alginates rich in mannuronic acid are believed to offer better long-term stability[32]. Alginates with a high molecular weight provide gels with more robust mechanical properties[33].

Alginate hydrogels respond to mechanical stress differently depending on whether they are ionically or covalently cross-linked. Ionotropic alginate hydrogels give rise to plastic

deformation under mechanical stress, which causes loss of water content and a stochastic reformation of ionic bonds. Covalently linked alginate hydrogels do not experience the dissociation of bonds, and therefore give rise to elastic deformation[34].

Alginate and its related salt forms are generally regarded as biocompatible [35-39], although impurities may remain as it is obtained from natural sources[40]. Thus, they are extensively employed within the biomedical, pharmaceutical and cosmetic industries due to their thickening, gel-forming and stabilizing properties[41]. The ability to controllably gel alginate into capsules or beads makes it suitable for encapsulation processes for drug delivery[25, 32, 39, 42, 43], cell encapsulation[38, 44-50] or the formation of biomimetic, soft matter constructs[51, 52]. Alginate hydrogels present numerous physical characteristics that are suitable for these encapsulation purposes, and make them ideal for the encapsulation of DIB networks, as it has already been shown that DIBs can form between aqueous droplets and hydrogels[2] and between alginate hydrogel shapes[53]. A summary of the physical characteristics of alginate hydrogels is given in Appendix 4.

Additionally, practical considerations allow alginate to be used to generate monodisperse capsules within a microfluidic device, using gelation methods that can be classified as being either internal or external[42]. Internal gelation requires an insoluble calcium salt to be present in the same solution containing alginate, such as calcium carbonate, which can solubilise upon acidification. Conversely, external gelation occurs when an alginate solution is brought into contact with a solution containing divalent cations, where this solution can be miscible with the alginate or not. Gelation method is reported to significantly change certain hydrogel properties such as pore size and matrix density[54], and particular purposes will benefit from an appropriately selected method. For example, for drug delivery, internally gelled alginate hydrogels offer a lower encapsulation efficiency and faster release than externally

gelled alginate hydrogels[42]. Internally gelled alginate hydrogels are reported to be more homogeneous[55], with externally gelled alginates beads often reported to contain a liquid core of the un-gelled alginate solution[51, 52, 56, 57].

In the context of the production of droplet interface bilayer networks encapsulated within a hydrogel shell, an internal mode of gelation is more desirable because of the improved homogeneity and permeability of such hydrogels[42, 55], which are required in order to provide with robustness and the ability to interact with an aqueous environment, respectively.

3.2.2.2 Alginate gelation & microfluidics

Alginate solutions are shear-thinning fluids (and therefore Non-Newtonian) [58] of which role in the rheology of droplet formation is not yet fully understood [59], but is known to be problematic with regards to droplet monodispersity[60, 61]. In comparison to Newtonian fluids, the extensional viscosity of shear-thinning fluids can cause an alginate solution stream to resist droplet pinch-off and give rise to fluid jets which break off into heterogeneous droplets[60]. Effective capillary numbers can be calculated that account for shear-thinning effects and used to generate monodisperse droplets via flow rate modulation [59].

Furthermore, it is important that the rate of gelation is controlled in order to avoid early and undesired formation of hydrogel which may obstruct continuous fluid flow, especially at the point of droplet formation. For this reason, an internal gelation method is preferred using low solubility calcium salts such as calcium sulphate and calcium carbonate, as this offers a higher degree of control than external gelation methods, which have been reported to give rise to quick, but poorly controlled gelation[62]. Using internal gelation methods, the rate of acidification, and hence gelation, can be extensively controlled[63] via the choice and concentration of acid, initial pH of the

alginate solution, the use of a buffer solution, and the concentration and particle size of calcium carbonate.

Alginate hydrogels in the form of capsules and beads have effectively been produced using microfluidic methods [47, 48, 64-69] which present with significant advantages in terms of control, homogeneity and uniformity in comparison to previous methods, including conventional emulsification[70] and electrostatic droplet extrusion[71]. Droplets of oil have been encapsulated within alginate shells[57, 67] using sequential coaxial droplet generating flows and an external gelation method relying on the partition of un-gelled O/W/O emulsion droplets from an oil phase into an aqueous phase containing calcium chloride[67].

3.1.3 Chapter aims

As described in this introduction, there is great value in producing hydrogel-encapsulated DIBs (eDIBs) which can contain DIB networks and communicate with an external aqueous environment via lipid bilayers. The hydrogel shell can provide with environmental compatibility and provide with robustness in comparison to previously described systems, such as multisomes and MCVs, allowing for the constructs to be fully freestanding and withstand mechanical handling. For this, the microfluidic methods used to produce W/O/W/O emulsions in the previous chapter will be adapted in order to controllably generate eDIBs in large numbers. The amphiphillic properties of lipids should allow for aqueous droplets to avoid coalescence, and thus forgo the use of surfactants as seen in section 2.3.2.2 and 2.3.2.3. Additionally, an external gelation method for alginate as described in section 3.2.2.2 should allow for the gelation of the alginate shell to occur after droplet formation, allowing for the continuous, *in situ* production of gelled eDIBs. Electrophysiology will be performed in order to demonstrate the formation of lipid bilayers between the internal compartments and the external environment of eDIBs, via capacitance measurements and also the incorporation of α-

Hemolysin membrane proteins. Finally, the ability of eDIBs to survive in aqueous, air and oil environments will be demonstrated.
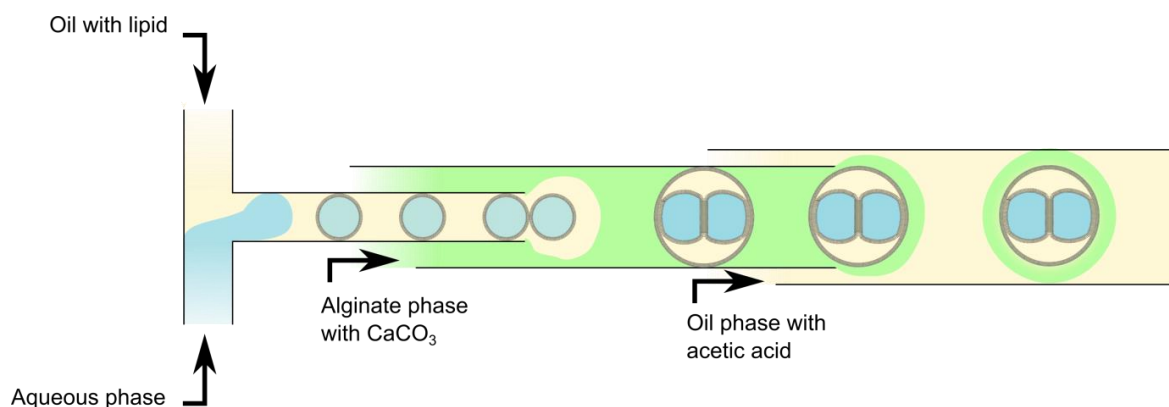

Figure 3.6 Diagram depicting the microfluidic approach employed to generate eDIBs. A T-junction is employed to generate droplets of water in oil with lipid, which is then passed through a first coaxial droplet generator flowing alginate with dispersed $CaCO_3$. The resulting flow is passed through a second coaxial droplet generator flowing oil with acetic acid, producing eDIBs. Gelation of the alginate phase occurs as the acetic acid from the oil phase partitions into the alginate phase, lowering the pH and dissolving $CaCO_3$ particles, which releases Ca^{2+} ions that trigger gelation.

3.2 Methods

All chemicals have been purchased from Sigma-Aldrich UK unless stated otherwise. Methods pertaining the design of the microfluidic devices employed are described in section 2.4.1.

3.2.1 Preparation of fluids

Lipid in oil solution: Lyophilised 1,2-diphytanoyl-*sn*-glycero-3-phosphocholine (Avanti Polar Lipids, USA) was dissolved in chloroform and dried down using nitrogen gas into a lipid film that adhered to the glass vial container. Once the lipid film was visibly dry and free of any chloroform, a 1:1 solution of hexadecane oil and silicone oil (AR20) was added to the vial to reach a lipid concentration of 5 mg mL^{-1}. The solution is rested overnight to allow the lipid to fully dissolve in the oil mixture.

Alginate solution: 2% w/v low viscosity sodium alginate, 5 mg mL^{-1} calcium carbonate nanoparticles and sodium chloride to make up a total ionic strength of 0.5 M are added to deionised water and stirred with use of a magnetic stirrer at 360 rpm for at least 3 hours, resulting in a homogeneously opaque and viscous solution.

Carrier oil solution: 0.5% v/v glacial acetic acid is added to light mineral oil (Sigma-Aldrich product nº M8410) and stirred for at least 30 minutes until the solution appears clear and homogeneous.

Aqueous solution: Aqueous solutions used for droplet interface bilayers consisted of 50 mM dibasic sodium phosphate and sodium chloride to make up a total ionic strength of 0.5 M. 50 µM Sulphorhodamine B or 1 mM Lissamine Green are added for colour (resulting in a pink or blue colour, respectively).

α-Hemolysin: α-Hemolysin heptamers were prepared by Dr. Oliver Castell[1] at a concentration of ≈30 nM in a 10 mM imidazole, 0.5 M NaCl, 20 mM HEPES, pH 8 buffer. The solution was kept at -80ºC, and aliquots were diluted to ≈3 nM, and kept at 5ºC for electrophysiology experiments. These aliquots were used within a week of their preparation and kept on ice during use.

3.2.2 Microfluidics

A 3D-printed microfluidic device for the generation of triple emulsions via coaxial droplet generating geometries is employed as described in Chapter 2. 3 mL or 25 mL plastic, luer lock syringes (Fisher Scientific, UK) are filled with the fluids and air bubbles are expelled. The fluids are dispensed using perfusion syringe pumps (Legato™ series single and double syringe pumps, KD Scientific, USA).

Table 1 shows a typical regime of flow rates employed to generated eDIBs as well as notes regarding the operation of the microfluidic device.

Fluid	Syringe Size	Flow Rate (mL hr^{-1})	Order of flow	Notes
Internal aqueous phase	3mL syringe			These fluids are pumped using the same syringe pump.
Lipid-in-oil phase	3mL syringe	11.76	3rd	Prior to the production of eDIBs, these fluids should be pumped until the FEP tube that delivers these fluids into the first coaxial droplet generator is filled with a monodisperse regime of droplets of water in oil. For the production of eDIBs, these fluids should be pumped only whence the device output FEP tube is filled with a monodisperse regime of alginate droplets in the carrier oil.
Alginate phase	25mL syringe	250	1st	The fluid must not be kept in the syringe for longer than 30 minutes prior to use as the CaCO$_3$ will separate from the mixture.
Carrier oil phase	25mL syringe	400	2nd	n/a

Table 1 Flow rates used per fluid in the microfluidic manufacture of eDIBs, plus additional comments regarding the operation of the microfluidic device.

As the device is used, an accumulation of polymerised alginate may occur at the orifice of the glass capillary, obstructing the even flow of both the alginate and oil phase. A 100 mM EDTA solution is used to dissolve the adhered hydrogel, which is pumped through both the alginate and carrier oil inlets of the microfluidic device so that the affected areas are kept in this solution for at least 30 minutes. This can then be rinsed to get rid of the dissolved alginate and EDTA, and microfluidic operation resumed.

3.2.3 Electrophysiology

Electrophysiology was performed using custom electrodes connected to an Axopatch 200B with a 203BU headstage (Molecular Devices, USA). The electrode tips are coated in a droplet (pL volume range) of agarose, performed by briefly dipping the tip of

the electrode onto a glass coverslip containing 5 μL of a 7.5 mg mL^{-1} solution of low melting point agarose in deionised water, which is kept at 90⁰ on a heating block.

Electrophysiology recordings of bilayer capacitance and ion flux were made under applied potentials of a +/- 23 mV triangle wave at 1 Hz or a fixed potential of 10-50 mV, respectively. Data was recorded with the software WinEDR (University of Strathclyde). Electrophysiology traces were analogue filtered using the Axopatch 200B equipment (low-pass, 5 Khz) and digitally filtered post-acquisition with either a 100 Hz low-pass filter.

Droplet-droplet DIB electrophysiology is performed by pipetting two 0.2 μL droplets into a micromilled PMMA trough filled with a 1:1 mixture of hexadecane and silicone oil AR20 containing 5 mg mL^{-1} DPhPC lipid. The droplets are anchored onto the electrodes. eDIB electrophysiology is performed by placing eDIBs in a petri dish submerged in mineral oil. The eDIB hydrogel shell is pierced to access the internal cores with the electrodes. The tip of the electrode containing a droplet of agarose is then inserted into the internal cores. Electrodes are mounted onto micromanipulators (Narishige, Japan).

3.2.3.1 Electrode preparation

A wire is prepared by stripping both sides of it (around 2 cm), exposing the internal wire filaments. A male crimp pin is soldered to one end and a female crimp pin to the other. The male crimp pin connects to the 203BU headstage whilst the female crimp pin connects to the Ag/AgCl electrode used for either droplet-droplet DIB or eDIB electrophysiology measurements.

Droplet-droplet Ag/AgCl electrodes are prepared from 3-6 cm of 0.1 mm diameter silver wire. The AgCl tip is prepared by lightly sanding the wire tip (around 2 mm) and exposing it to a solution of sodium hypochlorite for 30 minutes. The exposed tip will

129

darken, which indicates that the silver wire tip has undergone chlorination. This silver wire can now be soldered to the female crimp pin to complete the electrode.

Electrodes used for eDIB measurements are prepared differently, as they must be able to pierce the alginate shell and also be shielded from it in order to avoid short circuits when probing the internal droplets. When electrophysiology is performed to probe the bilayers formed between internal eDIB cores and the alginate shell, only the electrode that pierces the internal cores needs to be prepared in this way.

Firstly, a glass capillary (1 mm ID, CM Scientific, UK) is pulled using a capillary puller, in order to produce a tapered and sharp capillary tip. The glass capillary is then cut from the non-tapered end so that the non-tapered part of the glass sheath is around 3 cm long. Ag/AgCl silver wire treated as described above is inserted into the glass capillary through the non-tapered side of the glass sheath so that it reaches the inside of the tapered side of the glass. Then, the tapered tip can be broken with aid of tweezers in order for the silver wire to exit through the tapered end of the glass. The electrode wire is then passed through the glass capillary so that roughly 1 mm of untreated wire is exposed from the tip (Figure 3.7a). Epoxy resin is applied to the non-tapered end of the glass capillary in order to fix the silver wire in place, and set aside for 20 minutes in order to dry.
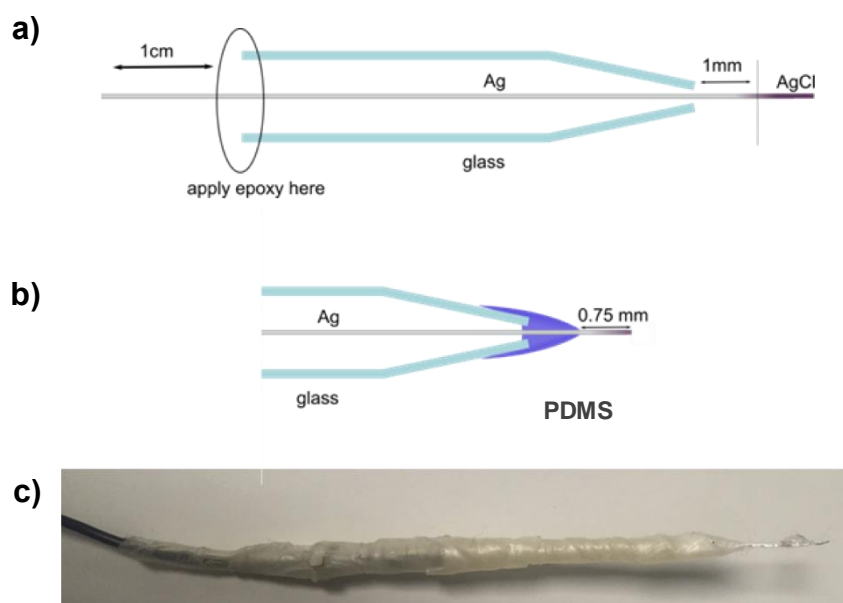
Figure 3.7 Preparation of electrodes for eDIB electrophysiology. a) Schematic depicting the stages in the preparation of an eDIB electrode prior to the fixing of the electrode wire within the pulled glass capillary with epoxy resin. b) Schematic of the tip of the eDIB electrode at its final stage. c) Photograph showing the finished electrode, which has mostly been covered in parafilm in order to protect the fragile glass sheath around the silver wire.

Polydimethoxysilane (PDMS) (2-part Sylgard 184 elastomer, DOW Corning, UK) is prepared to seal the junction between the tapered side of the glass and the tip of the electrode (Figure 3.7b). The tip of the electrode is briefly dipped into the PDMS solution, which forms a droplet of PDMS between the glass capillary and the silver wire. The electrode is then heated in an oven at 120 ºC for 30 minutes to cure the PDMS. The process of dipping the tip in PDMS and curing the resulting droplet is repeated until only 0.75 mm of un-chlorinated silver wire is left exposed at the tip. Each subsequent repetition will grow onto the solid droplet of PDMS cured from the first instance which gradually reduces the exposed length of the wire. Once the desired length of 0.75 mm is reached, the excess chlorinated silver wire can be cut off using a scalpel, and the glass electrode soldered onto the female crimp pin. To finalise the process, parafilm is used to secure the glass electrode in place, especially at the junction between the crimp pin and the glass capillary where it is most fragile (Figure 3.7c).

A 7.5 mg ml^{-1} solution of low-melting point agarose in DI water was prepared and kept at 90°C. The electrode tip was dipped in this solution prior to its use for electrophysiology, in order to encourage the wetting and hence the penetration of the electrode tip into water droplets contained within an eDIB.

3.3 Results & discussion

3.3.1 Droplet-droplet electrophysiology

Firstly, DIB formation between two droplets in bulk oil (1:1 ratio of silicon oil and hexadecane with 5 mg mL^{-1} DPhPC) was attempted in order to characterise bilayer capacitance and ion flux resulting from the insertion of α-Hemolysin pores. This was performed in order to provide a foundation for DIB formation and establish a benchmark via which subsequent eDIB bilayer measurement could be compared to.

Droplet-droplet electrophysiology demonstrated the formation of DIBs between aqueous droplets as well as the insertion of α-Hemolysin membrane protein pores into the bilayer (Figure 3.8).
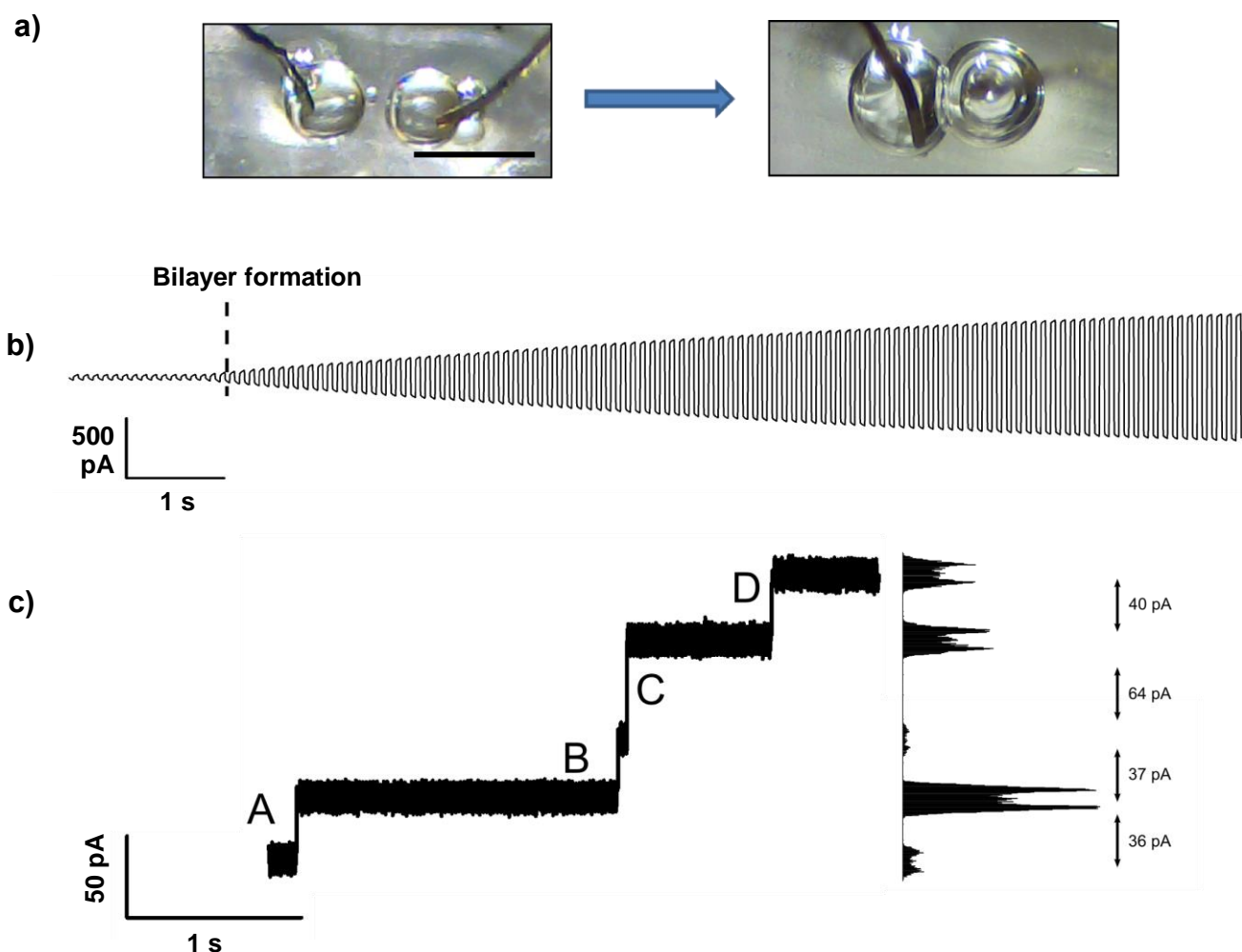
a)

b)

Bilayer formation

500 pA

1 s

c)

Figure 3.8 Droplet-droplet electrophysiology experiments. a) Photographs showing the formation of a DIB between two 0.2 µL aqueous droplets submerged in a 1:1 mix of hexadecane and silicone oil (AR20) containing 5 mg mL^{-1} DPhPC. The droplets are anchored on electrodes mounted on micromanipulators. A lipid bilayer forms between the droplets when they are brought in close proximity. Scale bar = 1 mm. b) Electrophysiology traces of the droplets shown in a). A 10 Hz, +/- 23 mV triangle wave potential is applied between the droplets, showing a capacitive current trace (above). This capacitive current trace increases in amplitude as the bilayer forms and increases its area. The dotted line represents the approximate point in time at which the bilayer starts to form. c) Electrophysiology trace of a droplet-droplet DIB under an applied voltage of 50 mV. The droplets contain 1M KCl, 50 mM NaH2PO4 and the transmembrane protein α-Hemolysin. A, B, C and D designate steps in current that correspond to α-Hemolysin insertions.

3.3.1.1. Bilayer formation

Bilayer formation between two aqueous droplets was evidenced via electrophysiology

traces which demonstrated characteristic bilayer capacitance when a triangle wave

potential is applied to the bilayer (Figure 3.8b). Prior to bilayer formation, minor capacitance is seen displaying a peak-to-peak amplitude of around 30 pA, which indicates the close proximity of the droplet interfaces (Figure 3.8b). This dramatically increases up to 1010 pA which corresponds to the formation of a droplet interface bilayer which can be visually confirmed (Figure 3.8a). The capacitive current trace displays a small gradient at its peaks which is an indication of bilayer leakage. The capacitance of the bilayer is given by:

$$F = \frac{A}{dV/dt}$$

Where F is capacitance (Farads), A is current (Amperes), V is voltage (Volts) and t is time (seconds).

This gives a bilayer capacitance of 2174 pF. According to the referenced publication, this gives a bilayer area of 0.33 mm^2 for DPhPC DIBs in hexadecane, which would correspond to a circle diameter of 0.63 mm[72]. This is within range of an expected bilayer diameter for a pair of 0.2 µL droplets of which diameter (assuming they are spheres) is 0.73 mm. Specific capacitance is calculated to be 0.667 µF cm^{-2} which is identical to that reported in the selected literature, for DPhPC DIBs formed in a 1:1 mixture of hexadecane and silicon oil AR-20[72].

3.3.1.2. Insertion of the membrane protein α-Hemolysin

The incorporation of the transmembrane protein pore α-Hemolysin into droplet-droplet bilayers was demonstrated. Once a DIB has formed, insertions of the transmembrane pore in the membrane were visualised using electrophysiology as stepped increases in current under an applied 50 mV potential (Figure 3.8c). A number of steps in current can be seen in the trace (A, B, C and D in Figure 3.8c), which likely correspond to insertions of α-Hemolysin single channels into the membrane. Assuming that step C

constitutes a simultaneous insertion of two α-Hemolysin channels, the average step size is 35.4 ± 3.44 pA.

3.3.2 Microfluidic production of encapsulated droplet interface bilayers (eDIBs)

3.3.2.1 Production of multisomes with control over the number and identity of inner aqueous cores.

Using the 3D-printed microfluidic device for the production of W/O/W emulsions described in Chapter 2, multisomes were produced by using squalene with 5 mg/mL DPhPC as the oil phase, providing the lipid in order to produce DIBs between the internal cores and between the internal cores and the external aqueous environment. Control over the number of inner cores was demonstrated by varying the flow rate of the inner, middle and outer phases of the droplet system, with the ability to controllably produce multisomes containing up to four inner aqueous cores (Figure 3.9a-c). The diameters of these multisomes appear to be 2 mm, which is the internal diameter of the capillary in which they are produced.

The ability to produce multisomes containing cores of different identity is also demonstrated. A 3D-printed microfluidic device (Figure 3.9e) is used which allows for the sequential generation of droplets of water in oil of alternating composition (Figure 3.9d and f), using two droplet-generating T-junctions, and a hydrophobic channel surface composed of PLA polymer. It was possible to generate multisomes containing two cores of different identities at a frequency of 2.5 Hz using a flow rate of 1 ml hr^{-1} for the internal aqueous phases, 4 ml hr^{-1} for the oil phase and 300 ml hr^{-1} for the external aqueous phase.

c)
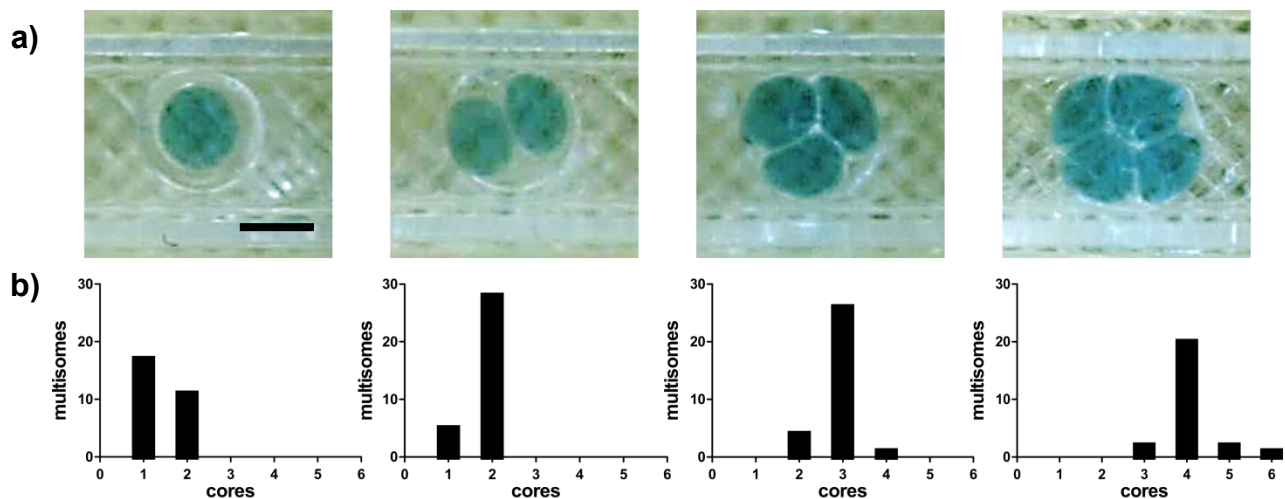
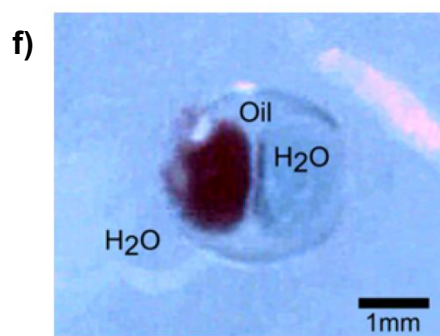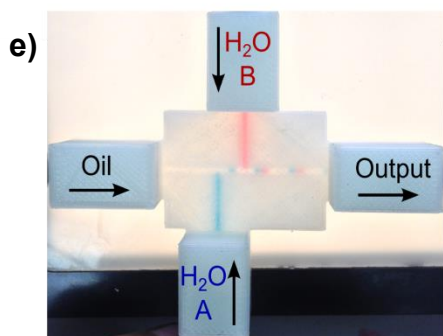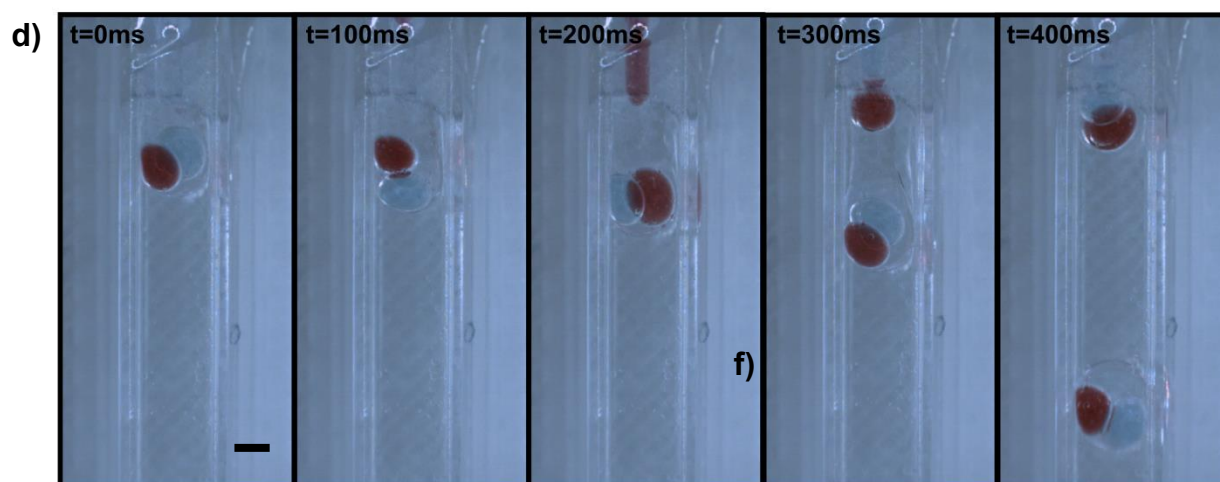| Internal cores (n^0)	Flow rate (ml/hr)		
	Inner phase (water)	Middle phase (oil)	Outer phase (water)
1	2	8	900
2	2	8	600
3	6	4	900
4	5	5	600

Figure 3.9 Production of multisomes using a 3D-printed microfluidic device described in Chapter 2. a) Photographs of multisomes containing 1-4 inner aqueous cores (dyed with 1mM Malachite Green) in squalene containing 5 mg mL-1 DPhPC. The multisomes are contained within a 2mm ID square channel. b) Graphs showing the number of aqueous cores per multisome produced in 8 seconds of microfluidic operation at the flow rates described in c). c) Table showing the flow rates of the inner, middle and outer phases used to generate multisomes containing 1-4 inner aqueous cores, as shown in a) and b). d) Time lapse images showing the production of a multisome containing two inner aqueous cores of different identity, dyed with blue and red food dyes. The flow rates employed are 1 ml hr^{-1} for the inner aqueous phases, 4 ml hr^{-1} for the oil phase and 300 ml hr^{-1} for the external aqueous phase. e) Photograph of the 3D-printed microfluidic device that was designed and used to produce aqueous droplets in oil of alternating identity. f) Image of a multisome containing two inner aqueous cores of different identity that has been collected in a 3D-printed collection chamber. Section a) is adapted from referenced publication[73]. Scale bars = 1 mm.

Following from the microfluidic production of multisomes, it was attempted to transfer them into an observation chamber in order to test their ability to remain stable untethered and outside of the microfluidic device used to produce them (Figure 3.10). The chamber was filled with an aqueous solution equivalent to the aqueous solution used for the inner aqueous droplets of the multisomes (excluding dyes), and consisted of a 3D-printed chamber with a hydrophilic, silanised glass lid (methods described in section 2.2.1.2). It was found that multisomes could not remain stable in the device and a number of them would coalesce when in close proximity (Figure 3.10).
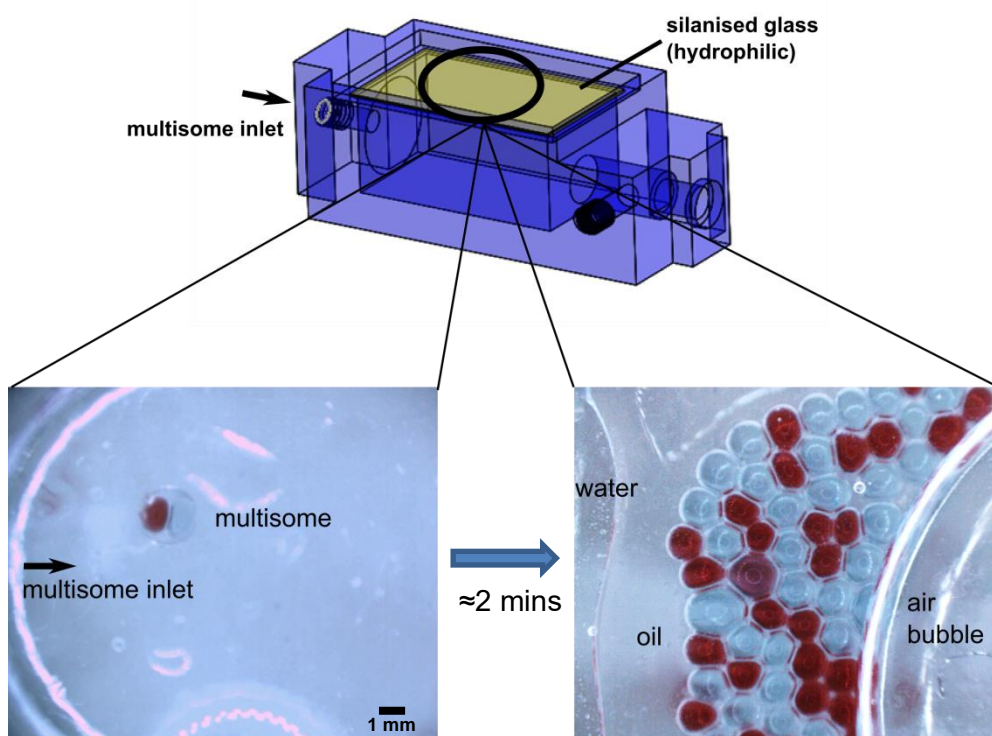

137

Figure 3.10 Images showing the use of a 3D-printed collection chamber (above) designed to collect and store microfluidically-produced multisomes. The photograph on the left depicts a multisome containing one red and one blue aqueous core that is contained in buffer within the collection chamber. The photograph on the right shows the collection chamber after ≈2 minutes of microfluidic operation, where a number of multisomes have coalesced to form a large network of blue and red DIBs in oil.

3.3.2.2 Production of droplet interface bilayers encapsulated in an alginate hydrogel shell (eDIBs).

Using the 3D-printed microfluidic device described in section 2.3.1.2, Figure 3.18, it was possible to produce W/O/W/O emulsions which formed encapsulated droplet interface bilayers (eDIBs) comprised of a number of aqueous cores contained within an oil droplet with dissolved lipid, which is encased in a hydrogel shell.

3.3.2.2.1 Microfluidic manufacture

The process for the production of eDIBs is outlined in

Figure 3.11 (a-d). A regular stream of aqueous droplets in oil containing dissolved lipid was produced using an external ETFE T-junction or a 3D-printed device for the generation of droplets of water of alternating composition. These droplets flowed into the 3D-printed microfluidic device using FEP tubing which terminated within a silanised glass capillary embedded in the 3D-printed microfluidic device. An input channel into the 3D-printed device allowed for an alginate solution to flow into the glass capillary and around the aqueous droplets in oil delivered by the FEP tubing, creating a coaxial droplet-generating geometry. This enabled the formation of oil droplets containing a prescribed amount of inner aqueous droplets. Another input channel of the 3D-printed device received a continuous flow of mineral oil containing 0.5% v/v acetic acid. This flowed into a second FEP tube within which the glass capillary carrying the oil droplets containing aqueous droplets terminated. This second, hydrophobic, coaxial flow

geometry, created the triple emulsion comprising a flow of alginate droplets, each containing an internal oil droplet with aqueous droplets inside (Figure 3.11).

Modulation of the relative flow rates of the different fluids provided control over the number of internal aqueous cores and the frequency of production. For example, the flow rates 11.76 ml hr^{-1} for both the internal aqueous and oil phases, 250 ml hr^{-1} for the alginate phase and 400 ml hr^{-1} for the carrier oil phase resulted in eDIBs where 96% of them containing 10±1 aqueous cores, produced at a frequency of 2 Hz (Figure 3.11e).
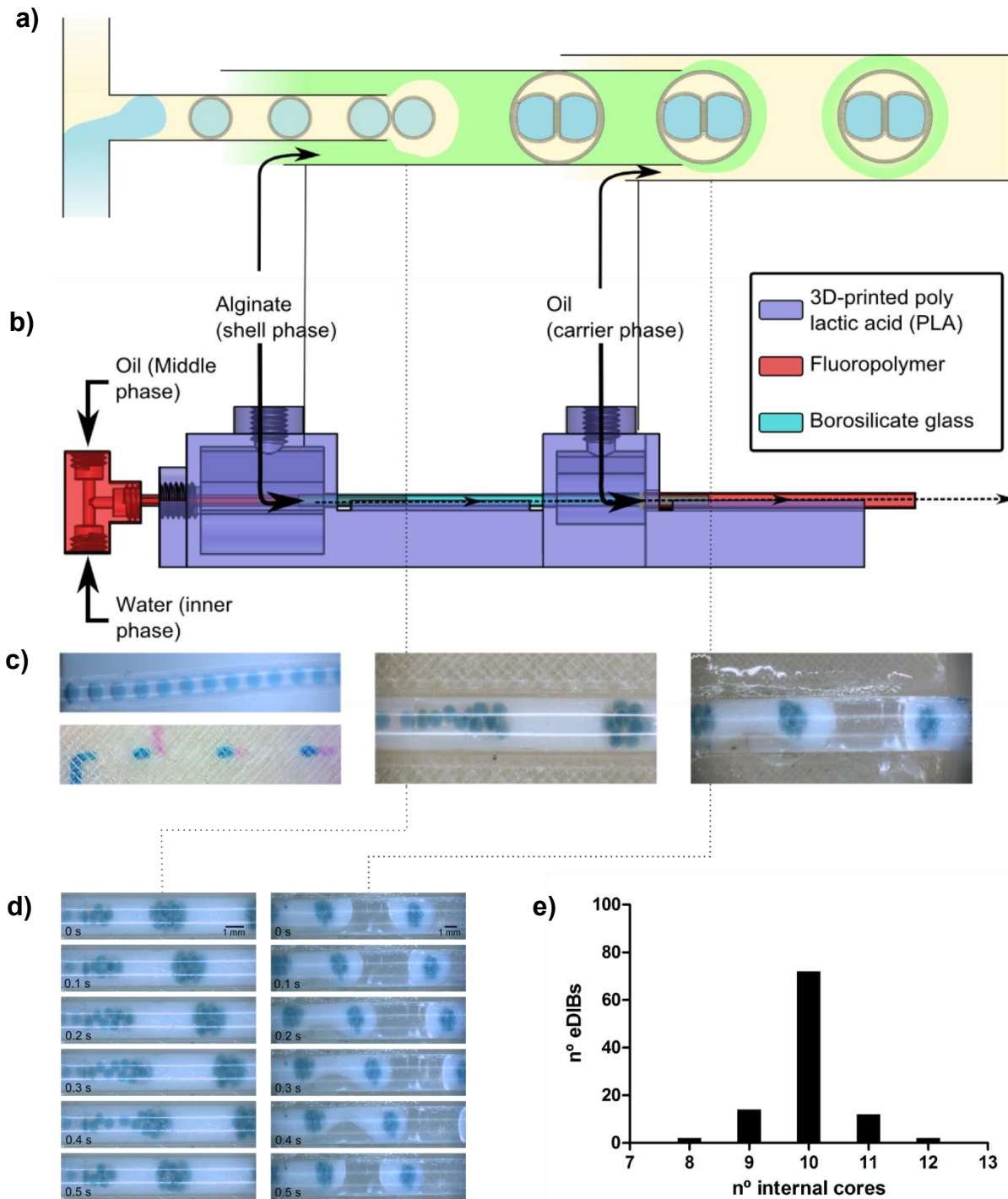
Figure 3.11 The microfluidic production of encapsulated droplet interface bilayers (eDIBs). a) Diagram of the method via which eDIBs are produced depicting a T-junction to generate water droplets and coaxial droplet-generating geometries for the subsequent encapsulations stages. b) CAD schematic of the 3D-printed microfluidic device used to produced eDIBs as per the method described in a). c) Photographs depicting the three different stages in eDIB formation. d) Time sequence photographs showing the formation of W/O/W (left) and W/O/W/O (right) emulsions within the coaxial droplet generating geometries in the 3D-printed microfluidic device. e) Graph showing the number of aqueous cores encapsulated per eDIB for 100 eDIBs using the flow rates 11.76:11.76:250:400 (aqueous, oil, alginate, oil).

140

The microfluidic production of eDIBs was found to be suitably reliable and reproducible for the purposes described in this chapter. Flow rates were experimentally selected and optimised (Appendix 5) to produce monodisperse eDIBs with regards to the number of encapsulated aqueous cores (Figure 3.11e). eDIB monodispersity was not characterised although the geometrically-driven regime of droplet formation prevents large variances in droplet volumes and geometries (as described in sections 1.3.3.3 and 2.3.2)[74]. The flow rate of the oil carrier was selected to be suitably high (400 ml hr^{-1}) in order to overcome the shear-thinning properties of alginate which can resist droplet pinch off, as lower flow rates resulted in cylindrical alginate fluid jets [60]. Careful alignment of the tubes forming the second coaxial geometry within the microfluidic device was required in order to prevent the ejection of the oil droplet from the alginate shell in flow, and proved to be a critical step in the microfluidic device fabrication processes outlined in Chapter 2 (section 2.3.1.2).

It is expected that the volume of the different phases and the frequency of production should follow a similar model as outlined in Chapter 2 (section 2.3.2.1) despite differences in fluid properties and the use of different surfactants, due to the maintenance of coaxial, geometrically-driven droplet formation regimes. However, variability in the number of aqueous cores encapsulated per eDIB was observed. For example, for the set of flow rates employed in these experiments, 72% of eDIBs contained the anticipated number of internal droplets (10 aqueous droplets per eDIB) whilst 26% contained one droplet more or less. This was attributed to an early formation of bilayers between adjacent aqueous droplets in the microfluidic encapsulation process, proving an adhesive force between contacting droplets which resulted in the droplet pair being either included or excluded from the forming oil droplet (Figure 3.12). The microfluidic device was able to tolerate these fluctuations for periods of up to 1 minute at least, without much other impact on droplet formation,

141

despite the non-linear pressure profiles of droplet formation and breakup mechanisms [75, 76].
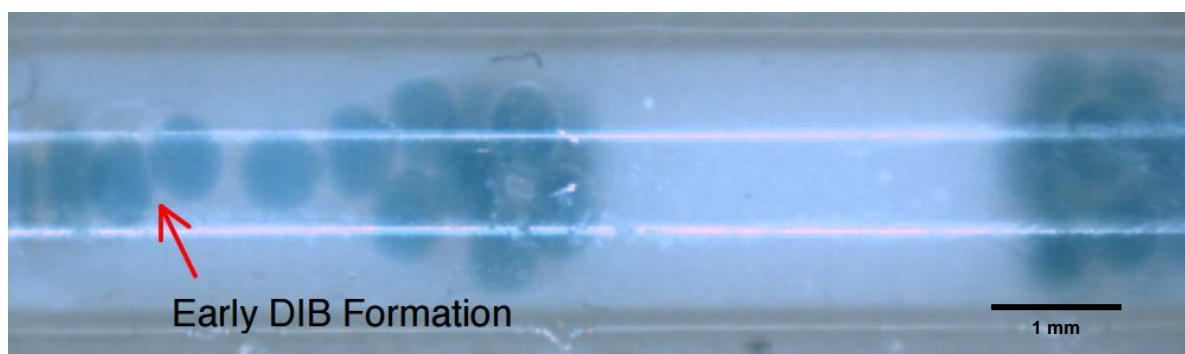

Early DIB Formation

1 mm

Figure 3.12 A bilayer forming between adjacent droplets early in the encapsulation process, providing with adhesion between droplets close to the oil droplet break-up point. This occurred occasionally and could result in either the inclusion or exclusion of the droplet pair, giving rise to variability in the number of aqueous cores encapsulated for a given set of flow rates (Figure 3.11e).

3.3.2.2.2 Alginate shell gelation

The alginate phase of the eDIBs proceeded in-flow and appeared to gel sufficiently in the length of the final FEP tube within the microfluidic device (typically 15 cm long) to be able to act as a solid upon exit from the device, and withstand mechanical handling or being placed in aqueous or oil environments (Figure 3.16). This was caused by the partitioning of acetic acid from the mineral oil phase to the aqueous phase, initiating the liberation of free calcium cations from the dissolution of calcium carbonate particles suspended in the alginate solution, which cross-link the alginate monomers to form a hydrogel. The dissolution of calcium carbonate in a low pH environment is in accordance with the following reaction:

$$CaCO_3 + 2H^+ \, (aq) \rightarrow Ca^{2+} \, (aq) + CO_2 + H_2O$$
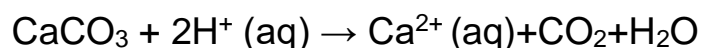
It was observed that there were two circumstances where alginate would gel and adhere to the orifice of the glass capillary at the second coaxial geometry. Firstly, a

plug of gelled alginate would develop at the orifice when flow was paused after generating eDIBs. This was usually resolved by resuming flow, as the plug of alginate would be dislodged from the orifice and expelled from the device. Alginate would also gel and adhere to the glass capillary after prolonged microfluidic flow which required the use of an EDTA solution to dissolve the gelled alginate, as described in section 3.2.2. A method that was not employed here that would circumvent this issue would be the use of a chaperone fluid, where the alginate droplet formation occurs in a non-gelling carrier solution that is miscible with the gelling carrier solution, which is introduced later on in the microfluidic device. In this way, the droplet-forming geometry would be protected from early gelation[50].

The presence of suspended calcium carbonate particles accounts for the initial opacity of the alginate shell. As the reaction described above takes place, the alginate shell is rendered transparent from the outside to the inside, as the acetic acid penetrates deeper into the alginate shell. Thus, the transparency of the alginate shell can be used to assess the extent of its gelation. Full transparency is achieved after approximately 15 minutes (Figure 3.13).

Figure 3.13 Photographs demonstrating how the alginate shell of an eDIB becomes transparent over a period of approximately 15 minutes. This occurs as acetic acid from the carrier oil phase partitions into the alginate phase, which contains suspended calcium carbonate particles that confer an initial opacity to the phase. The lowering of pH caused by the partitioning process causes these particles to be dissolved, resulting in transparency of the eDIB shell. These eDIBs have been output into a petri dish and are submerged in mineral oil containing 0.5 % v/v acetic acid.

The rate at which calcium cations are liberated can be modified to provide control over the shell morphology. The majority of eDIBs produced in this chapter are of an

asymmetric, ovoid morphology, with the internal cores often not residing in the centre of the construct. This is because eDIBs are produced as channel-occluding slugs within the microfluidic device, and the onset of gelation of the alginate shell occurs at this point. This asymmetrical shape can be desirable for bottom-up synthetic biology applications, where it can provide with directionality and geometrical polarity, which can be useful for the implementation of eDIB motility, for example. For other applications a spherical shape may be preferable to ensure a more homogeneous access to the DIBs contained within. It is possible to produce more spherical eDIBs by delaying gelation until after they have exited the microfluidic device, as shown in Figure 3.14.
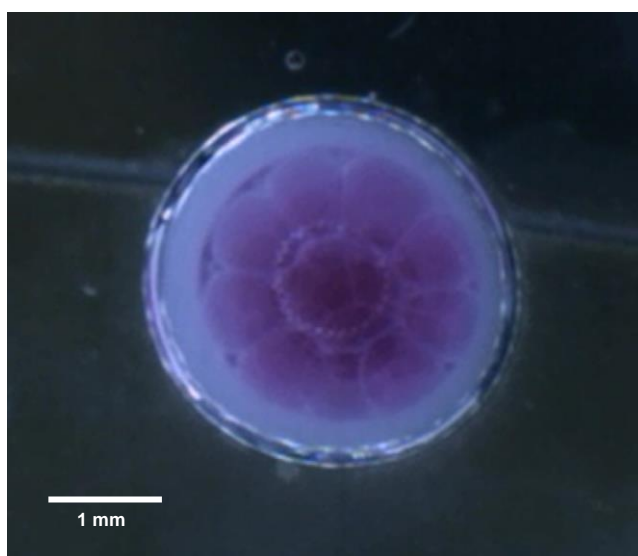
Figure 3.14 Photograph of a spherical eDIB produced by delaying the alginate shell gelation process by using a carrier oil phase with no dissolved acid. Gelation occurs once it has been submerged in a petri dish containing mineral oil with 0.5% glacial acetic acid.

It is noted that the control of the alginate shell gelation may be achieved by modulating the rate of calcium cation liberation from calcium carbonate. For example, calcium carbonate particle size and concentration, acetic acid concentration, buffering of the alginate phase, surface area to volume ratio of the capsule, capsule size and flow

conditions (i.e. flow-dependent advective mixing and the volume ratio of alginate to carrier oil) can all be modulated to control the rate of gelation. This may be useful in order to modulate not only the shape, but the rigidity and adhesiveness between a number of individual eDIBs.

Osmotic balancing between the internal cores and the alginate shell was a challenge because the alginate shell is comprised of a number of chemicals that affect osmotic pressure and that undergo a dynamic process during gelation. As acetic acid partitions into the alginate phase, the pH drops which causes $CaCO_3$ particles to dissolve releasing Ca^{2+} cations, and sodium alginate molecules to cross-link which releases Na^+ ions. Uncertainty exists in the amount of acetic acid present in the hydrogel, the amount of $CaCO_3$ dissolution and the degree of alginate cross-linking. In order to address this, assumptions were made in order to calculate the approximate ionic strength of the alginate shell prior to the addition of a relatively high concentration of salt (NaCl) to osmotically balance the inner aqueous phases with the alginate shell, causing any differences in ionic strength of the alginate phase due to the uncertainties described above to be less significant. These assumptions were a) all of the $CaCO_3$ in the alginate phase is dissolved and b) all of the alginate is cross-linked. The ionic strength of the alginate phase prior to the addition of salt was calculated to be 0.0505 M, and both the alginate and internal aqueous phase were balanced up to an ionic strength of 0.5 M using NaCl. Due to the ability of eDIBs to survive in aqueous environments, it should be possible to overcome these issues by incubating eDIBs in aqueous solutions that are osmotically matched with the internal cores, as the alginate shell will osmotically equilibrate with its surroundings.

Other methods of alginate gelation may also be employed and the kinetics of calcium delivery harnessed to control alginate morphology. For example, the release of photo-caged calcium may provide an internal gelation method[31] that dispenses with the

145

requirement of acid exposure and calcium carbonate particle suspension. An alternative method of alginate gelation was explored where the carrier phase was substituted for 1-octanol containing 150 mM dissolved calcium chloride (Figure 3.15). This external method of gelation relies on the partitioning of calcium cations from the octanol to the alginate phase[77]. This method offers the potential to circumvent potential issues with the internal gelation method described in this chapter, such as the initial opacity of the alginate phase, uncertainties regarding the pH and ionic strength of the hydrogel shell, and the unnecessary production of CO_2 via the dissolution of $CaCO_3$.
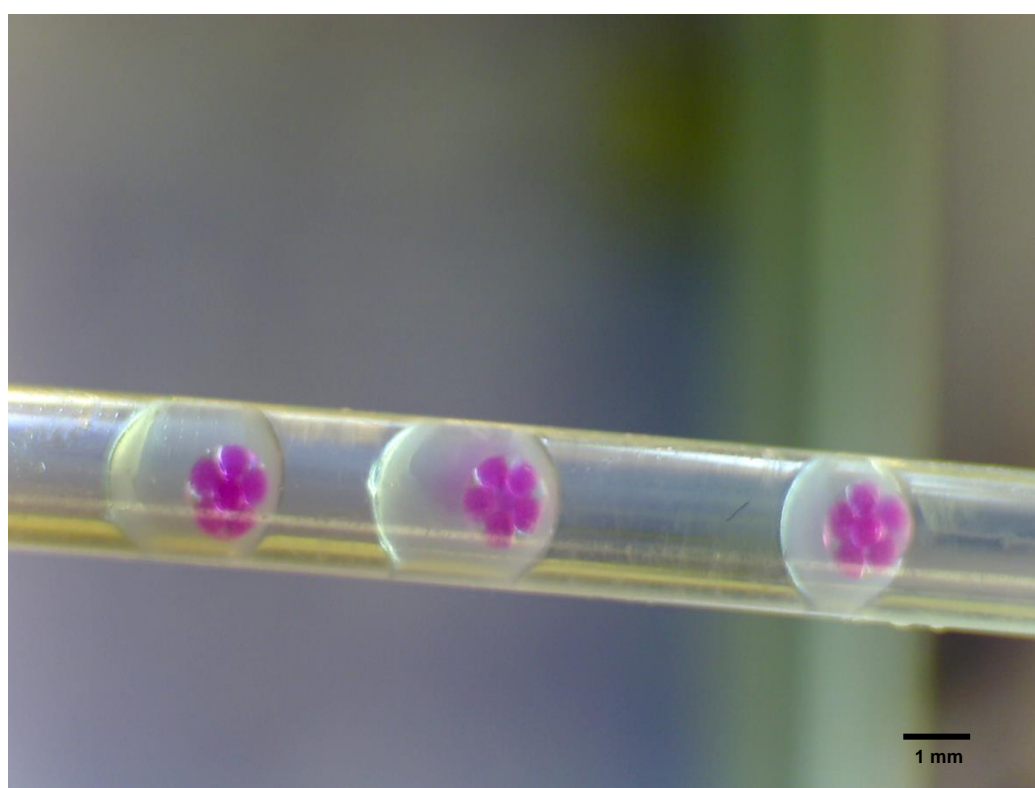

Figure 3.15 Photograph of eDIBs in an FEP tube (internal diameter = 2.5 mm) produced using an external gelation method relying on the partitioning of calcium chloride between a carrier 1-octanol phase containing 150 mM calcium chloride and the alginate phase.

3.3.2.2.3 eDIB stability

Unlike multisomes, eDIBs could be collected on exit from the device intact, and demonstrated to be self-supporting and resistant to rupture on contacting liquid air or container interfaces. The eDIBs were found to be stable in aqueous, oil and air environments (Figure 3.16) and were able to withstand careful manipulation using hands or tweezers (Figure 3.16b and c), as well as being manipulated using a pipette (Figure 3.16c) or stored in a 1.5 mL Eppendorf vial (Figure 3.16b).
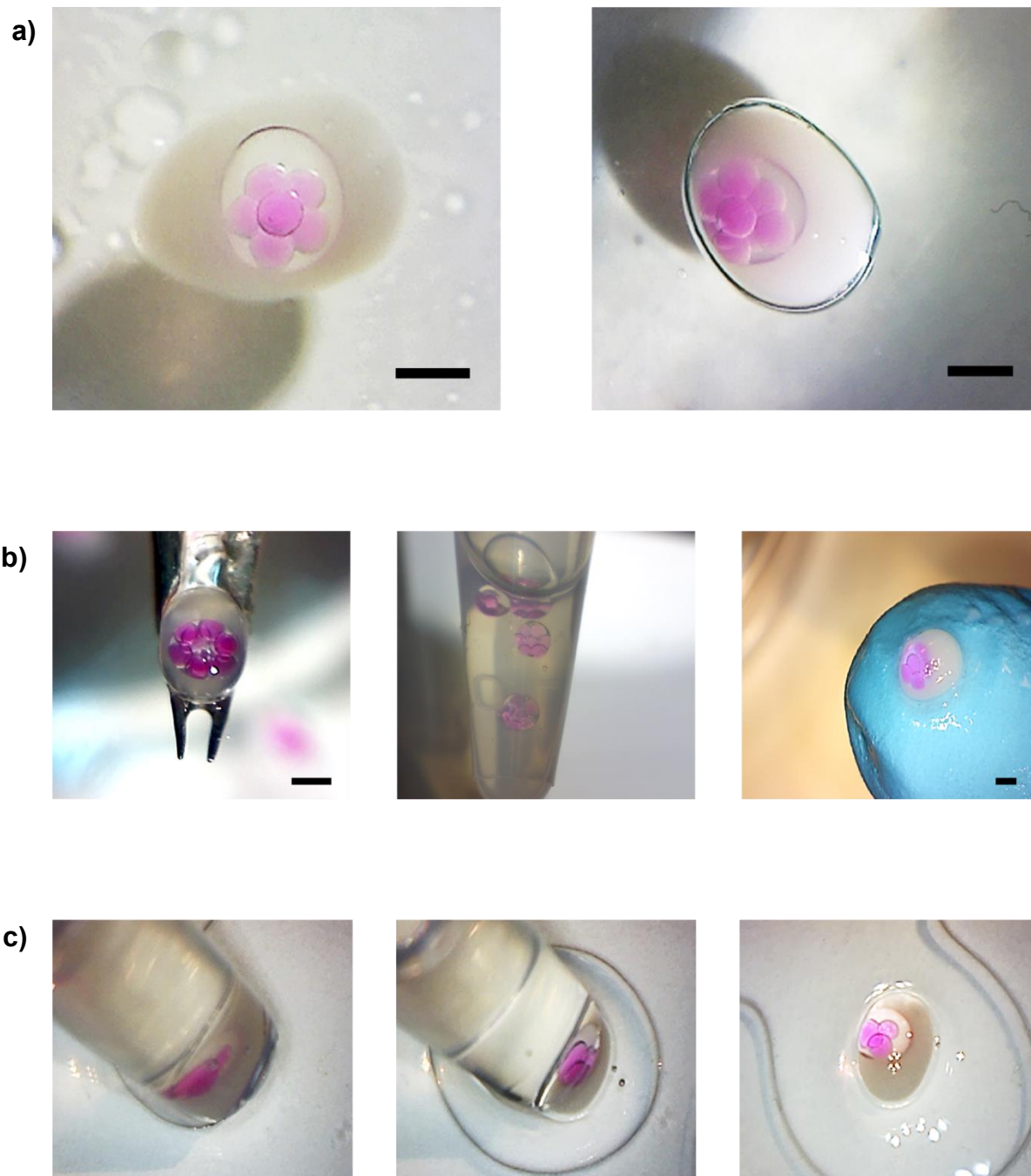
Figure 3.16 Photographs of encapsulated droplet interface bilayers (eDIBs). a) eDIBs floating in water (left) or submerged in oil (right). b) From left to right: an eDIB being handled using fine tweezers, four eDIBs contained in oil within a 1.5 mL Eppendorf tube, an eDIB being held on a gloved finger. All eDIBs depicted here were output directly from the microfluidic device. c) A sequence of images depicting the pipetting of an eDIB into an empty petri dish. This eDIB is absorbed from another petri dish containing eDIBs submerged in oil, using a 1 mL pipette with a cut pipette tip. Scale bars = 1 mm.

Additionally, it was found that eDIBs could be interfaced with the natural World, and were found to remain stable when placed upon a leaf found from the local flora of the Cardiff University grounds (Figure 3.17). This provides a basis via which eDIBs can be used outside of a laboratory environment.

Figure 3.17 Photograph of eDIB placed on a leaf collected from the outdoors of Redwood Building (Cardiff, UK). This demonstrates the potential of eDIBs to interact with materials in the outside World. For photographic purposes this image was taken indoors.

eDIBs could be kept intact for periods of weeks at room temperature when kept in oil, as this prevented evaporation of the hydrogel shells. During the course of the experiments described in this chapter, it was noted that eDIBs were able to survive over two weeks submerged in oil in a petri dish, and withstand the mechanical agitation of being transported by foot in an Eppendorf tube from different Cardiff University departments (approximately 1.2 km apart) This is a somewhat remarkable feat due to the notorious instability of artificial lipid bilayers and certain conditions for DIB formation within the experiments of this chapter that are expected to be detrimental to bilayer stability. For example, the bilayers produced in this chapter are considerably larger than many of those seen in the literature[3], which is likely to decrease the stability of the DIBs. Also, unlike other methods of DIB production, the continuous, microfluidic method of eDIB production employed here did not allow for the incubation of droplets

149

that is seen and suggested in the DIB literature[2, 11], which allows for the formation of lipid monolayers around the droplets. This process is considered a prerequisite for bilayer formation. This may be offset by reports that suggest that microfluidic flow enhances the speed at which lipid monolayers form around droplets[19]. The amount of time between the formation of the droplets of water in oil and their encapsulation within an oil droplet was usually less than 20 seconds in the experiments reported here, compared to incubation times in the order of 5-15 minutes that are suggested in the literature. Incubation time can be increased in eDIB production by increasing the length of the FEP tube prior to the encapsulation of the droplets of water in an oil droplet, and the ETFE T-junction where the droplets are formed. However, it was found that increasing the length of this tube affected the homogeneity of droplet production, especially the distance between the droplets, which was due to the flexible nature of the FEP tube that likely allowed for a heterogeneous flow of oil around the droplets. This can be circumvented by using different methods of water-in-oil droplet production, or using a rigid material to deliver the droplets into the 3D-printed device, such as a glass capillary. It is also likely that the hydrogel shell around the DIBs increases the stability of the bilayers formed. Observations support this hypothesis as, in the case of DIB failure within eDIBs, it is usually the DIBs between the internal cores that fail before the DIBs between the internal cores and the hydrogel shell, despite the internal cores being osmotically balanced for the large majority of experiments performed.

Different lipids and lipid compositions can be explored in order to increase the stability of the bilayers contained within the eDIBs or to modulate bilayer stability in response to different environments. For the experiments reported here, DPhPC was used as the sole constituent of the lipid bilayers due to its reported formation of high stability lipid bilayers [78, 79]. It was found that the use of 1,2-dioleoyl-sn-glycero-3-phosphocholine (DOPC) instead of DPhPC caused a significant amount of bilayer failure within the microfluidic production stages where the aqueous droplets are first brought into close

proximity. eDIB bilayer stability may benefit from the inclusion or use of polymerisable lipids[80, 81]. Also, lipid mixtures or cell lipid extracts may be used to generate more biomimetic bilayers within the eDIBs[82]. Asymmetrical lipid bilayers may be achievable via the delivery of lipids as vesicles within the aqueous droplets instead of dissolved in the oil phase[83].

3.3.2.3 eDIB electrophysiology

The presence of lipid bilayers segregating compartments was confirmed by electrophysiology (Figure 3.18). A characteristic square wave current was recorded in response to a triangular wave voltage, giving a bilayer capacitance of 2826 pF (Figure 3.18a). This corresponds to a bilayer area of approximately 0.42 mm^2 for DPhPC in hexadecane (Specific capacitance 0.652 µF cm^{-2} [72]). Electroporation of the bilayer was observed under an applied potential of 50 mV (Figure 3.18b), giving rise to transient increases in current.

In subsequent experiments, it was attempted to insert α-Hemolysin membrane pores into the eDIBs in order to electrically measure single-channel insertions and the resulting ion flux. This was performed by pipetting 0.2 µL aqueous droplets of the α-Hemolysin (≈3 nM) solution onto the alginate shells of the eDIBs being electrically probed. The droplets would wet the alginate shell and thus allow for the α-Hemolysin pores to diffuse to the eDIB bilayers. For these experiments, a 30 mV potential was applied across the bilayer. Step-wise increases in current were seen when probing the bilayers between the alginate shell and the internal aqueous cores, associated to individual pores inserting in the bilayer resulting in an ion flux across the membrane. Two types of insertion events were observed: a) step increases in current associated with α-Hemolysin inserting into the bilayer that directly separated both electrodes (Figure 3.18c, inset red pore and trace) and b) capacitive transient increases in current that decayed (Figure 3.18c, inset blue pore and trace). The latter behaviour has

151

previously been reported as a result of pore insertion into bilayers connected to the droplet being probed from the wider droplet bilayer network [5, 84]. A combination of these behaviours was also seen (Figure 3.18d).
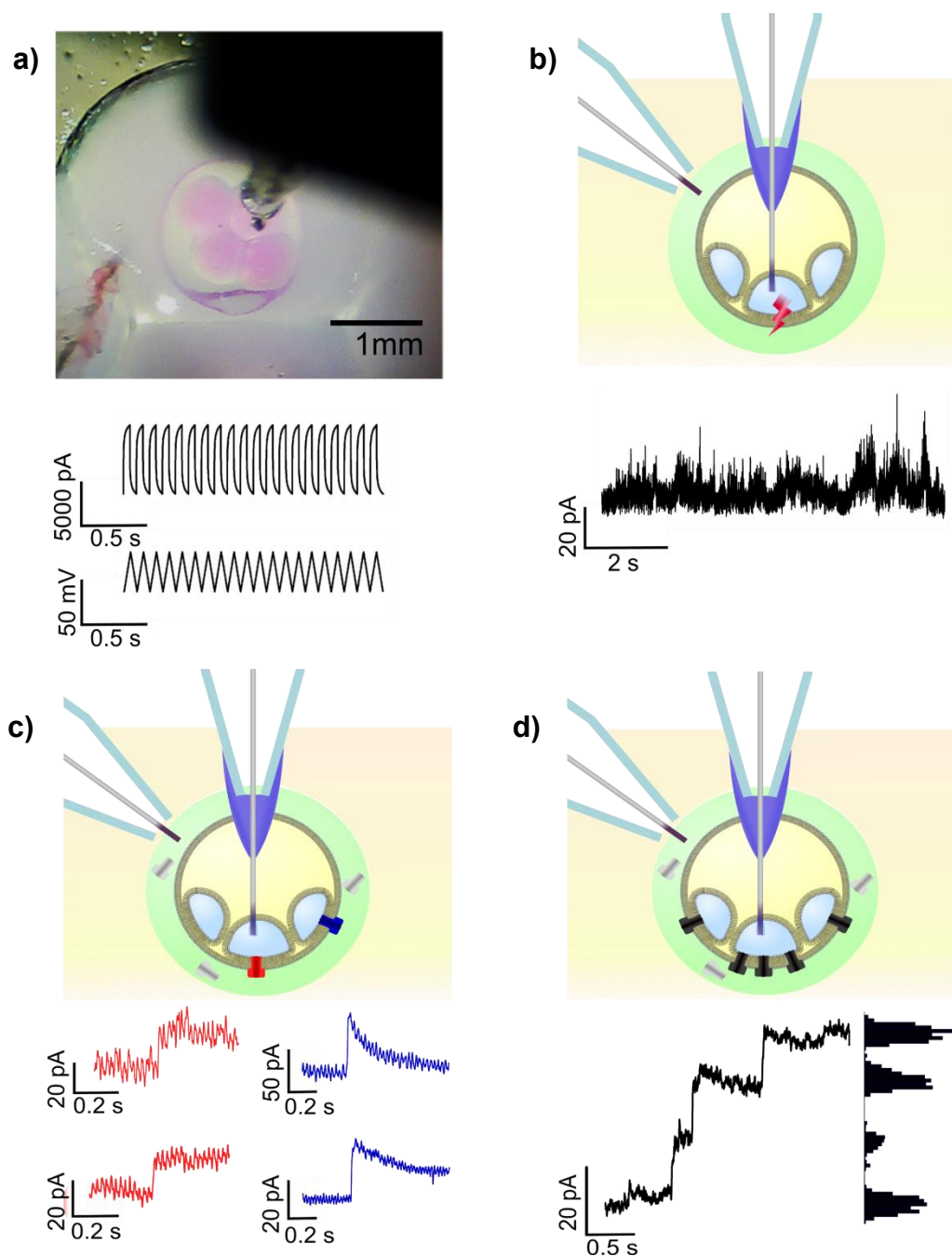

Figure 3.18 Electrophysiology experiments performed on eDIBs. a) A photograph depicting an eDIB with Ag/AgCl electrodes (top), where one is inserted in one of the internal aqueous cores and the other is in the alginate shell. In response to a ±23 mV triangle wave, a capacitive

current is measured, signifying the presence of a lipid bilayer (bottom). b) A short period of electroporation in an eDIB membrane is observed during a period under an applied potential of 50 mV. c) Following the contacting of the external shell of an eDIB with an aqueous droplet containing the protein pore α-Hemolysin, protein insertion events are detected which facilitate ion flux across the bilayer (red traces). Transient current spikes are also observed (blue traces) due to protein insertion into neighbouring bilayers of the droplet bilayer network of the eDIB. d) Successive step-wise increases in current are measured as multiple protein pores insert (Step size ca. 18 pA), with both types of protein pore insertions seen in c).

Electrophysiology experiments proved challenging for eDIBs due to the requirement of having to pierce an alginate shell in order to access the internal droplets. This required the piercing electrode to be shielded from the conductive alginate phase via the preparation of custom electrodes (as described in section 3.2.3.1). Also, the eDIBs proved to be susceptible to this kind of mechanical manipulation, and often the mechanical force of the electrode on the eDIB would cause its internal droplets to coalesce with the alginate shell and hence bilayer failure. To circumvent this issue, a 0.5x phosphate buffered saline solution was used in the alginate phase for the microfluidic generation of eDIBs that had a more flexible outer shell that could be pierced with little impact on the integrity of the bilayers within.

Electrophysiology experiments served to prove the formation of lipid bilayers between the internal aqueous cores and the alginate shell. Droplet-droplet electrophysiology was performed as it is a well characterised technique which was used to benchmark the electrophysiology performance of the eDIBs[2]. DIBs formed via this method displayed capacitance with little current leakage and abundant individual α-Hemolysin insertions. In comparison, the capacitance of the bilayers within the eDIB displayed more leakage and less abundant α-Hemolysin insertions. The increased leakage of eDIB bilayers is possibly due to the eDIB bilayers being larger than the droplet-droplet bilayers. Using a specific capacitance of 0.652 μF cm^{-2} for DPhPC in hexadecane[72], the eDIB bilayer demonstrated in Figure 3.18 has an area of 0.42 mm^2 as opposed to 0.082 mm^2 of the droplet-droplet bilayer in Figure 3.8. It was found that increasing

concentrations of dye in the aqueous cores increased the gradient of bilayer capacitance traces, which indicated an effect on bilayer leakage (Figure 3.19).
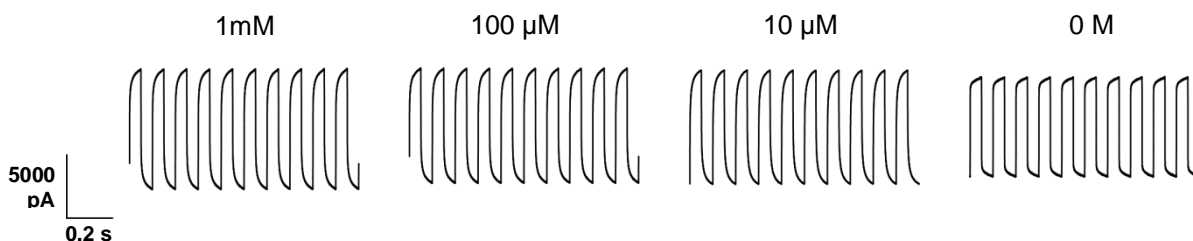

Figure 3.19 Electrophyiology traces representing the capacitance of eDIB bilayers between internal cores of varying Lissamine Green concentration (1mM, 100μM, 10μM, 0) and the hydrogel shell. Capacitance is observed with varying amounts of leakage under an applied 10 Hz ±23 mV triangle wave potential. Leakage is visible as a gradient at the capacitance peaks.

α-Hemolysin insertions were less abundant in eDIBs due to the method of α-Hemolysin delivery to the bilayers. Droplet-droplet bilayers allowed for α-Hemolysin to be contained within the bilayer droplets. For eDIBs, α-Hemolysin was delivered by adding droplets of α-Hemolysin to the alginate shell, which involves the proteins having to diffuse distances in the order of millimetres through an alginate hydrogel which comprises a relatively large volume (ca. 10 μL), resulting in fewer pores reaching the membrane despite the use of a higher concentration. Indirect α-Hemolysin insertions (Figure 3.10c inset blue pore and trace) were observed for eDIBs as capacitive transient increases in current that subsequently decayed. This behaviour has previously been reported as a result of pore insertion into indirectly interrogated bilayers within a wider droplet bilayer network [5, 84]. Consequently, we attribute this behaviour to insertions into neighbouring bilayers of the connected network that are not directly probed by the Ag/AgCl electrode that is inserted into an internal aqueous core. The conductivity of these pores was difficult to ascertain due to uncertainties with regards to the ionic concentrations of the alginate phase but were found to be comparable to other experiments in the literature for similar conditions[23].

3.4 Conclusion

In this chapter, it is shown that encapsulated droplet interface bilayer networks (eDIBs) based on W/O/W/O emulsions represent a robust and freestanding artificial bilayer network platform with the ability to interface with an external aqueous environment, as well as remain stable in aqueous, air and oil environments. eDIBs have been shown to be able to withstand mechanical handling and remain intact for prolonged periods of time. This goes beyond current reports in the literature that have aimed at producing mechanically stable DIBs in solid substrates [85, 86] which do not allow for communication with an external environment, attempts to stabilise DIBs in air[87], which are not freestanding or compatible with aqueous environments, and attempts to produce freestanding droplet networks in water[12] which are not stable in other environments and lack the handling capacity, rigidity, and the oil phase that eDIBs provide, which can act as a reservoir for lipids and other oil soluble substances.

The microfluidic method described here represents a cost effective, scalable and reliable method of producing eDIBs, and provides a means to control both aqueous core number as well as aqueous cores of different contents. This control enables eDIBs to retain favourable properties of DIBs, such as asymmetrical droplet contents or bilayer lipid composition, the insertion of functional membrane proteins, and communication between droplets, whilst affording an unprecedented combination of mechanical stability and environmental compatibility.

eDIB monodispersity is yet to be characterised, and further exploration of flow rates and the use of an additional syringe pump to independently control the internal aqueous and oil phase flow rates will allow greater control over droplet encapsulation. Automation of eDIB production is thought to be possible. Further developments should focus on the miniaturisation of eDIBs into the microscale (<100 µm in total diameter),

which is expected to be readily possible by scaling down channel diameters within the microfluidic device, and might improve eDIB manufacture in terms of bilayer stability and alginate gelation by increasing surface area to volume ratios.

The developments described here expand on the potential of artificial lipid bilayers for applications within fundamental science and bottom-up synthetic biology, and enables DIBs and droplet networks to be used outside of the laboratory for the development of functional materials in the external World (Figure 3.17). It is proposed that eDIBs may enable lab-in-a-capsule technologies through droplet network compartmentalisation, and could therefore represent self-contained assay platforms for use in environments that are not readily reducible to laboratory settings. With alginate being biocompatible and their widespread use in internal medicine, eDIBs could develop into diagnostic and therapeutic complex capsules capable of dynamic interaction with biological cells, tissues and organisms. Individual eDIB constructs may be engineered to physically interact with one another and form higher order structures, akin to artificial tissues[84]. Additionally, freestanding DIB networks may be able to integrate with other advances within the field of bottom-up synthetic biology, such as the ability to form motile droplets[88-91], further aiding in the development of self-sustaining artificial cell systems[90].

3.5 References

1. Elani, Y., Construction of membrane-bound artificial cells using microfluidics: a new frontier in bottom-up synthetic biology. *Biochemical Society Transactions* **2016,** *44* (3), 723-730.

2. Leptihn, S.; Castell, O. K.; Cronin, B.; Lee, E.-H.; Gross, L. C. M.; Marshall, D. P.; Thompson, J. R.; Holden, M.; Wallace, M. I., Constructing droplet interface bilayers from the contact of aqueous droplets in oil. *Nature Protocols* **2013,** *8* (6), 1048-1057.

3. Bayley, H.; Cronin, B.; Heron, A.; Holden, M. A.; Hwang, W.; Syeda, R.; Thompson, J.; Wallace, M., Droplet interface bilayers. *Molecular bioSystems* **2008,** *4* (12), 1191-1208.

4. S. Friddin, M.; Bolognesi, G.; Elani, Y.; J. Brooks, N.; V. Law, R.; M. Seddon, J.; A. Neil, M. A.; Ces, O., Optically assembled droplet interface bilayer (OptiDIB) networks from cell-sized microdroplets. *Soft Matter* **2016,** *12* (37), 7731-7734.

5. Hwang, W. L.; Holden, M. A.; White, S.; Bayley, H., Electrical Behavior of Droplet Interface Bilayer Networks: Experimental Analysis and Modeling. *Journal of the American Chemical Society* **2007,** *129* (38), 11854-11864.

6. Castell, O. K.; Berridge, J.; Wallace, M. I., Quantification of Membrane Protein Inhibition by Optical Ion Flux in a Droplet Interface Bilayer Array. *Angewandte Chemie International Edition* **2012,** *51* (13), 3134-3138.

7. Huang, S.; Romero-Ruiz, M.; Castell, O. K.; Bayley, H.; Wallace, M. I., High-throughput optical sensing of nucleic acids in a nanopore array. *Nature Nanotechnology* **2015,** *10* (11), 986-991.

8. Syeda, R.; Holden, M. A.; Hwang, W. L.; Bayley, H., Screening Blockers Against a Potassium Channel with a Droplet Interface Bilayer Array. *Journal of the American Chemical Society* **2008,** *130* (46), 15543-15548.

9. Leptihn, S.; Thompson, J. R.; Ellory, J. C.; Tucker, S. J.; Wallace, M. I., In vitro reconstitution of eukaryotic ion channels using droplet interface bilayers. *Journal of the American Chemical Society* **2011,** *133* (24), 9370-9375.

10. Maglia, G.; Heron, A. J.; Hwang, W. L.; Holden, M. A.; Mikhailova, E.; Li, Q.; Cheley, S.; Bayley, H., Droplet networks with incorporated protein diodes show collective properties. *Nature Nanotechnology* **2009,** *4* (7), 437-440.

11. Holden, M. A.; Needham, D.; Bayley, H., Functional Bionetworks from Nanoliter Water Droplets. *Journal of the American Chemical Society* **2007,** *129* (27), 8650-8655.

12. Elani, Y.; Law, R. V.; Ces, O., Vesicle-based artificial cells as chemical microreactors with spatially segregated reaction pathways. *Nature Communications* **2014,** *5*, 5305.

13. Elani, Y.; Solvas, X. C. I.; Edel, J. B.; Law, R. V.; Ces, O., Microfluidic generation of encapsulated droplet interface bilayer networks (multisomes) and their use as cell-like reactors. *Chemical Communications* **2016,** *52* (35), 5961-5964.

14. Elani, Y.; deMello, A. J.; Niu, X.; Ces, O., Novel technologies for the formation of 2-D and 3-D droplet interface bilayer networks. *Lab on a Chip* **2012,** *12* (18), 3514-3520.

15. A microfluidic platform for size-dependent generation of droplet interface bilayer networks on rails. *Biomicrofluidics* **2015,** *9* (6), 064121.

16. Schlicht, B.; Zagnoni, M., Droplet-interface-bilayer assays in microfluidic passive networks. *Scientific Reports* **2015,** *5*.

17. Czekalska, M. A.; Kaminski, T. S.; Jakiela, S.; Tanuj Sapra, K.; Bayley, H.; Garstecki, P., A droplet microfluidic system for sequential generation of lipid bilayers and transmembrane electrical recordings. *Lab Chip* **2015,** *15* (2), 541-548.

18. Barlow, N. E.; Bolognesi, G.; Flemming, A. J.; Brooks, N. J.; Barter, L. M. C.; Ces, O., Multiplexed droplet Interface bilayer formation. *Lab on a Chip* **2016,** *16* (24), 4653-4657.

19. Thutupalli, S.; Fleury, J.-B.; Steinberger, A.; Herminghaus, S.; Seemann, R., Why can artificial membranes be fabricated so rapidly in microfluidics? *Chemical Communications* **2013,** *49* (14), 1443-1445.

20. Funakoshi, K.; Suzuki, H.; Takeuchi, S., Lipid Bilayer Formation by Contacting Monolayers in a Microfluidic Device for Membrane Protein Analysis. *Analytical Chemistry* **2006,** *78* (24), 8169-8174.

21. Elani, Y.; Gee, A.; Law, R. V.; Ces, O., Engineering multi-compartment vesicle networks. *Chemical Science* **2013,** *4* (8), 3332-3338.

22.   Eisenstein, M., Synthetic Biology: Building better bubbles. *Nature Methods* **2012,** *9* (1), 13-13.

23.   Villar, G.; Heron, A. J.; Bayley, H., Formation of droplet networks that function in aqueous environments. *Nature Nanotechnology* **2011,** *6* (12), 803-808.

24.   Hirst, E.; Rees, D. A., 208. The structure of alginic acid. Part V. Isolation and unambiguous characterization of some hydrolysis products of the methylated polysaccharide. *Journal of the Chemical Society (Resumed)* **1965,** (0), 1182-1187.

25.   Lee, K. Y.; Mooney, D. J., Alginate: properties and biomedical applications. *Progress in polymer science* **2012,** *37* (1), 106-126.

26.   Imeson, A., *Food Stabilisers, Thickeners and Gelling Agents*. John Wiley & Sons: 2011; p 454.

27.   Hidalgo San Jose, L. Microfluidic production of stem-cell microcapsules for spinal cord injury repair. phd, Cardiff University, 2017.

28.   Grant, G. T.; Morris, E. R.; Rees, D. A.; Smith, P. J. C.; Thom, D., Biological interactions between polysaccharides and divalent cations: The egg-box model. *FEBS Letters* **1973,** *32* (1), 195-198.

29.   Gacesa, P., Enzymic degradation of alginates. *International Journal of Biochemistry* **1992,** *24* (4), 545-552.

30.   Klinger, M.; Toqeer, A.; Juul, A. G.; StenbÆK, D. Depolymerisation of alginic acid. WO2014102332 A1, 2014/07/03/, 2014.

31.   Chueh, B.-h.; Zheng, Y.; Torisawa, Y.-s.; Hsiao, A. Y.; Ge, C.; Hsiong, S.; Huebsch, N.; Franceschi, R.; Mooney, D. J.; Takayama, S., Patterning alginate hydrogels using light-directed release of caged calcium in a microfluidic device. *Biomedical microdevices* **2010,** *12* (1), 145-151.

32.   Sun, J.; Tan, H., Alginate-Based Biomaterials for Regenerative Medicine Applications. *Materials* **2013,** *6* (4), 1285-1309.

33.   Kong, H. J.; Kaigler, D.; Kim, K.; Mooney, D. J., Controlling rigidity and degradation of alginate hydrogels via molecular weight distribution. *Biomacromolecules* **2004,** *5* (5), 1720-1727.

34.   Stress-relaxation behavior in gels with ionic and covalent crosslinks. *Journal of Applied Physics* **2010,** *107* (6), 063509.

35.   Becker, T. A.; Kipke, D. R.; Brandon, T., Calcium alginate gel: a biocompatible and mechanically stable polymer for endovascular embolization. *Journal of Biomedical Materials Research* **2001,** *54* (1), 76-86.

36.   Li, H.-B.; Jiang, H.; Wang, C.-Y.; Duan, C.-M.; Ye, Y.; Su, X.-P.; Kong, Q.-X.; Wu, J.-F.; Guo, X.-M., Comparison of two types of alginate microcapsules on stability and biocompatibility in vitro and in vivo. *Biomedical Materials (Bristol, England)* **2006,** *1* (1), 42-47.

37.   Orive, G.; Carcaboso, A. M.; Hernández, R. M.; Gascón, A. R.; Pedraz, J. L., Biocompatibility Evaluation of Different Alginates and Alginate-Based Microcapsules. *Biomacromolecules* **2005,** *6* (2), 927-931.

38.   Rabanel, J.-M.; Banquy, X.; Zouaoui, H.; Mokhtar, M.; Hildgen, P., Progress technology in microencapsulation methods for cell therapy. *Biotechnology Progress* **2009,** *25* (4), 946-963.

39.   Tønnesen, H. H.; Karlsen, J., Alginate in drug delivery systems. *Drug Development and Industrial Pharmacy* **2002,** *28* (6), 621-630.

40.   Tam, S. K.; Dusseault, J.; Polizu, S.; Ménard, M.; Hallé, J.-P.; Yahia, L. H., Impact of residual contamination on the biofunctional properties of purified alginates used for cell encapsulation. *Biomaterials* **2006,** *27* (8), 1296-1305.

41.   Onsoyen, E., Commercial applications of alginates. *Carbohydrates Europe* **1996,** *14*, 26-31.

42.   Chan, L. W.; Lee, H. Y.; Heng, P. W. S., Mechanisms of external and internal gelation and their impact on the functions of alginate as a coat and delivery system. *Carbohydrate Polymers* **2006,** *63* (2), 176-187.

43.   Choi, B. Y.; Park, H. J.; Hwang, S. J.; Park, J. B., Preparation of alginate beads for floating drug delivery system: effects of CO_2 gas-forming agents. *International Journal of Pharmaceutics* **2002,** *239* (1–2), 81-91.

44.   Al-Hajry, H. A.; Al-Maskry, S. A.; Al-Kharousi, L. M.; El-Mardi, O.; Shayya, W. H.; Goosen, M. F. A., Electrostatic Encapsulation and Growth of Plant Cell Cultures in Alginate. *Biotechnology Progress* **1999,** *15* (4), 768-774.

45.　　Li, R. H.; Altreuter, D. H.; Gentile, F. T., Transport characterization of hydrogel matrices for cell encapsulation. *Biotechnology and Bioengineering* **1996,** *50* (4), 365-373.

46.　　Paul, A.; Ge, Y.; Prakash, S.; Shum-Tim, D., Microencapsulated stem cells for tissue repairing: implications in cell-based myocardial therapy. *Regenerative Medicine* **2009,** *4* (5), 733-745.

47.　　Tan, W. H.; Takeuchi, S., Monodisperse Alginate Hydrogel Microbeads for Cell Encapsulation. *Advanced Materials* **2007,** *19* (18), 2696-2701.

48.　　Utech, S.; Prodanovic, R.; Mao, A. S.; Ostafe, R.; Mooney, D. J.; Weitz, D. A., Microfluidic generation of monodisperse, structurally homogeneous alginate microgels for cell encapsulation and 3D cell culture. *Advanced healthcare materials* **2015,** *4* (11), 1628-1633.

49.　　Wang, N.; Adams, G.; Buttery, L.; Falcone, F. H.; Stolnik, S., Alginate encapsulation technology supports embryonic stem cells differentiation into insulin-producing cells. *Journal of Biotechnology* **2009,** *144* (4), 304-312.

50.　　Workman, V. L.; Dunnett, S. B.; Kille, P.; Palmer, D. D., Microfluidic chip-based synthesis of alginate microspheres for encapsulation of immortalized human cells. *Biomicrofluidics* **2007,** *1* (1).

51.　　Jiang, Z.; Zhang, Y.; Li, J.; Jiang, W.; Yang, D.; Wu, H., Encapsulation of β-Glucuronidase in Biomimetic Alginate Capsules for Bioconversion of Baicalin to Baicalein. *Industrial & Engineering Chemistry Research* **2007,** *46* (7), 1883-1890.

52.　　He, F.; Wang, W.; He, X.-H.; Yang, X.-L.; Li, M.; Xie, R.; Ju, X.-J.; Liu, Z.; Chu, L.-Y., Controllable Multicompartmental Capsules with Distinct Cores and Shells for Synergistic Release. *ACS Applied Materials & Interfaces* **2016,** *8* (13), 8743-8754.

53.　　Sapra, K. T.; Bayley, H., Lipid-coated hydrogel shapes as components of electrical circuits and mechanical devices. *Scientific Reports* **2012,** *2*, 848.

54.　　Quong, D.; Neufeld, R. J.; Skjåk-Braek, G.; Poncelet, D., External versus internal source of calcium during the gelation of alginate beads for DNA encapsulation. *Biotechnology and Bioengineering* **1998,** *57* (4), 438-446.

55.　　Ingar Draget, K.; Østgaard, K.; Smidsrød, O., Homogeneous alginate gels: A technical approach. *Carbohydrate Polymers* **1990,** *14* (2), 159-178.

56.　　Rolland, L.; Santanach-Carreras, E.; Delmas, T.; Bibette, J.; Bremond, N., Physicochemical properties of aqueous core hydrogel capsules. *Soft Matter* **2014,** *10* (48), 9668-9674.

57.　　Yow, H. N.; Routh, A. F., Formation of liquid core–polymer shell microcapsules. *Soft Matter* **2006,** *2* (11), 940-949.

58.　　Fu, S.; Thacker, A.; Sperger, D. M.; Boni, R. L.; Velankar, S.; Munson, E. J.; Block, L. H., Rheological Evaluation of Inter-grade and Inter-batch Variability of Sodium Alginate. *AAPS PharmSciTech* **2010,** *11* (4), 1662-1674.

59.　　Chiarello, E.; Gupta, A.; Mistura, G.; Pierno, M.; Sbragaglia, M., Droplet breakup driven by shear thinning solutions in a microfluidic T-Junction. *arXiv:1610.07800 [cond-mat]* **2016**.

60.　　Abate, A. R.; Kutsovsky, M.; Seiffert, S.; Windbergs, M.; Pinto, L. F. V.; Rotem, A.; Utada, A. S.; Weitz, D. A., Synthesis of Monodisperse Microparticles from Non-Newtonian Polymer Solutions with Microfluidic Devices. *Advanced Materials* **2011,** *23* (15), 1757-1760.

61.　　Seiffert, S.; Weitz, D. A., Controlled fabrication of polymer microgels by polymer-analogous gelation in droplet microfluidics. *Soft Matter* **2010,** *6* (14), 3184-3190.

62.　　Shintaku, H.; Kuwabara, T.; Kawano, S.; Suzuki, T.; Kanno, I.; Kotera, H., Micro cell encapsulation and its hydrogel-beads production using microfluidic device. *Microsystem Technologies* **2007,** *13* (8-10), 951-958.

63.　　Håti, A. G.; Bassett, D. C.; Ribe, J. M.; Sikorski, P.; Weitz, D. A.; Stokke, B. T., Versatile, cell and chip friendly method to gel alginate in microfluidic devices. *Lab on a Chip* **2016,** *16* (19), 3718-3727.

64.　　Chan, H. F.; Zhang, Y.; Ho, Y.-P.; Chiu, Y.-L.; Jung, Y.; Leong, K. W., Rapid formation of multicellular spheroids in double-emulsion droplets with controllable microenvironment. *Scientific Reports* **2013,** *3*.

65.　　Martinez, C. J.; Kim, J. W.; Ye, C.; Ortiz, I.; Rowat, A. C.; Marquez, M.; Weitz, D., A Microfluidic Approach to Encapsulate Living Cells in Uniform Alginate Hydrogel Microparticles. *Macromolecular Bioscience* **2012,** *12* (7), 946-951.

66.　　Morgan, A. J. L.; Jose, L. H. S.; Jamieson, W. D.; Wymant, J. M.; Song, B.; Stephens, P.; Barrow, D. A.; Castell, O. K., Simple and Versatile 3D Printed Microfluidics Using Fused Filament Fabrication. *PLOS ONE* **2016,** *11* (4), e0152023.

67.   Ren, P.-W.; Ju, X.-J.; Xie, R.; Chu, L.-Y., Monodisperse alginate microcapsules with oil core generated from a microfluidic device. *Journal of Colloid and Interface Science* **2010,** *343* (1), 392-395.

68.   Kim, C., Droplet-based microfluidics for making uniform-sized cellular spheroids in alginate beads with the regulation of encapsulated cell number. *BioChip Journal* **2015,** *9* (2), 105-113.

69.   Chen, W.; Kim, J.-H.; Zhang, D.; Lee, K.-H.; Cangelosi, G. A.; Soelberg, S. D.; Furlong, C. E.; Chung, J.-H.; Shen, A. Q., Microfluidic one-step synthesis of alginate microspheres immobilized with antibodies. *Journal of The Royal Society Interface* **2013,** *10* (88), 20130566.

70.   Poncelet, D.; Lencki, R.; Beaulieu, C.; Halle, J. P.; Neufeld, R. J.; Fournier, A., Production of alginate beads by emulsification/internal gelation. I. Methodology. *Applied Microbiology and Biotechnology* **1992,** *38* (1), 39-45.

71.   Bugarski, B.; Li, Q.; Goosen, M. F. A.; Poncelet, D.; Neufeld, R. J.; Vunjak, G., Electrostatic droplet generation: Mechanism of polymer droplet formation. *AIChE Journal* **1994,** *40* (6), 1026-1031.

72.   Taylor, G. J.; Venkatesan, G. A.; Collier, C. P.; Sarles, S. A., Direct in situ measurement of specific capacitance, monolayer tension, and bilayer tension in a droplet interface bilayer. *Soft Matter* **2015,** *11* (38), 7592-7605.

73.   Baxani, D. K.; Morgan, A. J. L.; Jamieson, W. D.; Allender, C. J.; Barrow, D. A.; Castell, O. K., Bilayer Networks within a Hydrogel Shell: A Robust Chassis for Artificial Cells and a Platform for Membrane Studies. *Angewandte Chemie International Edition* **2016,** *55* (46), 14240-14245.

74.   Nunes, J. K.; Tsai, S. S. H.; Wan, J.; Stone, H. A., Dripping and jetting in microfluidic multiphase flows applied to particle and fiber synthesis. *Journal of physics D: Applied physics* **2013,** *46* (11).

75.   Garstecki, P.; Fuerstman, M. J.; Whitesides, G. M., Oscillations with uniquely long periods in a microfluidic bubble generator. *Nature Physics* **2005,** *1* (3), 168-171.

76.   Garstecki, P.; Fuerstman, M. J.; Stone, H. A.; Whitesides, G. M., Formation of droplets and bubbles in a microfluidic T-junction—scaling and mechanism of break-up. *Lab on a Chip* **2006,** *6* (3), 437-446.

77.   Rezaei Mokarram, A.; Mortazavi, S. A.; Mohammadpour Dounighi, N.; Zolfagharian, H.; Alonso, M. J., Preparation and in-vitro evaluation of sodium alginate microspheres containing diphtheria toxoid as new vaccine delivery. *Archives of Razi Institute* **2008**.

78.   Redwood, W. R.; Pfeiffer, F. R.; Weisbach, J. A.; Thompson, T. E., Physical properties of bilayer membranes formed from a synthetic saturated phospholipid in n-decane. *Biochimica Et Biophysica Acta* **1971,** *233* (1), 1-6.

79.   van Uitert, I.; Le Gac, S.; van den Berg, A., The influence of different membrane components on the electrical stability of bilayer lipid membranes. *Biochimica et Biophysica Acta (BBA) - Biomembranes* **2010,** *1798* (1), 21-31.

80.   Orosz, K. S., Diffusion Coefficients and Mechanical Properties of Polymerizable Lipid Membranes. **2011**.

81.   Punnamaraju, S.; You, H.; Steckl, A. J., Triggered Release of Molecules across Droplet Interface Bilayer Lipid Membranes Using Photopolymerizable Lipids. *Langmuir* **2012,** *28* (20), 7657-7664.

82.   Engineering plant membranes using droplet interface bilayers. *Biomicrofluidics* **2017,** *11* (2), 024107.

83.   Hwang, W. L.; Chen, M.; Cronin, B.; Holden, M. A.; Bayley, H., Asymmetric Droplet Interface Bilayers. *Journal of the American Chemical Society* **2008,** *130* (18), 5878-5879.

84.   Villar, G.; Graham, A. D.; Bayley, H., A Tissue-Like Printed Material. *Science (New York, N.Y.)* **2013,** *340* (6128), 48-52.

85.   Venkatesan, G. A.; Sarles, S. A., Droplet immobilization within a polymeric organogel improves lipid bilayer durability and portability. *Lab on a Chip* **2016,** *16* (11), 2116-2125.

86.   Sarles, S. A.; Leo, D. J., Physical encapsulation of droplet interface bilayers for durable, portable biomolecular networks. *Lab on a Chip* **2010,** *10* (6), 710-717.

87.   Boreyko, J. B.; Polizos, G.; Datskos, P. G.; Sarles, S. A.; Collier, C. P., Air-stable droplet interface bilayers on oil-infused surfaces. *Proceedings of the National Academy of Sciences* **2014**, 201400381.

88.   Giomi, L.; DeSimone, A., Spontaneous division and motility in active nematic droplets. *Physical Review Letters* **2014,** *112* (14).

89.	Shioi, A.; Ban, T.; Morimune, Y., Autonomously Moving Colloidal Objects that Resemble Living Matter. *Entropy* **2010,** *12* (11), 2308-2332.
90.	Hanczyc, M. M., Metabolism and motility in prebiotic structures. *Philosophical Transactions of the Royal Society B: Biological Sciences* **2011,** *366* (1580), 2885-2893.
91.	Toyota, T.; Maru, N.; Hanczyc, M. M.; Ikegami, T.; Sugawara, T., Self-Propelled Oil Droplets Consuming "Fuel" Surfactant. *Journal of the American Chemical Society* **2009,** *131* (14), 5012-5013.

Chapter 4 – The Assembly of Encapsulated Droplet Interface Bilayers into Higher Order Structures

4.0 Chapter Summary

This chapter represents exploratory work in the assembly of higher order structures from individual encapsulated droplet interface bilayers (eDIBs), as developed in previous chapters. Their hydrogel shells are used as a means for a number of eDIBs to form higher order assemblies which can be regarded as artificial tissues. These novel constructs display multi-compartmentalisation at the level of their building blocks (the eDIBs), as well as at the level of the higher order assembly, providing a foundation for the continued development of functional, bottom-up synthetic biology constructs displaying hierarchical order and with the potential to give rise to complex functionality. Electrophysiology is employed in order to demonstrate electrical communication within an eDIB higher order assembly. Additionally, the microfluidic methods employed to produce eDIBs were used to produce alternative eDIB conformations, such as elongated chains and eDIBs containing a number of DIB networks within, which offer an alternative to producing higher order assemblies as well as potential models for the study of biological processes.

4.1 Introduction

Whilst the survival of single-cell organisms depends on the coaction of a number of different sub-cellular parts, multicellular organisms add subsequent layers of

complexity by depending on the cooperation of a number of higher order cellular organisations. This has allowed more complex biological systems to exist, applying the same fundamental functions that allow cells to survive (i.e. compartmentalisation, metabolism and replication) at a supra-cellular level (these functions are performed by groups of cells). Thus, whilst the development of artificial cells in itself is of great significance, it would be advantageous to develop a chassis for artificial cells that is capable of assembling into higher order structures akin to artificial tissues, as the continuous development of a system that can give rise to complexity via multi-compartmentalisation at different scales is expected to allow for more complex functionalities and emergent behaviours.

DIBs have often been referred to as potential structures for the development of artificial cells[1-6]. The development of DIB networks that function in aqueous environments[7], such as the encapsulated DIBs (eDIBs) described in this thesis[5], further realises this potential by allowing for its communication with an external, aqueous environment, and offers the ability to give rise to compartmentalised chemistry[8].

Villar et al. expanded the scale of droplet bilayer networks by several orders of magnitude, creating complex 3D networks of many thousands of droplets each individually printed[9]. By increasing the scale and dimensionality of droplet networks higher order behaviours could be introduced, ascribing tissue-like properties to the material. By printing 3D structures of two different droplet compositions with osmolality gradient between these different droplet types, passive diffusion of water across adjoining membranes was exploited to give rise to differential droplet swelling and shrinkage at defined locations in the 3D architecture. This introduced a responsive shape changing programmability into the synthetic tissue. Additionally, specific communicative paths could be engineered into the material by creating a path of droplets functionalised with membrane pores within a larger droplet assembly. This

163

allowed for rapid electrical communication along defined pathways within the artificial tissue structure. More recent developments have introduced light-responsive in vitro transcription and translation systems into the droplets, allowing for such paths to be directly written by exposure to light[10].

This work demonstrated a route to the development of tissue-like materials by expanding the scale of the number of droplets involved by several orders of magnitude, in comparison to previous DIB networks. Each "cellular" unit of the synthetic tissue is an individual droplet, which are connected by membranes to create a much larger structure. It would be advantageous to be able to create synthetic tissues comprised of multi-compartmentalised building blocks, affording the opportunity to engineer more sophisticated functionality into the cellular units of the tissue. It is anticipated that this would enable further complex tissue like properties and emergent behaviours to be exploited, creating a system closer to that of eukaryotic tissues. Towards fulfilling this ambition, it is proposed that eDIBs could constitute individual building blocks of a higher order structure, and consequently the production of tissue-like systems from eDIBs is the focus of this chapter.

The eDIBs developed in the previous chapter comprise a DIB network that is encapsulated within a hydrogel shell. The alginate shells can be used in order to segregate a number of DIB networks whilst allowing for diffusive communication between them due to the aqueous nature of the hydrogel. This provides a route towards which artificial tissues can be generated comprised of multi-compartmentalised, cellular units, as recently proposed by Bayoumi et al. [11]. This chapter aims to assemble eDIBs into higher-order, tissue-like structures whilst maintaining multi-compartment complexity at the cellular level. This will be attempted via the adherence of eDIBs to one another, which may be achieved via the incomplete gelling of the alginate shell as well as its elastic deformability (see section 3.1.2). An

164

alternative method will also be attempted via the production of eDIB conformations that comprise a number of oil-encapsulated DIB networks within a shared, alginate structure, which is expected to be achievable via the modulation of flow rates in the microfluidic production of eDIBs.

4.2 Materials and Methods

eDIBs were prepared as described in Chapter 3 (Section 3.3.2.2), using the microfluidic methods developed in chapter 2. Images were taken either with an iPhone 6, a USB microscope (Celestrion, USA), or a custom light microscope. eDIBs generated microfluidically were deliberately exited into containers for their assembly into higher order structures.

4.3 Results

4.3.1 eDIB "Proto-tissues"

eDIBs prepared as in Chapter 3 were output into a petri dish filled with mineral oil. Contacting eDIBs were found to adhere to each other when in close contact (Figure 4.1).
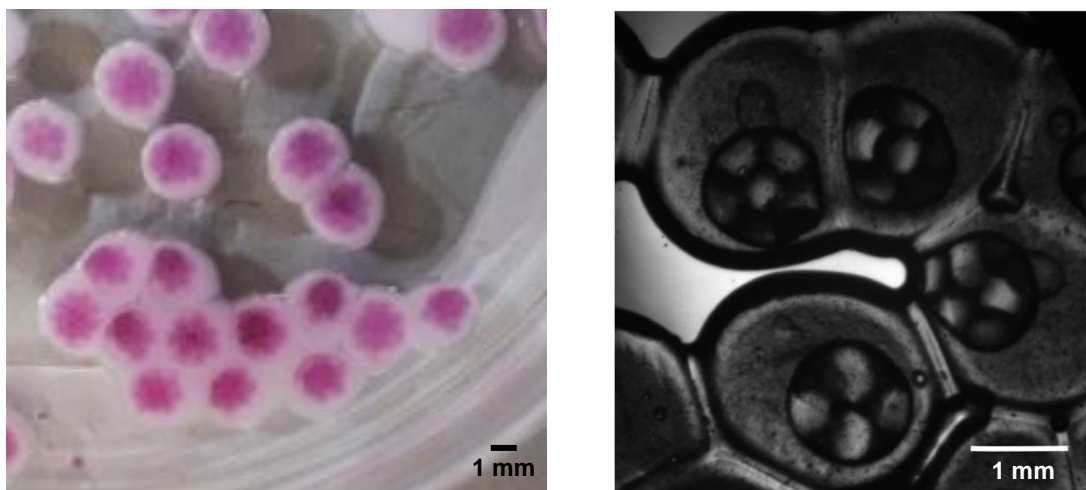
Figure 4.1 eDIBs in a petri dish filled with mineral oil which have been output directly from the microfluidic device. The eDIB aqueous cores are dyed pink with 25 µM sulphorhodamine B. The hydrogel shells of the eDIBs adhere to each other when in close proximity deforming their shape. Scale bars = 1 mm.

Figure 4.1 shows 2D conformations of eDIBs that are adhered to each other forming a

higher order, tissue-like structure. 3D conformations of eDIB proto-tissues were also

possible by outputting eDIBs at a higher density into a glass beaker, as shown in

Figure 4.2.

Figure 4.2 Beaker (5 mL) displaying a 3-dimensional network of adhered eDIBs in oil, forming 3D proto-tissues.

The eDIB shells appear to be deformable and adapt their shape to one another when in close proximity. Plastic deformability is a known property of ionically cross-linked alginate hydrogels[12], although it is likely that the adherence of eDIBs here is also aided by incomplete gelling of the hydrogel shells, as they are exited from the microfluidic device rapidly without any additional incubation time in the gelling solution (mineral oil + 0.5% acetic acid v/v). Additionally, the oil environment they are kept in likely provides a driving force for the alginate shells to minimise their contact area with the surrounding oil due to surface tension forces, and thus adhere to each other. It was found that eDIBs displayed some mechanical resistance when it was attempted to separate an eDIB from a group of adjoined eDIBs using a pair of tweezers (Figure 4.3i-iii), but it was possible to separate an eDIB without damage to the contained droplet networks, and also re-join the eDIB back into the larger assembly (Figure 4.3iii-v). This showcases the mechanical stability of the eDIBs, their ability to form mechanically resistant

167

assemblies, and also the ability of eDIB assemblies to be spatially re-configured. This

provides a route towards self-repairing and mechanically adaptable tissue-like
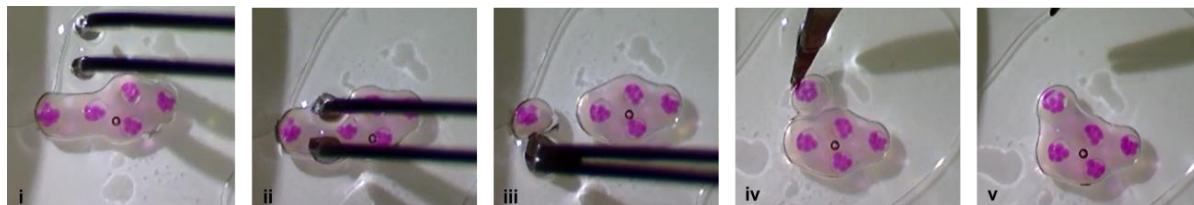
materials.

Figure 4.3 A group of 5 eDIBs forming a "proto-tissue". Tweezers are employed in order to separate an eDIB from the larger assembly, and then re-assemble the eDIB back into it without any apparent damage to the encapsulated bilayer network. The eDIB aqueous cores are dyed red with 25 µM sulphorhodamine B.

Similarly, it was found that eDIBs in oil in close proximity with each other would

spontaneously assemble into a higher order assembly, as shown in Figure 4.4. This is

likely due to surface tension forces between eDIBs in close proximity.

Figure 4.4 Time-course of eDIBs in oil in close proximity spontaneously assembling together into a "proto-tissue" over the course of 5 seconds. The eDIB aqueous cores are dyed red with 25 µM sulphorhodamine B.

eDIBs assemblies in oil could also be aspirated using a pipette and then pipetted back

out, with little or no damage to the eDIB structure, further demonstrating the robustness

of the eDIBs as well as of their higher order assemblies. This is shown in Figure 4.5.
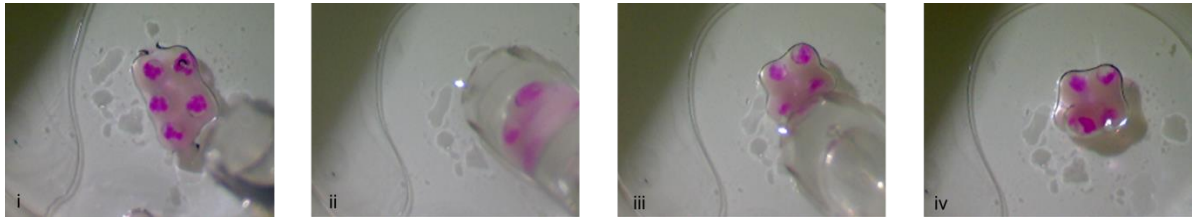
Figure 4.5 An assembly of 5 eDIBs in oil being aspirated into a cut pipette tip from a petri dish, and then being pipetted back out. The eDIB aqueous cores are dyed red with 25 µM sulphorhodamine B. Image iv appears to show one eDIB less, although this is because one eDIB is now sitting on top of another.

The adhesion of the eDIBs to each other was found to allow for diffusive electrical contact between eDIBs, evidenced by electrophysiology, where bilayers formed between the inner droplets of an eDIB and its hydrogel shell could be probed by having one electrode in an aqueous core of the probed eDIB and the other in the alginate shell of an adjacent eDIB within the larger eDIB assembly (Figure 4.6). Bilayer capacitance was observed when a +/- 23 mV, 10 Hz triangle wave potential was applied.
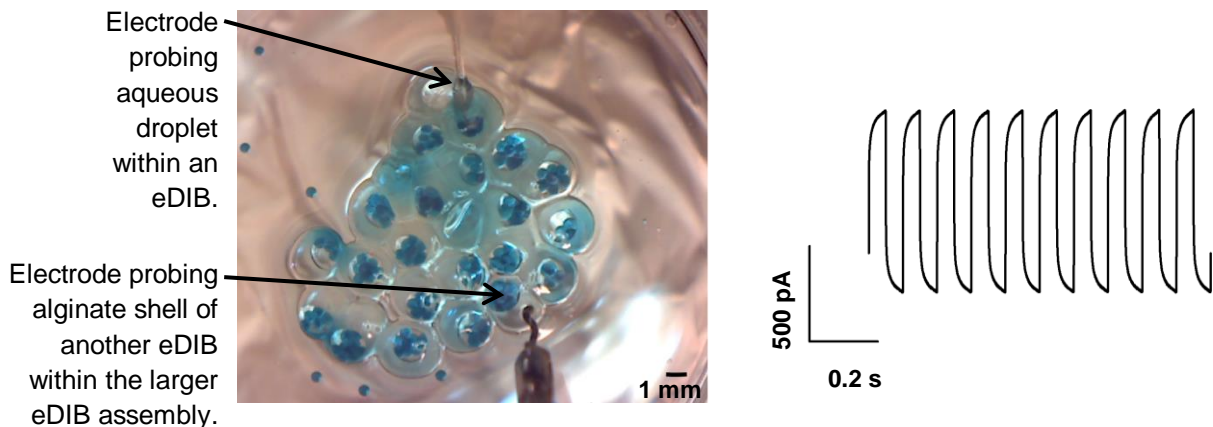

Figure 4.6 Diffusive electrical contact is demonstrated between eDIBs forming an artificial tissue in oil via electrophysiology. One electrode is present in the alginate shell of one eDIB, whilst the other is present inside an aqueous droplet contained within another eDIB, forming a bilayer between the aqueous droplet and its hydrogel shell. Capacitance was observed when a +/- 23 mV, 10 Hz triangle wave potential was applied (b), which demonstrates that the eDIBs share a conductive path between them due to the contact of the hydrogel shells. eDIBs are dyed blue with 50 µM Lissamine green. Scale bar = 1 mm.

4.3.2 Alternative eDIB conformations

Higher order eDIB assemblies could also be produced by encapsulating a number of eDIB networks within the same alginate hydrogel structure. In Chapter 2, the modulation of flow rates was used in order to affect the volume and generation frequency of aqueous droplets in a microfluidic device, giving rise to different numbers of encapsulated aqueous droplets per oil droplet (See section 2.3.2). A similar approach was employed here in order to produce higher order eDIB assemblies by modulating the alginate hydrogel formation in the carrier oil phase.

One example of this is the production of an eDIB chain, where a number of oil droplets containing aqueous cores inside was produced in an elongated alginate cylinder. This was achieved by using the microfluidic flow rate regimes used in chapter 3 (section 3.3.2.2) to produce eDIBs, except for the external oil phase flow rate which is halted after the tube has been prefilled with the oil solution. This avoided the breaking up of the alginate into droplets and allowed for an elongated alginate structure to form. The residual oil in the FEP outlet tube at either end of the alginate slug was sufficient to trigger initial gelation of the alginate exterior, before extruding the construct into a petri dish for complete gelation.
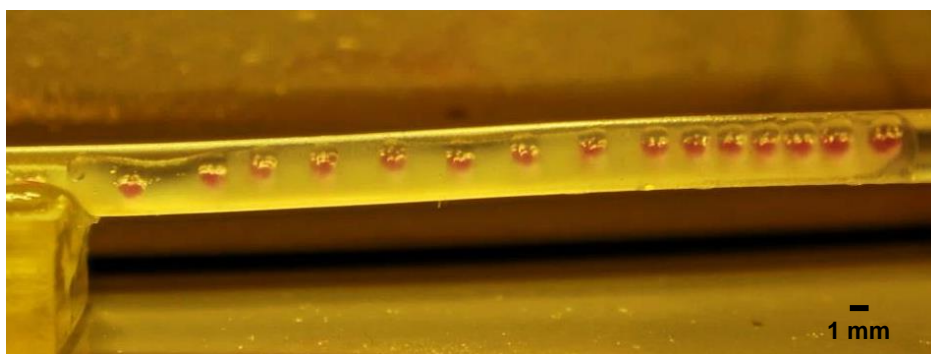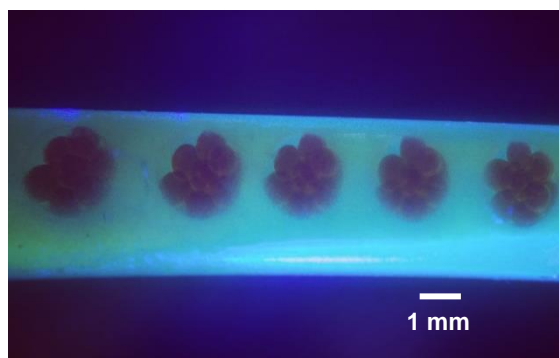
Figure 4.7 An eDIB chain within the final FEP tube of the microfluidic device employed to produce them (See section 2.3.2.3). The eDIB chain is comprised of a number of oil-encapsulated DIB networks within an elongated alginate hydrogel cylinder.

It was found that the alginate chains produced could be exited into a petri dish and manipulated with tweezers, with minimal damage to its structure and the DIBs contained within.
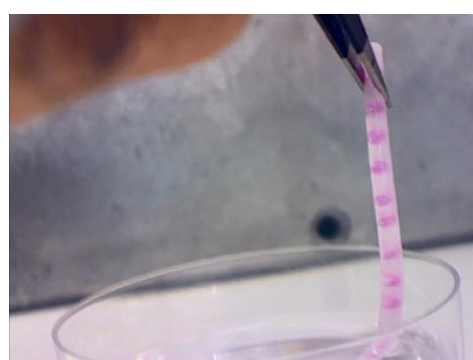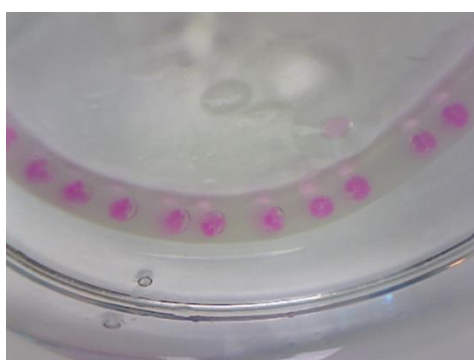

Figure 4.8 eDIB "chains" comprised of a number of oil-encapsulated DIB networks within an elongated hydrogel matrix. eDIB aqueous cores are dyed pink with 25 µM Sulphorhodamine. a) eDIB chain in a petri dish containing an aqueous solution. b) The eDIB chain can be manipulated and picked up with use of tweezers, demonstrating the robustness of the structure.

Additionally, it was also possible to produce eDIBs that comprised of two oil droplets containing droplet networks sharing the same alginate shell. These constructs could be produced by the slowing of the oil carrier phase relative to the preceding phases, resulting in a longer alginate droplet formation time and therefore the incorporation of additional oil droplets. In practice, this was achieved using the same flow rate regime employed to generate eDIBs as in section 3.3.2.2, and reducing the external oil carrier phase to a stop. The double-core eDIBs were produced for a short period of time between the use of flow rates for the generation of single-core eDIBs and the halting of the external oil carrier phase. It is likely that this can be achieved consistently be using relatively low carrier oil flow rates or a pulsatile flow regime. This kind of structure could find applications in the study of processes that occur where cells communicate in close contact with each other, bringing their respective membranes into close contact. Similarly, such architectures may pave the way for exploitation of close proximity and low diffusional volume between bilayers in synthetic systems, for example in the engineering of a synthetic synapse.
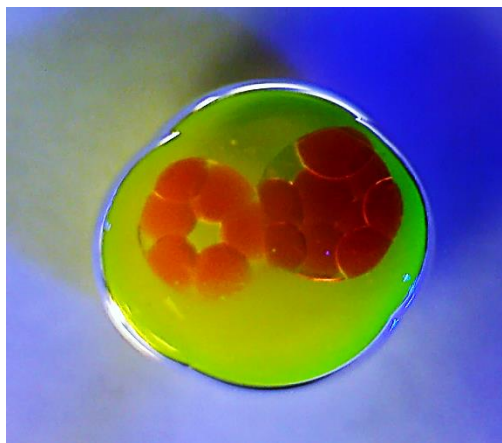

Figure 4.9 eDIB displaying two oil droplets with DIB networks within. The oil droplets are in close proximity to each other which could be used as a model for neuronal synapses or close cell-to-cell communication, for example. eDIB aqueous cores are dyed orange with 70 mM calcein (fluorescent yellow alginate is due to calcein contamination at the point of microfluidic manufacture).

4.4 Discussion & Conclusion

The work performed in this chapter shows initial work in the production of higher order assemblies using eDIBs as building blocks or artificial cells. It was demonstrated that eDIBs could form higher order assemblies where the hydrogel shells of a number of eDIBs adhered to each other when in close contact. This would occur spontaneously when eDIBs were placed in close contact with each other, displaying potential self-assembling properties likely due to surface forces. Additionally, eDIBs within a larger assembly could be mechanically separated and re-joined, which demonstrated the potential of eDIB artificial tissues to be spatially re-configurable and display self-repairing properties. Electrophysiology experiments confirmed that eDIBs forming a higher order assembly were in diffusive electrical contact with each other, and thus chemical and electrical communication between an eDIB artificial tissue should be achievable.

In comparison to the artificial tissues developed by Villar et al., the artificial tissues produced here achieve multi-compartmentalisation at the level of the individual building blocks, in addition to that of the higher order assembly. In the demonstrated system there are both connected and isolated components within the higher order structure, with the hydrogel in diffusive contact and internal droplet networks isolated by lipid bilayers. In contrast, the work of Villar et al. uses membranes to segregate all compartments of the larger structure. There are likely opportunities and drawbacks of each approach, depending on the requirement, for example, to isolate or perfuse. Given that it is possible to form DIBs between contacting hydrogels, the described approach with eDIBs could be extended to form bilayers between contacting alginate shells, thus generating similar membrane based selective connectivity between individual cellular units as that achieved by Villar et al.'s approach. It is notable that such an approach could be expected to generate significant complexity, affording

bilayer networks within bilayer networks. The employment of membrane protein regulated communication between and within droplet networks created the opportunity for feedback, interference, transmission as well as isolation of processes.

A similar concept to the eDIB tissue system reported in this chapter was proposed by Bayoumi et al., where hydrogel blocks containing a number of DIB networks within could be considered to be protocells or proto-tissues. It was reasoned that the formation of DIBs between a number of these units could be considered to be a proto-tissue or proto-organ. The capability to produce eDIBs rapidly and in large numbers by the microfluidic methods developed here, should facilitate the realisation and scaling of this concept, beyond of what is achievable using manual methods of production.

An alternative approach towards the production of higher order eDIB assemblies was also demonstrated here, achieved by modifying microfluidic flow regimes in the production of eDIBs, which gave rise to alginate structures containing a number of oil droplets with DIB networks within them. For example, an elongated cylinder of alginate containing a number of oil-encapsulated DIB networks was produced, as well as eDIBs containing two oil-encapsulated DIB networks in close proximity. The latter could find applications in the development of biomimetic models for scenarios of close cell-to-cell contact, such as in neuronal synapses. Control over the gelation process should allow for a myriad of eDIB proto-tissue shapes and conformations to be produced. For example, large eDIB proto-tissues can be formed by outputting eDIBs into a mould of a desired shape, where eDIBs can be output from the microfluidic device as gelled droplets or as a stream of un-gelled alginate containing DIB networks within oil droplets for subsequent, off-chip gelation.

The formation of DIBs between the alginate shells of eDIBs would be the immediate focus of future work. It is expected that this should be immediately achievable as the formation of DIBs between hydrogel shapes has been evidenced by others[13, 14]. This

can be achieved by incubating eDIBs in oil containing a suitable phospholipid, and bringing them into close contact after a period of incubation allowing for the assembly of lipid monolayers around the eDIB hydrogel shell. The formation of lipid bilayers would be evidenced using electrophysiology. This would allow for the exploitation of the collective properties and multi-compartmentalisation offered by DIB networks across two different scales, as depicted in Figure 4.10, which is envisaged to have the potential to give rise to complex, emergent behaviour which can mimic biological function or be used for industrial and medical application in the future.

a)

i) DIB

ii) eDIB

iii eDIB tissue

Communication through lipid bilayers
- level 1 (between aqueous droplets)
- level 2 (between eDIB and environment)
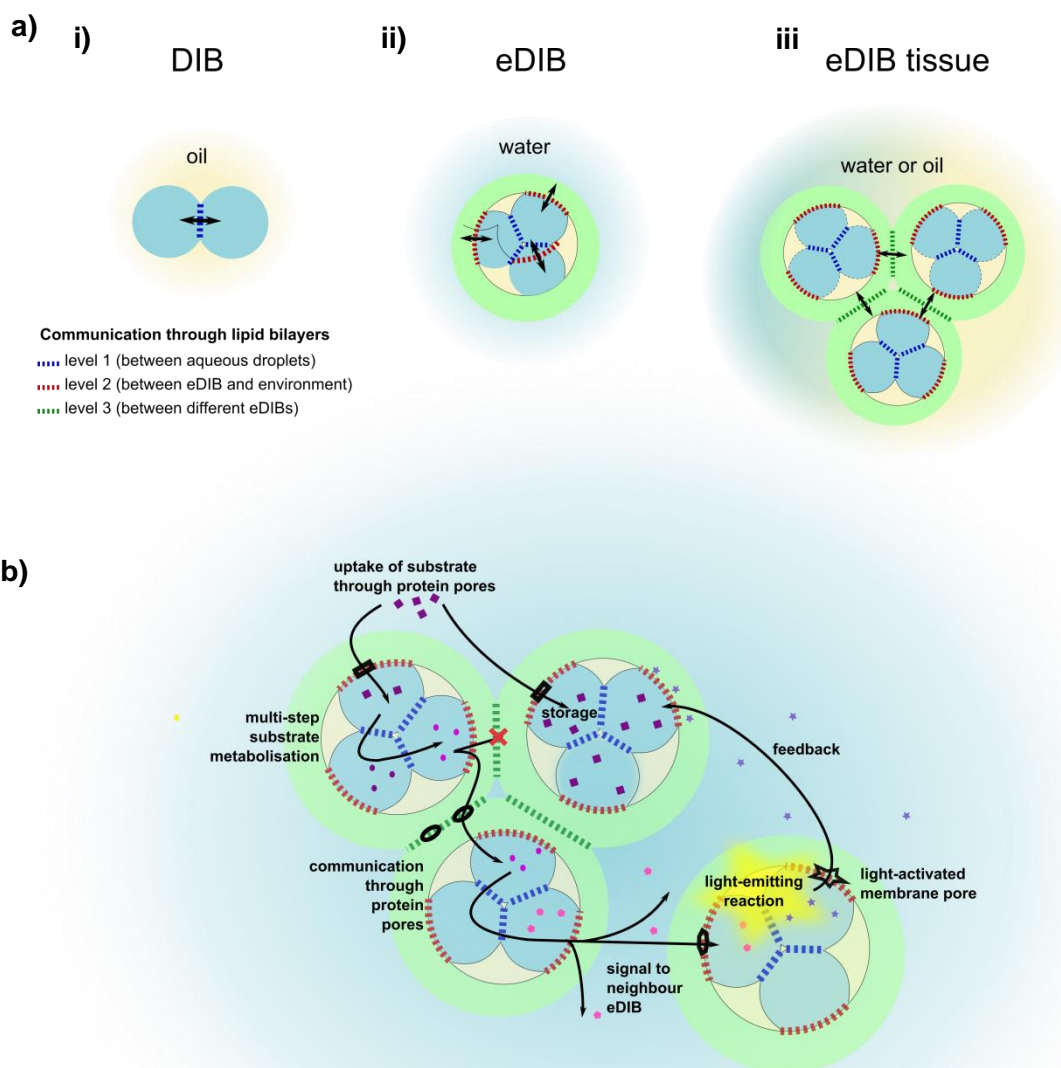- level 3 (between different eDIBs)

b)

Figure 4.10 a) Depiction of the different levels of communication achievable through bilayers with conventional DIBs, eDIBs and eDIB tissues. i) DIBs can only give rise to communication between one droplet and another. ii) eDIBs can also give rise to communication between DIB droplets and an external, aqueous environment. iii) eDIB tissues should be able to form bilayers between each other in oil and perhaps in water too with use of polymerisable lipids[15], for example, allowing for communication between a number of eDIBs. b) Different methods via which eDIBs forming tissues can communicate and interact with each other, with the use of the selective transfer of substrates from one eDIB compartment to another, or from one eDIB to another, with or without the use of membrane proteins that allow for the selective transfer of substances from one compartment to another.

DIB networks have been shown to give rise to collective properties, which can be exploited to give rise to electrical devices such as wave rectifiers[16].The assembly of

eDIBs containing readymade electrical devices could allow for the formation of complex electrical circuits in a soft matter system.

Additional work would involve the use of chemical systems and perhaps communication between eDIB populations of different chemical identity. One chemical system that could be employed is the conversion of resazurin to fluorescent resorufin in the presence of horseradish peroxidase and hydrogen peroxide. This could be employed for the detection of glucose present in an aqueous environment via its uptake into eDIB compartments and oxidation using glucose oxidase, for example[17]. Furthermore, it would be interesting to incorporate chemical waves that occur across an eDIB proto-tissue, as a method of chemical synchronisation, stasis and sensing between a number of eDIBs, akin to the behaviour of slime molds such as *physarum polycephalum*[18, 19], which pulsate via cytoplasmic streaming in order to give rise to homeostasis and locomotion. This could be imitated in a proto-tissue system via the incorporation of oscillating chemical reactions such as the Belousov-Zhabotinsky reaction[20].

It is anticipated that these kinds of higher order structures can be used to amplify the potential use of DIBs as bio-inspired devices, and may be used as arrays for membrane studies or optical sensing, akin to the pattern-recognising DIB array developed by Restrepo-Schild et al.[21]. eDIB assemblies may also find use as models for biological tissues. The alginate shells of the eDIBs can be considered to be mimetic of an extracellular matrix[22], which holds the artificial cells in place. Alginate hydrogels also limit the diffusion of large molecules[23], which could be useful for the maintenance of a local microenvironment within the synthetic tissue. Additionally, alginate can be functionalised with different chemical moieties for its selective adhesion or sequestering of substances[24].

4.5 References

1.   Bayley, H.; Cronin, B.; Heron, A.; Holden, M. A.; Hwang, W.; Syeda, R.; Thompson, J.; Wallace, M., Droplet interface bilayers. *Molecular bioSystems* **2008,** *4* (12), 1191-1208.

2.   Needham, D., Lipid structures: A brief history of multisomes. *Nature Nanotechnology* **2011,** *6* (12), 761-762.

3.   Elani, Y.; V. Law, R.; Ces, O., Protein synthesis in artificial cells: using compartmentalisation for spatial organisation in vesicle bioreactors. *Physical Chemistry Chemical Physics* **2015,** *17* (24), 15534-15537.

4.   Elani, Y., Construction of membrane-bound artificial cells using microfluidics: a new frontier in bottom-up synthetic biology. *Biochemical Society Transactions* **2016,** *44* (3), 723-730.

5.   Baxani, D. K.; Morgan, A. J. L.; Jamieson, W. D.; Allender, C. J.; Barrow, D. A.; Castell, O. K., Bilayer Networks within a Hydrogel Shell: A Robust Chassis for Artificial Cells and a Platform for Membrane Studies. *Angewandte Chemie International Edition* **2016,** *55* (46), 14240-14245.

6.   Trantidou, T.; Friddin, M.; Elani, Y.; Brooks, N. J.; Law, R. V.; Seddon, J. M.; Ces, O., Engineering Compartmentalized Biomimetic Micro- and Nanocontainers. *ACS nano* **2017**.

7.   Villar, G.; Heron, A. J.; Bayley, H., Formation of droplet networks that function in aqueous environments. *Nature Nanotechnology* **2011,** *6* (12), 803-808.

8.   Elani, Y.; Solvas, X. C. I.; Edel, J. B.; Law, R. V.; Ces, O., Microfluidic generation of encapsulated droplet interface bilayer networks (multisomes) and their use as cell-like reactors. *Chemical Communications* **2016,** *52* (35), 5961-5964.

9.   Villar, G.; Graham, A. D.; Bayley, H., A Tissue-Like Printed Material. *Science (New York, N.Y.)* **2013,** *340* (6128), 48-52.

10.   Booth, M. J.; Schild, V. R.; Graham, A. D.; Olof, S. N.; Bayley, H., Light-activated communication in synthetic tissues. *Science Advances* **2016,** *2* (4), e1600056.

11.   Bayoumi, M.; Bayley, H.; Maglia, G.; Sapra, K. T., Multi-compartment encapsulation of communicating droplets and droplet networks in hydrogel as a model for artificial cells. *Scientific Reports* **2017,** *7*, 45167.

12.   Stress-relaxation behavior in gels with ionic and covalent crosslinks. *Journal of Applied Physics* **2010,** *107* (6), 063509.

13.   Sapra, K. T.; Bayley, H., Lipid-coated hydrogel shapes as components of electrical circuits and mechanical devices. *Scientific Reports* **2012,** *2*, 848.

14.   Huang, S.; Romero-Ruiz, M.; Castell, O. K.; Bayley, H.; Wallace, M. I., High-throughput optical sensing of nucleic acids in a nanopore array. *Nature Nanotechnology* **2015,** *10* (11), 986-991.

15.   Cashion, M. P.; Long, T. E., Biomimetic design and performance of polymerizable lipids. *Accounts of Chemical Research* **2009,** *42* (8), 1016-1025.

16.   Maglia, G.; Heron, A. J.; Hwang, W. L.; Holden, M. A.; Mikhailova, E.; Li, Q.; Cheley, S.; Bayley, H., Droplet networks with incorporated protein diodes show collective properties. *Nature Nanotechnology* **2009,** *4* (7), 437-440.

17.   Elani, Y.; Law, R. V.; Ces, O., Vesicle-based artificial cells as chemical microreactors with spatially segregated reaction pathways. *Nature Communications* **2014,** *5*, 5305.

18.   Hejnowicz, Z.; Wohlfarth-Bottermann, K. E., Propagated Waves Induced by Gradients of Physiological Factors Within Plasmodia of Physarum polycephalum. *Planta* **1980,** *150* (2), 144-152.

19.   Jones, J.; Tsuda, S.; Adamatzky, A., Towards Physarum Robots. In *Bio-Inspired Self-Organizing Robotic Systems*, Meng, Y.; Jin, Y., Eds. Springer Berlin Heidelberg: 2011; pp 215-251.

20.   Torbensen, K.; Rossi, F.; Ristori, S.; Abou-Hassan, A., Chemical communication and dynamics of droplet emulsions in networks of Belousov–Zhabotinsky micro-oscillators produced by microfluidics. *Lab on a Chip* **2017,** *17* (7), 1179-1189.

21.   Schild, V. R.; Booth, M. J.; Box, S. J.; Olof, S. N.; Mahendran, K. R.; Bayley, H., Light-Patterned Current Generation in a Droplet Bilayer Array. *Scientific Reports* **2017,** *7*, 46585.

22.   Rowley, J. A.; Madlambayan, G.; Mooney, D. J., Alginate hydrogels as synthetic extracellular matrix materials. *Biomaterials* **1999,** *20* (1), 45-53.

23.   Tanaka, H.; Matsumura, M.; Veliky, I. A., Diffusion characteristics of substrates in Ca-alginate gel beads. *Biotechnology and Bioengineering* **1984,** *26* (1), 53-58.
24.   Dalheim, M. Ø.; Vanacker, J.; Najmi, M. A.; Aachmann, F. L.; Strand, B. L.; Christensen, B. E., Efficient functionalization of alginate biomaterials. *Biomaterials* **2016,** *80*, 146-156.

Chapter 5 – eDIB Arrays as a High-Throughput Assay Platform for Membrane Leakage and Disruption

5.0 Chapter Summary

This chapter concerns the development of a high-throughput assay platform for artificial lipid membranes (ALMs) using eDIBs as developed in Chapter 3. For this, eDIBs with aqueous cores containing a self-quenched solution of calcein are placed individually within wells of 96-well plates. Changes in fluorescence resulting from the de-quenching of calcein upon its release into the alginate shell of the eDIB are measured using a plate reader. Firstly, the assay is shown to be able to detect calcein droplet coalescence with the alginate shell, resulting from bilayer failure and giving rise to large and rapid increases in fluorescence. Secondly, the assay is shown to be able to detect leakage from bilayers, which gives rise to steady increases in fluorescence, as one would expect from the formation of bilayer pores. Validation experiments are performed by spiking eDIB wells with known amounts of fluorophore and comparing standard plate reading (single value) and well scanning measurements providing spatial information, in order to account for artefacts that may arise from spatial variations within the well. The assay platform is demonstrated via the exposure of eDIBs in 96-well plates to the detergents Triton-X100 and sodium dodecyl sulphate (SDS), which are known to stochastically form pores in bilayers. Following the demonstrations that the assay can detect different kind of bilayer disruption, proof-of-concept experiments are performed via exposing eDIBs to concentrations of the pore-forming peptides

Magainin 2 and PGLa, demonstrating the ability of eDIBs to serve as a high-throughput
platform for optical membrane assays.

5.1 Introduction

As mentioned in section 1.2, lipid membranes and membrane proteins are vital to the
function of cells and organisms, and are implicated in a large number of diseases. For
example, type II familial hypercholesterolemia and cystic fibrosis are membrane
receptor related diseases[1], and many types of haemolytic anaemia are cell membrane
disorders[2]. A significant amount of pathogenic microbes interact with membranes in
one form or another[3], many causing pathogenesis via membrane-interacting or pore-
forming toxins (i.e. α-Hemolysin from *staphylococcus aureus*). Additionally, a large
amount of antibiotics work by targeting bacterial cell membranes[1].

Despite the importance of lipid membranes and membrane proteins, few high-
throughput methods exist for their study. Taking from the success of DNA[4] and protein-
protein interaction microarrays and chips[5], there is great potential in the production of
lipid bilayer arrays which are necessary for the high-throughput study and function of
membrane proteins. This would provide the potential to accelerate drug screening and
discovery, as well as improve fundamental studies into membrane and membrane
protein function and interactions. It would also open up the possibility to develop novel
medical care devices at the point-of-care for early detection of pathogens or other
disease-related markers[6].

The difficulties in producing lipid membrane and membrane protein arrays lie in the
somewhat fragile nature of lipid membranes as well as challenges in inserting
functional membrane proteins within a lipid membrane[6]. Additionally, common
electrophysiological methods for recording membrane protein function and lipid
membrane properties suffer from scaling issues, with arrays requiring increasingly

complex electronic set-ups. Optical methods are more easily scalable and are commonly used for membrane protein pore flux experiments[7].

High-throughput bilayer arrays have few basic requirements. They require to be composed of a geometrically-defined pattern of biomolecules (in this case, artificial lipid membranes) which allow for parallel screening via the addition of samples[6], thus requiring access to one or both sides of the lipid membrane. They also require assays that allow for measurements to be taken rapidly and accurately, preferably in an automated manner. The ALMs should be reproducibly stable. Such arrays would benefit from methods that allow for the automated production of ALMs and sample handling, as well as the ability to assay via a number of different means i.e. both optical methods and electrophysiology. Furthermore, it is also advantageous to produce arrays which can interface with existing technology, such as robots, sample handlers and measurement tools, such as those that are optimised for a microplate format.

5.1.1 Current ALM array technologies

Virtually all methods of producing ALMs have been converted into arrays with varying degrees of success. This section will provide an overview of planar and supported lipid membrane, vesicle and DIB arrays.

5.1.1.1 Planar lipid membranes

Planar lipid membranes, or black lipid membranes (BLMs), are formed by "painting" lipid in an adequate solvent in an aperture between two aqueous compartments[8]. Methods for BLM formation are known to be laborious, and the resultant bilayers often contain excess solvent due to the mechanism of formation, and are known to be somewhat unstable[9]. Microfabrication techniques have allowed BLM methods to be significantly improved, via the use of micrometer-sized apertures (15 -50 μm) to form BLMs[10, 11]. Le Pioufle et al. developed a 5 x 5 BLM array[12] with over 15 hours of

survivability, and able to give rise to simultaneous and parallel electrophysiology recordings of protein channels.

5.1.1.2 Supported lipid membranes

In 1997 Groves et al. created the first array of supported lipid bilayers (SLBs)[13]. Diffusion barriers were produced using photolithographic techniques, whereby membrane patches were partitioned homogeneously into an array format. The ability to produce concentration gradients of charged lipid via exposure to an electric field is preserved, although bilayer fluidity is likely limited to the upper leaflet of the bilayer as the lower is anchored to the surface. Heterogeneous arrays are also possible using a microcapillary tube to place vesicle solutions in different areas of the array[14]. Over the years, different methods of depositing SLB arrays on surfaces have been developed[15], with a few delving into the microfluidic realm[16]. These kinds of arrays allow for largely optical assays and have been used for the high-throughput screening of drugs[17], immune cell interactions[18], and other applications. Overall, SLB arrays provide the ability to produce high-throughput, optical, parallelised measurements on either identical or heterogeneous SLBs. Individually addressable SLB arrays have also been produced[14], which allows for parallel sample analysis. Challenges remain inherent to the use of SLBs, such as the lack of access to one side and difficulty in inserting transmembrane proteins. Microcavity SLBs have arisen in the recent years in order to circumvent the issue of accessibility to either sides of the bilayer and have been used to monitor transport into a bilayer-separated compartment[19], however electrophysiological methods in such systems remain still a challenge. Another drawback of SLB arrays is their scant resemblance to biological membranes, as they lack in curvature and facile methods to achieve bilayer asymmetry, aside from not enclosing a volume of fluid as cell membranes and vesicles do.

5.1.1.3 Vesicles

Methods to produce vesicle arrays have been extensively studies in the last couple of decades due to their potential for high throughput membrane protein analysis[20]. Vesicles are naturally more biomimetic than supported or planar lipid bilayers due to their curvature and their relevance within cell biology, and are usually generated in large numbers as dispersions[21]. Vesicle-based assays for pore-forming substances, for example, are usually confined to bulk, ensemble measurements which can be less revealing than measurements on individual bilayers[22-24]. Thus, the ability to tether vesicles to a surface allows for the generation of high-throughput, multiplexed assays with the ability to assay individual bilayers.

Vesicle arrays usually rely on the patterning of surfaces where an array of vesicle-adhesive patches sit in a non-adhesive background. A number of microfabrication techniques have been used to develop such arrays, which have been reviewed by Bally et al.[6] and Mazur et al.[20]. For the immobilisation of vesicles, complementary DNA strands have been employed[25], where one strand is present on the supporting surface and a complementary strand is present on the vesicle surface, attached to it using cholesterol-linked DNA. Another method involves the use of disulphide-based linkage, which was reported to simplify the process as well as make the array reusable[26]. This method was used to quantify growth hormone related peptides at a nanogram level. Saliba et al. used another kind of vesicle array to assay protein recruitment to membranes in "a quantitative, automated, multiplexed and high-throughput manner"[27]. In this study, liposomes were formed on agarose patches where they remained for at least 6 hours, and were used to detect fluorescent-tagged proteins derived from bacterial and mammalian cells.

GUV arrays have also been created containing membrane proteins (aquaporin Z in this case) [28], whereby 30 GUV were created via electro-formation. The functional

184

preservation of aquaporin Z was suggested via the change in size of the GUVs arising from increased water transport facilitated by the Aquaporin pores in comparison to control GUVs, in response to osmotic imbalances. The use of GUV arrays carry the inherent benefit of looking at individual constructs that can be generated with controlled size and composition, allowing for single bilayer studies.

5.1.1.4 Droplet interface bilayers

Droplet interface bilayers (DIBs) offer exciting potential in producing bilayer arrays, due to the ease and robustness of their formation, as well as the large variety of manipulation techniques available to aqueous droplets[29-31]. A few examples of DIB arrays exist in the short history of DIB technology.

One of the first examples of a DIB array was demonstrated by Syeda et al., whereby a droplet anchored on a micromanipulator-attached electrode is used to form a DIB between itself and any one of droplets from a 4 x 4 array of droplets[32]. This was employed to sequentially screen a potassium channel against channel blockers in different droplets by electrophysiology. Castell et al. developed a microfabricated device whereby DIBs were formed between droplets and a hydrogel surface[7] in a 6 x 3 array. This was used to optically quantify the inhibition of the membrane pore α-Hemolysin via the fluorescent detection of Ca^{2+} flux into the droplets using wide-field total internal reflection (TIRF) microscopy. The use of total internal reflection (TIRF) s employed here to visualise a number of bilayers in parallel offers the potential to visualise transmembrane proteins and ion flux with single-molecule resolution. This is employed by Huang et al., who developed a hydrogel-hydrogel DIB array comprised of up to 2500 DIBs, able to visualise and optically encode the transfer of nucleic acid sequences across the transmembrane pores α-hemolysin and Mycobacterium smegmatis porin A (MspA) for sequencing purposes. Optical recordings were taken at an impressive density of $\approx 10^4$ pores per mm^2. Soga et al. developed a device able to

185

form ≈ 10,000 DIBs between a droplet and a volume of fluid within a cylindrical chamber[33]. The size of the chambers, droplets, and bilayers formed are of importance here, as they form 4 µm wide bilayers across volumes of fluid ranging between 3.3 fL and 200 aL, and a much larger volume of fluid shared between all bilayers. Such a set-up allowed for the measurement of the diffusion of a fluorescent dye (Alexa 488) across α-Hemolysin pores within a large number of lipid bilayers. The low volume of fluid within the chambers allowed for relatively rapid measurements of low numbers of α-Hemolysin channels in the membranes (1 or 2 per membrane). The same system has been employed to generate asymmetric lipid bilayers[34]. The main drawback of this set-up is that the bilayers are not fully individually addressable, as they all share the same aqueous volume on one side of the bilayer.

Furthermore, microfluidic systems are being developed which allow for the automated or facilitated production of DIB arrays, although demonstrations of their use as high-throughput assays have yet to be performed. In one instance, microfluidic droplet-trapping geometries are used to bring aqueous droplets (in lipid-containing oil) in close proximity to each other in groups of 3, forming bilayers between them[35]. Up to 27 of these DIB networks are produced in a single device, and a limited demonstration of the passive transfer of fluorophores across the bilayers was used to suggest the formation of DIBs, and demonstrates the ability to optically image transport between the droplets. Another example of an automated method of DIB array production involves the use of a PMMA microdevice with movable chambers, whereby droplets are initially separated from one another and upon sliding the moving parts of the device against each other, a number of DIB droplet pairs form[36]. Although these systems demonstrate potential in rapidly producing large numbers of DIBs, further experiments are required in order to demonstrate their application in high-throughput assays.

186

This chapter will focus on the development of a DIB platform for high-throughput studies, using eDIBs in 96-well plates. eDIBs can be output in an array that is compatible with common-place laboratory equipment, such as optical plate readers, further facilitating a compatible, bilayer array assay platform. Demonstration of the capabilities of the array is performed by exposing the eDIBs to bilayer-disrupting molecules, namely detergents and pore-forming peptides, and the leakage, or transfer of dye from one bilayer compartment to another is measured.

5.1.2 Membrane disruption

Bilayer disruption often occurs from membrane pore formation, which can occur via the insertion of transmembrane protein pores, such as α-Hemolysin, which structurally contain a pore, or via a number of different molecular species which form pores via disruption of lipid packing and order within a membrane. Such substances include detergent-like peptides, pore-forming peptides, as well as a number of detergents. Membrane lysis, solubilisation and pore formation caused by these molecules are important in many biological and technical applications[37]. For example, peptides that disrupt membranes, either via their lysis or the formation of pores, constitute a pathogenic or defence mechanism of certain organisms and microorganisms[3]. As such, they can be exploited as anti-microbial and other therapeutic small molecules[38]. Additionally, membrane solubilisation is an important biophysical technique used to isolate, purify, extract or reconstitute membrane structures such as proteins[37, 39].

The mechanisms of membrane disruption of many of these substances remain somewhat elusive due to their complexity and dependence on a number of variables including concentration, pH, lipid head polarity, and the presence of cholesterol or other membrane constituents. Initially, it was thought that the main mechanism via which micelle-forming amphiphiles disrupted bilayers was via their insertion into the bilayer and the induction of curvature stress, as the micellar curvature contrasts with the

187

relatively planar structure of the lipid bilayer[40, 41]. However, diversity in the action and kinetics of different detergents clarified that the disruption of lipid bilayers could not be a cause of curvature stress alone. Kragh-Hansen[42] described two different mechanisms of amphiphile-induced bilayer disruption: 1) the trans-bilayer insertion of amphiphiles into the bilayer and 2) the stripping of lipids from the bilayer caused by the presence of amphiphile micelles in solution. Some detergents and peptides are thought to give rise to pores in a lipid bilayer or local defects which increase bilayer permeability, and cause lysis in this way, whilst others thought to cause a more "fulminant" bilayer disruption where the bilayer is destroyed once a critical curvature stress is reached[41]. This has made it convenient to classify the activity of bilayer-disrupting amphiphiles as either homogeneously or heterogeneously membrane-disrupting[41, 43].

The debate regarding the exact mechanisms of action for many peptides and amphiphiles is largely due to the challenges in their study, as many currently available techniques rely on ensemble averaging (e.g. x-ray diffraction[44], ensemble vesicle leakage assays[20, 23]). Suggested models of bilayer disruption include the "barrel-stave" and toroidal models of pore formation, and the "carpet model"[45] (Figure 5.1). The barrel-stave describes the assembly of peptides into a barrel-like bundle where individual, helical peptides would be the staves, and was found to be unique to the action of alamethicin[46, 47]. The toroidal pore model involves peptides that only associate with the lipid head groups, where the pore is lined by the peptides and lipid head groups, as the bilayer leaflets bend continuously from one monolayer to another, protecting the lipid tail groups[48]. The carpet model involves the accumulation of peptides parallel to the membrane surface (the formation of a "carpet" of peptide along the membrane) which causes membrane disruption at a critical peptide concentration[49], similar to the homogeneous method of bilayer disruption described by Kragh-Hansen.
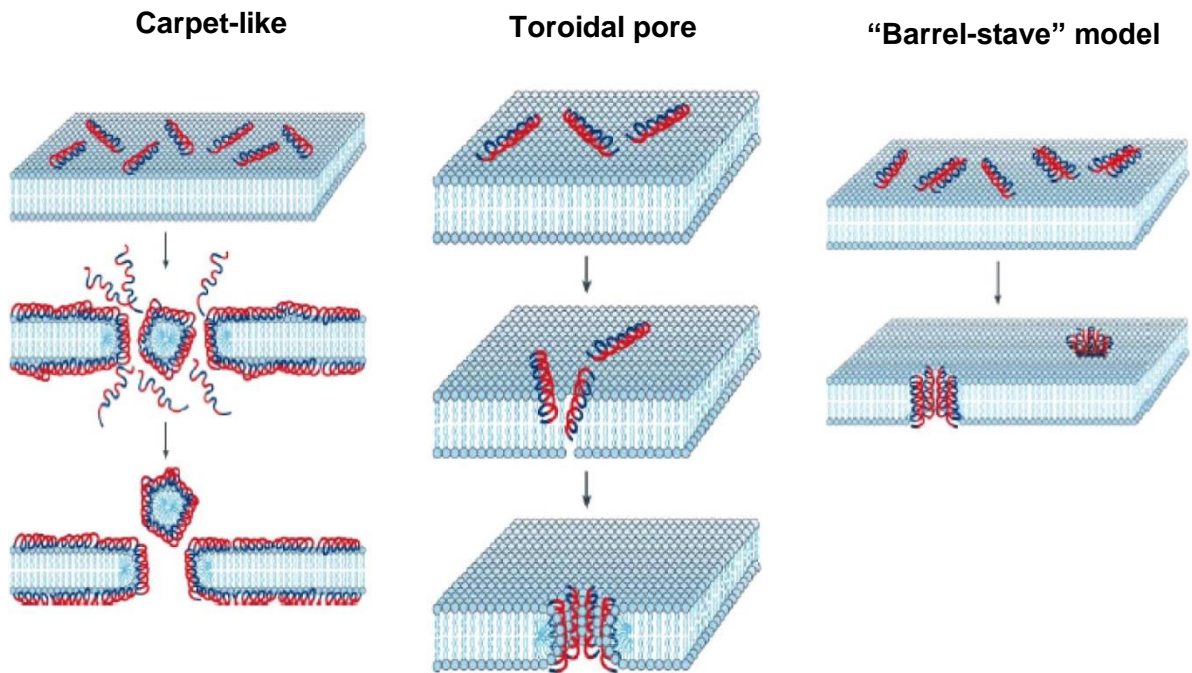
188

Carpet-like   **Toroidal pore**   **"Barrel-stave" model**

Figure 5.1 Depiction of the three main mechanisms of pore-forming peptides on lipid bilayers. Image adapted from referenced publication[50].

A subsequent, more updated model suggests that both the toroidal pore and carpet-like mechanisms can occur under exposure of bilayers to the same peptide, depending on membrane lipid composition, peptide concentration, pH, and salt and buffer concentration[51]. This led to the development of the Shai-Matsuzaki-Huang (SMH) model for pore formation[52], whereby peptides in a carpet-like conformation on the membrane surface thin out the outer lipid bilayer leaflet, causing a strain which is relieved via stochastic bilayer pore formation.

More recent techniques using GUVs have allowed for single bilayer resolution leakage assays[53] which has further clarified the action of certain peptides on bilayers, however the field would still largely benefit from a scalable single bilayer resolution system that simultaneously allows for leakage assays, electrophysiology experiments and potentially microscopy studies such as TIRF as well. The production of such a system is the focus of this chapter. A particularly interesting pore-forming peptide system to

189

interrogate is the Magainin 2 and PGLa system, which are known to have synergistic effects[54]. Experiments using these peptides will provide proof-of-concept of the system reported here.

5.1.2.1 Magainins

Magainins are a family of cationic linear peptides that exhibit antimicrobial properties, secreted as a mixture from the glands of the *Xenopus Laevis* frog[55]. Magainins are active against bacteria[54], demonstrated via their effect of membrane-potential dissipation in *Escherichia Coli*, and also against some eukaryotic cells such as spermatozoa[56], and certain tumor cells[57]. Indeed, membrane disrupting peptides have garnered significant interest as a novel class of therapeutic molecules[58].

By the 1990s, it was theorised that the mechanism of action of magainins was one of transmembrane pore formation, due to their relatively short length and tendency to form α-helices, conforming to archetypes of channel-forming peptides, such as alamethicin[57]. Subsequently, interest increased in the action of specific magainins Magainin 2 and PGLa, due to the discovery of a synergistic, cell-disrupting effect on *E. coli*, tumour cells and liposomes[54]. Elucidation of their mechanism of action has been a subject of study and debate ever since.

Early experiments on the effects of PGLa and Magainin 2 demonstrated that they preferentially interact with negatively-charged lipids, both forming lipid-peptide supramolecular pores that induced the release of the water-soluble dye calcein from large unilamellar vesicles (LUVs)[59]. This was subsequently confirmed for Magainin 2 via a calcein leakage assay performed on singular GUVs, which showed a gradual decrease in fluorescent intensity when exposed to the peptide[53], indicative of the formation of transmembrane pores. It has since been thought that Magainins induce the formation of variable-sized toroidal pores composed of between 4-7 Magainin

peptides and with an inner diameter between 3 and 5 nm[47, 60]. With regards to the synergism of Magainin 2 with PGLa, solid-state NMR has shown that Magainin 2 enhances the ability of PGLa to transition from a membrane-parallel to a transmembrane (more tilted) conformation[61], which seems to support an SMH model of bilayer disruption by which PGLa aids in the transition from a carpet-like assembly to the formation of pores. It has also been found that single amino acid mutations in Magainin 2 significantly altered its synergistic effects with PGLa, indicating towards specific molecular recognition between the peptides[59].

5.1.3 Chapter Aims

This chapter aims to develop an ALM array using eDIBs output into a 96-well plate. Via the incorporation of self-quenched calcein in the eDIB cores, the array can be used as a high-throughput assay for membrane disruption by measuring the de-quenching of calcein upon its release or transfer across the bilayer and into the alginate shell and buffer present in the well.

Firstly, eDIBs are produced as outlined in Chapter 3, containing a self-quenched solution of calcein. These are placed individually into the wells of a 96-well plate. Plate reader measurements are used to correlate observations with fluorescence measurements, in order to assess the ability of the plate reader to detect the de-quenching of calcein as resulting from bilayer failure or leakage.

Secondly, eDIBs are exposed to different conditions, such as different ionic strengths, in order to a) demonstrate the ability of the eDIB array to give information regarding their stability when exposed to different conditions, and b) optimise the assay in order to produce eDIBs that are as stable as possible.

Thirdly, validation experiments are performed in order to assess the ability of the eDIB array to measure small increases in fluorescence as a result of the formation of bilayer

pores. For this, the buffer in the wells is spiked with known amount of calcein in order
to simulate leakage of calcein from the eDIB. Well scanning measurements are
performed and used to compare plate reader measurements and account for any
spatial variations that may occur during the course of an experiment, which is expected
to give rise to potential measurement artefacts.

Finally, 96-well plates containing eDIBs are exposed to different concentrations of
detergents (Triton-X100 and sodium dodecyl sulphate), as well as the synergistic, pore-
forming peptides Magainin 2 and PGLa. This provides proof-of-concept that the
platform is a useful tool in producing high-throughput fluorescence measurements on
eDIBs in order to assess bilayer integrity when exposed to bilayer-disrupting
molecules, thus demonstrating their ability to form individually addressable ALM arrays
and their potential as a platform for membrane studies.

5.2 Methods

All chemicals were purchased from Sigma-Aldrich, except for Magainin 2 (Genscript,
USA) and PGLa (Generon, UK).

5.2.1 Generation of eDIBs

eDIBs were generated as described in Chapter 3, with the microfluidic equipment
developed and characterised in Chapter 2.

5.2.2 Imaging

Images were taken using the camera of an iPhone 6 with or without the use of an
attachable 0.67x macro lens (Wilko, UK), or a USB microscope (Celestron, USA).

192

5.2.3 Fluorescence measurements

Fluorescence measurements were taken using a Fluostar Optima (BMG Labtech, Germany). The filters used are 485 for excitation and 520 for emission. Fluorescence values are given as arbitrary units ranging from 0 to 1 (where 1 = saturation of the plate reader measurement at the particular gain employed).

5.2.4 Preparation of detergents and peptides

The detergents Triton-X100 and SDS were prepared from a liquid stock by dissolving in a buffer composed of 10 mM HEPES adjusted to a pH of 7 using HCl and NaOH. The solution was adjusted to an ionic strength of 500 mM using NaCl in order to maintain ionic balance across bilayers. This same buffer conditions were employed to dissolve the lyophilised peptides Magainin 2 and PGLa at a concentration of 100 µM, and used as a stock to add to the eDIB wells for peptide exposure experiments.

5.3 Results & Discussion

5.3.1 Method Development

This section comprises the development of a dye release assay using eDIBs in 96 well plates, able to detect both bilayer failure and leakage.

5.3.1.1 Preparation of 96 well plates containing eDIBs

The first step in producing an eDIB array was to output eDIBs individually into the wells of a 96-well plate. The wells were first prepared by adding 150 µL of buffer, matched to the internal cores of the eDIB (10 mM HEPES, pH7, ionic strength adjusted to 0.5 M using NaCl), in order to provide the external aqueous media for the eDIB. 100 µL (unless stated otherwise) of mineral oil was added on top of the buffer in order to

provide conditions that prevent evaporation of the aqueous phase and of the eDIB,
once placed in the wells.

eDIBs were generated microfluidically as described in Chapter 3, but the microfluidic
flow was halted periodically when the final FEP tube was filled with eDIBs. The eDIBs
were then kept in this tube for 5 minutes in order to allow for the full gelling of the
alginate shell (Figure 5.2a), before being flowed into the wells. In order to flow the
eDIBs into the wells, the carrier oil phase flow was resumed at a flow rate of 30 ml hr^{-1},
which allowed for the eDIBs to be slowly and carefully delivered in individual wells
alongside a small volume of the oil carrier phase. Figure 5.2b shows an eDIB in a well,
which is submerged in the aqueous volume within the well, and sits below the water/oil
interface due to it being less dense than the aqueous phase. The alginate shell of the
eDIB appears to be invisible as it is fully gelled and equilibrated with the aqueous
volume around it, and thus displays similar refractive indexes.
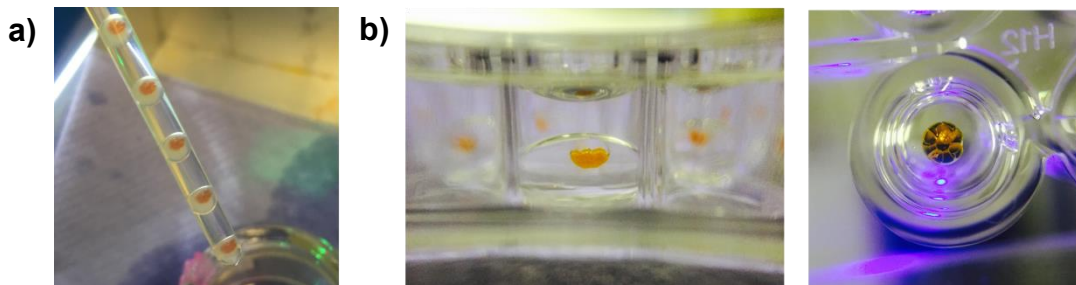
Figure 5.2 Photographs showing a) eDIBs in the exit tube of the microfluidic device, and b)
eDIBs in wells of a 96 well plate imaged from the side (left inset) and from the top (right inset).
The eDIBs are submerged in an aqueous buffer which is covered with mineral oil. The inner
aqueous cores of the eDIBs are an orange-brown colour as they contain 70 mM calcein, and
the alginate shell of the eDIB is not visible as it is equilibrated with the surrounding buffer and
thus displays the same refractive index.

eDIBs were delivered to the wells by submerging the tip of the FEP tube in the oil
phase of the well, and allowing for the eDIB to exit the tube and sit at the oil/water
interface within the well. This method allowed for batches of 12 eDIBs to be placed in
wells in under 15 minutes, dependant on the length of the final FEP tube of the
microfluidic device. It is anticipated that increasing the exit tube length or altering

194

gelling conditions (as described in chapter 3) would enable a significant increase in the rate of this process.

5.3.1.2 Selection and characterisation of a fluorescent, content release assay compatible with eDIBs

Optical bilayer leakage assays commonly rely on content release assays, where the transfer of a fluorophore, of a fluorophore-activating species[7], gives rise to a detectable, fluorescent signal. One such method relies on the use of a self-quenching fluorophore, such as calcein[62], which upon its release from a DIB droplet or a vesicle into an aqueous media, gives rise to a fluorescent signal as it is diluted and un-quenched at the other side of the bilayer. This system is a good candidate for a leakage assay using eDIBs, as a self-quenching concentration of calcein can be contained within the eDIB internal droplets, which would give rise to fluorescence when it is transferred to the external, aqueous media through bilayer pores, or by droplet coalescence, which is an expected result from bilayer failure.

In order to characterise the fluorescence of calcein, fluorescence measurements were taken using a 96-well plate filled with aqueous solutions with varying concentrations of calcein (0.001 mM to 50 mM). Calcein is excited at a wavelength of 495 nm and emits at 515 nm. As shown in Figure 5.3, fluorescence decreases above a concentration of ≈1 mM, and displays very low fluorescence at a concentration of 50 mM, indicative of self-quenching. Based on this experiment and on other reports, a concentration of 70 mM was selected to be contained within the eDIB cores for the content release assay[22].
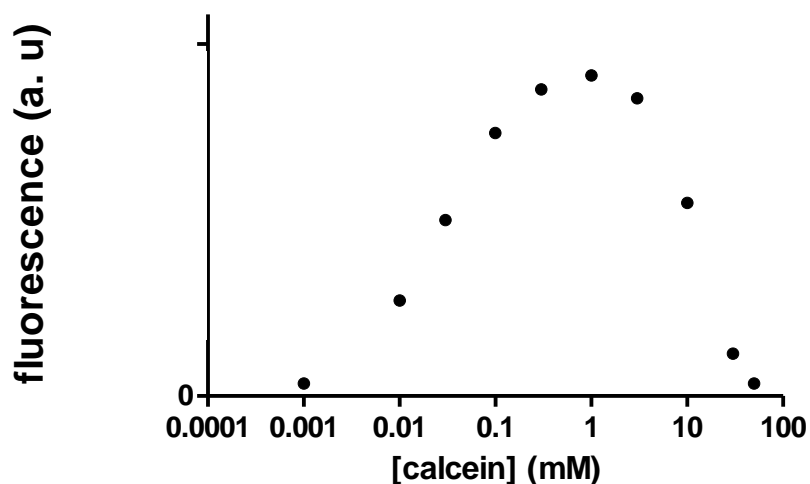
Figure 5.3 Fluorescence of calcein solutions of different concentrations (from 0.001 mM to 50 mM) as determined by the plate reader using a 96-well plate. Peak fluorescence is given at 1 mM, and increasing concentrations give rise to self-quenching. At 50 mM, the solution is mostly self-quenched displaying low levels of fluorescence. 150 µL of the calcein solutions are added to the wells (n = 3 per concentration), and the gain employed was 850.

Subsequently, it was found that eDIBs in wells containing 70 mM calcein in its cores gave rise to a sharp increase in fluorescence in the well upon the coalescence of one or more cores with the external aqueous media within the well. This could be visualised by exposing the eDIB wells to a blue light LED, as shown in Figure 5.4**.**
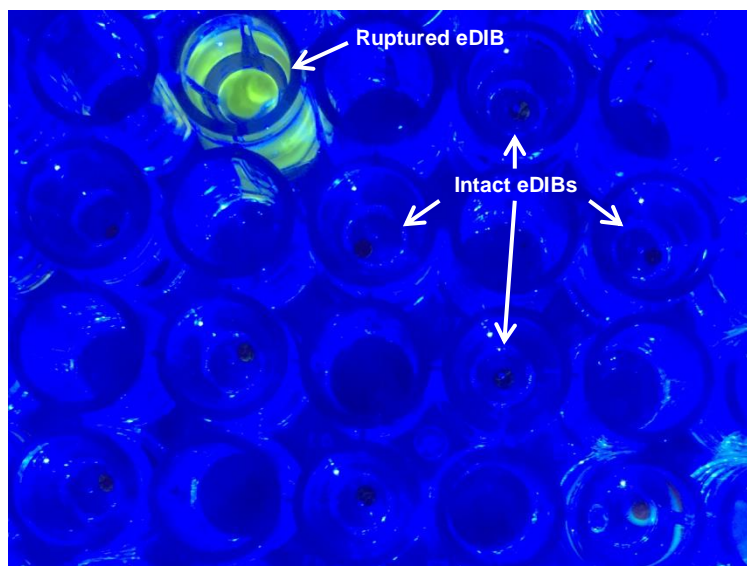
Figure 5.4 Photograph showing the appearance of intact and ruptured (bilayer failed resulting in droplet coalescence) eDIBs in a 96 well plate, imaged using a USB microscope under a blue light LED. Ruptured eDIBs display a strong, yellow fluorescent output across the entire well whilst intact eDIBs display no visible fluorescence.

This demonstrates that the assay is able to detect bilayer failure, as the resulting coalescence of an eDIB aqueous core gives rise to a large fluorescent response. This allows for a "digital" kind of assay, where either bilayers fail over a period of time or remain intact. It was possible to obtain time-resolved data via time-lapse imaging of eDIB wells over a period of time. This is shown in Figure 5.5, where eDIBs are exposed to a high ionic strength buffer (0.7 M) and imaged over time with a USB camera under a blue light LED.
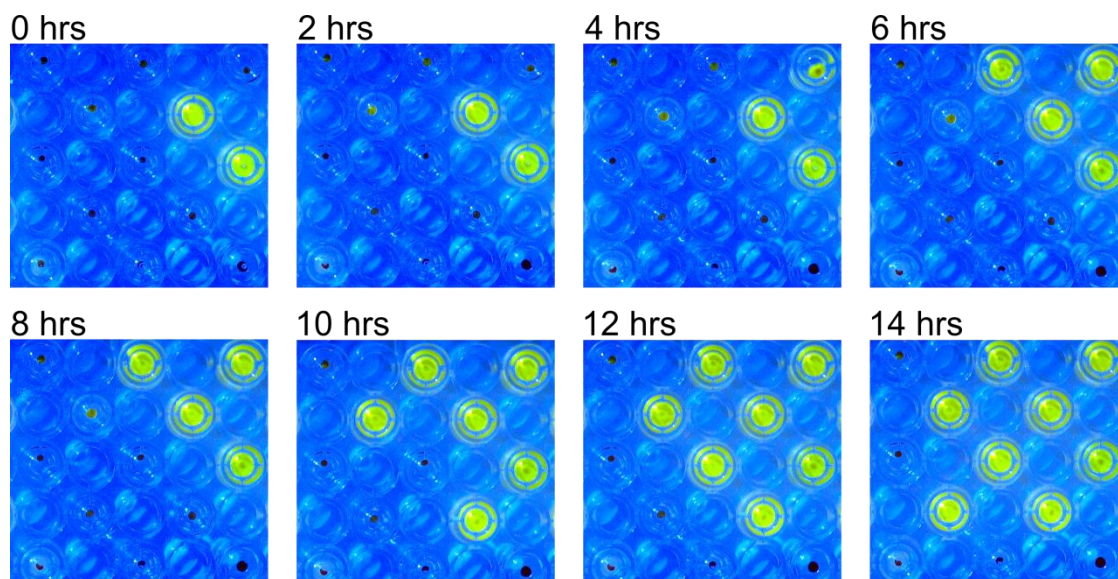
Figure 5.5 Time-lapse photographs showing a number of eDIBs imaged in a 96-well plate under a blue light LED, of which a number of them rupture over the 14 hour period as they are exposed to a high ionic strength buffer (10 mM HEPES, pH 7, adjusted to 0.7 M ionic strength using NaCl).

Additionally, it was observed that eDIBs sometimes leaked small amounts of fluorophore whilst in the microfluidic exit tube, which did not correspond to the coalescence of an eDIB aqueous core with the alginate shell (as this gives rise to a much larger increase in fluorescence, as seen with other eDIBs where internal cores did coalesce with the alginate shell), and thus is likely due to the stochastic formation of transient bilayer holes during the early stages of DIB formation, as shown in Figure 5.6**.**
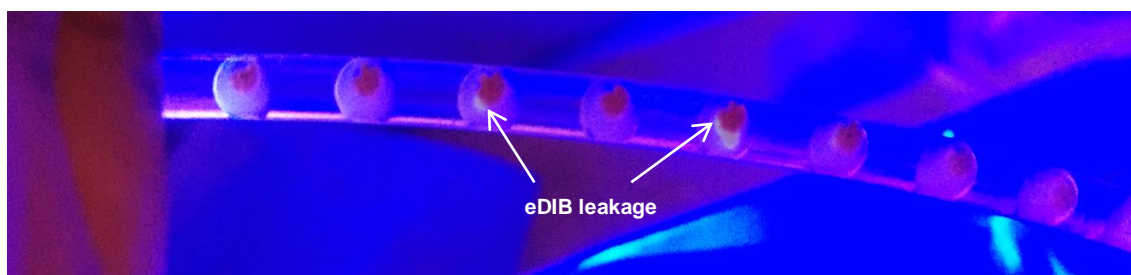
Figure 5.6 Photograph of eDIBs in the microfluidic exit tube, where two eDIBs display some fluorescence due to calcein leakage through the bilayers. The eDIBS are exposed to a blue light LED in order to excite the fluorophore.

This phenomenon was likely to occur for some eDIBs in all cases where eDIBs have been produced, such as in Chapter 3, but not visible until the incorporation of the

calcein release assay into the eDIBs. This suggests that the assay is highly sensitive and indicates that it would be possible to detect calcein leakage through bilayer pores formed by exposure to pore-forming peptides or detergents.

5.3.1.2.1 Use of plate reader fluorescence measurements for calcein leakage assay in eDIBs to determine bilayer failure

Following the demonstrations that the assay is able to detect bilayer failure in eDIB wells via visual confirmation, it was attempted to corroborate such observations with fluorescent data using a plate reader. This would allow for increased throughput via automation, using methods that are compatible with common-place laboratory equipment.

In the first instance, eDIBs were placed in adjacent wells containing buffer, and SWR measurements were taken on them at hourly intervals for 11 hours. This provided an opportunity to correlate observations with fluorescent measurements. The eDIBs presented with varying levels of initial fluorescence, as the alginate phase would commonly be contaminated with calcein from internal droplet coalescence during the process of microfluidic production and initial bilayer leakage as shown in Figure 5.6. This was resolved in subsequent experiments (from section 5.3.1.3 onwards) via the more careful alignment of the microfluidic channels in further iterations of the microfluidic devices, which caused less calcein droplet coalescence in the microfluidic manufacture process. Additionally, the buffer within the well of an eDIB could be exchanged with fresh buffer in order to eliminate any fluorescence visible under a blue light LED, arising from calcein contamination. This was performed routinely in future experiments to achieve comparably low levels of initial fluorescence in the eDIB wells.

As shown in Figure 5.7a, each eDIB displayed a different amount of fluorescence change from the beginning (t = 0) to the end (t = 11 hours) of the experiment. Figure

5.7b shows representative traces for the three different eDIB behaviours as well as
before and after photographs used to correlate fluorescence measurements with
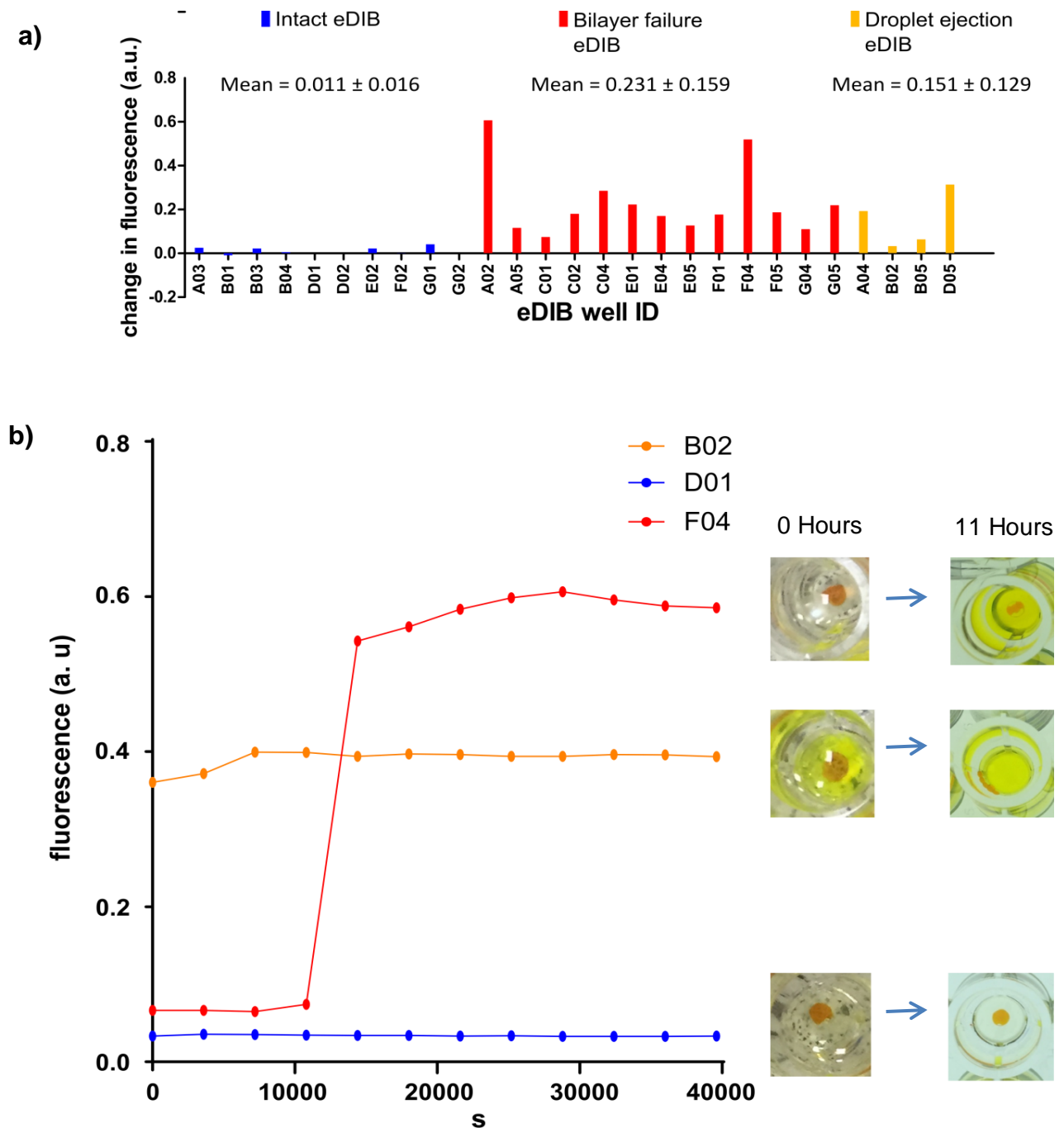observations.

Figure 5.7 a) Change in fluorescence over a period of 16 hours for eDIBs in a 96 well plate.
eDIBs that remained intact throughout the experiment showed little change in fluorescence
(0.011±0.016 a.u.), whilst eDIBs that ruptured gave rise to a larger change in fluorescence
(0.231±0.159 a.u.). Some eDIBs ejected their cores without necessary giving rise to
coalescence with the external well media, which showed a moderate increase in fluorescence

(0.151±0.129). b) Representative graphs showing the change in fluorescence over time for the three behaviours described in a), as well as before and after photographs of the wells in question.

eDIB behaviours could be classified into three categories based on observations and comparing the eDIBs at the beginning and end of the experiment. A number of eDIBs remained intact throughout the experiment (Figure 5.7a, blue bars), which displayed little total change in fluorescence. Many others contained bilayers that failed at different points throughout the experiment, showing a net rise in fluorescence (Figure 5.7a, red bars), corresponding to the coalescence of calcein droplets with the external aqueous environment. Bilayer failure in these eDIBs was likely due to a number of reasons, such as differences in osmotic pressure between the inside and outside of the eDIB, stochastic bilayer failure, or the effect of vibrations within the plate reader, causing mechanical stress on the bilayers.

The variability regarding the change in fluorescence is likely due to a number of reasons. Firstly, the buffer around the eDIB displayed different concentrations of calcein, which, upon further addition of calcein gave rise to a variable increase due to the non-linear correlation of calcein fluorescence with concentration. This is because the alginate shell of the eDIBs would commonly be contaminated with calcein in the microfluidic manufacture process. The lower the level of initial fluorescence, the greater the increase upon coalescence of calcein-containing droplets with the alginate phase and the external buffer, as seen with eDIBs A02 and F04 in Figure 5.7a. Secondly, there is variability in the number of aqueous droplets contained within each eDIB, as well as the number of droplets that coalesce with the alginate shell due to bilayer failure. Thus different amounts of calcein are transferred from the inside of the eDIB to the outside, from a self-quenched to a more fluorescent state.

A small number of other eDIBs ejected their internal cores without these coalescing with the alginate phase or the buffer around the eDIB, hence the third classification

201

(Figure 5.7a, orange bars). However, some of these eDIBs did give rise to an increase in fluorescence (Figure 5.7b, orange trace), indicating that some calcein within the eDIB had coalesced with the outer buffer or alginate shell. This was resolved in subsequent experiments via the use of further iterations of the microfluidic device where the coaxial alignment was improved, giving rise to eDIBs where the oil droplet is more centred within the alginate shell; and also via the addition of 100 µL of oil to the well instead of 50 µL. It is hypothesised that droplet ejection might have been due to the oil droplet being un-centred within the alginate shell, which would asymmetrically reduce its protective effects on the oil droplet contained within, enabling its expulsion. Additionally, the increased volume of oil might have reduced the radius of curvature of the water-oil interface, and the surface tension stress imparted by the water/oil interface onto the eDIBs, which could allow for them to maintain their integrity better. Uncertainty exists regarding the cause of such observations, and was deemed beyond the scope of this thesis as it was resolved in subsequent experiments via the changes mentioned above.

This experiment demonstrates that the platform is able to distinguish between eDIBs where bilayers fail and eDIBs where bilayers remain stable throughout a period of time. Of importance, for an eDIB to give rise to a "negative" result, a number of bilayers must remain intact, as each eDIB contains a number of aqueous droplets forming DIBs with the hydrogel shell. Furthermore, with improvements on microfluidic manufacture methods, allowing for the production of eDIBs displaying low initial levels of fluorescence, the platform as described here should allow for quantitative measurements that determine bilayer integrity when exposed to conditions that can cause bilayer failure, for example in the presence of peptides or detergents that disrupt bilayers in a homogeneous manner.

5.3.1.3 Determination of eDIB stability using plate reader fluorescence measurements.

The platform described in the previous sections was employed in order to determine conditions that gave rise to stable eDIBs. For these experiments, the number of eDIBs that remain intact after a period of time can be counted and compared between different conditions. This could be done using the plate reader as described in Section 5.3.1.2.1 or with visual confirmation using periodic imaging and a blue light source as described in Section 5.3.1.2. eDIB survival percentage was assessed 16 hours after the start of the experiment, and eDIBs were left to rest for one hour in the wells after being outputted from the microfluidic device.

In the first instance, eDIBs were incubated with 150 µL of a 10 mM HEPES buffer of different ionic strengths, adjusted using NaCl. The ionic strength of the inner cores was adjusted to 0.5 M (70 mM calcein, 10 mM HEPES and 397 mM NaCl), and therefore it was hypothesised that a 0.5 M buffer on the outside would give rise to a higher number of stable eDIBs as this would entail a low osmotic pressure. The alginate shell was also adjusted to 0.5 M using NaCl. As shown in Figure 5.8, over 80% of eDIBs incubated in a 0.5 M buffer composed of 10 mM HEPES adjusted to a pH 7 using NaOH and NaCl, and to an ionic strength of 0.5 M using NaCl, survived after 16 hours, with decreasing survivability the more ionically unbalanced the buffer solution is to the internal cores.
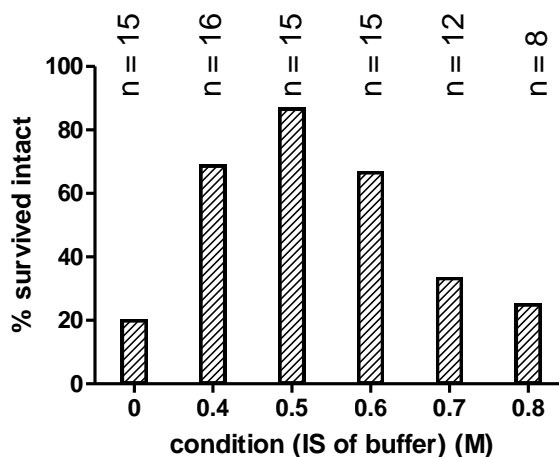
Figure 5.8 16 hour survival of eDIBs incubated in a 96-well plate with different ionic strength buffers. Ionic strength was adjusted using sodium chloride. Survival is reported as the percentage of eDIBs that remained intact throughout a 16 hour period, and was determined as shown in Figure 5.7. As expected, eDIBs display best survival when incubated in a buffer that is osmotically matched with the internal cores.

Additionally, eDIB stability was tested via comparing eDIBs in wells in oil alone or in oil and buffer, measured either with the plate reader or via imaging on the laboratory bench, in order to establish the methods that give rise to the most stable eDIBs (Figure 5.9). In the experiment performed in Section 5.3.1.2.1, fluorescent measurements indicated that eDIB bilayers ruptured mostly within the first two hours of the experiment, which could indicate that the plate reader measurements were disrupting the bilayers, possibly via mechanical. However, it was found that around 80% of the eDIBs measured in buffer both with and without the plate reader remained intact throughout the experiment, and stability only decreased down to 70% when eDIBs were measured using the plate reader and were kept in oil without any buffer. This could possibly due to the fact that eDIBs in oil are in contact with the well walls, whilst eDIBs in buffer are suspended within the well, possibly dampening any effect of the vibrations on the eDIBs.
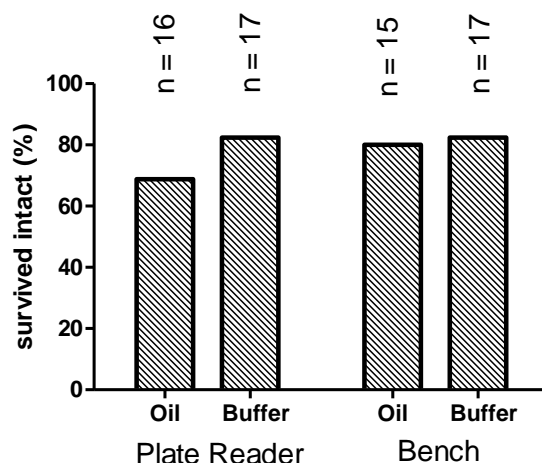
Figure 5.9 16 hour survival of eDIBs incubated in either oil or oil and buffer (0.5 M buffer) in 96-well plates, measured either in a plate reader as described in Figure 5.7, or on the laboratory bench as described in Figure 5.5. Survival is reported as the percentage of eDIBs that remained intact throughout a 16 hour period.

These experiments aided in determining the best conditions to use the platform and to rule out any possible effects the plate reader might have on eDIB stability. Over 80% of eDIBs in wells were consistently found to remain intact over the course of 16 hours when the external buffer was adjusted to 0.5 M, and up to 81 wells containing eDIBs were measured at once, with each well containing at least 6 bilayers per eDIB. This was considered to be a suitable level of initial bilayer stability.

5.3.1.4 Characterisation and validation of the eDIB content release assay to measure dye leakage through bilayer pores

The next step in the development of the assay platform was to enable plate reader measurements to accurately measure small increases in fluorescence over time, as opposed to large and rapid increases in fluorescence as seen in the previous sections. This would allow the platform to be used to measure the leakage of dyes such as calcein as resulting from exposure to substances that heterogeneously disrupt membranes by forming transmembrane pores or holes.

205

It is possible to envisage two kinds of assay for leakage through lipid bilayers. One involves the leakage of dye through bilayers measured as a change in the spatial distribution of fluorescence within a well, and the other measuring a total change in fluorescence in a well upon bilayer leakage. For example, the de-quenching of a fluorophore when leaked from the inside of an eDIB droplet to the outside would allow for this. For the second kind of assay, spatial information within the well would improve the sensitivity of measurements but is not a necessary requirement, as it is with the first kind of assay described. This method is the most suitable for plate reader assays in the first instance, as it only involves the extraction of single data values and is thus a more accessible technique, whilst the first kind of leakage assay method would involve spatial resolution achieved by well microscopy or more sophisticated plate reading methods such as well scanning. Thus, this kind of assay is the one chosen to measure leakage of calcein through bilayer pores in eDIB wells here.

It is noted that the presence of the eDIB within the well may give rise to artefacts in single measurements (i.e SWR measurements), as spatial variations within the well may arise from the low, initial levels of fluorescence that the eDIBs display, and movements of the eDIB throughout the course of an experiment. In order to characterise the effect of such possible artefacts and validate the ability of SWR measurements to accurately measure changes in well fluorescence arising from eDIB leakage, control experiments are performed and SWR data compared against well scanning data, as the latter provides with increased spatial resolution which allows for the effects of spatial variations within the well to be characterised and accounted for.

In the first instance, eDIBs spiked with a known concentration of calcein from 0 –49 μM were compared against control wells containing the same concentration of calcein and the same volume of buffer (150 μL), which was maintained at the same pH and ionic strength throughout the experiments (Figure 5.10). The SWR fluorescent values of the

eDIBs after the addition of calcein could be subtracted from the initial eDIB fluorescence, in order to reduce the variable fluorescent output of eDIBs prior to being spiked. This showed that increasing concentrations of calcein in wells containing eDIB could be measured for at least 7 μM calcein, which would be the equivalent of 6.67% of the volume of an eDIB internal core leaking into the external buffer volume. The fluorescent output and gradient was lower than for wells containing no eDIBs. This is possibly due to the shorter optical length for wells with eDIBs due to the presence of the eDIB, or light scatter caused by the different interfaces.
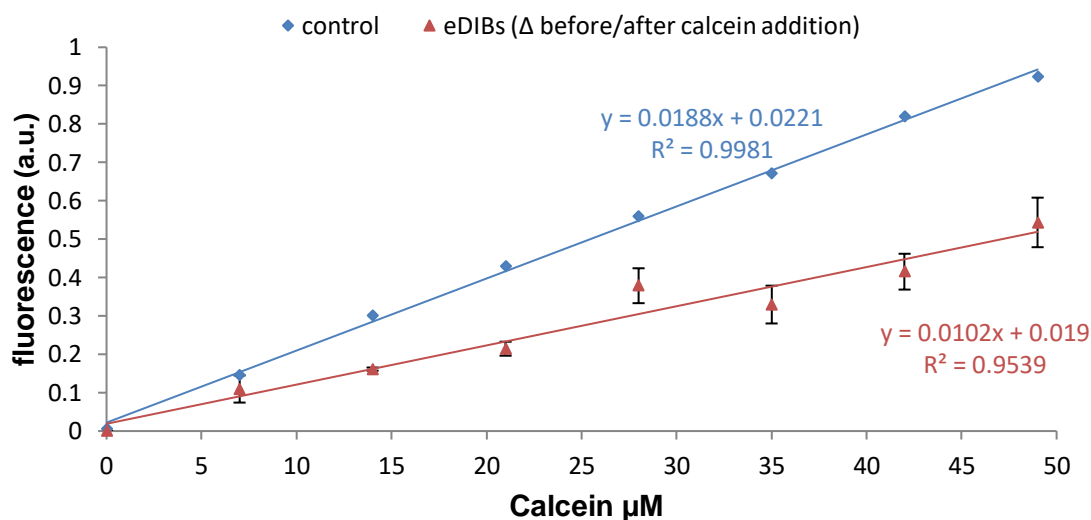
Figure 5.10 Fluorescence of wells in a 96-well plate containing different concentrations of calcein, as determined using single-value measurements on the plate reader. Data in blue refers to wells with no eDIBs (control wells), whilst data in red refers to wells containing an eDIB. For the latter data set, the fluorescence of the wells prior to the addition of calcein is subtracted from the fluorescence after the addition of calcein. For all measurements, n = 3. The gain employed is 1150.

It is noted that plate readers are typically designed to measure optical parameters from homogeneous solutions in wells. However, eDIBs introduce heterogeneity into the wells, which can produce artefacts in measured fluorescence, such as variations in eDIB position and shape, initial contamination of the eDIB shell, movement of the eDIB throughout the experiment, potential light scatter from the different phases and

interfaces, and low amounts of measured fluorescence from the quenched calcein cores. It is likely that these factors give rise to the higher standard deviation of measured eDIBs vs. control as seen in Figure 5.10.

In order to characterise the spatial variations within the eDIB wells, well scanning was performed on the wells both before and after spiking with calcein, as shown in Figure 5.12. Well scanning experiments were enabled by the plate reader employed and performed by measuring points in a 15 x 15 grid spanning across 5 mm of the diameter of the well (total well diameter = 6 mm) (Figure 5.11a). Code was developed in MATLAB (courtesy of Dr. Oliver Castell) which reconstructed a fluorescent image of the well and extracted useful metrics from well scanning pixel data, such as the mean, median, top and bottom values (given as the mean fluorescent value for the top or bottom 5%, 10% or 20% of the pixels), centre of mass (CoM) and CoM displacement from the centre pixel of the well. This was also used to generate coloured intensity map images of the wells as shown in Figure 5.12 and Figure 5.24**.**
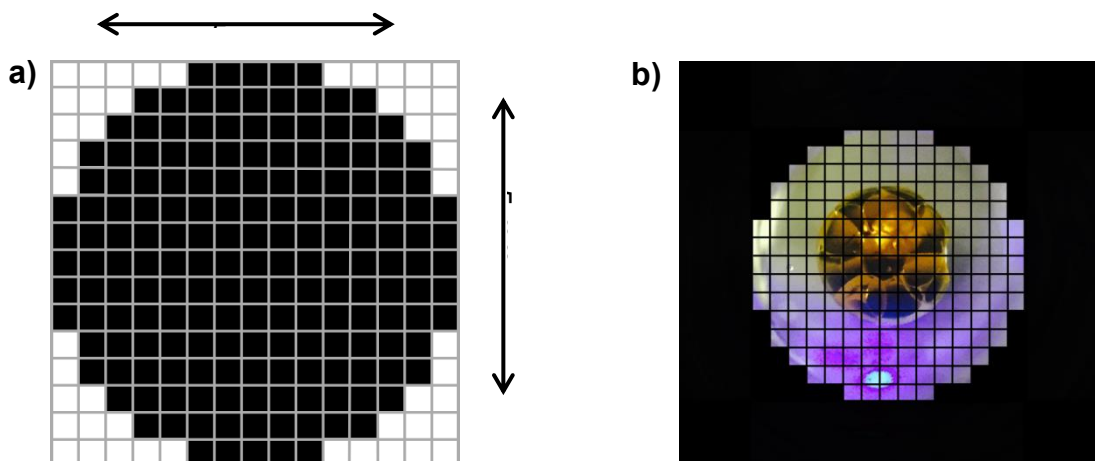

Figure 5.11 a) Image representing the 15 x 15 grid used for well scanning using the plate reader. Fluorescence data is taken for the black squares, adding up to a total of 177 data points per well. b) Representation of the points measured on an eDIB within a well, where a measurement is made for every square. The photograph is taken from above, although fluorescent measurements are taken from the bottom of the well.

Well scanning data could be compared against SWR data in order to gain confidence in the ability of SWR to measure leakage of dye through the bilayers and to account for potential spatial variations within wells. Additionally, by comparing different WS metrics, it is possible to understand whether SWR data values represent the mean fluorescence across the whole well, or the fluorescence of a defined area within the well.
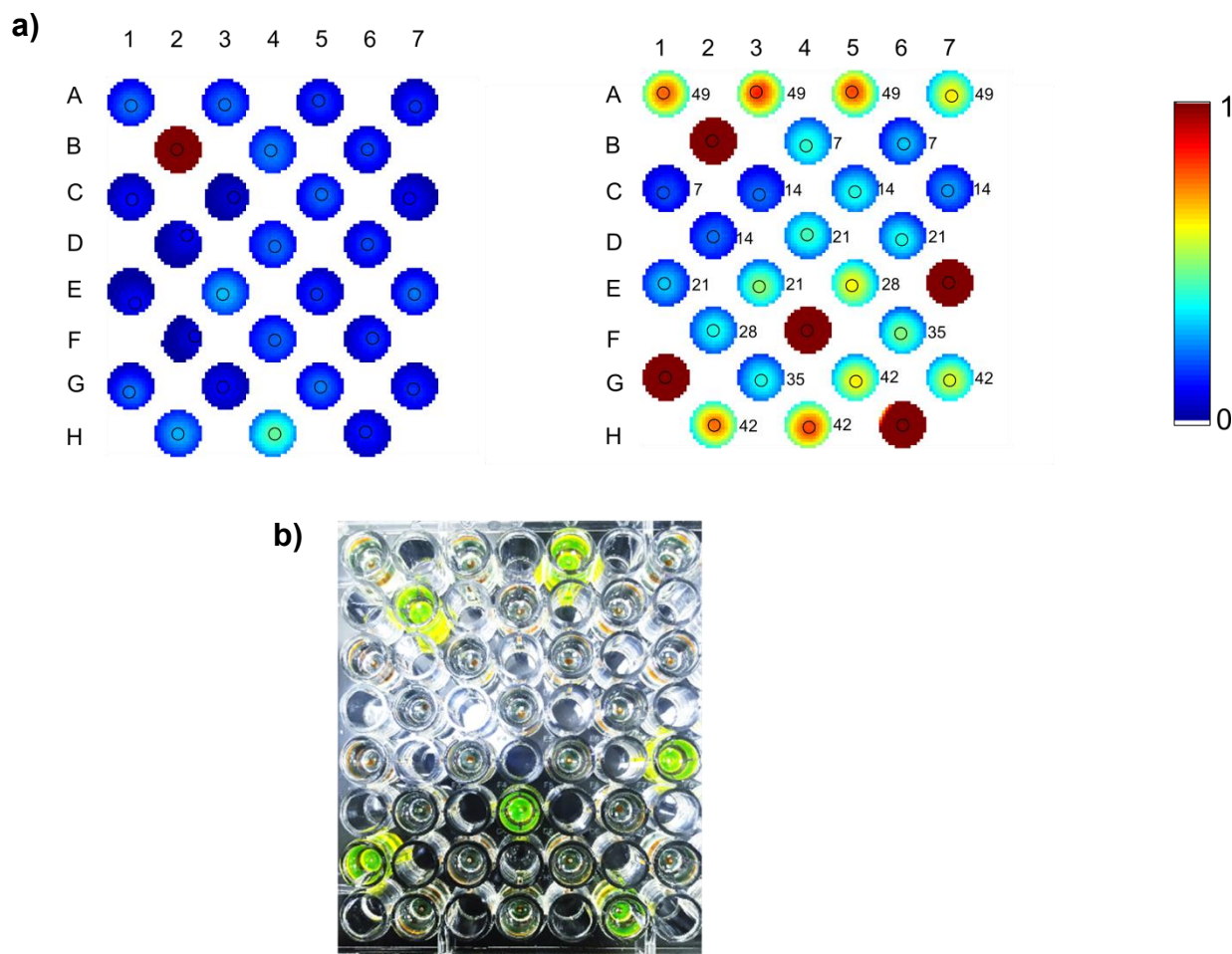

Figure 5.12 a) Well scanning images of eDIBs before and after the addition of calcein. The concentration of calcein added per well is shown in the "after" well scanning images adjacent to the wells, in μM. b) Photograph showing the 96-well plate after the addition of calcein and the taking of well scanning measurements.

The well scanning data, along with the photograph of the wells, show that before the addition of calcein to the wells, CoM (represented as a black circle in the well scanning plots) appears to represent where the eDIB cores are, as they generate low levels of fluorescence due to incomplete quenching. However, once calcein concentration is

increased in the surrounding well medium, the CoM is skewed towards the centre of the well as the eDIB ceases to represent the most fluorescent area within the well. For example, it is visible in the photograph that the eDIBS inn wells D02 and F02 are displaced towards the right, but are not represented as such in the "after" well scanning plot, but are in the "before" well scanning plot. For the majority of "after" well scanning plots, fluorescent intensity appears to radiate outwards from the centre of the well, despite the calcein concentration being homogeneous throughout the well. This could possibly be due to reflections or scatter of light at the borders of the well.

It is possible to estimate the point at which the CoM ceases to represent the position of the eDIB, via comparing the total fluorescent output of eDIBs spiked with different concentrations against control wells (Figure 5.13).
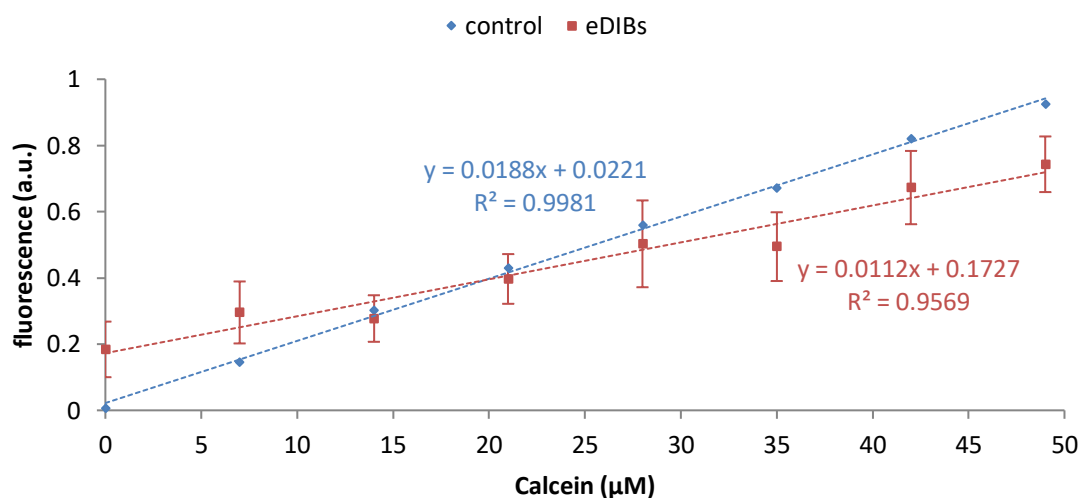

Figure 5.13 Graph showing the fluorescence of wells in a 96-well plate containing different concentrations of calcein, as determined using SWR measurements in the plate reader at a gain setting of 1150. Data in blue refers to wells with no eDIBs (control wells), whilst data in red refers to wells containing an eDIB. In comparison to the data shown in Figure 5.10, eDIB fluorescence prior to the addition of calcein is not subtracted from the fluorescence values obtain after the addition of calcein. N = 3 except for all measurements except the 0 data point for the eDIB-containing wells, where n = 27. The gain employed is 1150.

According to Figure 5.13, it appears that a calcein concentration above 21 µM is the point at which its fluorescence is higher than initial levels of eDIB fluorescence caused

by the quasi-quenched inner cores and potential calcein contamination of the alginate shell from the eDIB manufacture process. Therefore, it is expected that, above this concentration, CoM as determined by well scanning will cease to represent the position of the eDIB within the well. Additionally, the gradient of the spiked eDIB is lesser than that of the control wells, which is possibly due to the fact that the eDIB reduces the total amount of external fluorescent medium around the eDIB that is measured, as the fluorescence within the eDIB (inside the alginate shell) does not increase with added calcein in the external medium.

In order to characterise the effect of eDIB displacement from the centre across a range of fluorescent outputs, the mean pixel value (Figure 5.14) and top 10% of pixels (Figure 5.15) values can be compared against SWR measurements, and also against CoM displacement from the centre of the well. The correlation between mean pixel value and the top 10% of pixels will allow for the determination of the nature of SWR measurements (i.e. whether it measures the mean fluorescence emitted by the whole of the well or only an area within the well). The top 10% of pixel values are likely to represent the fluorescence emitted by the eDIB at low concentrations of spiked calcein, or the centre of the well for higher concentrations of calcein that give rise to a fluorescent output that is larger than the initial fluorescence of an eDIB in a given well. On the other hand, one would expect the mean to give an accurate representation of the fluorescence of the external media; however this might not be the case as well scanning images show that less fluorescence is detected at the side of the wells than at the centre. For low concentrations of spiked calcein, it is expected that mean pixel values overestimate the fluorescence of the well medium due to the contribution of the eDIB. For these graphs, measurements are included from both before and after the eDIBs have been spiked with calcein in order to characterise a large range of fluorescent values.
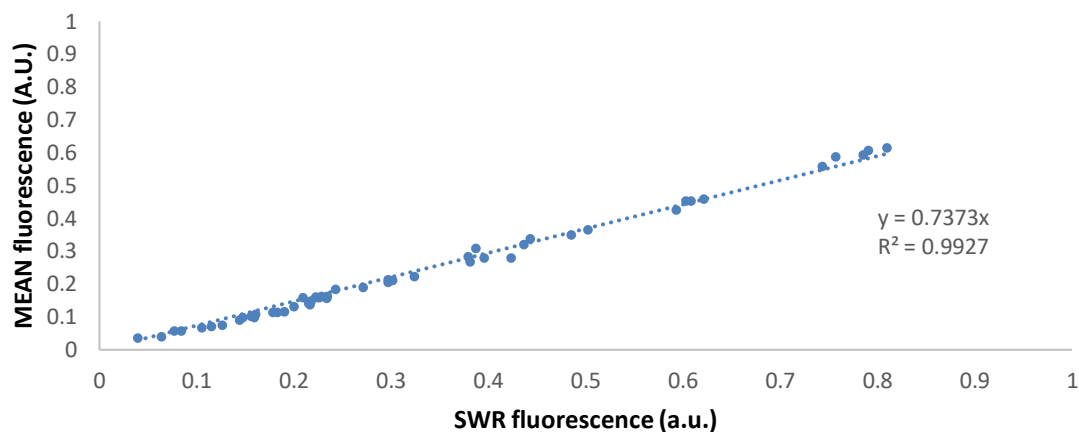
Figure 5.14 Correlation of mean pixel values and standard well reading values for eDIB wells both before and after the addition of calcein to the wells. The values correlate well along a linear regression (R^2 =0.9927). eDIBs that ruptured during the course of the experiment were excluded from the graph.
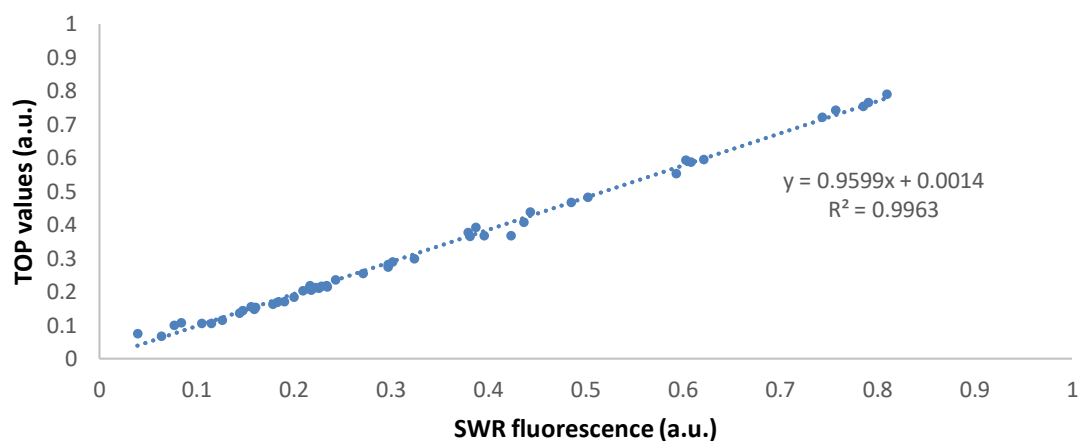

Figure 5.15 Correlation of the top 10% pixel values and standard well reading value for eDIB wells both before and after the addition of calcein to the wells. The values correlate well along a linear regression (R^2 = 0.9963), as well as displaying a gradient close to 1. This likely indicates that standard well reading measures the centre of the well, as for most well scanning top 10% values, the highest point of fluorescence in the well is in the centre of the well. eDIBs that ruptured during the course of the experiment were excluded from the graph.

For both mean pixel and the top 10% of pixel values, the fluorescence data correlated well with SWR across the whole range of fluorescent outputs (R^2 > 0.99). Thus, spatial variability of the eDIB in the well does not appear to have a large effect on SWR measurements, indicating that SWR measurements are generally an accurate representation of the fluorescent output of the wells. The strong correlation between

212

the top 10% of pixel values and SWR ($WS_{top10\%} = 0.9599 * SWR + 0.0014$), along with the fact that most wells display highest fluorescence values at the centre, indicate that SWR measurements are likely measuring a small number of pixels at the centre of the well.

For lower fluorescence values (approximately < 0.1), it appears that the mean pixel value correlates better with SWR than the top 10% of pixel values, as the latter is measuring the fluorescence of the eDIB cores, which are not necessarily in the centre of the well. For higher values, top 10% of pixel values appear to correlate with SWR better than the mean pixel value, as increasingly, the centre of the well becomes the highest point of fluorescence in the well surpassing the low levels of fluorescence emitted by the eDIB quenched calcein cores. Thus, as fluorescence increases in the well (or as leakage occurs), the effect of eDIB displacement from the centre is diminished.

For further clarification of the effect of eDIB displacement on fluorescent output, SWR and well scanning data can be compared, taking into account CoM displacement values for each eDIB (Figure 5.16).
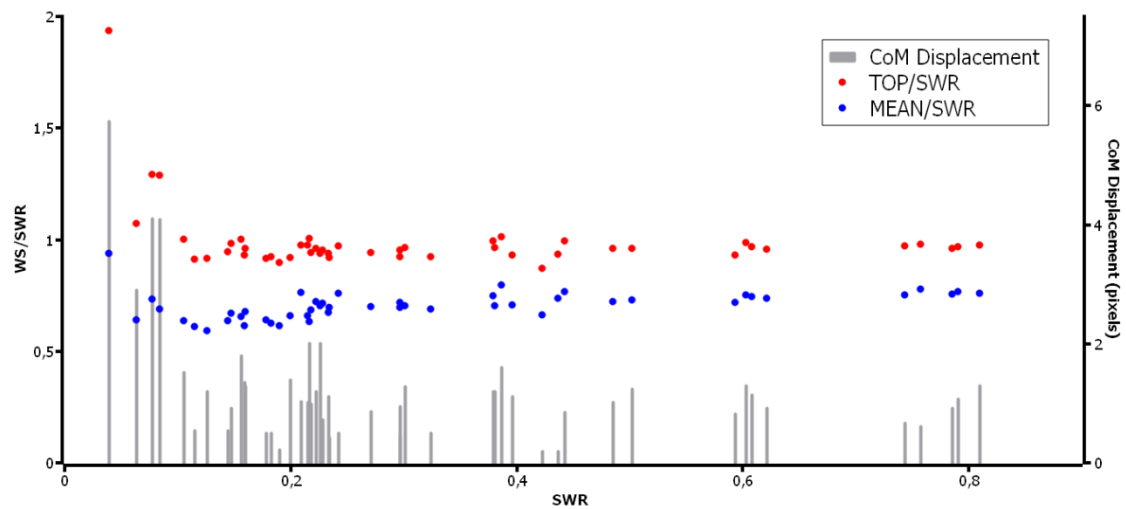
Figure 5.16 Ratio of well scanning top 10% and mean to standard well reading values both before and after the addition of calcein to the wells. The displacement of the centre of mass of the well is shown per individual point. The ratio of well scanning top 10% and mean values to standard well reading values I roughly 1 and 0.7, respectively, and individual points that deviate from this ratio correlate well with high centre of mass displacement from the centre of the well. Additionally, high centre of mass displacement from the centre of the well occurs at low standard well reading values mostly, which corroborates findings that increased fluorescence in the well skews the centre of mass towards the middle of the well. Therefore, displacement of an eDIB from the centre of well is only of relevance for low fluorescence values as determined via standard well readings or well scanning.

The graph shows the ratio of the top 10% of pixel values to SWR and mean pixel value to SWR measurements along with CoM displacement for each data point, corresponding to individual well measurements. It is visible that, for SWR fluorescence values below approximately 0.1, CoM displacement values are significantly larger than the rest, whereas for values above this, it doesn´t exceed a value of 2 pixels. It is notable in the graph that the ratio of the top 10% of pixel values and SWR appears to be around 1, except for values of low fluorescence and high displacement, where the top 10%of pixel values appears to be larger than SWR. This is expected as the eDIB is the major source of fluorescence, and thus when it is displaced, SWR is not measuring the highest point of fluorescence in the well, whilst the top 10% of pixel values is. The ratio between mean pixel value and SWR is lower than the top 10% of pixel values and SWR, as SWR measures central pixels within the well, whilst the mean pixel value takes the sides of the well, displaying lower fluorescence than the middle, into account. The difference between both ratios appears to decrease with increasing fluorescence,

as the well becomes more homogeneous and the eDIB ceases to be the major source of fluorescence. However, the mean pixel value to SWR ratio is also deviated by CoM displacement at low fluorescence, albeit less, for the same reasons as described above for the top 10% of pixel values to SWR ratio.

The significance of this is that, for low fluorescence values, it is reasonable to expect that SWR may be underestimating the fluorescence of the well as would be measured by the top 10% of pixel values or mean pixel value, depending on the CoM displacement and thus the displacement of the eDIB from the centre. The movement of an eDIB throughout a time-course experiment could give rise to measurement artefacts such as false positive values for leakage, if the eDIB moves from the periphery of the well into the middle. Because of the good correlation of well scanning metrics such as the top 10 of pixel values with SWR measurements, it is possible to account for these situations and provide correction factors for different displacement values. Such a method would allow time-resolved leakage experiments to be measured via SWR, and spatial variations controlled for with use of periodic well scanning measurements.

In order to correct for CoM variations, it is necessary to understand how the distribution of fluorescence in the well is affected by displacement. The top 1% of pixel values represents eDIB fluorescence independent of its position, whilst we hypothesise that SWR measures the centre of the well as established earlier. Therefore we propose that it should be possible to predict the top 10% of pixel values based on SWR if we can understand their relationship, as given by Figure 5.17. For these graphs, only un-spiked eDIBs are used as for spiked eDIBs, the CoM increasingly represents the centre of the well despite eDIB position, as described earlier.
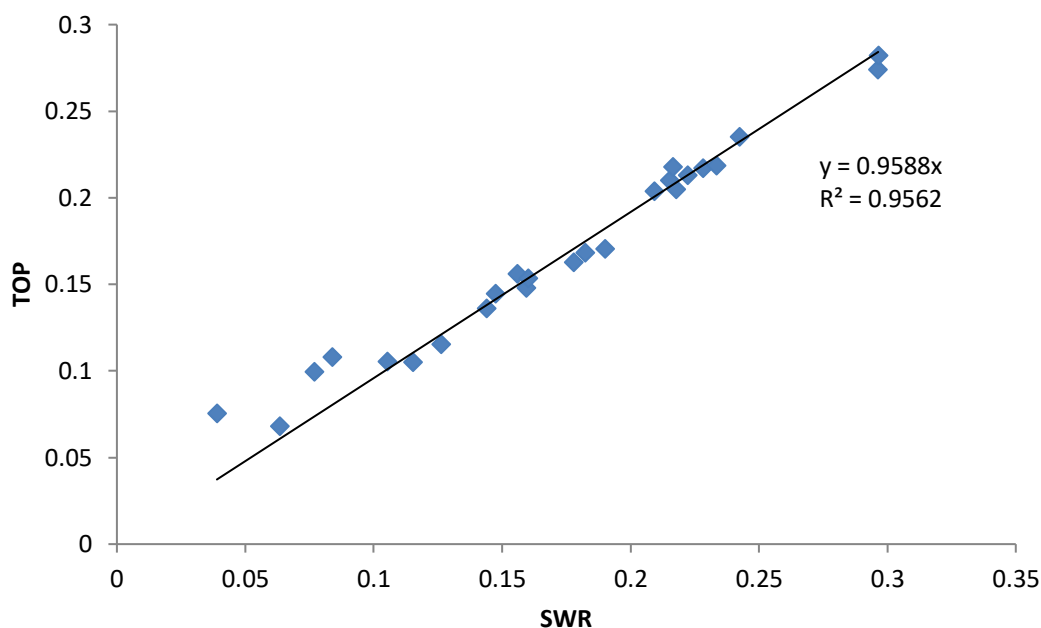
Figure 5.17 Correlation of well scanning top 10% values with standard well reading values taken on eDIB wells before the addition of calcein to the external buffer.

From the relationship ($WS_{top10\%}$ = 0.9588 * SWR), a set of predicted top 10% pixel values can be generated and compared against measured measured top 10% pixel values. The ratio between the measured and predicted values indicate the accuracy of the predicted values, and it is expected that accuracy will decrease (i.e. the ratio will deviate further from 1) as displacement increases, as the highest area of fluorescence within the well (measured by the top 10% of pixel values) is no longer in the centre of the well (measured by SWR). This is shown in Figure 5.18.
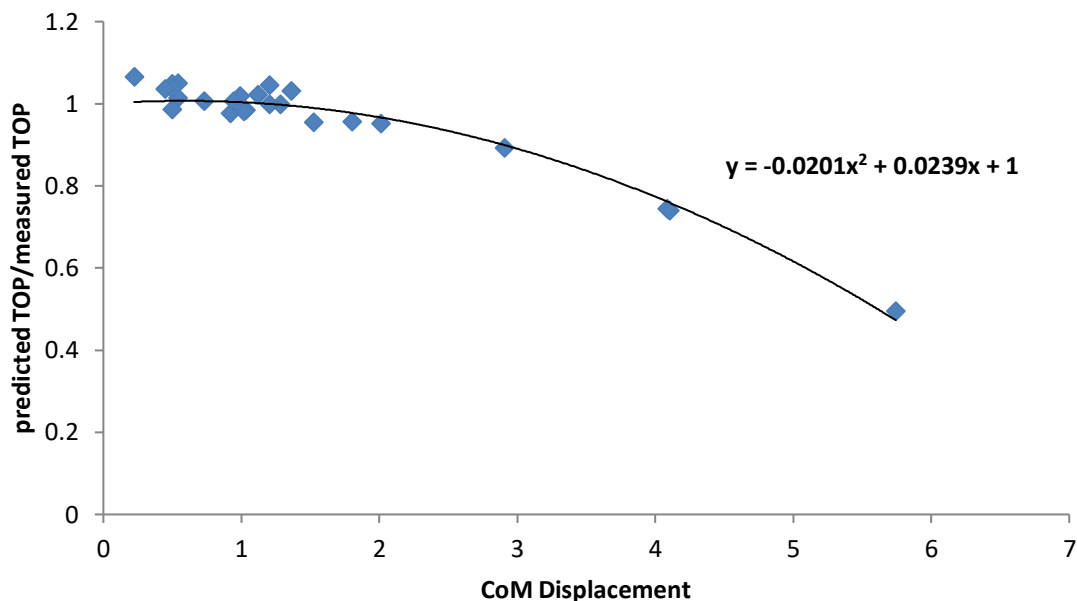
Figure 5.18 Correlation of the ratio of predicted well scanning top 10% values to measured well scanning top 10% values, as determined using the data and equation obtained from Figure 5.17, against displacement of the centre of mass from the centre of the well, as determined via well scanning. This shows how the accuracy of the predicted well scanning top 10% values is affected by the displacement of the centre of the mass from the centre of the well, and can be used to provide a correction factor to determine what the top 10% values would be based on displacement and standard well reading data.

The graph shows that predicted TOP is increasingly inaccurate with increasing CoM displacement as the eDIB moves away from the area measured via SWR. Therefore, the polynomial equation generated indicates the deviation in accuracy as displacement increases, and can be used to generate a correction factor which can be used to obtain accurate top 10% of pixel values based on SWR and CoM displacement (Figure 5.19). This shows that eDIB fluorescence values can be accurately determined from SWR independent of its displacement ($R^2 = 0.9944$).
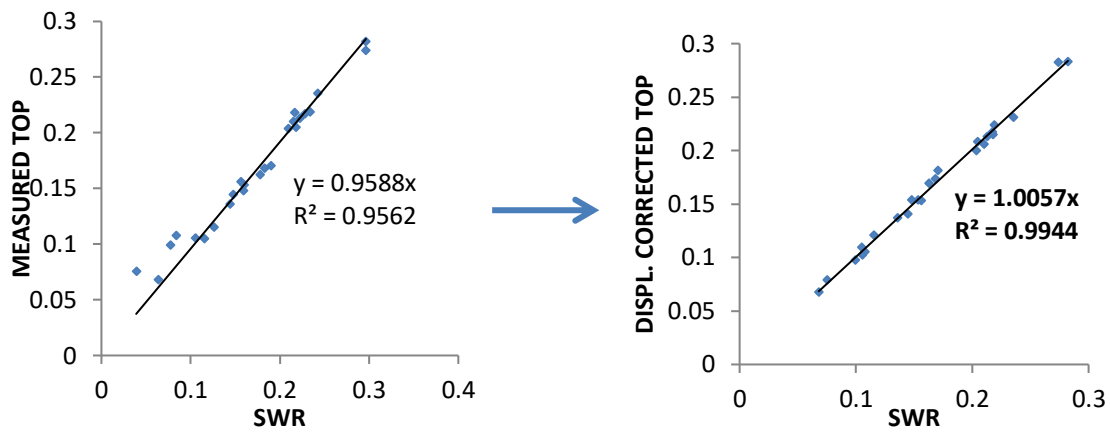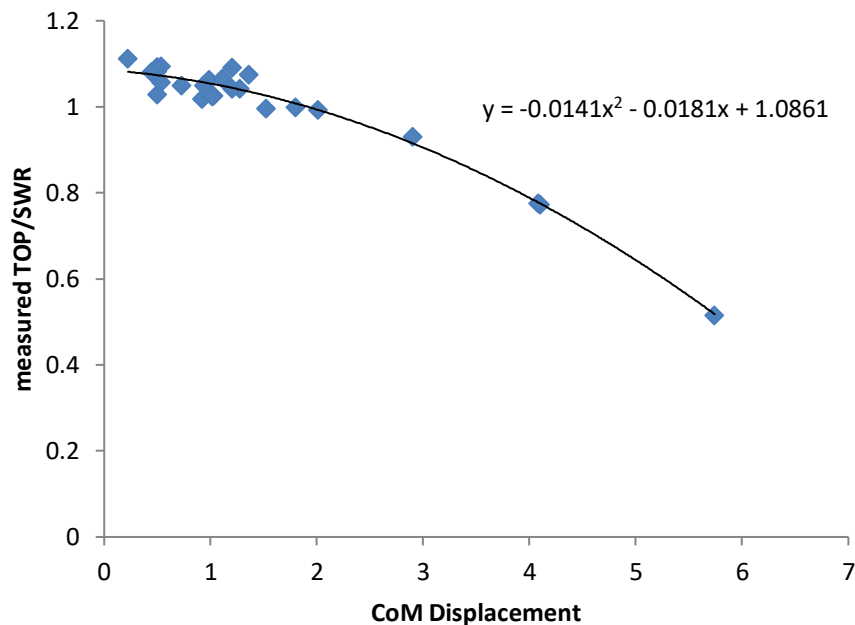
Figure 5.19 Correlation of measured well scanning top 10% values and standard well reading data, as well as the correlation of top 10% values as obtained from standard well reading and centre of mass displacement values(i.e. displacement corrected top values) (see Figure 5.17 and Figure 5.18).

Additionally, the same logic can be applied in order to produce accurate SWR measurements from the top 10% of pixel values and CoM data (Figure 5.20a). This would allow SWR to be adjusted for displacement, and to unpick the effects of displacement, or variations in displacement throughout a leakage experiment (Figure 5.20b)
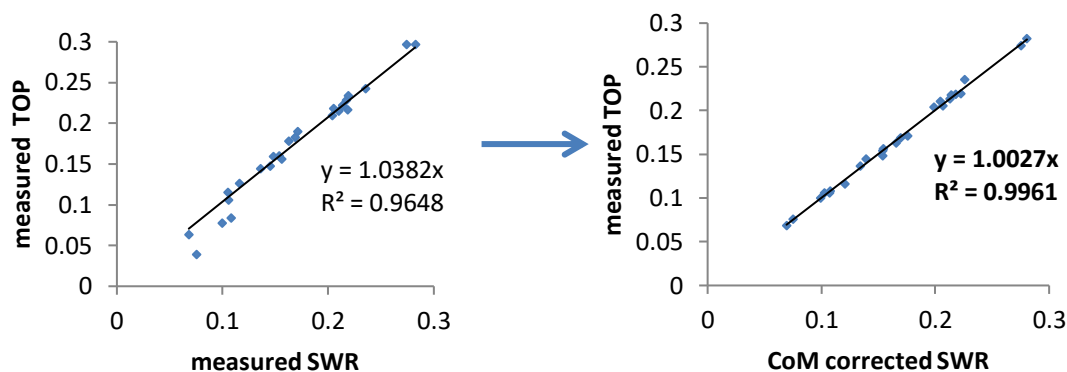
Figure 5.20 a) Correlation of the ratio of well scanning top 10% and standard well reading values with displacement of the centre of mass from the centre of wells. This is used to assess the accuracy of standard well reading in representing the highest area of fluorescence in a well, in relation to the displacement of this area from the centre of the well, which is the area hat standard well readings measure. b) Correlation between measured well scanning top 10% values and standard well readings, as well as between measured well scanning top 10% values and predicted standard well reading values as obtained from a). This allows for standard well reading values to be accurately predicted from well scanning data, in order to correct for eDIBs that show displacement of the centre of mass from the cenre of the well.

The data shows that deviations in fluorescence measured via SWR caused by eDIB displacement and movement can be corrected for using WS measurements. This should allow for the measurement of small amounts of eDIB dye leakage when the CoM of fluorescence is representative of eDIB position, allowing for higher sensitivity in measuring bilayer leakage.

In conclusion, this section demonstrates that eDIBs can be used in a high-throughput manner assay to assess bilayer leakage via the release of a self-quenched dye into an external buffer in a well. As leakage increases, the well becomes more homogeneous which allows for accurate measurements of increases in fluorescence associated to dye release from the inner cores of an eDIB, whereas for low levels of leakage, accuracy is reduced as the eDIB displays some fluorescence as the calcein-containing aqueous cores are not fully quenched, which allows for movement of the eDIB within the well to affect the fluorescent output as measured via SWR. However, a method to

account for such movement has been devised by comparing the top 10% of pixel values to SWR measurements, and producing a correction factor via which displacement of the well CoM can be accounted for. This should allow for SWR measurements to be taken frequently over the course of an experiment, whilst well scanning can be used periodically in order to correct for the movement of an eDIB within a well which can give rise to measurement artefacts that can obscure low levels of leakage. This is a desirable format of leakage measurement, as well scanning measurements take a longer time to perform, reducing the amount of measurements possible per given time, and the measurements inherently give rise to increased mechanical vibrations within the machine which may have the potential to disrupt eDIB bilayers. Thus, SWR measurements have been validated to measure leakage, with sensitivity governed by the gain settings employed on the plate reader.

5.3.2 Plate reader measurements of bilayer failure and leakage using the eDIB assay platform

5.3.2.1 Use of the assay platform to determine bilayer leakage caused by the detergents Triton-X100 and sodium dodecyl sulphate (SDS)

Following from the previous set of experiments aimed at validating SWR measurements to measure leakage from bilayers, proof-of-concept experiments were performed to assess bilayer leakage in eDIBs under exposure to different concentrations of the detergents sodium dodecyl sulphate (SDS) and Triton-X100 as they are known to give rise to stochastically formed pores conducive to the leakage and de-quenching of calcein from the inner eDIB cores[43].

5.3.2.1.1 SDS

In the first instance, eDIBs were exposed to 5, 10 and 50 µM SDS and measured over a 16 hour period via SWR measurements using a high gain setting (1150). Data was generated for individual wells showing changes in fluorescence over time (Figure 5.21). As such, each graph in the panel represents the change in fluorescence over a 16 hour period for an individual well. Wells displayed a variable amount of initial fluorescence due to eDIB contamination in the manufacturing process, likely affected by eDIB position. Coalescence of calcein-containing eDIB cores with the alginate shell and well media consistently gave rise to a saturated response under the gain setting employed, which was convenient in distinguishing bilayer failure in eDIBs in contrast to leakage. This could be visually confirmed at the end of the experiment as described in Figure 5.7.
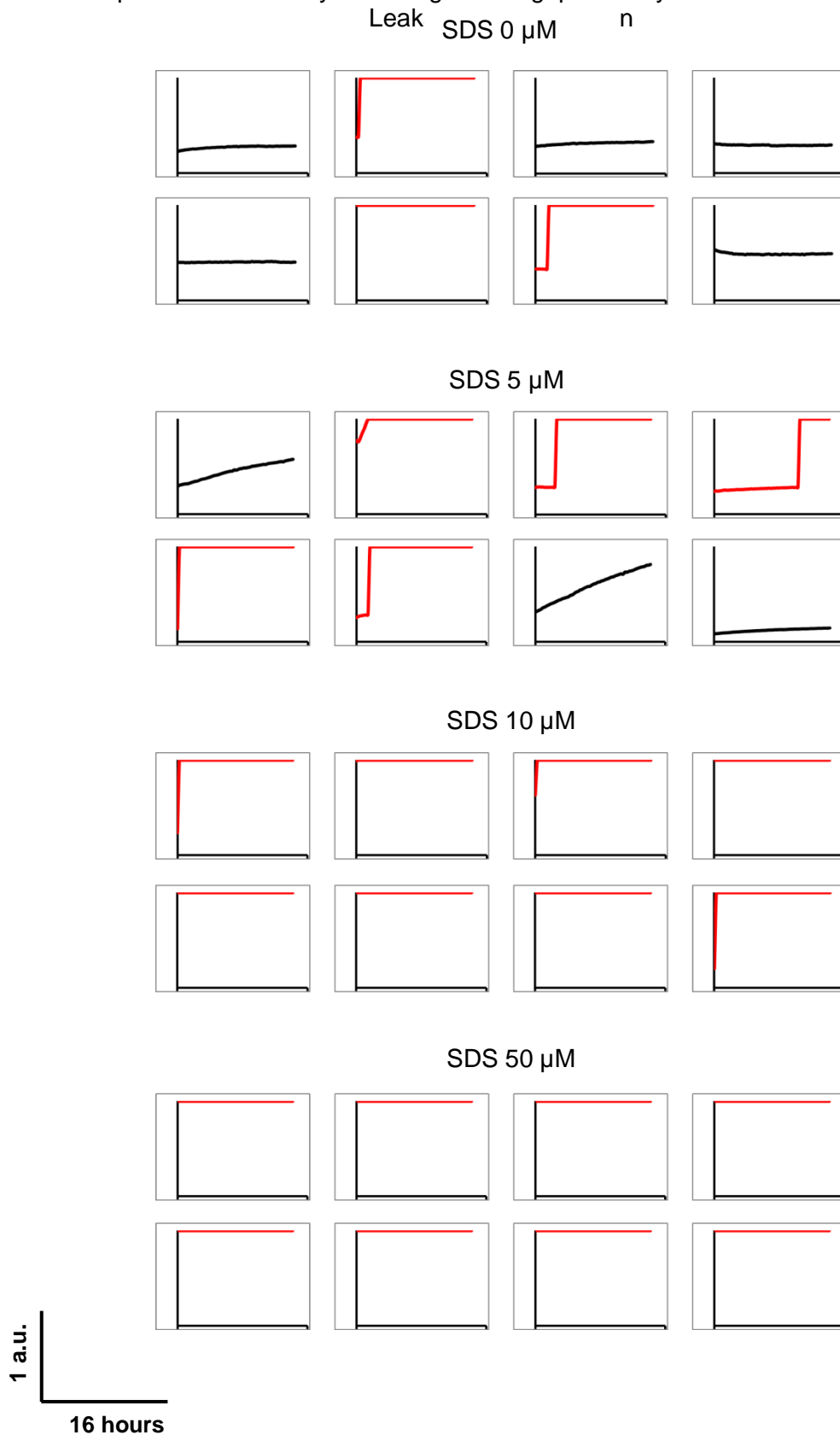
Figure 5.21 Graphs showing the fluorescence of eDIBs in a 96-well plate incubated with varying concentrations of SDS over a period of 16 hours, measured using standard well reading measurements. Each graph represents an individual well. A high gain setting (1150) is employed in order to visualise small changes in fluorescence. eDIBs that undergo bilayer failure were found to saturate the measurement at the gain settings employed, and are represented with red lines.

It was found that 50 µM SDS caused eDIB bilayer failure very rapidly, which resulted in an initial saturated response in all eDIBs tested, as bilayers ruptured between the addition of SDS and the start of SWR measurements. 10 µM SDS gave rise to similar results, with most eDIBs rupturing before the start of measurements and some in the first 30 minutes. 5 µM SDS caused some eDIB bilayers to fail, and a steady increase in fluorescence in other eDIBs, likely indicative of bilayer leakage. Survivability of eDIBs was therefore affected by the presence of SDS, as seen in Figure 5.22.
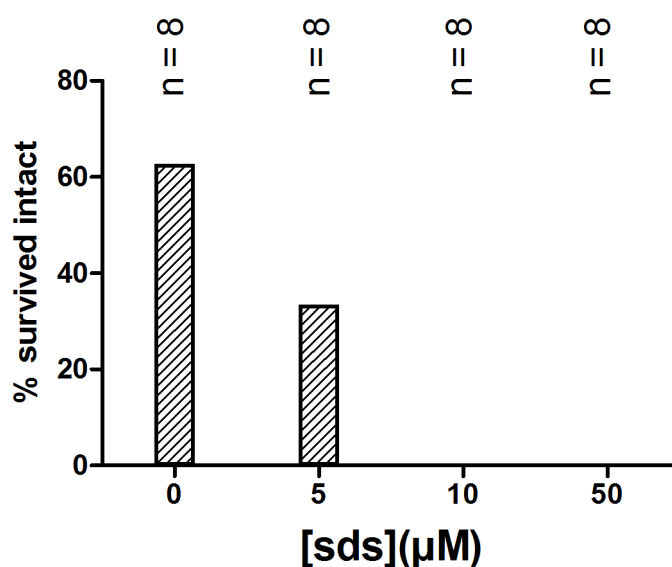

Figure 5.22 Survivability of eDIBs (as shown in Figure 5.21) exposed to varying concentrations of the detergent sodium dodecyl sulphate (SDS), showing the percentage of eDIBs that do not undergo bilayer failure over the course of the 16 hour experiment. The data is obtained by looking at SWR measurements that give rise to saturation over the course of the experiment, as well as visual confirmation after the plate reader measurements have taken place.

In order to further assess leakage, the initial fluorescence value obtained per individual eDIB was subtracted from the rest of values, in order to produce fluorescence graphs normalised to zero, and better be able to cross-compare the different eDIBs and conditions. This is shown in

Figure **5.23**. Due to the subtraction, well fluorescence saturation appears to be at variable levels of fluorescence depending on the starting point of fluorescence for each well, as eDIBs were not measured prior to the addition of SDS. For example, eDIB wells measured at saturation for the first measurement will display a fluorescence of zero throughout the experiment as there is no change in fluorescence throughout the course of the experiment. This effect can be circumvented in future experiments via the measurement of eDIB fluorescence prior to the addition of bilayer-disrupting agents, achieving a true zero measurement which can be subtracted from subsequent measurements.
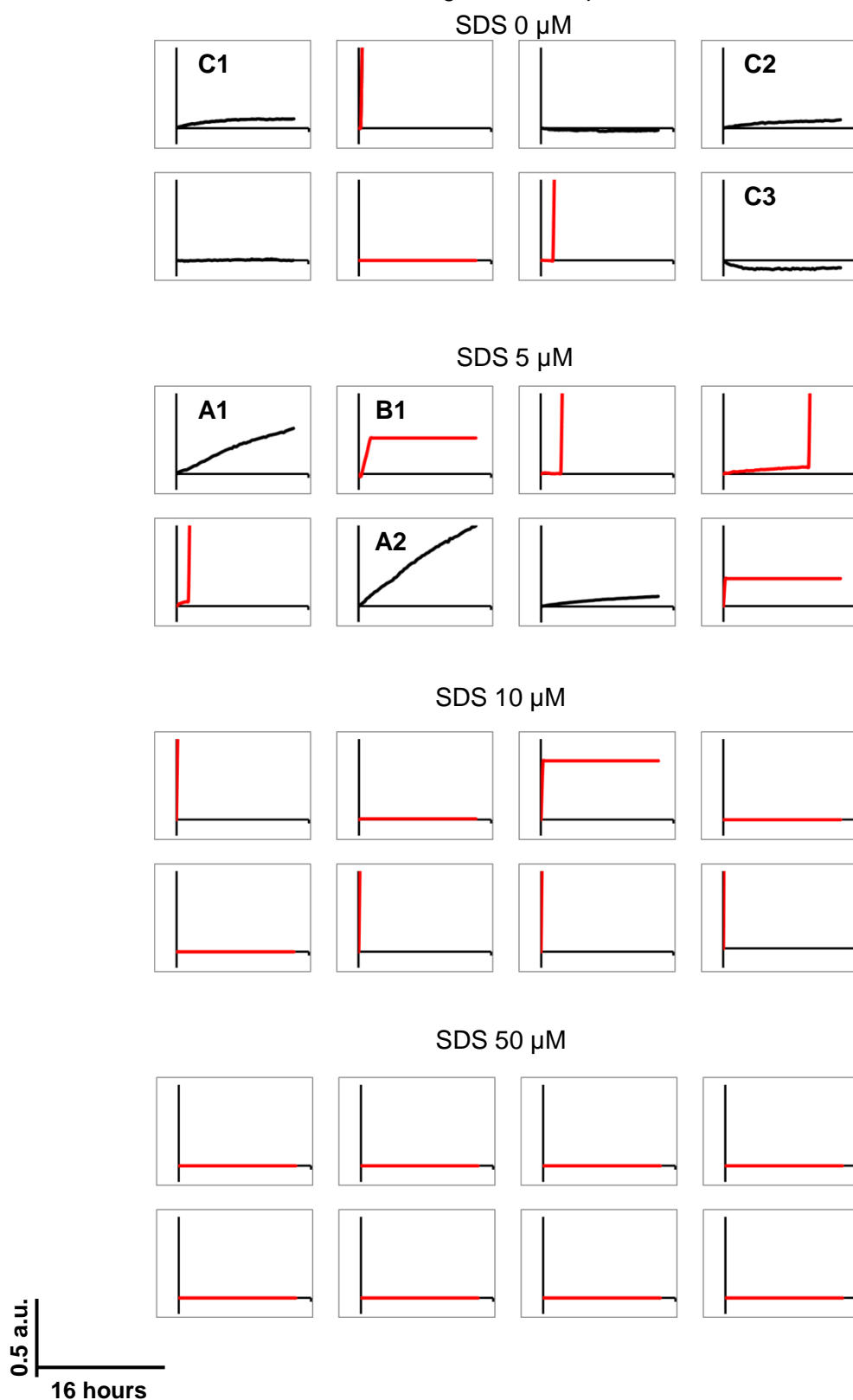
Figure 5.23 Graphs showing the change in fluorescence over a period of 16 hours of eDIBs in a 96-well plate incubated with varying concentrations of SDS, measured via SWR. Each graph represents an individual well and change in fluorescence is normalised to 0 via subtraction of the first SWR measurement from the rest of measurements. A number of graphs have been labelled (C1, C2, C3, A1, A2, B1) for reference in text. A high gain setting (1150) is employed in order to visualise small changes in fluorescence. eDIBs that underwent bilayer failure during the course of the experiment are represented with red lines.

225

The normalised data shows that two out of the three surviving eDIBs incubated in 5 µM SDS display a large, steady increase in fluorescence (labelled as A1 and A2 in Figure 5.23) which is indicative of dye leakage through eDIB bilayers, as the increases in fluorescence are significantly larger than as seen with control eDIBs. Two control eDIBs (C1 and C2) display a visible increase in fluorescence over time, which could be due to eDIB movement within the well, likely towards the centre of the well. One eDIB displays a decrease in fluorescence (C3) over time which may be due to the movement of an eDIB away from the centre of the well.

Well scanning images are shown in Figure 5.24 displaying example wells from Figure 5.23 for control eDIBs, leaking eDIBs and eDIBs showing bilayer failure. eDIBs that displayed bilayer rupture gave rise to a saturated response across the whole well (B1), whilst eDIBs that displayed leakage show a localised focal point of fluorescence close to the centre of the well with an increase in fluorescence throughout the whole well (A1), independent of eDIB position. Control eDIBs that showed an increase in fluorescence according to SWR measurements appeared to increase their fluorescence in a similar manner to the leakage eDIB, albeit much less, coinciding with the SWR measurements. The CoM of C1 appears to move towards the centre of the well, although this might also be due to low levels of leakage, whilst C2 doesn´t show a change in CoM although does increase in fluorescence akin to the leakage trace. This could be because fluorescence does not increase sufficiently so that the CoM ceases to represent the position of the eDIB, and thus the CoM at 16 hours still reflects the position of the eDIB within the well.
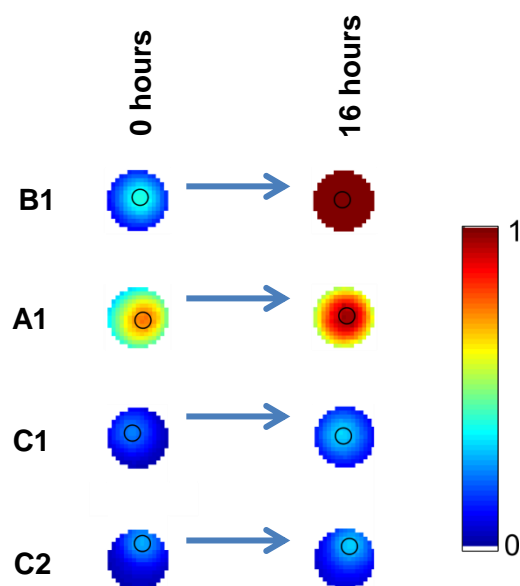
Figure 5.24 Well scanning images of selected eDIB wells as shown in Figure 5.23, displaying the change in fluorescence over a period of 16 hours. The black circle in the well scanning images represent the CoM of fluorescence in the well. B1 shows an eDIB that ruptures over the course of the experiment, giving rise to a saturated fluorescence response across the well due to the high gains setting employed, A1 shows an eDIB that displays high amounts of leakage throughout the course of the experiment due to the presence of 5 µM SDS. C1 and C2 are control eDIBs, where C1 appears to show low levels of eDIB leakage skewing the CoM towards the centre, and C2 also appears to leak although CoM remains away from the centre, likely reflecting the position of the eDIB within the well.

The experiment shows that it is possible to use the eDIB assay platform and SWR plate reader measurements to obtain high-throughput data showing changes in fluorescence over time, which can be attributed to either bilayer failure and hence the rapid de-quenching of calcein giving a sharp increase in fluorescence, or the leakage of dye through bilayer pores, visible as a steady rise in fluorescence over time. Thus it was found that SDS appears to be able to form such pores which allow for the leakage of calcein from the inside of an eDIB to the outside.

5.3.2.1.2 Triton-X100

A similar experiment was performed using different concentrations of Triton-X100, determined via previous range-finding experiments aimed at using concentrations that

227

do not result in the immediate rupture of all eDIB bilayers. The Triton-X100 experiment

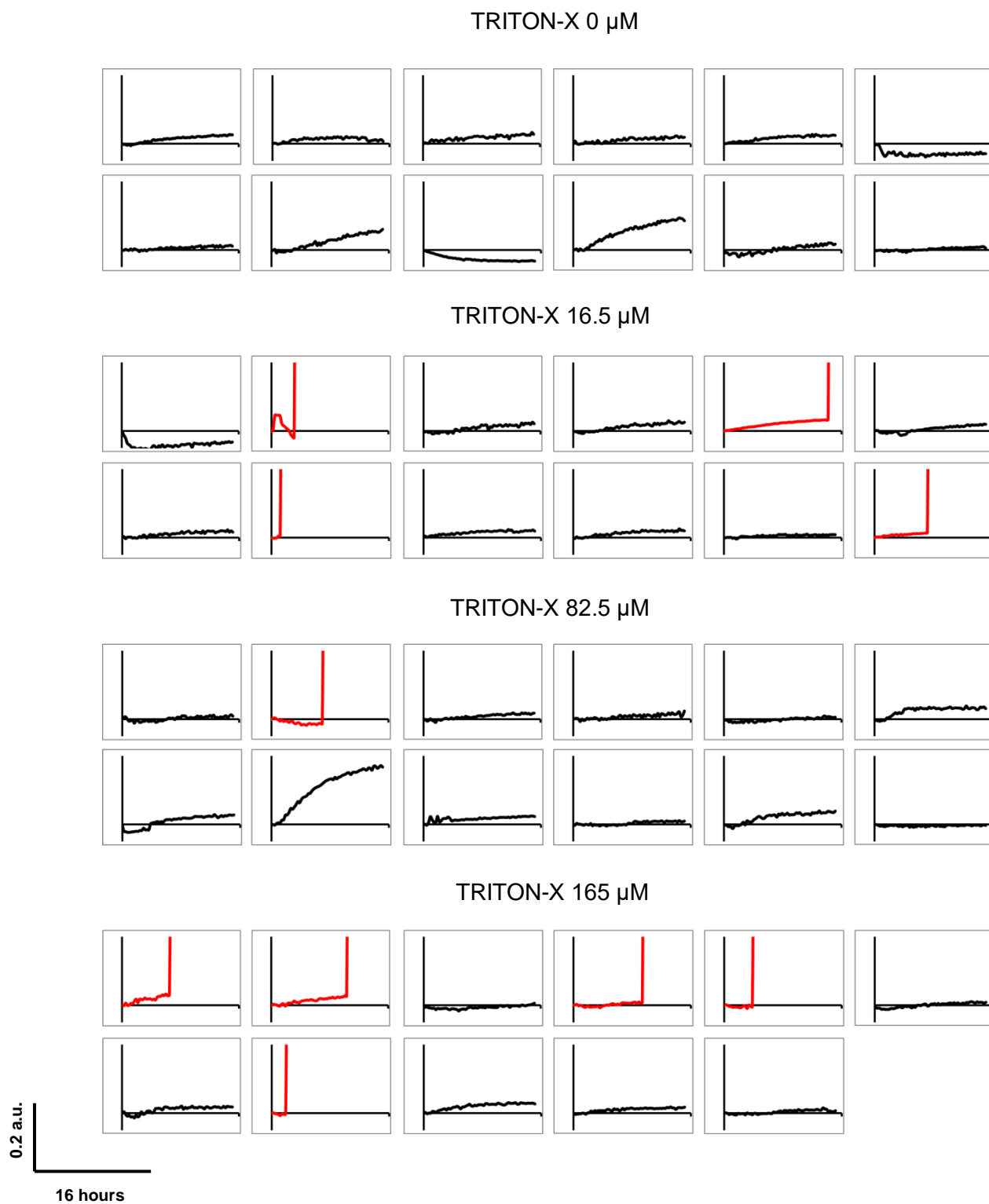is shown in Figure 5.25, using only normalised data in order to better visualise bilayer

leakage.

TRITON-X 0 µM

TRITON-X 16.5 µM

TRITON-X 82.5 µM

TRITON-X 165 µM

0.2 a.u.

16 hours

228

Figure 5.25 Change in fluorescence over a period of 16 hours of eDIBs in a 96-well plate incubated with varying concentrations of Triton-X100, measured via SWR. Each graph represents an individual well and change in fluorescence is normalised to 0 via subtraction of the first SWR measurement from the rest of measurements. A high gain setting (1150) is employed in order to visualise small changes in fluorescence. eDIBs that underwent bilayer failure during the course of the experiment are represented with red lines.
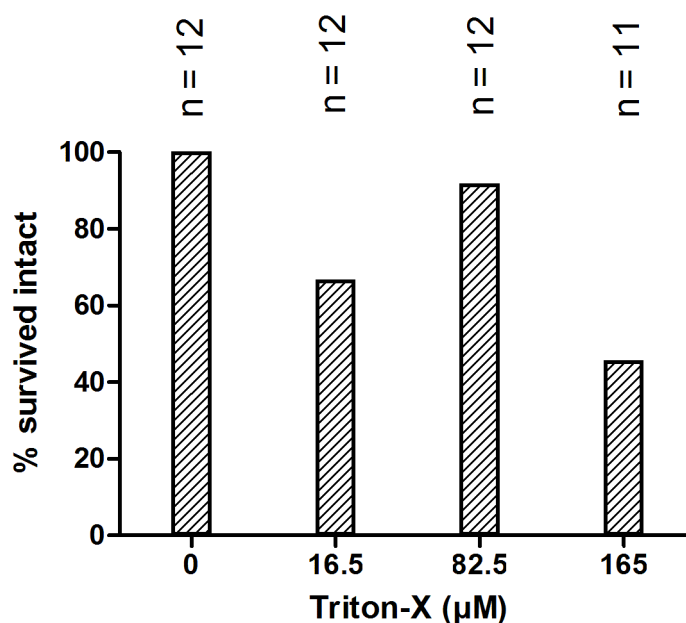

Figure 5.26 Survivability of eDIBs (as shown in Figure 5.25) exposed to varying concentrations of the detergent Triton-X100, showing the percentage of eDIBs that do not undergo bilayer failure over the course of the 16 hour experiment. The data is obtained by looking at SWR measurements that give rise to saturation over the course of the experiment, as well as visual confirmation after the plate reader measurements have taken place.

Results show that the presence of Triton-X100 decreases the survivability of eDIBs (Figure 5.26) in comparison to the control group. However, eDIBs incubated in 82.5 µM Triton-X100 display better survivability than eDIBs incubated in 16.5 µM Triton-X100, whereas one would expect increasing concentrations of Triton-X100 to give rise to decreasing survivability. However, this could be an artefact of relatively low sample numbers. Regarding bilayer leakage, it appears that Triton-X100 causes bilayer failure without giving rise to previous leakage, as steady increases in fluorescence in Triton-X100 wells do not differ significantly from controls. Therefore it is likely that small

increases or decreases in fluorescence over time are likely due to eDIB movement within the well. Two eDIBs display a higher increase in fluorescence than the rest of eDIBs, one pertaining to the control group (A1) and another incubated in 82.5 µM Triton-X100, and therefore cannot be attributed to leakage caused by the presence of Triton-X100 unless further evidenced in future experiments. Thus, the data points towards a homogeneous mechanism of action of the detergent Triton-X100 on the bilayers.

Comparing the effect of SDS vs. Triton-X100 on the eDIB bilayers, it appears that SDS has a more potent effect in causing bilayer rupture than Triton-X100 (i.e. 0% survival of eDIBs incubated with 10 µM SDS vs. 42.5% survival of eDIBs incubated with 165 µM Triton-X100). However, it appears that SDS is capable of causing leakage of dye through the bilayer at concentrations of 5 µM, visible via a steady increase in fluorescence at a rate beyond what is seen for any control eDIBs. This is indicative of a heterogeneous mode of action of SDS on the eDIBs. In comparison, Triton-X100 does not give rise to steady increases in fluorescence that is different than control eDIBs, but with increasing concentrations, gives rise to bilayer rupture and decreased eDIB survivability without prior leakage. Thus, albeit limited by low sample numbers, the findings are consistent with reports in the literature regarding the differences in the mechanisms of bilayer solubilisation caused by Triton-X100 or SDS[63]. Microscopy experiments on GUVs indicate that Triton-X100 inserts into bilayers and rapidly equilibrates between the bilayer leaflets, giving rise to rapid-forming holes once a solubility threshold is reached that results in bilayer failure, whilst it is thought that SDS causes local membrane curvature stresses as it remains mostly contained in one bilayer leaflet, leading to the formation of transient macropores at sufficient concentrations[43, 64].

Further experiments with eDIBs would aim to clarify such different mechanisms of actions by increasing the range of Triton-X100 concentrations tested, and further exploring a range of concentrations at which leakage appears to be more likely for SDS, between 0 – 10 µM.

5.3.2.2 Use of the eDIB assay platform to determine bilayer disruption caused by the synergistic pore-forming peptides Magainin 2 and PGLa

Following from demonstrations that the eDIB assay platform can detect leakage using SWR measurements, the system was employed to test the ability of pore-forming peptides Magainin 2 and PGLa to disrupt eDIB lipid bilayers. As described in section 5.1.2.1, these peptides are thought to act synergistically and debate exists regarding their mechanism of bilayer disruption. Thus, a high-throughput method to assay their ability to disrupt membranes at varying peptide concentrations and ratios would be beneficial in elucidating their activity.

Firstly, eDIBs were incubated with a range of concentrations of either Magainin 2 or PGLa, and then with both, in order to assess the synergistic effects reported for the peptides. As with previous experiments, SWR measurements were taken for 16 hours using a high gain setting (1150). The range of concentrations tested were selected to be below the concentrations at which all eDIBs immediately ruptured based on previous range-finding experiments with Magainin 2. This concentration was found to be between 0.7 and 3.5 µM, and the range of concentrations tested in subsequent experiments was 0.1 – 1.5 µM. This is in contrast with reports in the literature showing that concentrations between 3 – 10 µM cause leakage of calcein dye from GUVs but no overall bilayer disruption[53], however this difference is likely due to different experimental conditions such as the use of GUVs and the use of charged lipid mixtures, in comparison to DIBs and the zwitterionic lipid DPhPC employed in the experiments reported here.

231

Figure 5.27a and Figure 5.28a show the change in fluorescence over time for eDIBs incubated with either Magainin 2 or PGLa at different concentrations, respectively. The data shown is normalised to zero as described for the SDS and Triton-X100 data. Figure 5.27b and Figure 5.28b show the percentage of eDIBs surviving without any bilayer rupture for Magainin 2 and PGLa, respectively.
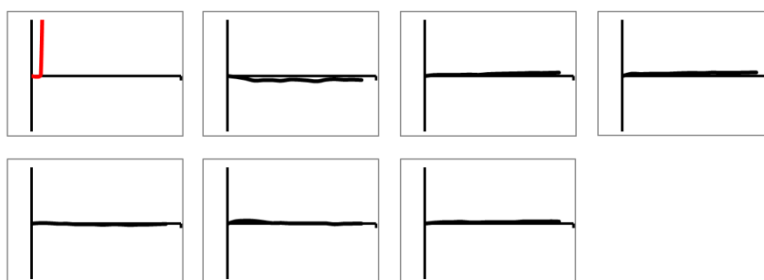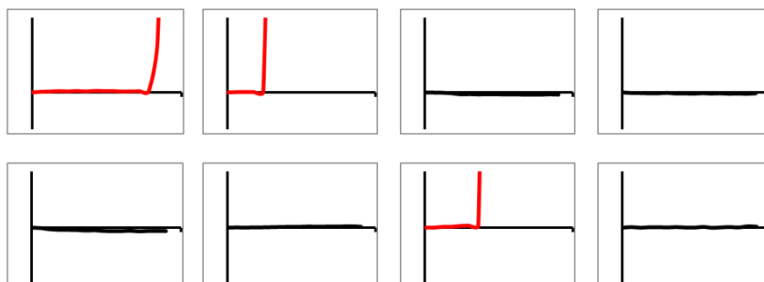
a)
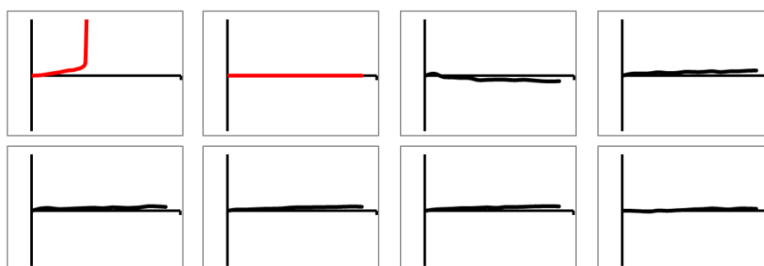
Magainin 2 0 μM

Magainin 2 0.1 μM

Magainin 2 0.5 μM

Magainin 2 1 μM

Magainin 2 1.5 μM

0.2 a.u.

16 hours

233

b)
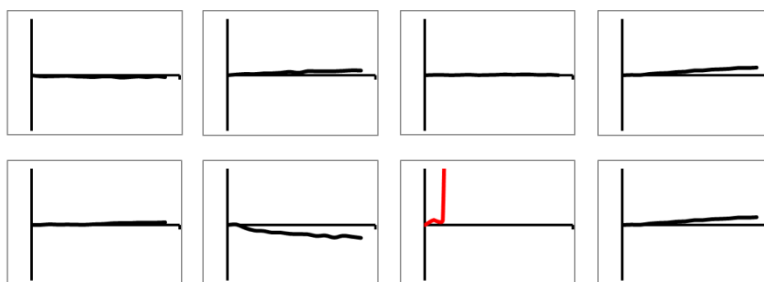
Figure 5.27 a) Graphs showing the change in fluorescence over a period of 16 hours of eDIBs in a 96-well plate incubated with varying concentrations of Magainin 2, measured via SWR. Each graph represents an individual well and change in fluorescence is normalised to 0 via subtraction of the first SWR measurement from the rest of measurements. eDIBs that underwent bilayer failure during the course of the experiment are represented with red lines. A high gain setting (1150) is employed in order to visualise small changes in fluorescence. b) Survivability of eDIBs as shown in the graphs in a), shown as the percentage of eDIBs that do not undergo bilayer failure over the course of the 16 hour experiment. The data is obtained by looking at SWR measurements that give rise to saturation over the course of the experiment, as well as visual confirmation after the plate reader measurements have taken place.

PGLa 0 µM

a)

PGLa 0.1 µM
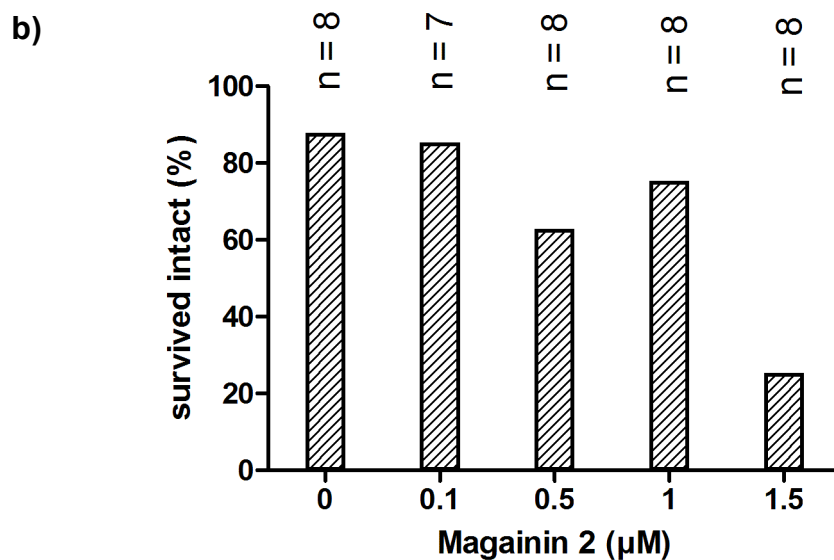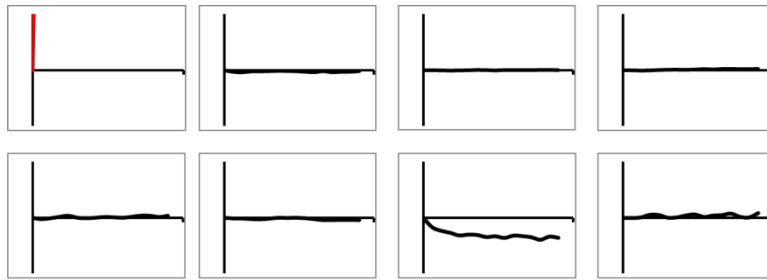
PGLa 0.5 µM

1 µM PGLa

PGLa 1.5 µM

0.2 a.u.

16 hours

b)

Figure 5.28 a) Change in fluorescence over a period of 16 hours of eDIBs in a 96-well plate incubated with varying concentrations of PGLa, measured via SWR. Each graph represents an individual well and change in fluorescence is normalised to 0 via subtraction of the first SWR measurement from the rest of measurements. eDIBs that underwent bilayer failure during the course of the experiment are represented with red lines. A high gain setting (1150) is employed in order to visualise small changes in fluorescence. b) Survivability of eDIBs as shown in the graphs in a), showing the percentage of eDIBs that do not undergo bilayer failure over the course of the 16 hour experiment. The data is obtained by looking at SWR measurements that give rise to saturation over the course of the experiment, as well as visual confirmation after the plate reader measurements have taken place.
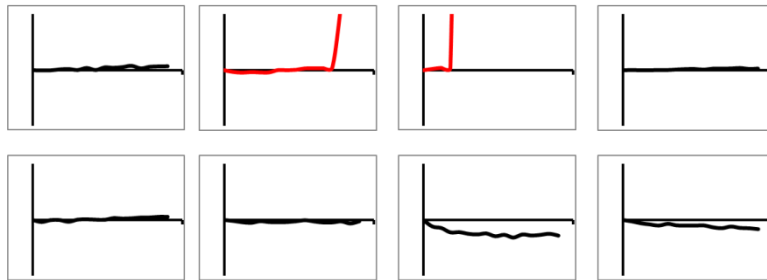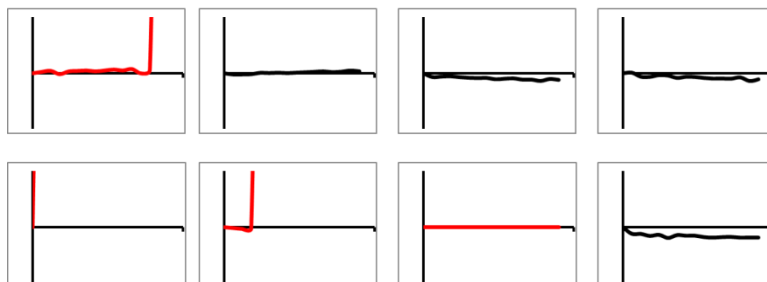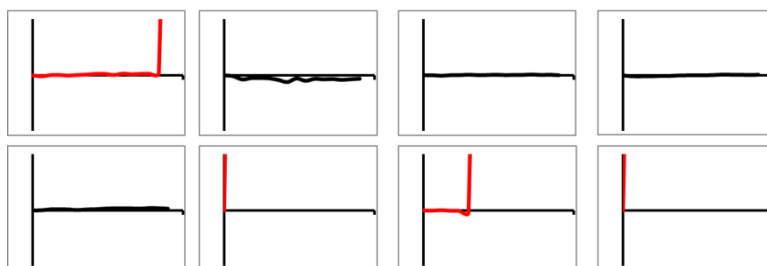
For both Magainin 2 and PGLa, decreasing eDIB survivability is seen with increasing concentrations of peptide, demonstrating that the peptides are indeed active at disrupting zwitterionic bilayers. However, it appears that eDIBs were more susceptible to bilayer failure in the presence of PGLa than Magainin 2 at higher concentrations (1 - 1.5 µM). The data for the peptides are comparable as evidenced by similar survivability of the control groups (82.5% of eDIBs survived intact for both experiments). Bilayer leakage does not appear to occur for either peptides, as few eDIBS demonstrate a steady rise in fluorescence, and those that do are indistinguishable from control. The fact that some eDIBs show a steady decrease in fluorescence from baseline further indicates that these small variations in fluorescence are likely due to spatial variations within the well, or other measurement artefacts. Therefore the data suggests that the

peptides disrupt bilayers in a homogeneous manner, at least for the zwitterionic lipid bilayers tested in these experiments.

Next, the synergistic effects of Magainin 2 and PGLa were tested by incubating eDIBs in a concentration of both peptides and comparing against the same concentration of single peptide. Figure 5.29a and b shows change in fluorescence over time for eDIBs incubated with Magainin 2, PGLa or both peptides, as well as the percentage of eDIBs surviving without any bilayer rupture, respectively.

No peptide

a)

Magainin 2 0.5 µM

PGLa 0.5 µM

Magainin 2 0.25 µM + PGLa 0.25 µM

0.2 a.u.

16 hours

238

b)
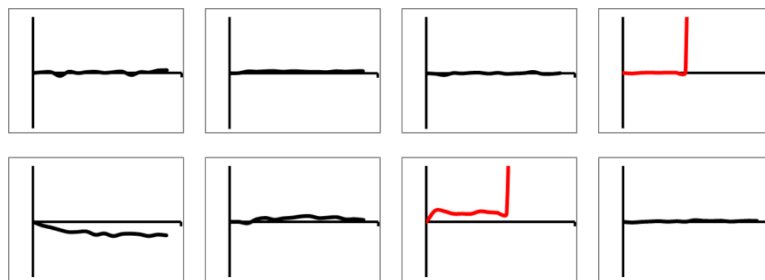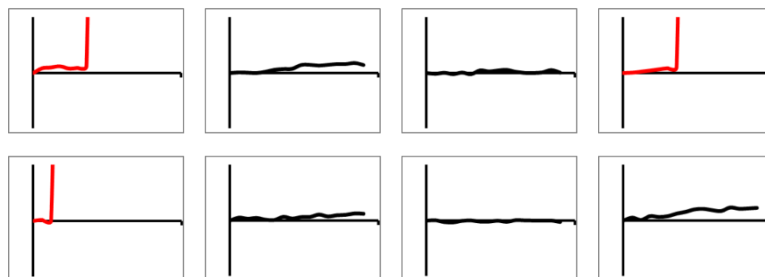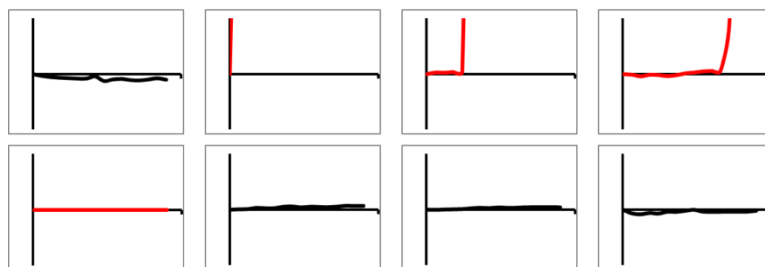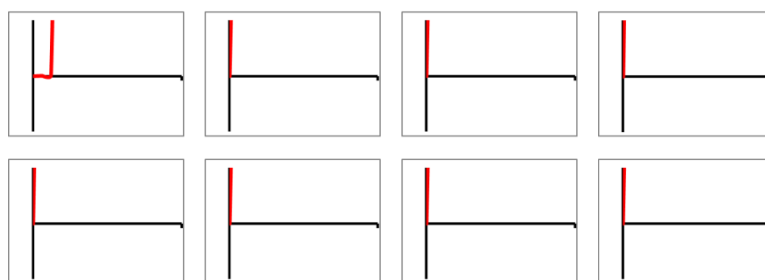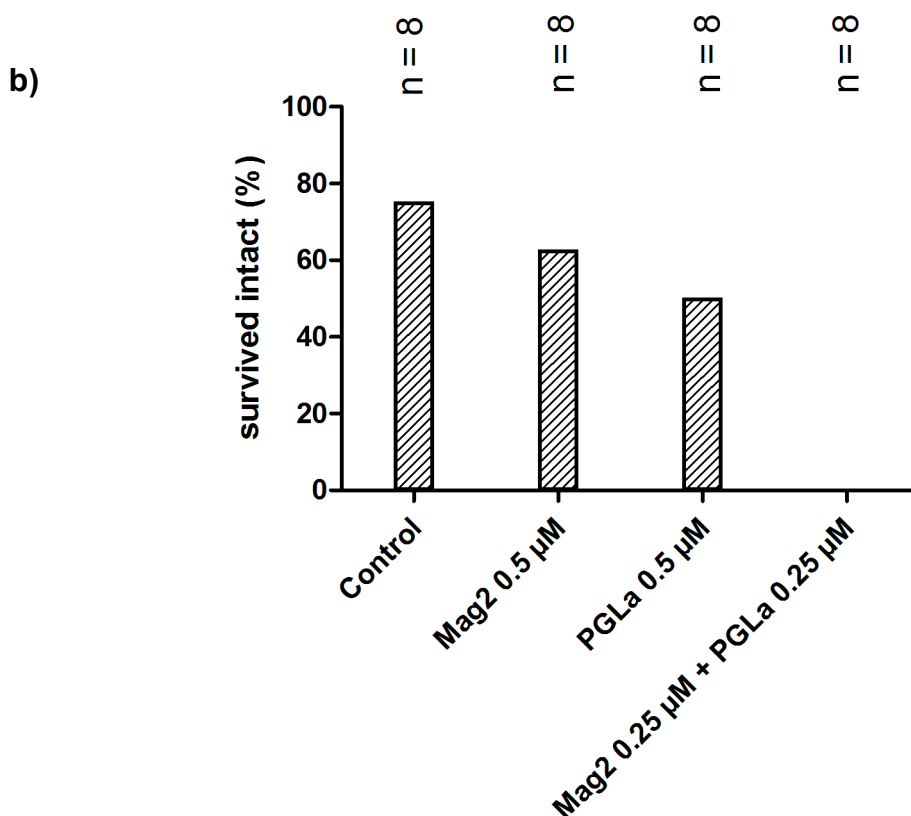
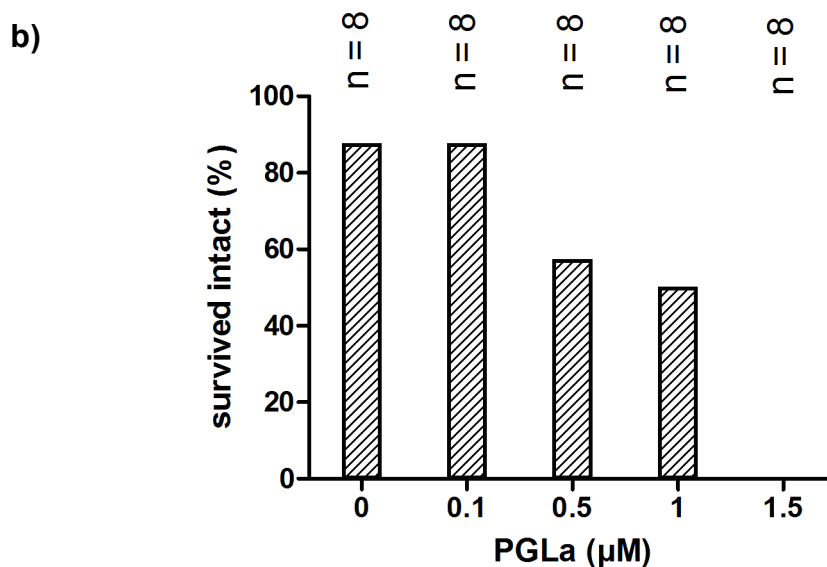**Figure 5.29** a) Graphs showing the change in fluorescence over a period of 16 hours of eDIBs in a 96-well plate incubated with varying concentrations of Magainin 2, measured via SWR. Each graph represents an individual well and change in fluorescence is normalised to 0 via subtraction of the first SWR measurement from the rest of measurements. eDIBs that underwent bilayer failure during the course of the experiment are represented with red lines. A high gain setting (1150) is employed in order to visualise small changes in fluorescence. b) Survivability of eDIBs as shown in the graphs in a), showing the percentage of eDIBs that do not undergo bilayer failure over the course of the 16 hour experiment. The data is obtained by looking at SWR measurements that give rise to saturation over the course of the experiment, as well as visual confirmation after the plate reader measurements have taken place.

The experiment demonstrates the synergistic effects of Magainin 2 and PGLa in giving rise to bilayer failure, as survivability of eDIBs incubated in a 1:1 ratio for the peptides drops to 0% over a 16 hour period in comparison to the same concentration of either of the peptides. Because of this, it is yet unconfirmed whether peptide synergy can give rise to leakage, as the eDIBs ruptured within the first hour of the experiment at the concentration tested. Therefore, subsequent experiments would focus on testing a suitable range of concentrations that would allow for the detection of leakage, lower than the concentrations employed here.

5.4 Conclusion

The experiments performed in this chapter have shown that eDIBs can be used as a high-throughput assay platform to measure the leakage of the self-quenching fluorescent dye calcein from its internal aqueous cores into the alginate shell and an aqueous buffer in a 96-well plate. For this, eDIBs can be output individually into a 96-well plate, and measurements taken using a plate reader via single-value, standard well reading (SWR) or well scanning measurements. As they are individually addressable and can be generated in large numbers, this system conforms to the basic requirements for an ALM array as described in section 5.1.

The assay platform has been demonstrated to be able to distinguish between two types of bilayer disruption. The first kind is bilayer failure, which caused the coalescence of eDIB aqueous cores with the external media, resulting in a sharp increase in measured fluorescence within the well. This could be determined via SWR measurements as well as visual confirmation due to the high resultant fluorescent output. The second kind is bilayer leakage resulting in the steady leakage of calcein from the internal eDIB aqueous cores, which can occur when bilayer pores are formed. eDIB stability within the wells was found to be variable but sufficiently high in order to carry out high-throughput experiments, ranging between 62.5 % and 100% of control eDIBs in the experiments performed in this chapter remaining measurably intact by the end of the experiment.

For the measurement of bilayer leakage, validation experiments were performed by adding known amounts of calcein to the external media within an eDIB-containing well, and comparing SWR measurements against well scanning measurements in order to account for SWR measurement artefacts that can arise from variations in the position of an eDIB within a well. It was found that SWR is able to detect concentrations of

calcein added to the well independent of eDIB position, although for low concentrations the position of an eDIB can affect SWR measurements as SWR was found to measure an area within the centre of the well. However, by comparing well scanning metrics such as the top 10% and mean pixel values with SWR, it was possible to produce correction factors to account for these variations which would allow for SWR measurements to be adjusted based on the known position of an eDIB within a well. Therefore, this would allow for SWR measurements to be taken frequently and well scanning measurements to be taken periodically over the course of an experiment, in order to distinguish between low levels of leakage and eDIB movement within a well. This is a favourable system for the measurement of leakage from eDIB bilayers as SWR measurements are significantly more rapid than well scanning measurements, allowing for increased time resolution (i.e. measurements every 15 minutes).

Following the validation experiments, proof-of-concept experiments aimed at measuring leakage of eDIBs arising from exposure to the detergents Triton-X100 and SDS were performed. These experiments showed that SDS can give rise to leakage of calcein from eDIBs at a concentration of 5 µM, with increasing concentrations resulting in bilayer rupture, whilst Triton-X100 gives rise to bilayer rupture without any measurable bilayer leakage at the concentrations tested. These findings corroborate reports regarding the differences in the mechanisms via which the detergents act on lipid bilayers[41].

Finally, the assay platform was employed in order to assess the behaviour of the pore-forming peptides Magainin 2 and PGLa, which are known to act synergistically to disrupt lipid bilayers composed of charged lipids. It was found that Magainin 2 and PGLa can separately cause failure of bilayers composed of zwitterionic lipid (DPhPC), related to the concentration of the peptide, without any discernible bilayer leakage prior to bilayer failure. The synergistic effects of the peptides were also corroborated, as

incubation of eDIBs with a 1:1 ratio of peptides caused the failure of more eDIBs than incubation with the same concentration of either peptide. Further experiments are required in order to elucidate whether the peptides synergistically give rise to bilayer leakage, exploring a larger range of concentrations, and using different kinds of lipids to form lipid bilayers. The nature of the assay allows for 2D-screens of peptide concentrations, which would be the focus of further experiments. The lack of visible leakage seen here is likely due to reports that the peptides only form pores in bilayers formed from charged lipids. However, the experiments performed here indicate that they also interact with zwitterionic lipid bilayers, albeit likely via different mechanisms and in a homogeneous manner, giving rise to bilayer failure without prior discernible leakage. Further experiments would aim to test the activity of the peptides on different lipid compositions, including the use of charged lipids.

The nature of eDIBs presents with novel opportunities in lipid bilayer array systems, in particular due to their robustness and ability to contain DIB networks. The assay described in this chapter would allow for the eDIBs to be additionally measured via electrophysiology or microscopy techniques, either directly in the wells or by extracting selected eDIBs from the wells via suction or mechanical handling, which has been demonstrated to be possible in Chapter 3. This remains yet to be demonstrated and would be a focus of future experiments. Additionally, eDIBs can be produced with a prescribed number of inner cores of different contents, which could be used to increase screening throughput, assess bilayer-compartmentalised chemical pathways or allow for the inclusion of a number of fluorescence assays per eDIB. For example, a "lipid-in" method could be employed where different aqueous cores contain different lipid mixtures and fluorescent dyes, allowing for simultaneous assaying of different asymmetric membranes, which upon bilayer leakage or rupture would give rise to distinguishable fluorescent outputs. It is therefore proposed that the array system produced in this Chapter may find numerous, ingenious applications in high-throughput

242

ALM studies, due to the intrinsic advantages of microfluidic manufacture and the eDIB chassis.

Current limitations of the experiments performed here meant that the number of inner cores per eDIB could not be modulated. For example, it might be beneficial to include only one aqueous core per eDIB, which would mean that only one DIB is assessed per well. This would allow for better characterisation and quantification of leakage in a well, as the number of bilayers and bilayer area could be readily known. This would indeed be possible with use of an additional syringe pump to control the ratio of flow rates for the inner aqueous and oil phases during the eDIB manufacture process, allowing for control over the frequency of droplet generation and hence the number of droplets encapsulated per eDIB. Furthermore, the contamination of the alginate shell of eDIBs with the inner aqueous core fluids, caused by the microfluidic manufacture process can be a problem, especially when assessing small amounts of leakage that may occur from membrane proteins, for example. However, this can be circumvented via buffer exchanging the aqueous contents of the well, or via the use of fluorescent dyes that can be controllably and externally quenched. For example, calcein can be quenched via the addition of ferric iron[65]. Additionally, different assays can be employed that give rise to optical responses that diminish over time. For example, luciferin can be contained within the aqueous cores of the eDIB aqueous cores, which upon leakage or bilayer failure mixes with luciferase in the alginate shell or the external aqueous media[66], giving rise to bioluminescence. Any luminescence that arises from initial contamination of the alginate shell with luciferin can be eliminated by waiting until luminescence naturally subsides before starting an experiment, for example.

In conclusion, this chapter has demonstrated the ability of eDIBs to be used as a high-throughput bilayer array assay platform to measure bilayer disruption where each eDIB is individually addressable, and it has been demonstrated here to provide single-bilayer

resolution for up to 47 eDIBs simultaneously (Figure 5.25) (or 78 as shown in Figure 5.8, if measuring only bilayer failure and not leakage), containing a number of DIBs each related to the number of aqueous cores contained per eDIB. The nature of the microfluidic manufacture of eDIBs and plate reader measurements allow for an assay platform that is low cost, high-throughput, scalable, and flexible, which might allow for its future development and use in applications such as drug screening and point-of-care diagnostics.

5.5 References

1.   Goldberg, D. M.; Riordan, J. R., Role of membranes in disease. *Clinical Physiology and Biochemistry* **1986,** *4* (5), 305-336.

2.   Gallagher, P. G., Red cell membrane disorders. *Hematology. American Society of Hematology. Education Program* **2005**, 13-18.

3.   Goot, G. v. d., *Pore-Forming Toxins*. Springer Science & Business Media: 2001; p 188.

4.   Heller, M. J., DNA microarray technology: devices, systems, and applications. *Annual Review of Biomedical Engineering* **2002,** *4*, 129-153.

5.   Reymond Sutandy, F. X.; Qian, J.; Chen, C.-S.; Zhu, H., Overview of Protein Microarrays. *Current protocols in protein science / editorial board, John E. Coligan ... [et al.]* **2013,** *0 27*, Unit-27.1.

6.   Bally, M.; Bailey, K.; Sugihara, K.; Grieshaber, D.; Vörös, J.; Städler, B., Liposome and Lipid Bilayer Arrays Towards Biosensing Applications. *Small* **2010,** *6* (22), 2481-2497.

7.   Castell, O. K.; Berridge, J.; Wallace, M. I., Quantification of Membrane Protein Inhibition by Optical Ion Flux in a Droplet Interface Bilayer Array. *Angewandte Chemie International Edition* **2012,** *51* (13), 3134-3138.

8.   Montal, M.; Mueller, P., Formation of Bimolecular Membranes from Lipid Monolayers and a Study of Their Electrical Properties. *Proceedings of the National Academy of Sciences of the United States of America* **1972,** *69* (12), 3561-3566.

9.   Ti Tien, H., Black Lipid Membranes at Bifaces : Formation characteristics, optical and some thermodynamic properties. *The Journal of General Physiology* **1968,** *52* (1), 125-144.

10.   Fertig, N.; Meyer, C.; Blick, R. H.; Trautmann, C.; Behrends, J. C., Microstructured glass chip for ion-channel electrophysiology. *Physical Review. E, Statistical, Nonlinear, and Soft Matter Physics* **2001,** *64* (4 Pt 1), 040901.

11.   Peterman, M. C.; Ziebarth, J. M.; Braha, O.; Bayley, H.; Fishman, H. A.; Bloom, D. M., Ion Channels and Lipid Bilayer Membranes Under High Potentials Using Microfabricated Apertures. *Biomedical Microdevices* **2002,** *4* (3), 231-236.

12.   Le Pioufle, B.; Suzuki, H.; Tabata, K. V.; Noji, H.; Takeuchi, S., Lipid Bilayer Microarray for Parallel Recording of Transmembrane Ion Currents. *Analytical Chemistry* **2008,** *80* (1), 328-332.

13.   Groves, J. T.; Ulman, N.; Boxer, S. G., Micropatterning Fluid Lipid Bilayers on Solid Supports. *Science* **1997,** *275* (5300), 651-653.

14.   Cremer, P. S.; Yang, T., Creating Spatially Addressed Arrays of Planar Supported Fluid Phospholipid Membranes. *Journal of the American Chemical Society* **1999,** *121* (35), 8130-8131.

15.   Castellana, E. T.; Cremer, P. S., Solid supported lipid bilayers: From biophysical studies to sensor design. *Surface Science Reports* **2006,** *61* (10), 429-444.

16.   Kam, L.; Boxer, S. G., Spatially Selective Manipulation of Supported Lipid Bilayers by Laminar Flow: Steps Toward Biomembrane Microfluidics. *Langmuir* **2003,** *19* (5), 1624-1631.

17.   Yamazaki, V.; Sirenko, O.; Schafer, R. J.; Nguyen, L.; Gutsmann, T.; Brade, L.; Groves, J. T., Cell membrane array fabrication and assay technology. *BMC Biotechnology* **2005,** *5*, 18.

18.   Shen, K.; Tsai, J.; Shi, P.; Kam, L. C., Self-Aligned Supported Lipid Bilayers for Patterning the Cell−Substrate Interface. *Journal of the American Chemical Society* **2009,** *131* (37), 13204-13205.

19.   Maher, S.; Basit, H.; Forster, R. J.; Keyes, T. E., Micron dimensioned cavity array supported lipid bilayers for the electrochemical investigation of ionophore activity. *Bioelectrochemistry* **2016,** *112*, 16-23.

20.   Mazur, F.; Bally, M.; Städler, B.; Chandrawati, R., Liposomes and lipid bilayers in biosensors. *Advances in Colloid and Interface Science*.

21.   F Szoka, Jr.; Papahadjopoulos, a. D., Comparative Properties and Methods of Preparation of Lipid Vesicles (Liposomes). *Annual Review of Biophysics and Bioengineering* **1980,** *9* (1), 467-508.

22.   Patel, H.; Tscheka, C.; Heerklotz, H., Characterizing vesicle leakage by fluorescence lifetime measurements. *Soft Matter* **2009,** *5* (15), 2849-2851.

23. Ahyayauch, H.; Requero, M. A.; Alonso, A.; Bennouna, M.; Goñi, F. M., Surfactant effects of chlorpromazine and imipramine on lipid bilayers containing sphingomyelin and cholesterol. *Journal of Colloid and Interface Science* **2002,** *256* (2), 284-289.

24. Hovakeemian, S. G.; Liu, R.; Gellman, S. H.; Heerklotz, H., Correlating antimicrobial activity and model membrane leakage induced by nylon-3 polymers and detergents. *Soft matter* **2015,** *11* (34), 6840-6851.

25. Städler, B.; Falconnet, D.; Pfeiffer, I.; Höök, F.; Vörös, J., Micropatterning of DNA-Tagged Vesicles. *Langmuir* **2004,** *20* (26), 11348-11354.

26. Shoji, A.; Sugimoto, E.; Orita, S.; Nozawa, K.; Yanagida, A.; Shibusawa, Y.; Sugawara, M., A reusable liposome array and its application to assay of growth-hormone-related peptides. *Analytical and Bioanalytical Chemistry* **2010,** *397* (3), 1377-1381.

27. Saliba, A.-E.; Vonkova, I.; Ceschia, S.; Findlay, G. M.; Maeda, K.; Tischer, C.; Deghou, S.; van Noort, V.; Bork, P.; Pawson, T.; Ellenberg, J.; Gavin, A.-C., A quantitative liposome microarray to systematically characterize protein-lipid interactions. *Nature Methods* **2014,** *11* (1), 47-50.

28. Kang, Y. J.; Wostein, H. S.; Majd, S., A Simple and Versatile Method for the Formation of Arrays of Giant Vesicles with Controlled Size and Composition. *Advanced Materials* **2013,** *25* (47), 6834-6838.

29. Gross, L. C. M.; Castell, O. K.; Wallace, M. I., Dynamic and Reversible Control of 2D Membrane Protein Concentration in a Droplet Interface Bilayer. *Nano Letters* **2011,** *11* (8), 3324-3328.

30. S. Friddin, M.; Bolognesi, G.; Elani, Y.; J. Brooks, N.; V. Law, R.; M. Seddon, J.; A. Neil, M. A.; Ces, O., Optically assembled droplet interface bilayer (OptiDIB) networks from cell-sized microdroplets. *Soft Matter* **2016,** *12* (37), 7731-7734.

31. Bayley, H.; Cronin, B.; Heron, A.; Holden, M. A.; Hwang, W.; Syeda, R.; Thompson, J.; Wallace, M., Droplet interface bilayers. *Molecular bioSystems* **2008,** *4* (12), 1191-1208.

32. Syeda, R.; Holden, M. A.; Hwang, W. L.; Bayley, H., Screening Blockers Against a Potassium Channel with a Droplet Interface Bilayer Array. *Journal of the American Chemical Society* **2008,** *130* (46), 15543-15548.

33. Soga, N.; Watanabe, R.; Noji, H., Attolitre-sized lipid bilayer chamber array for rapid detection of single transporters. *Scientific Reports* **2015,** *5*, srep11025.

34. Watanabe, R.; Soga, N.; Yamanaka, T.; Noji, H., High-throughput formation of lipid bilayer membrane arrays with an asymmetric lipid composition. *Scientific Reports* **2014,** *4*, srep07076.

35. Schlicht, B.; Zagnoni, M., Droplet-interface-bilayer assays in microfluidic passive networks. *Scientific Reports* **2015,** *5.*

36. Barlow, N. E.; Bolognesi, G.; Flemming, A. J.; Brooks, N. J.; Barter, L. M. C.; Ces, O., Multiplexed droplet Interface bilayer formation. *Lab on a Chip* **2016,** *16* (24), 4653-4657.

37. Seddon, A. M.; Curnow, P.; Booth, P. J., Membrane proteins, lipids and detergents: not just a soap opera. *Biochimica et Biophysica Acta (BBA) - Biomembranes* **2004,** *1666* (1–2), 105-117.

38. Pushpanathan, M.; Gunasekaran, P.; Rajendhran, J., Antimicrobial Peptides: Versatile Biological Properties. *International Journal of Peptides* **2013**.

39. Bordier, C., Phase separation of integral membrane proteins in Triton X-114 solution. *Journal of Biological Chemistry* **1981,** *256* (4), 1604-1607.

40. Heerklotz, H., Interactions of surfactants with lipid membranes. *Quarterly Reviews of Biophysics* **2008,** *41* (3-4), 205-264.

41. Nazari, M.; Kurdi, M.; Heerklotz, H., Classifying Surfactants with Respect to Their Effect on Lipid Membrane Order. *Biophysical Journal* **2012,** *102* (3), 498-506.

42. Kragh-Hansen, U.; le Maire, M.; Møller, J. V., The mechanism of detergent solubilization of liposomes and protein-containing membranes. *Biophysical Journal* **1998,** *75* (6), 2932-2946.

43. Lichtenberg, D.; Ahyayauch, H.; Goñi, Félix M., The Mechanism of Detergent Solubilization of Lipid Bilayers. *Biophysical Journal* **2013,** *105* (2), 289-299.

44. Ladbrooke, B. D.; Williams, R. M.; Chapman, D., Studies on lecithin-cholesterol-water interactions by differential scanning calorimetry and X-ray diffraction. *Biochimica et Biophysica Acta (BBA) - Biomembranes* **1968,** *150* (3), 333-340.

45. Brogden, K. A., Antimicrobial peptides: pore formers or metabolic inhibitors in bacteria? *Nature Reviews Microbiology* **2005,** *3* (3), 238-250.

46.   Laver, D. R., The barrel-stave model as applied to alamethicin and its analogs reevaluated. *Biophysical Journal* **1994,** *66* (2 Pt 1), 355-359.

47.   Yang, L.; Harroun, T. A.; Weiss, T. M.; Ding, L.; Huang, H. W., Barrel-stave model or toroidal model? A case study on melittin pores. *Biophysical Journal* **2001,** *81* (3), 1475-1485.

48.   Ludtke, S. J.; He, K.; Heller, W. T.; Harroun, T. A.; Yang, L.; Huang, H. W., Membrane pores induced by magainin. *Biochemistry* **1996,** *35* (43), 13723-13728.

49.   Shai, Y., Mechanism of the binding, insertion and destabilization of phospholipid bilayer membranes by alpha-helical antimicrobial and cell non-selective membrane-lytic peptides. *Biochimica Et Biophysica Acta* **1999,** *1462* (1-2), 55-70.

50.   Costa, F.; Carvalho, I. F.; Montelaro, R. C.; Gomes, P.; Martins, M. C. L., Covalent immobilization of antimicrobial peptides (AMPs) onto biomaterial surfaces. *Acta Biomaterialia* **2011,** *7* (4), 1431-1440.

51.   Bechinger, B., The SMART model: Soft Membranes Adapt and Respond, also Transiently, in the presence of antimicrobial peptides. *Journal of Peptide Science* **2015,** *21* (5), 346-355.

52.   Zasloff, M., Antimicrobial peptides of multicellular organisms. *Nature* **2002,** *415* (6870), 389-395.

53.   Tamba, Y.; Yamazaki, M., Single giant unilamellar vesicle method reveals effect of antimicrobial peptide magainin 2 on membrane permeability. *Biochemistry* **2005,** *44* (48), 15823-15833.

54.   Westerhoff, H. V.; Zasloff, M.; Rosner, J. L.; Hendler, R. W.; De Waal, A.; Vaz Gomes, A.; Jongsma, P. M.; Riethorst, A.; Juretić, D., Functional synergism of the magainins PGLa and magainin-2 in Escherichia coli, tumor cells and liposomes. *European Journal of Biochemistry* **1995,** *228* (2), 257-264.

55.   Zasloff, M., Magainins, a class of antimicrobial peptides from Xenopus skin: isolation, characterization of two active forms, and partial cDNA sequence of a precursor. *Proceedings of the National Academy of Sciences of the United States of America* **1987,** *84* (15), 5449-5453.

56.   de Waal, A.; Gomes, A. V.; Mensink, A.; Grootegoed, J. A.; Westerhoff, H. V., Magainins affect respiratory control, membrane potential and motility of hamster spermatozoa. *FEBS Letters* **1991,** *293* (1), 219-223.

57.   Cruciani, R. A.; Barker, J. L.; Durell, S. R.; Raghunathan, G.; Guy, H. R.; Zasloff, M.; Stanley, E. F., Magainin 2, a natural antibiotic from frog skin, forms ion channels in lipid bilayer membranes. *European Journal of Pharmacology* **1992,** *226* (4), 287-296.

58.   Giuliani, A.; Pirri, G.; Nicoletto, S. F., Antimicrobial peptides: an overview of a promising class of therapeutics. *Central European Journal of Biology* **2007,** *2* (1), 1-33.

59.   Matsuzaki, K.; Mitani, Y.; Akada, K.-y.; Murase, O.; Yoneyama, S.; Zasloff, M.; Miyajima, K., Mechanism of Synergism between Antimicrobial Peptides Magainin 2 and PGLa. *Biochemistry* **1998,** *37* (43), 15144-15153.

60.   Matsuzaki, K.; Sugishita, K.; Ishibe, N.; Ueha, M.; Nakata, S.; Miyajima, K.; Epand, R. M., Relationship of membrane curvature to the formation of pores by magainin 2. *Biochemistry* **1998,** *37* (34), 11856-11863.

61.   Tremouilhac, P.; Strandberg, E.; Wadhwani, P.; Ulrich, A. S., Synergistic transmembrane alignment of the antimicrobial heterodimer PGLa/magainin. *The Journal of Biological Chemistry* **2006,** *281* (43), 32089-32094.

62.   Benachir, T.; Lafleur, M., Study of vesicle leakage induced by melittin. *Biochimica et Biophysica Acta (BBA) - Biomembranes* **1995,** *1235* (2), 452-460.

63.   Ahyayauch, H.; Bennouna, M.; Alonso, A.; Goñi, F. M., Detergent Effects on Membranes at Subsolubilizing Concentrations: Transmembrane Lipid Motion, Bilayer Permeabilization, and Vesicle Lysis/Reassembly Are Independent Phenomena. *Langmuir* **2010,** *26* (10), 7307-7313.

64.   Sudbrack, T. P.; Archilha, N. L.; Itri, R.; Riske, K. A., Observing the Solubilization of Lipid Bilayers by Detergents with Optical Microscopy of GUVs. *The Journal of Physical Chemistry B* **2011,** *115* (2), 269-277.

65.   Thomas, F.; Serratrice, G.; Beguin, C.; Saint Aman, E.; Pierre, J. L.; Fontecave, M.; Laulhere, J. P., Calcein as a fluorescent probe for ferric iron - Application to iron nutrition in plant cells. *Journal of Biological Chemistry* **1999,** *274* (19), 13375-13383.

66.   Johnson, F. H.; Eyring, H., The nature of the luciferin-luciferase system. *Journal of the American Chemical Society* **1944,** *66*, 848-848.

Chapter 6 – Summary, Conclusions and Future Directions

6.1 Summary of findings

The work performed in this thesis has revolved around the generation of a novel kind of encapsulated droplet interface bilayer network (eDIB)[1], and its subsequent development as a chassis for artificial cells and a platform for lipid membrane studies. In comparison to other DIB networks, as developed primarily by Villar et al.[2, 3] and Elani et al.[4-6], the eDIBs described here are uniquely rugged thanks to their alginate shell, which enables them to be freestanding, mechanically handled and survive in air, water and oil environments. Alongside the microfluidic manufacture methods developed, which allows for their rapid and reproducible production, it is expected that eDIBs can give rise to novel applications using freestanding DIB networks, namely in the development of artificial cells and tissues, and novel biosensors. The multi-compartmentalised nature of eDIBs alongside their robustness may allow for the prospect of novel "lab-in-a-droplet" applications which could be used to bring the laboratory to the natural World.

The experimental work in this thesis can be divided into three main blocks: the development of the microfluidics used to produce complex emulsions required to make eDIBs, the characterisation of eDIBs, and their use as a high-throughput assay for the study of lipid membrane disruption.

Microfluidic manufacture methods were explored in order to generate both water-in-oil-in-water (W/O/W) and W/O/W/O emulsions, required in order to produce the eDIB

architecture, which comprises a network of DIBs formed from aqueous droplets inside an oil droplet containing dissolved lipid, encapsulated within a hydrogel shell. Firstly, micromilled PMMA devices were explored, however it was found that silanisation techniques for surface modification, required to produce droplets of oil, were unsuccessful (see section 2.2). Thus, a novel microfluidic device was produced, comprising sequentially aligned coaxial droplet generators made from glass capillaries, which were assembled together and aligned using a 3D-printed scaffold. In the device, W/O droplets are produced using an external T-junction, which flow into the coaxial device flowing a second aqueous phase through a glass capillary. This glass capillary was silanised in order to produce a hydrophilic surface, which was assessed using contact angle measurements. The volume and generation frequency of both the W/O droplets and the O/W droplets produced were found to be controllable via flow rate modulation, and in this way gave rise to W/O/W emulsions reproducibly encapsulating between 7 and 23 aqueous droplets per emulsion. W/O/W emulsions could then be passed through a second coaxial droplet generator within the same microfluidic device, flowing oil through a larger FEP tube, resulting in W/O/W/O emulsions. The hybrid, coaxial microfluidic device produced presented used common-place laboratory materials , and was found to be accessible due its low cost and ease of assembly, granted by the 3D-printed scaffold; and versatile due to it sequential alignment, allowing for the production of double and triple emulsions as demonstrated here, although further emulsions are also likely possible via further sequentially aligned coaxial geometries using channels of alternating wettabilities[7].

Using the microfluidic methods described above for the generation of W/O/W/O emulsions, encapsulated droplet interface bilayers (eDIBs) were generated. This was achieved by using a lipid-containing oil solution for the oil droplet phase resulting in the formation of DIBs between the internal droplets and also between the internal droplets and the alginate shell. The alginate shell was produced via the gelation of the external

aqueous phase within the microfluidic device, using an internal gelation mechanism[8]. The resulting eDIBs were found to be considerably rugged, in comparison to similar structures that do not contain a hydrogel shell (i.e. multisomes[2]), which were found to commonly rupture upon contact with surfaces and phase interfaces. The hydrogel-encapsulated eDIBs were shown to be able to remain intact in both aqueous, oil and air environments and could survive in oil for periods of weeks, when kept in conditions that prevented evaporation (such as when submerged in oil). Additionally, eDIBs were shown to be able to withstand manual handling such as with tweezers, and could be sucked-up and expelled using a pipette. Electrophysiology techniques were employed in order to demonstrate the formation of lipid bilayers between the internal droplets and the hydrogel shell, as well as the insertion of the membrane protein α-Hemolysin. This demonstrated the ability of eDIBs to selectively communicate with their environment.

Additionally, it was shown that eDIBs could form higher order structures in 2 and 3 dimensions, via the adherence of eDIBs to one another. This forms a basis via which a number of DIB networks can give rise to larger, tissue-like assemblies. Moreover, eDIBs could be made to form into elongated structures comprising a number of oil-droplets containing DIB networks within an alginate "snake", which might find applications in drug delivery or as biological models for communication between cells in close proximity. Furthermore, eDIBs could also be produced within a polymerisable substance, such as TMPTA, instead of alginate, which could in principle be used in order to produce storable and shippable DIB networks.

Finally, eDIBs were employed in order to generate an artificial lipid membrane (ALM) array, which was demonstrated with use of a fluorescence release assay based on calcein de-quenching in order to obtain high-throughput data on membrane disruption. For this, the internal eDIB droplets contained a self-quenched solution of calcein, which gave rise to fluorescence upon its release into the alginate shell. eDIBs could be

250

individually placed within the oil- and buffer-filled wells of a 96-well plate, and fluorescently measured over time using a plate reader. It was found that internal droplets coalesced with the alginate phase upon bilayer failure, which gave rise to a sharp increase in well fluorescence. Leakage through bilayer pores could also be detected, and was validated using control experiments where wells containing eDIBs were spiked with known concentrations of calcein and the resulting well scanning and standard well reading measurements compared, in order to account for spatial variations within the wells. It was found that spatial variations gave rise to minimal effects in standard well read measurements and could be accounted for by using well scanning data. Proof-of-concept experiments were performed by exposing eDIBs in 96-well plates to concentrations of the detergents Triton-X100 and sodium dodecyl sulphate (SDS), as well as the pore-forming peptides Magainin 2 and PGLa. It was found that SDS was able to give rise to steady increases in fluorescence indicating the formation of stochastic bilayer pores, whilst Triton-X100 caused bilayer failure without prior detectable leakage. These results were found to be coherent with mechanisms proposed in the literature[9]. It was also found that Magainin 2 and PGLa caused bilayer failure in eDIBs, and their potency in disrupting the bilayers increased when acting synergistically in a 1:1 ratio. This was also found to be coherent with reports on the literature about their function, as Magainin 2 and PGLa are known to act synergistically[10, 11], and form pores in charged lipid bilayers[12-14]. The lipids employed here (DPhPC) are zwitterionic and it was therefore expected that the peptides might disrupt the eDIB bilayers differently. It was thus demonstrated that the eDIB assay platform was able to detect different profiles of membrane disruption, and presents a number of favourable aspects such as the fact that the assay is high-throughput, scalable and likely automatable, and low-cost due to the use of common laboratory equipment such as a plate reader. Further, optical measurements can be supplemented with gold-standard electrophysiology measurements on identified

constructs of interest. The eDIBs are individually addressable within each well and also remain suitably stable throughout the course of 16 hour experiment.

6.2 Short term future work

Short-term future work comprises work which would immediately improve or follow from the work that has already been performed in this thesis. This section will be divided into work concerning microfluidics, eDIB characterisation, and the eDIB array for high-throughput bilayer measurements.

6.2.1 Microfluidics

Monodispersity: The monodispersity of the droplets and the double and triple emulsions was not characterised. Characterisation of the monodispersity aids in understanding the performance and reproducibility of the microfluidic device in producing eDIBs.

Use of ETFE junction resulted in unpredictable formation of W/O droplets: As shown in Figure 2.8 in Chapter 2 (section 2.3.2), the modulation of water and oil flow rates gave rise to erratic W/O formation regarding the size and frequency of generation of the droplets. The use of a more reproducible and predictable method of droplet formation would allow for better control over resulting double and triple emulsions and hence a better ability to predict the number of aqueous droplets contained per W/O/W emulsion for a given set of flow rates, for example.

Scaling down: The emulsions produced here are relatively large within the microfluidics realm: double and triple emulsions are around 2 mm and 3 mm in diameter, respectively. This is likely due to the use of large channels and a geometrically-driven regime of droplet formation. Thus, further experiments would focus on scaling down the device in order to produce emulsions that are significantly

smaller, likely to give rise to more controllable emulsion production, less reagent use, as well as more stable and useful eDIBs. Ideally, eDIBs would be produced that are at least smaller than 1 mm in diameter.

6.2.2 eDIBs

eDIB communication: Insofar, demonstration of communication between different internal eDIB compartments has not been performed. Further work would involve the use of chemical systems that allow eDIBs to selectively transfer chemicals from one compartment to another, and also uptake chemicals from the environment and give rise to a signal, such as a luminescent or fluorescent signal. For this, an Amplex Red system for the detection of glucose could be employed, as is employed in the referenced publication[5].

eDIB tissue communication: communication between a population of eDIBs would solidify the claim that they are able to act as synthetic tissues, as insofar they have only demonstrated to be able to adhere to one another. Firstly, it would be desirable to demonstrate the formation of lipid bilayers between eDIBs using electrophysiology. Alginate hydrogel shapes have been reported elsewhere to be able to form DIBs between them[15]. Secondly, the Amplex Red system as mentioned above[5] could be employed in order to demonstrate communication between two populations of eDIBs. For example, hydrogen peroxide produced by one population of eDIBs could be used to trigger the fluorescence in another population of eDIBs, via its passive diffusion into eDIB cores containing Amplex Red. Another interesting example of eDIB tissue communication could be achieved via the incorporation of oscillator reactions, such as the Belousov-Zabotinsky (BZ) reaction[16], which could be used to enable tissue-wide chemical synchronisation in an oscillating fashion.

6.2.3 eDIB array for high throughput membrane studies

Proof-of-concept experiments using Magainin 2 and PGLa: the experiments performed would be adequately completed via the demonstration of a 2D concentration screen in a 96-well plate, in order to test different concentrations and ratios of peptides. This would provide an example of the versatility and high-throughput of the eDIB array. Furthermore, the use of charged lipids in the eDIBs, such as 1,2-dioleoyl-sn-glycero-3-phospho-(1'-rac-glycerol) (DOPG)[12], would allow for further demonstrations of the ability of the array to detect bilayer leakage, as well as shed light on the ability of the peptides to affect lipid bilayers of different compositions.

Assaying via different means: it is hypothesised that the eDIB array allows for the ALMs to be probed *in situ* via different means aside from optical means. Thus further experiments would demonstrate the ability to probe eDIBs via electrophysiology within the wells following plate reader measurements.

Lower limit of detection: Determination of the lower limit of detection for bilayer leakage through eDIBs would be of benefit in understanding its limitations and assessing whether the assay would be able to measure leakage through fixed-diameter protein pores, for example.

6.3 Long-term future work

This section will highlight potential projects and aspects of work with eDIBs that have been identified in being able to bring value to the fields of bottom-up synthetic biology and the development of bio-inspired devices.

Adaptivity and Responsiveness: A key feature of biological cells is their ability to sense their environment or biological cues, and then respond or adapt accordingly. This can be emulated in artificial cells or eDIBs by coupling sensing with actuator

254

mechanisms[17]. For example, a luciferin-luciferase system can be used to generate light in response to chemical cues, and then activate light-responsive membrane proteins, such as bacteriorhodopsin[18, 19], which can give rise to an ion flux in response. Gelation and de-gelation can also be actuated in this way, which could give rise to the release of the inner contents of an eDIB[20]. Such a system can be envisaged to be useful in triggered drug delivery systems. It would be of great value to incorporate protein expression or energy generation systems such as ATP-synthase, which can be employed by the cell to produce suitable proteins or energise transport, locomotion, or other biomimetic processes in response to environmental stimuli.

Multi-compartmentalised chemical synthesis: Because of the multi-compartmentalised nature of eDIBs, it should be possible to incorporate multi-step enzymatic or chemical pathways for the production of valuable chemicals. The separation of reaction steps into different compartments would allow for the avoidance of reaction product-inhibition as well as the maintenance of concentration gradients and specific conditions (i.e. pH) that are most favourable for individual reaction steps, within an individual construct. Reaction steps can be separately assessed via the incorporation of optical sensing mechanisms (i.e. reaction products give rise to fluorescence or luminescence). Additionally, reaction products can be made to trigger gelation of internal eDIB cores in order for facile collection of the final reaction products. The ability to mass produce eDIBs using microfluidics makes this a feasible method to produce valuable chemicals with high yields. Furthermore, such strategies can be used to give rise to *in situ* chemical synthesis for the use of eDIBs as drug delivery vehicles, via the compartmentalisation of prodrugs and activators, for example.

Artificial cell communication with biological cells: eDIBs can be co-incubated with biological cells and made to interact with them, via the release of cytokines and hormones. Furthermore, eDIBs can be engineered to react to biological cell stimuli by

255

releasing substances in response to their chemical cues, establishing feedback loops or the sequential release of biological molecules for biological cell differentiation or pathogen modelling, for example.

6.4 Frontiers for the development of artificial cells

Natural, biological cells are enormously complex in their structure, behaviour and function. However, several advances have been developed over the recent decades for both bottom-up and top-down biology approaches. Artificial cells based on natural organisms have been produced containing entirely synthetic genomes[21]. Artificial cell chassis systems based around lipid membranes have been produced which have demonstrated to give rise to a number of biological behaviours, such as the ability to replicate and express genetic material[22], give rise to multi-compartmentalisation[4], adhere to each other[23], communicate with microorganisms[24], contain primitive metabolisms[5], incorporate cytoskeletal components[25] and form higher order structures such as tissues[3]. Other endeavours have also managed to demonstrate life-like behaviours arising from simple, droplet structures, such as spontaneous division[26] and motility[27]. It is expected that the successful development of truly artificial cells will depend on the co-operation of scientists across different fields and approaches to synthetic biology, and their ability to develop a single artificial cell platform able to incorporate many of the functionalities described here, so that such functions are dependent on each other and reactive to stimuli, as they are with living cells. For example, a significant achievement would be the incorporation and function of a minimal, synthetic genome inside a bottom-up synthetic cell chassis.

A common theme seen in biological systems is the ability of emergent behaviours to arise from the collective action of a number of discrete components. This occurs across all scales of biology via self-organisation[28] mechanisms, whether it is in the self-

assembly of molecules into supramolecular, functional structures, the co-operation of cells that give rise to multicellular organisms, or the collective action of individual organisms that give rise to super-organisms, seen with certain arthropods such as ants and bees[29]. In all of these cases, self-organisation arises from a set of initial conditions, parameters, and interaction rules, from which patterns and behaviours emerge that extend beyond the scale of the individual subunits of the system, without requirement of an external coordinator. Such interaction rules often give rise to negative and positive feedback loops, oscillations, threshold response criticality and other collective phenomena[30], which allow the emergent system to be qualitatively different than the sum of its subunits.

Whilst the current approaches and successes in the development of artificial cells have mostly been of a reductionist nature, it could be argued that if biology were truly to be replicated, one would require to implement a set of interaction rules between a number of discrete components that give rise to "living" behaviours at a higher-order, systems level. Outside of the realm of biology, this can be exemplified by the creation of Conway´s Game of Life, which is a computer program where a two-dimensional orthogonal grid of square cells evolve over time without any input beyond its initial configuration[31]. Synthetic biology has yet to incorporate such concepts in the design of artificial cells. This can be envisaged via the creation of an artificial cell platform which can incorporate a selection of reactive phenomena, such as the ability to express functional proteins as a reaction to stimuli, or the ability of individual cells to physically interact and communicate chemically when in close proximity. The engineering of self-organization and emergence in soft matter systems remains an exciting challenge as it offers the ability to cause system-level changes via the modification of subunit parameters. Additionally, this offers to shine new perspectives on our understanding of "living" and other complex systems.

6.5 Concluding statements

This thesis has shown the development process of a novel kind of DIB construct, herein named eDIBs, comprised of a DIB network encapsulated within a hydrogel shell. It has been demonstrated that these constructs are uniquely rugged, are able to communicate with their environment using membrane proteins, and form higher-order structures. These properties enable the use of eDIBs as chassis for artificial cells. Proof-of-concept experiments have shown that they can be employed as an artificial bilayer array for membrane studies, offering a flexible platform that is able to interrogate bilayer constructs individually in a high-throughput fashion. Additionally, the microfluidic methods used allow for the controlled and scalable generation of eDIBs in large numbers. The employment of relatively accessible methods and equipment throughout this thesis for the generation of eDIBs (i.e. 3D-printing, silanisation), and their use as an ALM array (i.e. plate reader) enable facile uptake of the production and use of eDIBs in other laboratories, further providing the tools to expand upon the potential that eDIBs offer.

For all of the reasons stated above, we propose that eDIBs may be able to harness previously unrealised potential of DIB networks for applications in healthcare and beyond, perhaps with the opportunity to create novel, "lab-in-a-capsule" technologies that can be used outside of typical laboratory settings, and a hierarchically-organised artificial cell system.

6.6 References

1.   Baxani, D. K.; Morgan, A. J. L.; Jamieson, W. D.; Allender, C. J.; Barrow, D. A.; Castell, O. K., Bilayer Networks within a Hydrogel Shell: A Robust Chassis for Artificial Cells and a Platform for Membrane Studies. *Angewandte Chemie International Edition* **2016,** *55* (46), 14240-14245.

2.   Villar, G.; Heron, A. J.; Bayley, H., Formation of droplet networks that function in aqueous environments. *Nature Nanotechnology* **2011,** *6* (12), 803-808.

3.   Villar, G.; Graham, A. D.; Bayley, H., A Tissue-Like Printed Material. *Science (New York, N.Y.)* **2013,** *340* (6128), 48-52.

4.   Elani, Y.; Gee, A.; Law, R. V.; Ces, O., Engineering multi-compartment vesicle networks. *Chemical Science* **2013,** *4* (8), 3332-3338.

5.   Elani, Y.; Law, R. V.; Ces, O., Vesicle-based artificial cells as chemical microreactors with spatially segregated reaction pathways. *Nature Communications* **2014,** *5*, 5305.

6.   Elani, Y.; Solvas, X. C. I.; Edel, J. B.; Law, R. V.; Ces, O., Microfluidic generation of encapsulated droplet interface bilayer networks (multisomes) and their use as cell-like reactors. *Chemical Communications* **2016,** *52* (35), 5961-5964.

7.   Abate, A. R.; Weitz, D. A., High-Order Multiple Emulsions Formed in Poly(dimethylsiloxane) Microfluidics. *Small* **2009,** *5* (18), 2030-2032.

8.   Tan, W. H.; Takeuchi, S., Monodisperse Alginate Hydrogel Microbeads for Cell Encapsulation. *Advanced Materials* **2007,** *19* (18), 2696-2701.

9.   Nazari, M.; Kurdi, M.; Heerklotz, H., Classifying Surfactants with Respect to Their Effect on Lipid Membrane Order. *Biophysical Journal* **2012,** *102* (3), 498-506.

10.   Westerhoff, H. V.; Zasloff, M.; Rosner, J. L.; Hendler, R. W.; De Waal, A.; Vaz Gomes, A.; Jongsma, P. M.; Riethorst, A.; Juretić, D., Functional synergism of the magainins PGLa and magainin-2 in Escherichia coli, tumor cells and liposomes. *European Journal of Biochemistry* **1995,** *228* (2), 257-264.

11.   Matsuzaki, K.; Mitani, Y.; Akada, K.-y.; Murase, O.; Yoneyama, S.; Zasloff, M.; Miyajima, K., Mechanism of Synergism between Antimicrobial Peptides Magainin 2 and PGLa. *Biochemistry* **1998,** *37* (43), 15144-15153.

12.   Tamba, Y.; Yamazaki, M., Single giant unilamellar vesicle method reveals effect of antimicrobial peptide magainin 2 on membrane permeability. *Biochemistry* **2005,** *44* (48), 15823-15833.

13.   Cruciani, R. A.; Barker, J. L.; Durell, S. R.; Raghunathan, G.; Guy, H. R.; Zasloff, M.; Stanley, E. F., Magainin 2, a natural antibiotic from frog skin, forms ion channels in lipid bilayer membranes. *European Journal of Pharmacology* **1992,** *226* (4), 287-296.

14.   Ludtke, S. J.; He, K.; Heller, W. T.; Harroun, T. A.; Yang, L.; Huang, H. W., Membrane pores induced by magainin. *Biochemistry* **1996,** *35* (43), 13723-13728.

15.   Sapra, K. T.; Bayley, H., Lipid-coated hydrogel shapes as components of electrical circuits and mechanical devices. *Scientific Reports* **2012,** *2*, 848.

16.   Torbensen, K.; Rossi, F.; Ristori, S.; Abou-Hassan, A., Chemical communication and dynamics of droplet emulsions in networks of Belousov–Zhabotinsky micro-oscillators produced by microfluidics. *Lab on a Chip* **2017,** *17* (7), 1179-1189.

17.   Trantidou, T.; Friddin, M.; Elani, Y.; Brooks, N. J.; Law, R. V.; Seddon, J. M.; Ces, O., Engineering Compartmentalized Biomimetic Micro- and Nanocontainers. *ACS nano* **2017**.

18.   Holden, M. A.; Needham, D.; Bayley, H., Functional Bionetworks from Nanoliter Water Droplets. *Journal of the American Chemical Society* **2007,** *129* (27), 8650-8655.

19.   Schild, V. R.; Booth, M. J.; Box, S. J.; Olof, S. N.; Mahendran, K. R.; Bayley, H., Light-Patterned Current Generation in a Droplet Bilayer Array. *Scientific Reports* **2017,** *7*, 46585.

20.   Kloxin, A. M.; Tibbitt, M. W.; Anseth, K. S., Synthesis of photodegradable hydrogels as dynamically tunable cell culture platforms. *Nature Protocols* **2010,** *5* (12), 1867-1887.

21.   Gibson, D. G.; Glass, J. I.; Lartigue, C.; Noskov, V. N.; Chuang, R.-Y.; Algire, M. A.; Benders, G. A.; Montague, M. G.; Ma, L.; Moodie, M. M.; Merryman, C.; Vashee, S.; Krishnakumar, R.; Assad-Garcia, N.; Andrews-Pfannkoch, C.; Denisova, E. A.; Young, L.; Qi, Z.-Q.; Segall-Shapiro, T. H.; Calvey, C. H.; Parmar, P. P.; Hutchison, C. A.; Smith, H. O.; Venter, J. C., Creation of a bacterial cell controlled by a chemically synthesized genome. *Science (New York, N.Y.)* **2010,** *329* (5987), 52-56.

22.   Kurihara, K.; Tamura, M.; Shohda, K.-I.; Toyota, T.; Suzuki, K.; Sugawara, T., Self-reproduction of supramolecular giant vesicles combined with the amplification of encapsulated DNA. *Nature Chemistry* **2011,** *3* (10), 775-781.

23.   Hadorn, M.; Boenzli, E.; Sørensen, K. T.; De Lucrezia, D.; Hanczyc, M. M.; Yomo, T., Defined DNA-mediated assemblies of gene-expressing giant unilamellar vesicles. *Langmuir: the ACS journal of surfaces and colloids* **2013,** *29* (49), 15309-15319.

24.   Gardner, P. M.; Winzer, K.; Davis, B. G., Sugar synthesis in a protocellular model leads to a cell signalling response in bacteria. *Nature Chemistry* **2009,** *1* (5), 377-383.

25.   Krishna Kumar, R.; Yu, X.; Patil, A. J.; Li, M.; Mann, S., Cytoskeletal-like Supramolecular Assembly and Nanoparticle-Based Motors in a Model Protocell. *Angewandte Chemie International Edition* **2011,** *50* (40), 9343-9347.

26.   Zhu, T. F.; Szostak, J. W., Coupled growth and division of model protocell membranes. *Journal of the American Chemical Society* **2009,** *131* (15), 5705-5713.

27.   Hanczyc, M. M., Metabolism and motility in prebiotic structures. *Philosophical Transactions of the Royal Society B: Biological Sciences* **2011,** *366* (1580), 2885-2893.

28.   Whitesides, G. M.; Grzybowski, B., Self-assembly at all scales. *Science (New York, N.Y.)* **2002,** *295* (5564), 2418-2421.

29.   Detrain, C.; Deneubourg, J.-L., Self-organized structures in a superorganism: do ants "behave" like molecules? *Physics of Life Reviews* **2006,** *3* (3), 162-187.

30.   Karsenti, E., Self-organization in cell biology: a brief history. *Nature Reviews Molecular Cell Biology* **2008,** *9* (3), 255-262.

31.   Bauchau, V., Emergence and Reductionism: from the Game of Life to Science of Life. In *SELF-ORGANIZATION AND EMERGENCE IN LIFE SCIENCES*, Feltz, B.; Crommelinck, M.; Goujon, P., Eds. Springer Netherlands: 2006; pp 29-40.

Appendix

APPENDIX 1 - Calculation of oil droplet volume from photographs

Oil droplet volume was calculated using the dimensions depicted in Figure 2.2 and using the following equation for the volume of an ellipsoid:

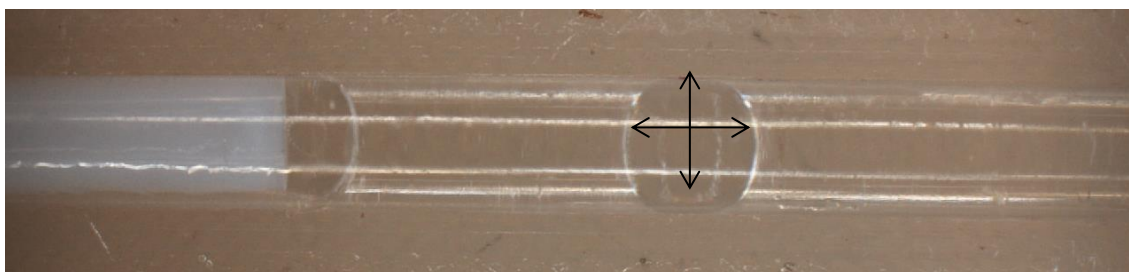$$V = \frac{4}{3}\pi\frac{x^2 y}{2}$$

Figure 1 Image of an oil droplet generated using the 3d-printed, hybrid device in the coaxial geometry, using a flow rate of 10 ml hr^{-1} for the oil phase and 300 ml hr^{-1} for the carrier aqueous phase.

However, the droplet is not an ellipsoid as its geometry is constricted by the inner diameter of the glass channel where it is contained, and thus could more accurately be represented as a cylinder with a spherical cap at either side. Another potentially more reliable method would be to output the droplets into a container filed with water and calculate their volume as a sphere.
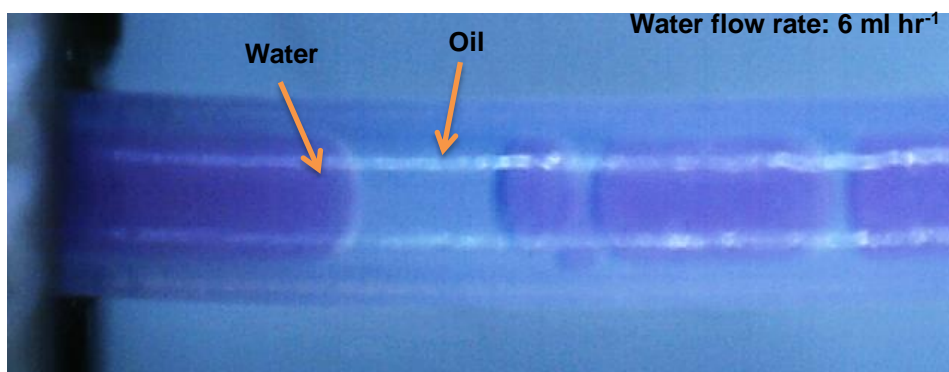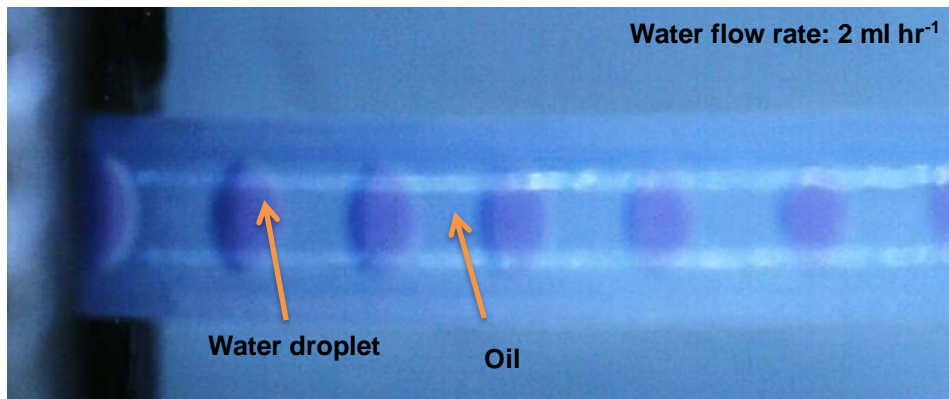
APPENDIX 2 - Flow rates that allow for the periodic generation of water droplets in oil using an ETFE T-junction as a droplet generator.

Table and photograph displaying the variability in water droplet production in squalene oil using an ETFE junction. a) Table displaying all of the flow rates tested. Green indicates flow rates which allow for the stable, periodic production of droplets whilst red indicates erratic droplet production. b) Photographs depicting examples of monodisperse droplet production (above) and erratic droplet production (below).

a)

b)

APPENDIX 3 - Capillary number calculations

The table shows the range of parameters (at room temperature and pressure) used to determine the Ca numbers for the generation of W/O droplets in an ETFE junction and the generation of O/W droplets in the coaxial junction. The equation for the Ca number can be found in section 1.3.2.1.1.

Parameter	Water	Oil (squalene)
Dynamic viscosity μ	$8.9*10^{-4}$ N s m^{-2} [2]	0.012 N s m^{-2} [3]
Velocity	$0.835 - 1.67$ m s^{-1} (for $10 - 20$ ml min^{-1} flowing through a 0.5 mm channel (diameter).	$5.4*10^{-5} - 2.7*10^{-4}$ (for $100 - 500$ ml min^{-1} flowing through a 2 mm channel (diameter)
Surface tension	$0.02 - 0.04$ N m^{-1} between water and squalene[3].	

Ca calculations are estimates and used to compare microfluidic behaviours to those seen in the literature. It is noted that the viscosity values for the oil as well as the surface tension values employed may be different due to the presence of surfactant.

The range of Ca obtained for all flow rate and surface tension values is $0.037 - 0.074$ for W/O droplets, and $0.000032 - 0.00016$ for O/W. These values correspond to a dripping and a geometrically-driven regime of droplet formation, respectively, as described in section 1.3.2.

APPENDIX 4 - Table of physicochemical properties of various alginate hydrogels.

Property	Value	Reference (s)	Conditions	Comments	Value
Viscosity	163 cP / shear thinning	Al-Hajry et al. 1999[4] Dimitriu et al. 2004[5]	Viscosity of a 2% w/v low visc. Sodium Alginate solution prior to gelation.	Low viscosity alginates are chosen because they are favourable for microfluidic flow.	Alginates of different viscosity can be used to suit a desired microfluidic flow regime (i.e. dripping vs. jetting). Also, alginates of different viscosity give rise to hydrogels with different physical properties such as gel density and stiffness.
Density	1.02 kg m^{-3}	n/a	2% v/v low viscosity alginate (as used here).	n/a	The density of the alginate hydrogel can be used to control capsule buoyancy.
Depolymeris ability	yes	Klinger et al. 2014	Alginate polymers can be depolymerised with microwave irradiation.	Other methods exist and depend on whether the alginate gel is covalently or ionotropically cross-linked.	This allows for capsules to perform as triggered release vehicles or in tissue repair, in circumstances where an internal cargo required to be delivered.
Compression modulus	2.539 GPa	Anne-Virginie et al. 2009[6]	Measured via ultrasound for a 2% w/v sodium alginate solution hydrogel beads.	n/a	By selecting different alginate types or by varying the concentration or gellng method, alginate beads and capsules can be produced to resist different degrees of mechanical stress.
Young´s Modulus	14±2 kPa	Ahearne et al. 2008[7]	2% w/v sodium alginate.	n/a	
Gel Strength	58.9 mN	Choi et al. 2002[8]	3% w/v sodium alginate hydrogel.	n/a	
Mesh Size	5.3±1.0 nm	Kaklamani et al. 2014[9]	Sodium alginate 2.5% w/v hydrogels prepared with 1M $CaCl_2$	n/a	By varying the type, concentration and gelling method of the alginate, alginate capsules and beads can be produced with varying permeability to differently sized molecules, offering a route towards selective and semi-permeability.
Porosity	88.84%± 3.21 (avg)	Choi et al. 2002		The gels prepared in this paper are made to contain air. This is done by the release of CO_2 from $CaCO_3$. Gelation is carried out by external $CaCl_2$ In our constructs, CO_2 is also released as it is reacting with acetic acid.	
Pore Size	0.50±0.14 nm (median pore diameter)	Choi et al. 2002	3% w/v sodium alginate hydrogel w/ 0.25:1 $CaCO_3$: sodium alginate (w/v).		
Swelling ratio	21±0.9	Kong et al. 2004	3% w/v sodium alginate solution prepared with $CaSO_4$ as gelation agent.	This is the swelling ratio of dry vs. wet sodium alginate (pre & after hydrogel formation), not the swelling ratio of alginate	The swelling ability of alginate beads and capsules can be exploited to cause structural changes which could be useful for biomedical applications. This also suggests alginate beads and capsules can be dry-stored and rehydrated into hydrogels.

					hydrogels.
Thermal stability	Up to 160ºC			According to paper, above this temperature dry alginate films start to lose weight.	Thermal stability demonstrates the potential robustness of alginate beads and capsules, and allows them to be heat sterilised for biological and medical purposes. They can also be used to carry out chemical reactions that benefit from heat or are triggered or ceased by temperature.
Conductivity (dry alginate film)	8.7×10^{-5} S/cm	Iwaki et al. 2012[9]	2% w/v medium/high viscosity sodium alginate.	Conductivity described here is of a dry alginate film. Conductivity of an alginate hydrogel will depend mostly on the buffer/water it is dissolved in.	Conductivity allows alginate beads and capsules the potential to electrically interact with each other and biological tissues, and to be used to carry out electrophysiologicy recordings in conjunction with DIBs, for example.
Transparency	Up to 90%			Transparency depends greatly on the way the hydrogel is prepared. E.g. hydrogels gelled with dispersed $CaCO_3$ will be turbid as long as $CaCO_3$ is unreacted.	Transparency of alginate beads and capsules allow them to be optically characterised or to be used to carry out optical assays. Also, potentially large structures composed of alginate can be produced with little impact on visibility.
Refractive index	1.37	Esteban et al. 2009[10]	0.7% w/v sodium alginate in deionised water gelled with $CaCl_2$.		A refractive index similar to water facilitates optical characterisation of alginate hydrogels stored in water.
UV-vis absorption	Peaks @ 970 and 1200 nm			Absorption peaks are that of water as it is the main constituent of alginate hydrogels.	Low UV-vis absorption allows alginate beads and capsules to be used as a medium for spectroscopy.

APPENDIX 5 - Optimisation of flow rates for the production of eDIBs containing a prescribed number of aqueous cores.

Initially, the following flow rates were employed, which were empirically determined to produce relatively monodisperse emulsions:

Phase	Flow rate (ml hr^{-1})
Inner aqueous	12
Inner oil	12
Alginate	150
Carrier oil	400

The distribution of the number of cores encapsulated per eDIB for 100 eDIBs flowing continually is shown in the following graph:
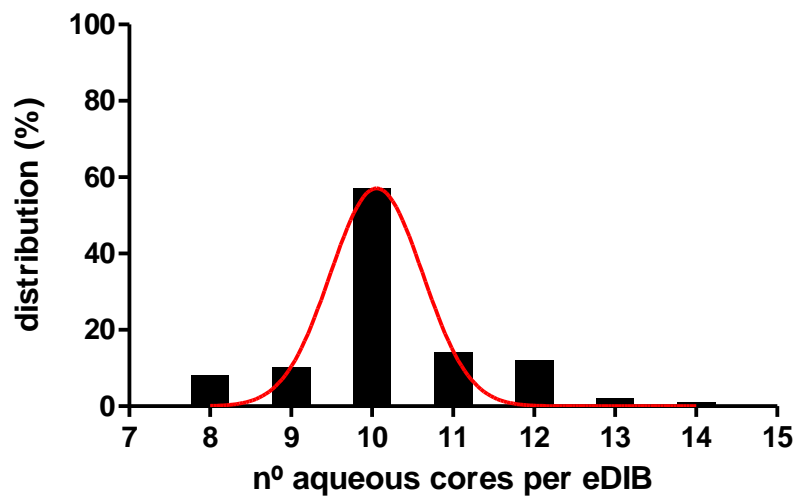

Figure 1 Graph depicting the distribution of the number of aqueous cores encapsulated per eDIB for 100 eDIBs produced continually using the following flow rates: inner aqueous phase: 12 ml hr^{-1}; inner oil phase: 12 ml hr^{-1}; alginate phase: 150 ml hr^{-1}; carrier oil phase: 400 ml hr^{-1}. A Gaussian distribution is fitted to the data (red line), displaying a peak at 10.28 cores per eDIB.

A Gaussian profile is fit to the distribution displaying a peak at 10.28. This can be used to adjust the inner aqueous and oil flow rates to approximate the peak to the nearest whole number (i.e. 10 cores per eDIB):

$$\frac{12}{10.28} \times 10 = 11.76$$

Thus, a flow rate of 11.76 ml hr^{-1} for both the inner aqueous and oil phases is tested which gives rise to the following distribution:
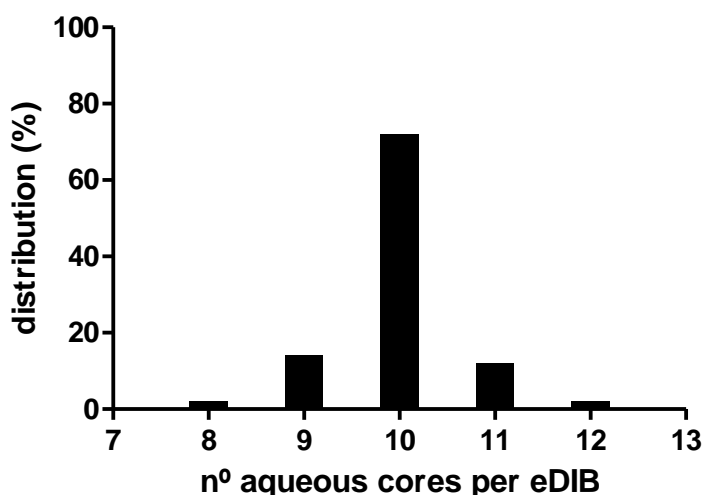

Figure 2 Graph depicting the distribution of the number of aqueous cores encapsulated per eDIB for 100 eDIBs produced continually using the following flow rates: inner aqueous phase: 11.76 ml hr^{-1}; inner oil phase: 11.76 ml hr^{-1}; alginate phase: 150 ml hr^{-1}; carrier oil phase: 400 ml hr^{-1}.

This method effectively reduced the polydispersity of the eDIBs produced with regards to the number of aqueous cores encapsulated per eDIB, via optimisation of the inner aqueous and oil flow rates. Whilst the initial flow rates employed gave rise to a wide distribution of the number of cores per eDIB (8-14 cores per eDIB) with 57% containing 10 cores and 78% containing 10±1 cores, the optimised flow rates produce a narrower range (8-12 cores) with 70% containing 10 cores and 96% containing 10±1 cores. The optimisation process could be repeated on the distribution obtained, but was found to increase polydispersity.

References

1.	Castell, O. K.; Berridge, J.; Wallace, M. I., *Angewandte Chemie International Edition* **2012,** *51* (13), 3134-3138.

2.	Pubchem.

3.	Pubchem.

4.	Al-Hajry, H. A.; Al-Maskry, S. A.; Al-Kharousi, L. M.; El-Mardi, O.; Shayya, W. H.; Goosen, M. F. A., *Biotechnology Progress* **1999,** *15* (4), 768-774.

5.	Klinger, M.; Toqeer, A.; Juul, A. G.; StenbÆK, D. Depolymerisation of alginic acid. WO2014102332 A1, 2014/07/03/, 2014.

6.	Anne-Virginie, S.; Liguo, Z.; Jean-Marc, G., *ResearchGate* **2009**.

7.	Ahearne, M.; Yang, Y.; Liu, K. K., *ResearchGate* **2008,** *4*.

8.	Choi, B. Y.; Park, H. J.; Hwang, S. J.; Park, J. B., *International Journal of Pharmaceutics* **2002,** *239* (1–2), 81-91.

9.	Kaklamani, G.; Cheneler, D.; Grover, L. M.; Adams, M. J.; Bowen, J., *Journal of the Mechanical Behavior of Biomedical Materials* **2014,** *36*, 135-142.

10.	Esteban, Ó.; Marvá, F.; Martínez-Antón, J. C., *Optical Materials* **2009,** *31* (4), 696-699.